UNDERSTANDING THE ROLE OF ADIPOSE TISSUE MICROENVIRONMENT IN OBESITY-INDUCED INFLAMMATION AND INSULIN RESISTANCE

A Thesis Submitted
In Partial Fulfillment of the Requirements
For the Degree of

DOCTOR OF PHILOSOPHY

by

DEBARUN PATRA

(2018BMZ0005)

DEPARTMENT OF BIOMEDICAL ENGINEERING

INDIAN INSTITUTE OF TECHNOLOGY ROPAR

January, 2024

Debarun Patra: *Understanding The Role of Adipose Tissue Microenvironment in Obesity-Induced Inflammation and Insulin Resistance*

DEDICATED

TO

MY TEACHERS

Declaration of Originality

I hereby declare that the work which is being presented in the thesis entitled UNDERSTANDING THE ROLE OF ADIPOSE TISSUE MICROENVIRONMENT IN OBESITY-INDUCED INFLAMMATION AND INSULIN RESISTANCE has been solely authored by me. It presents the result of my own independent investigation/research conducted during the time period from **January, 2019** of joining the Ph.D. program to **January, 2024** for final Ph.D. Thesis submission under the supervision of **Durba Pal, PhD**, Assistant Professor. To the best of my knowledge, it is an original work, both in terms of research content and narrative, and has not been submitted or accepted elsewhere, in part or in full, for the award of any degree, diploma, fellowship, associateship, or similar title of any university or institution. Further, due credit has been attributed to the relevant state-of-the-art and collaborations (NIPER SAS Nagar and DMC&H Ludhiana) with appropriate citations and acknowledgments, in line with established ethical norms and practices. I also declare that any idea/data/fact/source stated in my thesis has not been fabricated/ falsified/ misrepresented. All the principles of academic honesty and integrity have been followed. I fully understand that if the thesis is found to be unoriginal, fabricated, or plagiarized, the Institute reserves the right to withdraw the thesis from its archive and revoke the associated Degree conferred. Additionally, the Institute also reserves the right to appraise all concerned sections of society of the matter for their information and necessary action. If accepted, I hereby consent for my thesis to be available online in the Institute's Open Access repository, inter-library loan, and the title & abstract to be made available to outside organizations.

Signature

Name: Debarun Patra
Entry Number: 2018BMZ0005
Program: PhD
Department: Department of Biomedical Engineering
Indian Institute of Technology Ropar Rupnagar, Punjab 140001

Date: January 05, 2024

Acknowledgments

I extend my heartfelt gratitude to various individuals and organizations whose unwavering support and contributions have been instrumental throughout my Ph.D. journey. First and foremost, I express my deep appreciation to my family members for their unwavering support and encouragement during every phase of my doctoral studies. I extend my heartfelt gratitude to **Dr. Durba Pal**, my esteemed Ph.D. advisor, for her invaluable academic guidance, unwavering support, and dedicated supervision, without which the accomplishment of this scientific work would have remained out of reach. I am deeply thankful for her belief in my capabilities and for nurturing my self-assurance throughout this academic journey. Her expertise and commitment have not only played a pivotal role in molding my research but have also contributed significantly to my personal and professional development.

I am also immensely grateful to Dr. Suman Dasgupta, Tezpur University, whose support, diligence, kindness, and thought-provoking discussions continuously inspired me to delve deeper into my research and expand my horizons. My gratitude extends to Dr. Dipanjan Banerjee of Tezpur University for being a constant source of support and Mr. Upalabdha Dey of Tezpur University for his unwavering support during my bioinformatics studies.

I would like to acknowledge Prof. Kulbhushan Tikoo, NIPER SAS Nagar, who generously provided access to laboratory facilities, making the execution of animal studies possible. I am thankful to Dr. Rajat Pant of NIPER for his experience, and insightful discussions, which contributed significantly to my growth as a researcher. Special thanks go to Mr. Shivam Sharma and Mr. Shaheen Waseel Kabir for their assistance in conducting animal experiments.

I extend my appreciation to my doctoral committee members: Dr. Srivatsava Naidu, Prof. Javed N. Agrewala, Dr. Viswajeet Mehandia, and Dr. Kailash Chandra Jena for their timely suggestions and academic support. My heartfelt thanks also go to all my fellow lab members, whose unwavering support was a cornerstone of every research outcome. My sincere appreciation is directed towards the clinicians and team members of the Gastroenterology Unit at DMC&H, Prof. Satpal Singh, and the team for their assistance in collecting vWAT patient samples. I am thankful to Prof. Debasish Manna of IIT Guwahati for his support in performing SPR analyses.

I want to acknowledge my friend Dr. Adeel Zafar for his constant support and assistance in navigating both professional and personal challenges. A special mention goes to my dear friend, Mr. Soumyajit Roy, who has been by my side throughout my academic and personal journey, making many achievements possible. Last but not least I would like to thank my wife Puja for being part of my life and providing constant support.

Lastly, I wish to express my gratitude to the Ministry of Education (MoE), Indian Institute of Technology Ropar, for providing me with a fellowship, as well as the Department of Biomedical Engineering and Central Research Facilities (CRF) for granting access to research facilities. I am also thankful to Keystone Symposia for awarding me a Scholarship, which allowed me to present my work at the Hypoxia Conference in Ireland.

Debarun Patra

January 05, 2024

Certificate

This is to certify that the thesis entitled 'UNDERSTANDING THE ROLE OF ADIPOSE TISSUE MICROENVIRONMENT IN OBESITY-INDUCED INFLAMMATION AND INSULIN RESISTANCE', submitted by Debarun Patra (2018BMZ0005) for the award of the degree of Doctor of Philosophy of Indian Institute of Technology Ropar, is a record of bonafide research work carried out under my guidance and supervision. To the best of my knowledge and belief, the work presented in this thesis is original and has not been submitted, either in part or full, for the award of any other degree, diploma, fellowship, associateship or similar title of any university or institution.

In my opinion, the thesis has reached the standard fulfilling the requirements of the regulations relating to the Degree.

(Supervisor)

Name: Dr. Durba Pal
Department: Department of Biomedical Engineering
Indian Institute of Technology Ropar
Rupnagar, Punjab 140001
Date: January 05, 2024

Lay Summary

Obesity is a major health challenge that can lead to serious problems like diabetes and insulin resistance. In this thesis, we explored how obesity deteriorates body health and found some potential ways to treat these health issues. When a person becomes obese, their body's lower fat tissue, especially the one around the belly, gets expanded. We discovered that the lower abdominal fat tissue becomes a battleground, for certain special immune cells called macrophages, and they play a key role in disturbing fat tissue function. We found that a tiny nucleic acid molecule called microRNA-210-3p, abundantly presents in macrophages and converts them into more inflammatory. We also found if we can prevent miR-210-3p's function it can help to reduce the inflammation and restore fat tissue function, a novel way to manage obesity-related health problems. Additionally, we found that in obesity, the fat tissue macrophages send out tiny packages called extracellular vesicles to carry miR-210-3p and disburse to nearby fat tissues and other parts of the body like muscles and liver via circulation. These make the body's response to insulin worsens, which disturbs blood sugar level. But by blocking these vesicles we can improve the insulin function of fat, liver, and skeletal muscles. Lastly, we discovered that a well-known obese diabetic biomarker glycoprotein called fetuin-A, which was known to be secreted from the liver and fat tissue in the circulation, but during obesity, it can migrate to the nucleus and cause them to become old and damaged fat cells which quickly lose their function. These novel findings can open up a new direction for managing obese-induced type 2 diabetes.

In a nutshell, this study explores how obesity affects fat tissue health and finds a way to manage it by targeting specific molecules and processes, that might help to develop new treatments to improve the health of people globally who are suffering from obesity-related issues like diabetes and insulin resistance.

Abstract

Chronic obesity presents a formidable challenge to biomedical researchers as its association with metabolic disorders, notably insulin resistance (IR) and type 2 diabetes (T2D). In this study, we unravel a multifaceted interplay within the obese visceral white adipose tissue (vWAT) that drives adipocyte dysfunction, inflammation, and insulin resistance, offering potential therapeutic avenues for managing these conditions. During chronic obesity, the vWAT undergoes significant expansion generating a microenvironment (AT*env*), characterized by elevated free fatty acids (FFAs) and hypoxia, triggering a cascade of pathogenic events. Here in this thesis, we revealed microenvironment significantly upregulates the expression of miR-210-3p in adipose tissue macrophages (ATMs), promoting the polarization of proinflammatory ATMs and the release of proinflammatory cytokines. Notably, the delivery of miR-210-3p mimic exacerbates macrophage inflammation even in the absence of lipid surge (HL co-stimulation), while miR-210-3p inhibition mitigates HL-induced inflammation. Mechanistically, miR-210-3p targets SOCS1, a negative regulator of the NF-κB p65 subunit which negatively influences the inflammatory pathway. The direct delivery of anti-miR-210-3p LNA in the vWAT rescues mice from obesity-induced adipose tissue inflammation, highlighting miR-210-3p inhibition in ATMs as a promising therapeutic strategy. Furthermore, obese AT*env* orchestrates the release of miR-210-3p-enriched extracellular vesicles (EVs) from ATMs, which subsequently impair glucose metabolism in lean mice by targeting GLUT4 expression and disrupting the insulin signaling pathway. The therapeutic intervention using miR-210-3p inhibitor-LNA in vWAT rescues high-fat diet (HFD)-fed mice from obesity-induced systemic insulin resistance and glucose intolerance. Thus, targeting obese ATM-specific miR-210-3p holds promise as a therapeutic strategy for managing IR and T2D.

In the context of obesity, a tremendous increase in adipocyte senescence is observed as adipocytes undergo irreversible growth arrest associated with the secretion of various adipokines, cytokines, chemokines, and extracellular matrix proteins that contribute to IR and T2D. Here we reveal that fetuin-A, previously recognized as a hepatokine and adipokine, serves as a nuclear regulatory protein in adipocytes under obese AT*env* conditions. HIF-1α directly interacts with fetuin-A and mediates the nuclear migration, and activates senescence-associated secretory phenotypes (SASPs) leading to adipocyte senescence. Ectopic expression of HIF-1α and fetuin-A in adipocytes independently induces senescence, even in the absence of pathophysiological stimuli. Additionally, fetuin-A ablation rescues adipocytes from SASP activation and premature senescence in diet-induced obese mice. These findings shed light on a novel mechanism of adipocyte pathogenesis, underscoring the importance of nuclear fetuin-A and HIF-1α interaction in driving adipocyte senescence under obese AT*env* conditions.

Collectively, our study provides a comprehensive understanding of the multifaceted mechanisms underlying obesity-induced adipose tissue dysfunction and insulin resistance, offering potential therapeutic targets for addressing these critical health challenges.

Keywords

Obesity; Adipose Tissue microenvironment; Inflammation; Insulin Resistance; microRNA, macrophage, adipocyte, Adipocyte senescence; Type 2 Diabetes; miR-210-3p, NF-κB, SOCS1, GLUT4, Fetuin-A

List of Publications

From Thesis

Journal:

1. Patra, D., Roy, S., Arora, L., Kabeer, S.W., Singh, S., Dey, U., Banerjee, D., Sinha, A., Dasgupta, S., Tikoo, K., Kumar, A., Pal, D. (2023). miR-210-3p Promotes Obesity-Induced Adipose Tissue Inflammation and Insulin Resistance by Targeting SOCS1-Mediated NF-κB Pathway. *Diabetes 72*, 375–388. 10.2337/db22-0284.

2. Patra, D., Ramprasad, P., Sharma, S., Dey, U., Kumar, V., Singh, S., Nirmalkar, N., Dasgupta, S., Kumar, A., Tikoo, K., Pal, D. (2023) Obese adipose tissue macrophage-derived miR-210 disrupts systemic insulin sensitivity by GLUT4 silencing. (*under review*)

3. Patra, D., Vashisth, A., Ramprasad, P., Sharma, S., Prusty, B.M., Roy, S., Singh, S., Manna, D., Tikoo, K., Dasgupta, S., Pal, D. (2023) Nuclear Fetuin-A programs adipocyte senescence under chronic obesity. (*under review*)

4. Patra, D., Banerjee, D., Ramprasad, P., Roy, S., Pal, D., Dasgupta, S. (2023) Recent insights of obesity-induced gut and adipose tissue dysbiosis in type 2 diabetes. *Frontiers in Molecular Biosciences* 10.3389/fmolb.2023.1224982

5. Patra, D., Ramprasad, P., Joshi, R., Dey, U., Dasgupta, S., Pal, D. (2023) microRNA interplay in obesity affected insulin-responsive tissue microenvironment. (*about to submit*)

Conference Proceeding:

1. Patra, D., Pal, D. (2023) Macrophage derived miR-210-3p causes adipocyte insulin resistance in obesity. *Diabetes Technology & Therapeutics* 25(2) A-266. 10.1089/dia.2023.2525

Book chapter:

1. Patra, D., Roy, S., Ramprasad, P., Pal, D. (2023) Next-generation therapies for Type 2 diabetes mellitus. *Functional Smart Nanomaterials and Their Theranostics Approaches, Springer Nature; (accepted, in press)* ISBN: 978-981-99-6596-0

List of Publication

From Associated Projects

1. Banerjee, D*., Patra, D*., Sinha, A., Roy, S., Pant, R., Sarmah, R., Dutta, R., Bhagabati, S.K., Tikoo, K., Pal, D., Dasgupta S. (2022) Lipid-induced monokine Cyclophilin-A promotes adipose tissue dysfunction implementing insulin resistance and type 2 diabetes in zebrafish and mice models of obesity. *Cellular and Molecular Life Sciences* 79(5), 282. 10.1007/s00018-022-04306-1 (*joint first author)

2. Pant, R., Kabeer, S.W., Sharma, S., Kumar, V., Patra, D., Pal, D., Tikoo, K. (2023) Pharmacological inhibition of DNMT1 restores macrophage autophagy and M2 polarization in western diet-induced Nonalcoholic fatty liver disease. *Journal of Biological Chemistry* p. 104779. 10.1016/j.jbc.2023.104779

3. Choudhary, S., Patra, D., Sinha, A., Pant, R., Chouhan, R., Jha, A.N., Prusty, B.M., Manna, D., Das, S.K., Tikoo, K., Pal, D., Dasgupta, S. (2023) A small molecule potent IRAK4 inhibitor abrogates lipopolysaccharide-induced macrophage inflammation in-vitro and in-vivo. *European Journal of Pharmacology* 944, 17593. 10.1016/j.ejphar.2023.175593

4. Arora, L., Patra, D., Roy, S., Nanda, S., Singh, N., Verma, A.K., Chakraborti, A., Dasgupta, S., Pal, D. (2022) Hypoxia-induced miR-210-3p expression in lung adenocarcinoma potentiates tumor development by regulating CCL2-mediated monocyte infiltration. *Molecular Oncology*. 10.1002/1878-0261.13260

5. Banerjee, D., Patra, D., Sinha, A., Chakrabarty, D., Zafar, A., Patra, A., Sarmah, R., Dey, U., Dutta, R., Bhagabati, SK., Mukherjee, AK., Kumar, A., Pal, D., Dasgupta, S. (2023) Macrophage foam cells-derived mediator fetuin-A promotes insulin resistance in atherosclerosis through the induction of spontaneous fat lipolysis. *Biofactors* (*under review*)

6. Banerjee, D., Achari, A., Patra, D., Sinha, A., Sarmah, R., Dutta, R., Bhattacharya, S., Jaisankar, P., Dasgupta, S. (2023) Reversal of foam cells to macrophages by a plant-derived molecule which alleviates cellular cholesterol imbalance and atherosclerosis. *Phytomedicine*. (*under review*)

Book chapter:

1. Patra, D., Bhavya, K., Ramprasad, P., Kalia, M., Pal, D. (2023) Anti-cancer drug molecules targeting cancer cell cycle and proliferation. *Advances in Protein Chemistry and Structural Biology*; Academic Press, Elsevier. ISSN 1876-1623

List of conferences, awards, and honours

1. Abstract selected for Poster presentation in the Cell Symposia: *Molecular mechanisms and integrative physiology of obesity*. October 13–15, 2023, Shanghai

2. Delivered short talk and presented Poster on HypoxamiR-210 promotes obesity-induced adipose tissue inflammation via targeting SOCS1/NF-κB at the Keystone Conference 'Hypoxia: From Basic Mechanisms to Emerging Therapies', May 28-31, 2023, Ireland

3. Attended 7th Annual *Stanford Drug Discovery Symposium* (SDDS) organized by Stanford University (Virtual); April 24-25, 2023.

4. Poster presentation at the 16th International Conference on *Advanced Technologies & Treatment for Diabetes* (ATTD) 22-25 February 2023, Berlin & Online

5. Delivered a short talk on '*Immunotechniques*' (Western blotting) in SPARC INDO-US Workshop, Workshop on Immunology, jointly organized by Indian Institute of Technology Ropar and The George Washington University, 12-13 June 2020

6. Poster presentation in National Seminar 'XLIII All India Cell Biology Conference (AICBC)' 2019, IISER Mohali (Punjab), 19-21 December 2019

Awards

1. *Keystone Symposia Future of Science Fund Scholarship* awarded for attending "Hypoxia: From Basic Mechanisms to Emerging Therapies" Keystone Conference, May 28-31, 2023, Ireland

Table of Contents

Declaration of Originality v

Acknowledgments vii

Certificate ix

Lay Summary xi

Abstract xiii

List of Publications xv

List of conferences, awards, and honours xvii

Abbreviations xxi

List of Figures xxiv

List of Tables xxv

Chapter 1 | Introduction 1

1.1 Background: Adipose tissue microenvironment and type 2 diabetes 1

1.2 Context 2

1.3 Research Questions 3

1.4 Relevance 4

1.5 Specific aims 4

1.6 Thesis outline 4

References 7

Chapter 2 | Literature Review 9

2.1 Overview of Adipose tissue 9

2.2 Visceral white adipose tissue (vWAT) composition 11

2.2.1 Pre – and mature adipocytes 11

2.2.2 Macrophages 13

2.2.3 Dendritic cells 16

2.2.5 Endothelial cells 18

2.3 Obesity induced adipose tissue dysfunction causing inflammation and insulin resistance 18

2.4 microRNAs regulating adipose tissue dysfunction 22

2.4.1 miRNA regulates AT insulin signaling pathway 23

2.4.2 miRNA regulates AT inflammation that linked with IR 24

2.5 Extracellular vesicle-mediates AT dysfunction during obesity 27

2.6. Adipocyte senescence-mediated AT pathogenesis during obesity 32

References 34

Chapter 3 | miR-210-3p promotes Adipose Tissue Macrophage Inflammation in Obesity 43

3.1 Background 43

3.2 Results 44

3.2.1 Obesity-associated hypoxic state of adipose tissue microenvironment potentiates increased expression of *miR-210-3p* in ATMs 44
3.2.2 Inhibition of *miR-210-3p* protects HL-induced macrophage inflammation and its polarization 46
3.2.3 *miR-210-3p* drives obesity-induced ATM inflammation by targeting the SOCS1/NF-κB pathway 50
3.2.4 Anti-*miR-210-3p* delivery rescued obesity-induced ATM inflammation 54

3.3 Discussion **56**

3.4 Materials and Methods **59**
3.4.1 Reagents and antibodies 59
3.4.2 Mice models and treatments 60
3.4.3 Human subjects 60
3.4.4 Cell culture and treatments 61
3.4.5 miR-210-3p mimic/inhibitor transfection 62
3.4.6 Transwell co-culture and glucose uptake assay 62
3.4.7 Site directed mutagenesis 62
3.4.8 SOCS1 3'-UTR luciferase reporter assay 63
3.4.9 Flow cytometry 63
3.4.10 Immunocytochemistry 63
3.4.11 Immunofluorescence 64
3.4.12 Oil Red O staining 64
3.4.13 H&E staining and imaging 64
3.4.14 RNA extraction and Quantitative PCR 65
3.4.15 Immunoblotting 65
3.4.16 Enzyme-linked immunosorbent assay (ELISA) 66
3.4.17 Fluorescence-activated cell sorting (FACS) 66
3.4.18 miRNA transcriptomic analysis 66
3.4.19 Statistical analysis 66

References **67**

Chapter 4 | Obese adipose tissue macrophage-derived miR-210 disrupts systemic insulin sensitivity by GLUT4 silencing ***69***

4.1 Background **69**

4.2 Results **70**
4.2.1 Obese ATMs-derived extracellular vesicles (EVs) bestow miR-210-3p to adipocytes 70
4.2.2 miR-210-3p enriched EVs of obese ATMs promote glucose intolerance and insulin resistance 73
4.2.3 Suppression of GLUT4 expression by the direct interaction with miR-210-3p potentiates insulin resistance 76
4.2.4 miR-210-3p inhibition rescues DIO mice from glucose intolerance and insulin resistance 79

4.3 Discussion **81**

4.4 Materials and Methods **83**
4.4.1 Reagents and antibodies 83
4.4.2 Mice models and treatments 84
4.4.3 Human subjects 84
4.4.4 Cell culture and treatments 84
4.4.5 Extracellular vesicle experiments 86
4.4.6 Transmission Electron microscopy of Tissue sections 86
4.4.7 miR-210-3p mimic transfection 87
4.4.8 Transwell co-culture experiment 87
4.4.9 Glucose uptake assay 87
4.4.10 Cloning of GLUT4 3'UTR 87
4.4.11 Site directed mutagenesis 88

4.4.12 GLUT4 3'-UTR luciferase reporter assay ... 88
4.4.13 Immunocytochemistry ... 88
4.4.14 Oil-red O staining ... 88
4.4.15 Immunostaining and Confocal microscopy ... 88
4.4.16 H&E staining and imaging ... 89
4.4.17 RNA extraction and Quantitative PCR ... 89
4.4.18 Immunoblotting ... 89
4.4.19 Enzyme-linked immunosorbent assay (ELISA) ... 89
4.4.20 Flow cytometry ... 89
4.4.21 Reanalyses of publicly available snSeq dataset ... 89
4.4.22 Statistical analyses ... 89

Chapter 5 | Obese adipose tissue microenvironment-induced nuclear FetuinA that promotes adipocyte senescence ... ***93***

5.1 Background ... **93**

5.2 Results ... **94**
5.2.1 Nuclear localization of fetuin-A (fetA) in adipocytes of obese adipose tissue ... 94
5.2.2 Hypoxia-inducible factor-1α regulates the nuclear migration of FetA ... 96
5.2.3 Nuclear FetA induces adipocyte senescence and its' inhibition protects from senescence-induced pathogenesis ... 99

5.3 Discussion ... **102**

5.4. Materials and methods ... **103**
5.4.1 Reagents and antibodies ... 103
5.4.2 Cell culture and transfection ... 104
5.4.3 Mice experiments ... 105
5.4.4 Clinical samples ... 105
5.4.5 Adipocyte nuclei isolation and staining ... 105
5.4.6 Nuclear protein isolation ... 105
5.4.7 Co-immunoprecipitation ... 106
5.4.8 SPR analysis ... 106
5.4.9 Protein-protein docking analyses ... 106
5.4.10 Senescence-associated beta-galactosidase (SABG) assay ... 107
5.4.11 Immunofluorescence staining and Confocal microscopy ... 107
5.4.12 Oil-red O staining ... 107
5.4.13 H&E staining and imaging ... 107
5.4.14 RNA Extraction and Quantitative PCR ... 107
5.4.15 Immunoblotting ... 107
5.4.16 Statistical analyses ... 108

References ... **108**

Chapter 6 |Summary ... ***111***

6.1 Highlights ... **111**

6.2 Conclusions ... **112**

6.3 Future perspectives ... **113**

Table A | Antibody ... ***115***

Table B | Primer sequence ... ***117***

Table C | Patient demographic details ... ***119***

Abbreviations

AT	Adipose tissue
vWAT/VAT	Visceral white adipose tissue
WAT	White adipose tissue
BAT	Brown adipose tissue
SAT	Subcutaneous adipose tissue
AT*ENV*	Adipose tissue microenvironment
MIR	MicroRNA
ATM	Adipose tissue macrophage
CLS	Crown like cell
SVF	Stromal vascular fraction
ScRNASEQ	Single-cell RNA sequencing
SnRNASEQ	Single-nuclei RNA sequencing
T2D	Type 2 diabetes
IR	Insulin resistance
DIO	Diet-induced obesity
HFD	High fat diet
STNDD	Standard diet
FFAS	Free fatty acids
TGA	Triglyceride
db/db	Genetically obese, leptin deficient mice model
SM or Sk. M	Skeletal muscles
IR	Insulin resistance
NAFLD	Non-alcoholic fatty liver disease
CVD	Cardiovascular diseases
ob/ob	Genetically obese mouse strain.
GTT	Glucose tolerance test
ITT	Insulin tolerance test
HOMA-IR	Homeostatic model assessment for insulin resistance
IGG	Immunoglobulin γ
ECM	Extracellular matrix
SABG	Senescence-associated beta-galactosidase
ASPC	Adipose stem and progenitor cells
EXOs	Exosomes
FAPs	Fibor-adipogenic progenitors
EVs	Extracellular vesicles

sEVs	Small extracellular vesicles
ELISA	Enzyme-linked immunosorbent assay
FACS	Fluorescence-activated cell sorting
LNAS	Locked nucleic acid
mRNA	Messenger RNA
TEM	Transmission electron microscopy
NTA	Nanoparticle tracking analysis
RT-qPCR	Real-time quantitative polymerase chain reaction
FAM	Fluorescein amidite
UTR	Untranslated regions
H&E	Hematoxylin and eosin
SASP	Senescence-associated secretory phenotype
NK CELL	Natural killer cell
DC	Dendritic cell
MΦ	Macrophage
ILCs	Innate lymphoid cells
MOS	Monocytes
LAMs	Lipid-associated macrophages
PVMs	Perivascular macrophages
MSCs	Mesenchymal stem cells
adECa	Adipose tissue endothelial cells
PDGFR	Platelet-derived growth factor receptor
KLF4	Krüppel-like factor 4
ATGL	Adipose triglyceride lipase
PRDM16	Positive regulatory domain zinc finger region protein 16
DAG	Diacylglycerol
CRP	C-reactive protein
UCP1	Uncoupling protein 1
TNFα	Tumour necrosis factor alpha
TGF-β	Transforming growth factor-β
PDGF	Platelet derived growth factor
IGF1	Insulin-like growth factor 1
PAI1	Plasminogen activator inhibitor-1
β-GAL	β-galactosidase
NF-κB	Nuclear factor kappa β
PPAR-γ	Peroxisome proliferators–activated receptor γ
CEBPα	CCAAT/enhancer-binding protein alpha

TLRs	Toll like receptors
NLRs	Nod-like receptor
NLRP3	Nod-, lrr- and pyrin domain-containing protein 3
ARNT	Aryl hydrocarbon receptor nuclear translocator
NAD	Nicotinamide adenine dinucleotide
SIRT1	Sirtuin 1
ADIPOR1	Adiponectin receptor 1
JNK	C-jun n-terminal kinases
IKKB	Ikappab kinase β
PTEN	Phosphatase and tensin homolog deleted on chromosome 10
GLUT4	Glucose transporter type 4
PI3K	Phosphoinositide 3-kinases
INSR /IR-β	Insulin receptor / Insulin receptor β
PHLLP	PH domain and leucine rich repeat protein phosphatases
MAPK	Mitogen-activated protein kinase
CCND1	Cyclin D1
PKB/AKT	Protein kinase B or Akt
IKB	Inhibitor of nuclear factor kappa B
MCP-1	Monocyte chemoattractant protein-1
ND	Non Obese Non-Diabetic Patients
DM	Obese Diabetic Patients
HIF-1α	Hypoxia-inducible factor 1 alpha
CXCL	CXC chemokine ligand
CD	Cluster of differentiation
CCL	Chemokine (c-c motif) ligand
MHC	Major histocompatibility complex
CCR2	C-C motif chemokine receptor 2
SOCS1	Suppressor of cytokine signalling 1
MMP3	Matrix metalloproteinase-3
TIMP2	Tissue inhibitor of metalloproteinases 2
O_2	Oxygen
CO_2	Carbon dioxide
ANOVA	Analysis of variance
SD	Standard deviation
H	Hypoxia (1% oxygen)
L	Lipid (palmitate)
DAPI	4',6-diamidino-2-phenylindole

List of Figures

Figure 1.1| Lipid-rich hypoxic adipose tissue microenvironment (AT*env*) in obesity……..**2**

Figure 1.2 | Pictorial overview of thesis outline……**6**

Figure 2.1| Obesity-induced pathophysiological state causing inflammation and insulin resistance…**9**

Figure 2.2| Cellular heterogeneity in white adipose tissue …….…….**15**

Figure 2.3| Obese pathogenic factors' role in adipose tissue inflammation and insulin resistance……**21**

Figure 2.4| Overview of miRNAs expression in AT under obesity……..……..……..**27**

Figure 2.5| Adipose tissue-derived extracellular vesicles regulate obesity-induced pathogenesis……**31**

Figure 3.1| Lipid-rich low oxygen tension in obese AT*env* potentiates high *miR-210-3p* expression in ATMs…….**45**

Figure 3.2 |Chronic obese AT*env* promotes ATMs skewing towards M1……...**48-49**

Figure 3.3|*miR-210-3p* derives obesity-induced ATM polarization and inflammation by targeting the SOCS1-NF-κB pathway……..**52-53**

Figure 3.4| Anti-miR-210-3p LNA delivery rescues obesity-induced ATM inflammation and insulin resistance……...**55**

Figure 4.1 |Obese ATMs-derived extracellular vesicles (EVs) bestow miR-210-3p to adipocytes.**71-72**

Figure 4.2 |miR-210-3p-enriched EVs of obese ATMs promote glucose intolerance and insulin resistance…….**74-75**

Figure 4.3 | Suppression of GLUT4 expression by the direct interaction with miR-210-3p potentiates insulin resistance……..……**77-78**

Figure 4.4 | Suppression of GLUT4 expression by the direct interaction with miR-210-3p potentiates insulin resistance……..……**79-80**

Figure 5.1 |Nuclear localization of fetuin-A (FetA) in adipocytes of obese adipose tissue…….....**95**

Figure 5.2| Hypoxia-inducible factor-1α facilitates nuclear migration of fetuin-A……..……...…**97-98**

Figure 5.3| Nuclear fetuin-A induces adipocyte senescence…….…...…**100-101**

List of Tables

Table 2.1 | Categorizing Macrophages with a special focus on their roles, types and markers expression in White Adipose Tissue……...**14-15**

Table 2.2 | List of miRNAs regulating adipose tissue dysfunction in obesity ……...…**28-29**

Table A | List of antibody…….…….……...……....…**115-117**

Table B | List of Primers……..……..…..….**117-118**

Table C | Patient demographic details (Clinicopathological features of obese diabetic patients and non-obese non-diabetic patients)…….……..……..…....…..**119**

Chapter 1 | Introduction

Obesity, defined as excess fat accumulation in the body, becomes a vicious risk to human health, contributing to over 4 million deaths worldwide ("Health Effects," 2017). Once the world was struggling with malnutrition, obesity was only considered a high-income country health problem, but today's scenario is far away from the past, as low and middle-income country has a higher number of obese peoples and the number is much higher than the underweight population in almost every corner of this globe except few regions (Avenue et al., 2012; Bhurosy & Jeewon, 2014; "Health Effects," 2017; Popkin & Slining, 2013). It enhances significant risk factors for developing various metabolic disorders, including type 2 diabetes (T2D), non-alcoholic fatty liver disease, atherosclerosis, and cardiovascular disease (Jin et al., 2023; Ormazabal et al., 2018). Obesity has been known as a major causative factor for insulin resistance (IR), a major defect and an early sign of T2D (Kahn & Flier, 2000) which is now considered as a pandemic due to its growing pervasiveness worldwide. The major burden of T2D is taking place in developing countries and most recent studies anticipated that Asia has arisen as the world's 'diabetes epicenter' and India will have more than 120 million adults with diabetes by 2045 (Home et al., n.d.; Khan et al., 2019; Pradeepa & Mohan, 2021).

1.1 Background: Adipose tissue microenvironment and type 2 diabetes

Visceral white adipose tissue (vWAT), a specialized form of connective tissue predominantly composed of adipocytes and stromal cells, including adipose stem cells, progenitor cells, preadipocytes, macrophages, T cells, dendritic cells, various immune cell populations, endothelial cells, and fibroblasts. It was once considered a storage depot for energy but more recently, it has been discovered as a master regulatory tissue that maintains glucose and lipid homeostasis (Reyes-Farias et al., 2021; Rosen & Spiegelman, 2006). This tissue exhibits a remarkable degree of plasticity, expanding significantly in response to obesity. Adipocyte size can increase by up to 200-fold in obese individuals, with a notable increase in the presence of adipose tissue macrophages (ATMs), which constitute approximately 50% of stromal cells in obese adipose tissue, in contrast to 5–10% in lean adipose tissue (Boutens & Stienstra, 2016). Excess storage of fat inside the adipocytes is a major consequence of its functional defects that leads to the formation of hypertrophied adipocytes which release higher levels of circulatory free fatty acids (FFAs), accompanied by the reduction of adipose tissue vascularisation creating a zone deprived of adequate oxygen and nutrients (Goossens et al., 2011; Lempesis et al., 2020; Snodgrass et al., 2016). Evidence showed that a severe drop in partial pressure of oxygen (pO_2) (also called *hypoxia*) takes place in the vWAT of obese diabetic patients as compared to lean non-diabetic subjects, that correlates with the upregulation of HIF target genes expression which involved in macrophage chemotaxis, angiogenesis, oxidative stress, cellular stemness and proliferation (Lee et al., 2019; Snodgrass et al., 2016). Adipose tissue hypoxia plays a major role in adipose tissue

inflammation and cause IR during the state of chronic obesity by secreting various proinflammatory cytokines and chemokines (Pasarica et al., 2009). The chemokines, such as CCL2/MCP1, aggravate the adipose tissue inflammation by heightened infiltration of macrophages and its polarization toward the M1 phenotype, as evident in the obese adipose tissue of patients and mice (Wang et al., 2007; Ye et al., 2007). On the other side, accumulation of excess fat within adipocytes is a primary consequence of dysfunctional hypertrophied adipocytes, which, elevates the release free fatty acids (FFAs). Increased FFA generates a state of chronic low-grade inflammation within both adipocytes and adipose tissue macrophages (ATMs) by activating TLR4-NF-κB pathway (Pal et al., 2012). Altogether, lipid-enriched, hypoxia creates a pathophysiologic *Adipose Tissue Microenvironment'* (**AT*env***) within the visceral adipose tissue during obesity which significantly potentiating inflammation, IR, and causing metabolic dysfunction.

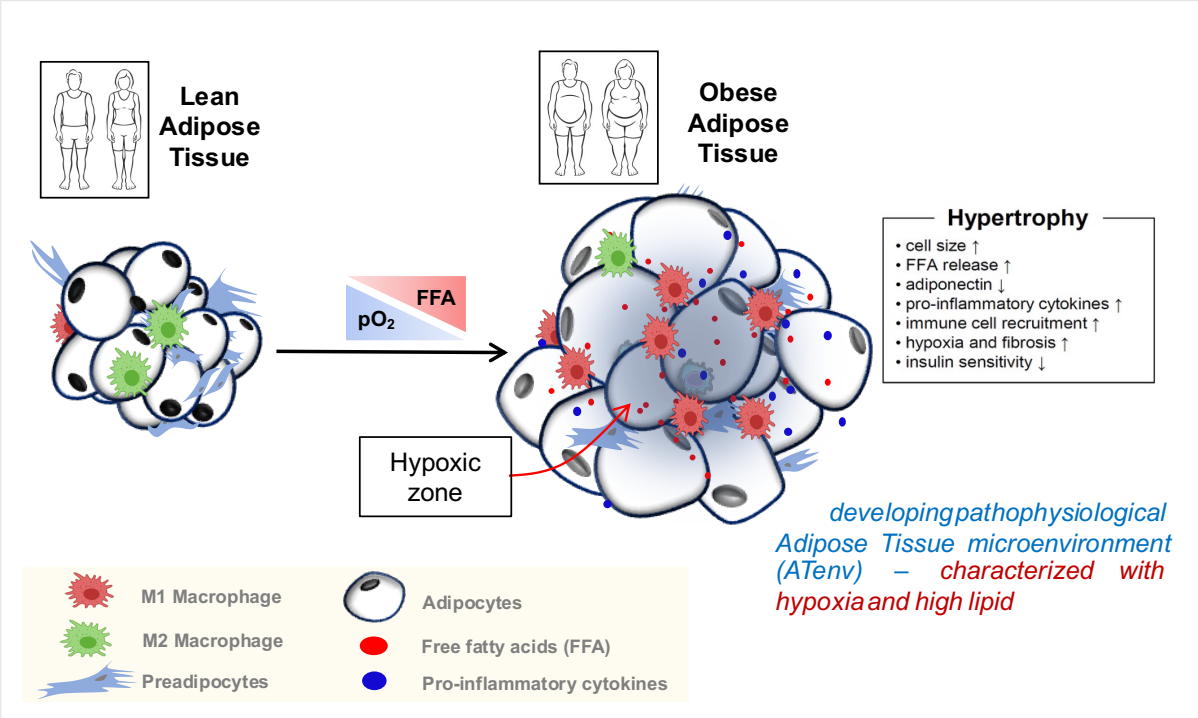

Figure 1.1| **Generation of lipid rich hypoxic adipose tissue microenvironment (AT*env*) in obese vWAT compared with lean ones.**

1.2 Context

The obese AT*env* dysregulates microRNA (miRNA) expression in adipocytes, macrophages, and other cells, significantly contributes to AT dysfunction (Kurylowicz, 2021; Oger et al., 2014). Several studies have reported altered miRNA profiles in obese adipose tissue, with distinct miRNAs being either upregulated or downregulated compared to lean individuals (Arner et al., 2012; Heyn et al., 2020; Kiran et al., 2021). These miRNA alterations extend their influence beyond adipose tissue, as they can impact systemic metabolic homeostasis via paracrine and endocrine actions (Kiran et al., 2021). The

consequences of adipose tissue dysfunction, including IR, dyslipidemia, and chronic inflammation, play pivotal roles in the pathogenesis of obesity-related metabolic diseases such as type 2 diabetes and cardiovascular disorders. Evidently, a few non-coding RNAs (e.g. miRNAs) can influence and modulate systemic insulin sensitivity and glucose tolerance in the onset of obesity by silencing critical signaling mediators. However, it was unclear whether ATenv-regulated non-coding RNAs directly influence the insulin function of adipocytes. Therefore, understanding the regulatory role of microenvironment-influenced miRNAs in adipose tissue dysfunction can offer potential insights for therapeutic interventions targeting obesity-related metabolic complications.

Moreover, recent studies evidenced that the initiation of adipocyte senescence in obesity marks a pivotal stage in the development of IR and metabolic disorders (Gustafson et al., 2022; Smith et al., 2021; Tchkonia et al., 2010; Palmer et al., 2019). Obesity enhances adipocyte senescence by stimulating the expression of multiple senescence-associated genes in vWAT (Tchkonia et al., 2010). Cellular oxidative stress, chronic inflammation, lipotoxicity, due to lipid overload in vWAT drives adipocytes into a state of senescence (Tchkonia et al., 2010; Manna & Jain, 2015). These senescent fat cells lose their normal functions and, instead, release pro-inflammatory molecules as part of the senescence-associated secretory phenotype (SASP) (Smith et al., 2021).

The complex interplay between adipocyte senescence, immune cell infiltration, inflammation, and IR underscores the critical role of adipose tissue dysfunction in the pathophysiological AT*env* to augment obesity-related metabolic complications. Therefore, understanding these processes may pave the way for innovative interventions aimed at alleviating the burden of metabolic disorders in the context of obesity.

1.3 Research Questions

To understand the regulation of AT*env* at the cellular and molecular level we quested for multiple unanswered questions which has been addressed in this thesis. Our first question was (1) how AT*env* alters non-coding RNAs in immune cells that are involved in chronic inflammation? (2) whether AT*env*-regulated non-coding RNAs directly influence the insulin signaling pathway? (3) Can targeted inhibition of epigenetic regulators at the pathophysiological environment protect from inflammatory burden and IR? Lastly, (4) how does AT*env*-influenced adipokine impact adipose senescence in obesity? In this thesis, much importance was given to deciphering the molecular action of such AT*env*-induced miRNA/adipokine in developing inflammation and IR. By answering these critical questions we understand the influence of AT*env* in obesity-induced AT pathogenesis.

1.4 Relevance

This thesis aims to understand the molecular factors involved in the progression of pathogenesis in terms of inflammation, metabolic dysfunction, and cellular heterogeneity under obese AT*env*. The initial purpose was to unravel the molecular mechanism contributing to proinflammatory macrophage enrichment in the visceral AT at the onset of obesity governed by lipid-rich hypoxic microenvironment. This will not only provide basic molecular information contributing to macrophage polarization in obesity but it will also identify the novel factor/s involved in pathogenesis, which can be further channelized for the development of novel therapeutic targets to combat obesity and T2D. Studies were designed to be performed on human patient samples and *in-vivo* models of obesity (DIO mice), for physiological relevance. Upon initial finding of the molecular target, it was aimed to understand the crosstalk between macrophages with adipocytes, and other insulin-responsive organs (e.g. liver, skeletal muscle) via releasing EVs at a systemic level. This led to the consideration of the macrophage-derived molecular target, as a critical therapeutic target molecule against this metabolic disorder. Furthermore, we aim to identify the novel obesity-induced adipokine(s) (OIAs) and its contribution to adipocyte senescence and insulin resistance in obesity-induced T2D. In addition, this study will also explore the therapeutic efficacy of targeted suppression of OIAs in obese T2D mice models. Altogether, the novel findings of obese AT microenvironment-influenced miRNAs and adipokines will open up new avenues for researchers and clinicians, to conduct further preclinical studies for the development of therapies against obesity-induced MM.

1.5 Specific aims

Specific aims of the study include:

1. To identify the role of hypoxia-induced miRNA in macrophage polarization in obese adipose tissue microenvironment (AT*env*).
2. To decipher the mechanism of AT macrophage-derived miRNAs function in contributing to insulin resistance in obesity.
3. To identify and delineate the molecular mechanism of obesity-induced adipokine in potentiating adipocyte senescence under AT*env*.

1.6 Thesis outline

This thesis is organized into **six chapters** starting with **chapter 1**, the *introduction*, and **chapter 2** is the *review of the literature*. Reports of the studies conducted to understand the obese adipose tissue microenvironment (AT*env*) are described in **chapters 3-5**. **Chapter 6** is the *concluding chapter*.

Briefly, **Chapter 3** highlights the molecular mechanism of *obese adipose tissue microenvironment in macrophage polarization to potentiate chronic inflammation* by using RAW264.7 murine macrophages, primary adipose tissue macrophage, 3T3-L1 murine adipocytes, diet-induced obese mice models and clinical samples from lean non-diabetic and obese diabetic patients. Here, we showed ATenv significantly increased miR-210-3p expression in ATMs which promotes NF-κB dependent proinflammatory cytokine expression along with the downregulation of anti-inflammatory cytokine expression through increased production of suppressor of cytokine signaling 1 (SOCS1), a negative regulator of the NF-kB inflammatory signaling pathway. Mechanistically, miR-210 directly binds to the 3′-UTR of SOCS1 mRNA and silences its expression, thus preventing proteasomal degradation of NF-κB p65. Direct delivery of anti–miR-210-3p LNA in the VAT (ATenv) of obese insulin-resistant mice, showed a significant reduction in obesity-induced adipose tissue inflammation. Thus, miR-210-3p inhibition in ATMs could be a novel therapeutic strategy for managing chronic inflammation in obesity-induced adipose tissue pathogenesis. This studies reveals anti-miR-210 therapy can rescue obese mice from inflammatory escalation.

In **Chapter 4**, the effect of *ATenv-induced ATM-driven miR-210 surge on neighboring adipocytes and other insulin target cells* was studied by using murine Bone marrow-derived macrophages (BMDMs), RAW 264.7 macrophages, 3T3-L1 adipocytes, HepG2 hepatocytes, C2C12 myoblasts, lean and obese mice models and human samples. We found that obese AT*env* intrigues excess release of extracellular vesicles (EVs) from the (ATMs) to dispense miR-210-3p to the neighboring adipocytes and the skeletal muscle and liver via paracrine and endocrine actions. EVs from Dicer silenced miR-210-3p overexpressed bone-marrow-derived macrophages (BMDMs) when administered in lean mice, it was found to potentiate glucose intolerance and IR in these mice. Mechanistically, miR-210-3p interacts with multiple insulin signaling pathway molecules, including GLUT4, and silences its expression, efficiently hindering the insulin signaling pathway. Therapeutic intervention by miR-210-3p inhibitor LNA rescue high-fat diet (HFD)-fed mice from obesity-induced IR and glucose intolerance by upregulating insulin signaling molecules in adipose tissue, skeletal muscle, and liver. Thus, obese ATM-specific miR-210-3p can be a promising therapeutic target for managing obesity-induced IR and T2D. This study claims Anti-miR-210 therapy can also bring back glycaemic homeostatic status in obese T2D mice.

Chapter 5, unravels the *molecular mechanism of adipocyte senescence under obese ATenv and its' regulation by obesity-induced adipokine* using clinical samples, diet-induced mice model, and 3T3-L1 murine adipocytes. Fetuin-A, a biomarker for obesity T2D, is released from liver tissue (hepatokine) or adipose tissue (adipokine), contributing to inflammation and insulin resistance in the onset of obesity (Chatterjee et al., 2013; Gerst et al., 2021; Pal et al., 2012). Here, we found that fetuin-A functioned as a nuclear protein in the adipocytes under obese AT*env*. The migration of fetuin-A from cytosol to the

nucleus is facilitated by HIF-1α, by directly interacting with fetuin-A under pathophysiological conditions that trigger adipocyte senescence, a significant contributor to white adipose tissue (WAT) dysfunction. Further fetuin-A inhibition significantly rescues them from senescence under obese. This study uncovers novel action of fetuin-A in the development of adipocyte-senescence in obesity and discovers fetuin-A as potential therapeutic candidate for managing obesity-induced AT senescence.

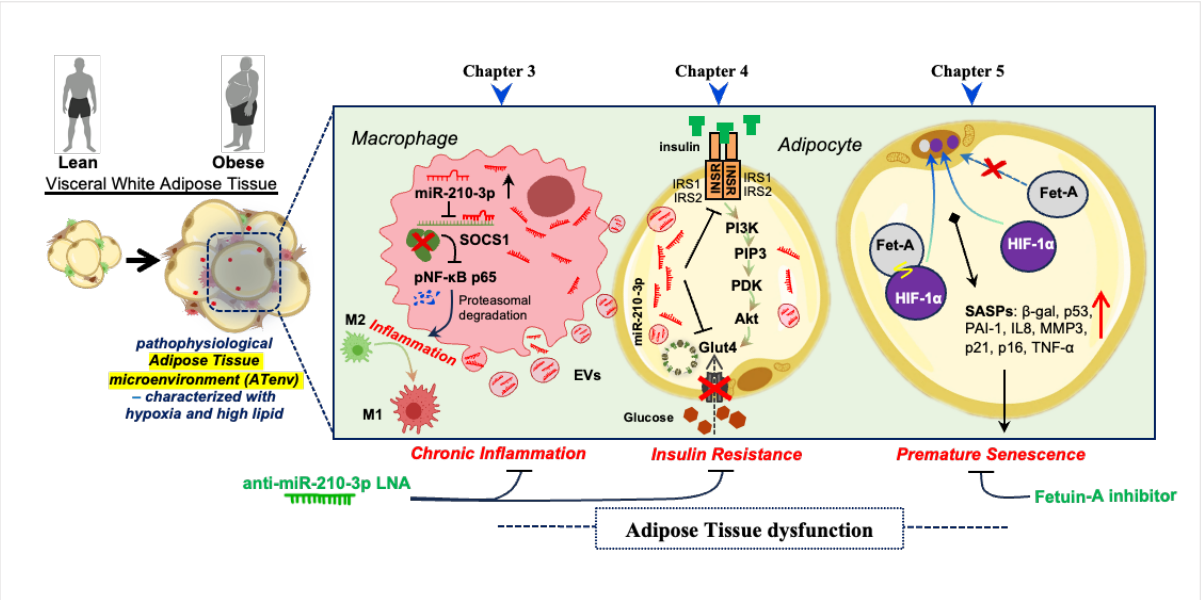

Figure 1.2| **Pictorial overview of thesis outline**

The research work done in the thesis is divided into three main chapters: 3-5. **Chapter 3** explains the role of AT*env*-induced miR-210-3p in ATM skewing under obese conditions that potentiate chronic AT inflammation. **Chapter 4** emphasizes the function of ATMs-derived miR-210-3p to aggravate systemic insulin resistance in the obese AT*env*. **Chapter 5**, explores the novel function of nuclear fetuin-A on adipocyte senescence, which exacerbates at obese AT*env*. Altogether, results obtained from these studies decipher the involvement of obese adipose tissue microenvironment in visceral white adipose tissue dysfunction.

References

Arner, E., Mejhert, N., Kulyté, A., Balwierz, P. J., Pachkov, M., Cormont, M., Lorente-Cebrián, S., Ehrlund, A., Laurencikiene, J., Hedén, P., Dahlman-Wright, K., Tanti, J.-F., Hayashizaki, Y., Rydén, M., Dahlman, I., van Nimwegen, E., Daub, C. O., & Arner, P. (2012). Adipose Tissue MicroRNAs as Regulators of CCL2 Production in Human Obesity. *Diabetes*, *61*(8), 1986–1993. https://doi.org/10.2337/db11-1508

Avenue, 677 Huntington, Boston, & Ma 02115. (2012, October 21). *Globalization*. Obesity Prevention Source. https://www.hsph.harvard.edu/obesity-prevention-source/obesity-causes/globalization-and-obesity/

Bhurosy, T., & Jeewon, R. (2014). Overweight and Obesity Epidemic in Developing Countries: A Problem with Diet, Physical Activity, or Socioeconomic Status? *The Scientific World Journal*, *2014*, e964236. https://doi.org/10.1155/2014/964236

Boutens, L., & Stienstra, R. (2016). Adipose tissue macrophages: Going off track during obesity. *Diabetologia*, *59*, 879–894. https://doi.org/10.1007/s00125-016-3904-9

Chatterjee, P., Seal, S., Mukherjee, S., Kundu, R., Mukherjee, S., Ray, S., Mukhopadhyay, S., Majumdar, S. S., & Bhattacharya, S. (2013). Adipocyte fetuin-A contributes to macrophage migration into adipose tissue and polarization of macrophages. *The Journal of Biological Chemistry*, *288*(39), 28324–28330. https://doi.org/10.1074/jbc.C113.495473

Gerst, F., Kemter, E., Lorza-Gil, E., Kaiser, G., Fritz, A.-K., Nano, R., Piemonti, L., Gauder, M., Dahl, A., Nadalin, S., Königsrainer, A., Fend, F., Birkenfeld, A. L., Wagner, R., Heni, M., Stefan, N., Wolf, E., Häring, H.-U., & Ullrich, S. (2021). The hepatokine fetuin-A disrupts functional maturation of pancreatic beta cells. *Diabetologia*, *64*(6), 1358–1374. https://doi.org/10.1007/s00125-021-05435-1

Goossens, G. H., Bizzarri, A., Venteclef, N., Essers, Y., Cleutjens, J. P., Konings, E., Jocken, J. W. E., Čajlaković, M., Ribitsch, V., Clément, K., & Blaak, E. E. (2011). Increased Adipose Tissue Oxygen Tension in Obese Compared With Lean Men Is Accompanied by Insulin Resistance, Impaired Adipose Tissue Capillarization, and Inflammation. *Circulation*, *124*(1), 67–76. https://doi.org/10.1161/CIRCULATIONAHA.111.027813

Gustafson, B., Nerstedt, A., Spinelli, R., Beguinot, F., & Smith, U. (2022). Type 2 Diabetes, Independent of Obesity and Age, Is Characterized by Senescent and Dysfunctional Mature Human Adipose Cells. *Diabetes*, *71*(11), 2372–2383. https://doi.org/10.2337/db22-0003

Health Effects of Overweight and Obesity in 195 Countries over 25 Years. (2017). *New England Journal of Medicine*, *377*(1), 13–27. https://doi.org/10.1056/NEJMoa1614362

Heyn, G. S., Corrêa, L. H., & Magalhães, K. G. (2020). The Impact of Adipose Tissue–Derived miRNAs in Metabolic Syndrome, Obesity, and Cancer. *Frontiers in Endocrinology*, *11*. https://www.frontiersin.org/articles/10.3389/fendo.2020.563816

Home, Resources, diabetes, L. with, Acknowledgement, FAQs, Contact, & Policy, P. (n.d.). *Citation usage | IDF Diabetes Atlas*. Retrieved May 17, 2023, from https://diabetesatlas.org/citation-usage/

Jin, X., Qiu, T., Li, L., Yu, R., Chen, X., Li, C., Proud, C. G., & Jiang, T. (2023). Pathophysiology of obesity and its associated diseases. *Acta Pharmaceutica Sinica B*, *13*(6), 2403–2424. https://doi.org/10.1016/j.apsb.2023.01.012

Kahn, B. B., & Flier, J. S. (2000). Obesity and insulin resistance. *The Journal of Clinical Investigation*, *106*(4), 473–481. https://doi.org/10.1172/JCI10842

Khan, M. A. B., Hashim, M. J., King, J. K., Govender, R. D., Mustafa, H., & Kaabi, J. A. (2019). Epidemiology of Type 2 Diabetes – Global Burden of Disease and Forecasted Trends. *Journal of Epidemiology and Global Health*, *10*(1), 107–111. https://doi.org/10.2991/jegh.k.191028.001

Kiran, S., Kumar, V., Kumar, S., Price, R. L., & Singh, U. P. (2021). Adipocyte, Immune Cells, and miRNA Crosstalk: A Novel Regulator of Metabolic Dysfunction and Obesity. *Cells*, *10*(5), Article 5. https://doi.org/10.3390/cells10051004

Kurylowicz, A. (2021). microRNAs in Human Adipose Tissue Physiology and Dysfunction. *Cells*, *10*(12), 3342. https://doi.org/10.3390/cells10123342

Lee, J. W., Ko, J., Ju, C., & Eltzschig, H. K. (2019). Hypoxia signaling in human diseases and therapeutic targets. *Experimental & Molecular Medicine*, *51*(6), Article 6. https://doi.org/10.1038/s12276-019-0235-1

Lempesis, I. G., van Meijel, R. L. J., Manolopoulos, K. N., & Goossens, G. H. (2020). Oxygenation of adipose tissue: A human perspective. *Acta Physiologica*, *228*(1), e13298. https://doi.org/10.1111/apha.13298

Manna, P., & Jain, S. K. (2015). Obesity, Oxidative Stress, Adipose Tissue Dysfunction, and the Associated Health Risks: Causes and Therapeutic Strategies. *Metabolic Syndrome and Related Disorders*, *13*(10), 423–444. https://doi.org/10.1089/met.2015.0095

Oger, F., Gheeraert, C., Mogilenko, D., Benomar, Y., Molendi-Coste, O., Bouchaert, E., Caron, S., Dombrowicz, D., Pattou, F., Duez, H., Eeckhoute, J., Staels, B., & Lefebvre, P. (2014). Cell-Specific Dysregulation of MicroRNA Expression in Obese White Adipose Tissue. *The Journal of Clinical Endocrinology & Metabolism*, *99*(8), 2821–2833. https://doi.org/10.1210/jc.2013-4259

Ormazabal, V., Nair, S., Elfeky, O., Aguayo, C., Salomon, C., & Zuñiga, F. A. (2018). Association between insulin resistance and the development of cardiovascular disease. *Cardiovascular Diabetology*, *17*(1), 122. https://doi.org/10.1186/s12933-018-0762-4

Pal, D., Dasgupta, S., Kundu, R., Maitra, S., Das, G., Mukhopadhyay, S., Ray, S., Majumdar, S. S., & Bhattacharya, S. (2012). Fetuin-A acts as an endogenous ligand of TLR4 to promote lipid-induced insulin resistance. *Nature Medicine*, *18*(8), Article 8. https://doi.org/10.1038/nm.2851

Pasarica, M., Sereda, O. R., Redman, L. M., Albarado, D. C., Hymel, D. T., Roan, L. E., Rood, J. C., Burk, D. H., & Smith, S. R. (2009). Reduced Adipose Tissue Oxygenation in Human Obesity: Evidence for Rarefaction, Macrophage Chemotaxis, and Inflammation Without an Angiogenic Response. *Diabetes*, *58*(3), 718–725. https://doi.org/10.2337/db08-1098

Popkin, B. M., & Slining, M. M. (2013). New dynamics in global obesity facing low- and middle-income countries. *Obesity Reviews*, *14*(S2), 11–20. https://doi.org/10.1111/obr.12102

Pradeepa, R., & Mohan, V. (2021). Epidemiology of type 2 diabetes in India. *Indian Journal of Ophthalmology*, *69*(11), 2932. https://doi.org/10.4103/ijo.IJO_1627_21

Reyes-Farias, M., Fos-Domenech, J., Serra, D., Herrero, L., & Sánchez-Infantes, D. (2021). White adipose tissue dysfunction in obesity and aging. *Biochemical Pharmacology*, *192*, 114723. https://doi.org/10.1016/j.bcp.2021.114723

Rosen, E. D., & Spiegelman, B. M. (2006). Adipocytes as regulators of energy balance and glucose homeostasis. *Nature*, *444*(7121), 847–853. https://doi.org/10.1038/nature05483

Smith, U., Li, Q., Rydén, M., & Spalding, K. L. (2021). Cellular senescence and its role in white adipose tissue. *International Journal of Obesity*, *45*(5), Article 5. https://doi.org/10.1038/s41366-021-00757-x

Snodgrass, R. G., Boß, M., Zezina, E., Weigert, A., Dehne, N., Fleming, I., Brüne, B., & Namgaladze, D. (2016). Hypoxia Potentiates Palmitate-induced Pro-inflammatory Activation of Primary Human Macrophages*. *Journal of Biological Chemistry*, *291*(1), 413–424. https://doi.org/10.1074/jbc.M115.686709

Tchkonia, T., Morbeck, D. E., Von Zglinicki, T., Van Deursen, J., Lustgarten, J., Scrable, H., Khosla, S., Jensen, M. D., & Kirkland, J. L. (2010). Fat tissue, aging, and cellular senescence. *Aging Cell*, *9*(5), 667–684. https://doi.org/10.1111/j.1474-9726.2010.00608.x

Wang, B., Wood, I. S., & Trayhurn, P. (2007). Dysregulation of the expression and secretion of inflammation-related adipokines by hypoxia in human adipocytes. *Pflügers Archiv - European Journal of Physiology*, *455*(3), 479–492. https://doi.org/10.1007/s00424-007-0301-8

Ye, J., Gao, Z., Yin, J., & He, Q. (2007). Hypoxia is a potential risk factor for chronic inflammation and adiponectin reduction in adipose tissue of ob/ob and dietary obese mice. *American Journal of Physiology-Endocrinology and Metabolism*, *293*(4), E1118–E1128. https://doi.org/10.1152/ajpendo.00435.2007

Obesity has now emerged as a global epidemic, posing a significant risk for several debilitating, and deadly diseases such as type 2 diabetes (T2D), cardiovascular diseases (CVD), immune disorders, nonalcoholic fatty liver disease (NAFLD), and various types of cancers. In addition, obesity also leads to a reduced quality of life, a shorter lifespan, and increased healthcare expenses. Given its complex pathophysiological nature, it is clear that obesity cannot be solely attributed to energy imbalance between calorie intake and expenditure. Consequently, a range of metabolic abnormalities, oxidative stress, mitochondrial dysfunction, immune system dysregulation, and persistent low-grade inflammation have been observed in individuals with excess weight. In obesity, expanded adipose tissue depots and altered glucose and lipid metabolism lead to systemic metabolic imbalance. Adipose tissue plays an active role in maintaining overall metabolic balance through a complex communication involving various tissues such as the liver, skeletal muscle, pancreatic endocrine cells, with the brain. Adipose tissue (AT) responds to overnutrition by initiating an immune response and triggering the inflammatory response (Jung & Choi, 2014; X. Lin & Li, 2021; Poirier et al., 2006).

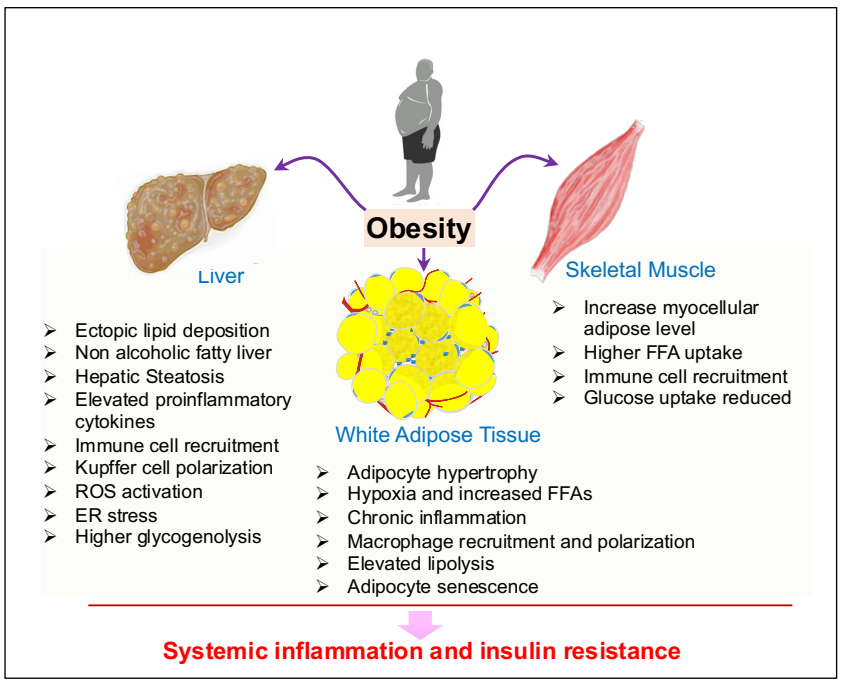

Figure 2.1| **Obesity mediated pathophysiological alteration in liver, adipose tissue, and skeletal muscle causing systemic inflammation and insulin resistance.**

2.1 Overview of Adipose tissue

What sets adipose tissue apart from most other tissues is its remarkable ability to undergo changes in size and cellular composition in response to both physiological and pathological conditions. These adaptations to environmental and physiological challenges encompass not only alterations in the size,

number, and function of adipocytes but also enduring quantitative and qualitative shifts in the tissue's cellular composition. Adipose tissue undergoes expansion through hyperplasia, involving an increase in adipocyte number, and hypertrophy, characterized by an increase in adipocyte size. Both hyperplasia and hypertrophy serve as potential mechanisms for the expansion of adipose tissue to accommodate surplus energy intake during obesity. Hyperplastic growth is observed primarily during the early stages of adipose tissue development, whereas hypertrophy takes precedence to address the need for increased fat storage capacity as obesity progresses; which underscores the dynamic and complex nature of adipose tissue growth in response to genetic and dietary factors. Adipose tissue, comprises various types, including white, brown, and beige adipose tissue, each with distinct functions. White adipose tissue primarily stores energy as triglycerides, secretes adipokines regulating metabolism and offers thermal insulation. Brown adipose tissue specializes in thermogenesis and energy expenditure through uncoupled mitochondrial respiration. Beige adipose tissue contributes to thermogenesis and metabolic flexibility. Subcutaneous White adipose tissue (sWAT) is situated beneath the skin and serves as both a mechanical cushion and thermal insulator. It also stores excess energy as triglycerides. In contrast, vWAT is located within the abdominal cavity, surrounding vital organs. vWAT is metabolically active, secreting pro-inflammatory substances that can lead to insulin resistance and metabolic dysfunction when present in excess. vWAT significant depots specifically the intra-abdominal organs (mesenteric, omental, perigonadal, perirenal, and retroperitoneal) and surrounding the heart (pericardial) in both humans and rodents. It is noteworthy that there is a difference between human and rodent vWAT, where humans possess detectable omental WAT (oWAT), while rodents exhibit large perigonadal WAT (gWAT). This demarcation highlights the variability in adipose tissue distribution between the two species.

Additionally, intrahepatic fat within the liver and intramuscular fat within skeletal muscles can impact organ function and muscle health, respectively, with implications for metabolic health. Notably, brown adipose tissue (BAT) is concentrated in specific regions like the supraclavicular area and specializes in thermogenesis and mitochondria enriched, contributing to the regulation of body temperature. Beige adipose tissue, on the other hand, can be induced within white adipose tissue depots and shares some characteristics with BAT, potentially providing metabolic benefits. Dysfunctions in adipose tissue are linked to metabolic disorders, emphasizing its critical role in health and disease. In the context of obesity, vWAT is the most critical subset due to its metabolic activity, hormone secretion, role in inflammation, strong association with health risks, responsiveness to weight loss, and relevance in surgical interventions. It plays a central role in regulating energy balance and is linked to various obesity-related health complications, making it a key focus in obesity research and management.

2.2 Visceral white adipose tissue (vWAT) composition

This tissue consists of several key elements, including mature adipocytes, fibroblast-like cellular populations that encompass adipocyte precursors, the vascular network, and various immune cells. These components not only coexist within the adipose tissue but also engage in intricate spatial and functional interactions. The term "stromal vascular fraction" (SVF) is employed to describe the non-adipocyte components within adipose tissue, which encompass highly diverse populations of immune cells, mesenchymal stromal cells, endothelial cells, and smaller groups of various cell types, including neurons. Within this environment, the vasculature plays a vital role by traversing the adipose tissue and supplying essential oxygen and nutrients to the resident tissue cells. Adipocyte progenitors predominantly inhabit the perivascular region, exhibiting their potential for adipogenesis. Concurrently, fibroblast-like cells contribute to the formation of connective tissue and can exhibit pro-fibrotic and pro-inflammatory characteristics. Furthermore, the adipose tissue hosts a diverse array of immune cells. Among the innate immune cells found in adipose tissue are macrophages, neutrophils, eosinophils, dendritic cells (DCs), mast cells, innate lymphoid cells (ILCs), and natural killer (NK) cells, while adaptive immune cells such as T and B lymphocytes are also present. In a healthy, lean state, these components work in harmony to maintain the tissue homeostasis (Choe et al., 2016; Jiang et al., 2014; Mohd. P. Khan et al., 2015; S. Khan et al., 2020). However, when subjected to overnutrition, metabolic stress disrupts this delicate balance, resulting in an enlarged, inflamed, hypoxic, and fibrotic adipose tissue.

The emergence of single-cell transcriptomics has rapidly transformed our understanding of the wide array of cell types and states residing within adipose tissue, providing fresh insights into how these distinct cell populations influence the tissue's overall function.

2.2.1 Pre – and mature adipocytes

The significance of adipocytes in regulating overall body physiology and the distinct metabolic functions of various adipose depots have prompted inquiries into how the functions of adipocytes are controlled within the tissue microenvironment. It is widely believed that the number of adipocytes in the body is largely established by early adulthood, with a relatively stable turnover rate estimated at approximately 8% per year in humans and approximately 18% per month in mice. Nevertheless, WAT exhibits remarkable plasticity and can undergo significant remodeling in response to metabolic, nutritional, and pharmacological stimuli

Investigation exhibits the presence of at least two distinct subclusters of adipocyte progenitors. One subcluster, often referred to by various names, including fibro-adipogenic progenitors, adipocyte progenitor cells, and mesenchymal stromal cells exhibits robust adipogenic potential, expresses key

adipocyte markers and shares common mesenchymal markers like PDGFRA and PDGFRB. These progenitors demonstrate high commitment to adipogenesis, expressing *adipoq* and *lep*, and often residing close to the adipose vasculature. In contrast, the second major cluster of mesenchymal stromal cells, often referred to as fibro-inflammatory precursors, interstitial progenitor cells, and collagen-rich progenitors, among others, lacks PPARγ expression. Instead, these cells are enriched in gene signatures associated with ECM remodeling and inflammation. They likely play roles in regulating inflammation, collagen deposition, and adipogenesis. This subcluster shares similarities with interstitial skeletal muscle fibro/adipogenic progenitors and can be identified as $DPP4^{+}$, primarily found within the interstitial regions of the adipose tissue depots. Importantly, human subcutaneous adipose tissue also contains DPP4+ and DPP4- populations closely resembling their murine counterparts, suggesting the existence of similar progenitor subpopulations in adult humans that can be distinguished based on DPP4 expression. This intriguing parallel between murine and human adipose tissue highlights the potential relevance of these findings in understanding adipose tissue biology across species. Both of these cells demonstrate a robust ability to differentiate into adipocytes both in vitro and upon transplantation into mice (Burl et al., 2018; Hepler et al., 2018; Hepler & Gupta, 2017; Nahmgoong et al., 2022; Q. A. Wang et al., 2013). Cell trajectory analysis suggests a hierarchical developmental relationship between preadipocytes and fibro/adipogenic progenitors. Lineage-tracing studies indicate that FAPs expressing DPP4 in eWAT can undergo de novo adipocyte differentiation at a low frequency, particularly in response to a high-fat diet (HFD) (Maniyadath et al., 2023). To comprehensively grasp the developmental relationship between FAPs and preadipocytes in each adipose tissue depot and to delineate the relative contributions of these subpopulations to the maintenance and expansion of the adipocyte pool in vivo, further investigations are warranted.

It has been observed in both humans and mice that individual WAT depots contain multiple subpopulations of adipocytes, each characterized by the expression of specific markers in addition to standard adipocyte identity markers like Adiponectin and Perilipin1. In a study employing single-nucleus RNA sequencing (snRNA-seq) of mice's epididymal WAT, three distinct subpopulations of mature white adipocytes were identified. These subpopulations were categorized as follows: lipogenic adipocytes, characterized by the expression of genes related to de novo fatty acid synthesis; lipid-scavenging adipocytes, which expressed genes associated with lipid uptake and transport; and stressed lipid-scavenging adipocytes, which also expressed genes related to hypoxia and autophagy, indicating a potential connection between the adipocyte size and insulin sensitivity, as stressed lipid-scavenging adipocytes were the largest adipocytes, while lipogenic adipocytes were the smallest. Nevertheless, it is probable that adipocytes can transition between different states in response to external and internal signals (Bäckdahl et al., 2021; Emont et al., 2022; Sárvári et al., 2021). The reduction in lipogenic adipocytes in response to HFD-induced obesity may explain the previously reported decrease in de

novo lipogenesis and insulin sensitivity in obese individuals. In the context of obesity, the abundance of the other subpopulations increased.

Spatial transcriptomics of human WAT revealed three distinct subpopulations of mature white adipocytes with unique transcriptomic signatures and spatial organization. One of these subpopulations, PERILPIN^{high}, displayed a transcriptomic profile similar to lipogenic adipocytes and was associated with higher in vivo insulin sensitivity. Another subpopulation was found to be enriched for genes involved in lipid uptake and handling, resembling lipid-scavenging adipocytes in mice. The LEPTIN^{high} subpopulation and stressed lipid-scavenging adipocytes appeared to share common enriched pathways related to leptin synthesis and ECM remodeling. Similar to findings in mice, the relative abundance of PERILPIN^{high} adipocytes decreased in obese individuals (Maniyadath et al., 2023).

In summary, various studies have consistently demonstrated the presence of multiple subpopulations of white adipocytes with varying degrees of lipogenic and lipid uptake characteristics in both mice and humans. Future research should focus on understanding the developmental and transitional trajectories of these subpopulations, exploring whether specific adipogenic progenitors give rise to distinct adipocyte subpopulations, and unravelling the influence of the tissue microenvironment on adipocyte cell states. Additionally, investigating the roles of different adipocyte subpopulations in shaping the short-term and long-term plasticity of WAT is crucial.

2.2.2 Macrophages

Macrophages have garnered significant attention due to their pivotal role in the functioning of adipose tissue. In lean mice and humans, macrophages typically account for approximately 5% of the cellular composition within adipose tissue. However, in cases of obesity, their prevalence dramatically escalates, making up as much as 50% of all adipose tissue cells. Furthermore, during obesity, adipose tissue macrophages (ATMs) not only increase in number but also undergo significant changes in their distribution and inflammatory characteristics. Unlike their distribution in the lean state, where ATMs are evenly dispersed throughout adipose tissue and exhibit limited inflammatory properties, in obese adipose tissue, they cluster around deceased adipocytes, forming structures known as crown-like structures (CLSs). Importantly, ATMs in obese adipose tissue exhibit pronounced proinflammatory features. The presence of macrophages within CLSs in obese adipose tissue has been directly associated with the development of insulin resistance (Boutens & Stienstra, 2016).

Initially, there was a prevailing belief that in the presence of obesity, ATMs would shift towards a proinflammatory M1 macrophage phenotype. However, a more thorough examination of immune cell populations within adipose tissue, proposed that obesity predominantly steers ATMs towards functions related to lipid uptake, storage, and breakdown. Recent strides in single-cell technologies collective

showed some ATMs subpopulations exhibit heightened proinflammatory traits, while others are more metabolically active. Lin^+ cells in both mouse and human obese conditions revealed that obesity induces a unique ATM subpopulation marked by the presence of Cd9 and Trem2 markers. This specific subpopulation expresses elevated levels of genes associated with lipid handling, such as Cd36, Lpl, and Lipa. It is now commonly referred to as lipid-associated macrophages (LAMs). LAMs are notably enriched in CLSs within adipose tissue, where they appear to play a significant role in tissue remodeling. Intriguingly, certain studies have identified a smaller subset of LAMs expressing genes linked to proliferation, hence named proliferative LAMs, suggesting that the LAM pool can expand not only through increased recruitment and activation of monocytes but also through local proliferation. In addition to LAMs, there are subpopulations of inflammatory macrophages (IMs) that exhibit heightened expression of inflammatory genes, and these have been positively associated with obesity (Hildreth et al., 2021; Jaitin et al., 2019; C. Li et al., 2019; Massier et al., 2023; Vijay et al., 2020).Single-cell studies have revealed a significant reduction in lipid-associated macrophages populations during the regression of obesity. However, even after achieving complete normalization of body and tissue weight, the abundance of LAMs in the tissue remained higher than in lean controls. Interestingly, the group that experienced weight regain exhibited a rapid increase in LAMs, surpassing the obese cohort, suggesting that these cells may retain an obesity memory. Despite variations across different fat depots and species concerning obesity-associated ATMs, there exists a relatively consistent pattern of metabolic and inflammatory programming across WAT depots and species. Although some variations in the relative abundance of myeloid and lymphoid cell populations have been noted, the transcriptomic profiles of individual macrophage populations remain largely analogous. Nevertheless, it is important to mention that a recent study did not seem to identify the lipid-handling gene program in their $Trem2^+$ LAMs (Emont et al., 2022; Maniyadath et al., 2023).Numerous investigations across diverse adipose tissue depots and species have unveiled distinct macrophage subpopulations characterized by the expression of genes associated with vascular development and extracellular matrix remodeling and maintenance. Collectively, these findings suggest that these specialized macrophages, referred to as perivascular macrophages (PVMs), identified by the presence of the Lyve1 marker, represent a prominent constituent among tissue-resident macrophages (TRMs) in lean WAT (Corvera, 2021; Silva et al., 2019).

Macrophage type	Stimulus	Function	Secretory markers	Surface markers
M1	LPS, IFN-γ, FFAs, TNF-α	Pro-inflammatory, Works against infection, Autoimmune disease progression	iNOS, IL-1β , IL-6/-12/-23, TNF-α, CXCL-9/10/11	CD80, CD86, HLA-DR, CD11c , TLR4
M2a	IL-4, IL-13	Enhance endocytosis, parasite elimination, and induce tissue repair	IL-10, TGF-β, CCL17/18/22	CD206, IL-1R

M2b	LPS+IL-1β	Immune regulation	TNF-α, IL-1, IL-6	CD86, MHC-II
M2c	IL-10, TGFβ, Glucocorticoids	Apoptotic cells clearance, Matrix remodelling	IL-10, TGF-β, CCL-16/-18	CD206, CD163
M2d	IL-6, Adenosine	Promotes angiogenesis	IL-10, VEGF,IL-12, TGF-β	
ATM population	**Polarization**	**function**	**Markers**	**Onset of obesity**
LAM	M1 type	Lipid handling, Chemokine signalling, proinflammatory pathways, lysosomal pathways	Trem2, Cd9, Lpl, Lamp2	Increased
P-LAM	M1 type	local proliferation of LAMs in VAT depots to maintain ATMs abundance	Pola1, Kif11, Kif15	Increased
PVM	M2 type	Perivascular-like tissue resident macrophages regulating EGFR signalling and statin pathways.	Lyve1, Cd163, Klf4, Cbr2, CD206, Cd209f, Stab1, Mrc1, Clec10a	Decreased

Table 2.1 | **Categorizing Macrophages with a special focus on their roles, types and markers expression in White Adipose Tissue.**

However, their relative prevalence appears to diminish in the context of obesity. The underlying cause of this decrease remains a subject of investigation, with potential factors including a possible transformation of PVMs into inflammatory macrophages (IMs), as suggested by RNA velocity analyses, or the notable expansion of LAM and IM populations. Intriguingly, a reduction in PVMs' abundance in epididymal white adipose tissue has been observed in response to acute fasting. Furthermore, it is noteworthy that PVMs concurrently express markers indicative of M2-like macrophages, such as Mrc1, Clec10a, and CD163, in addition to genes implicated in vascular and extracellular matrix functions (Maniyadath et al., 2023; Massier et al., 2023).

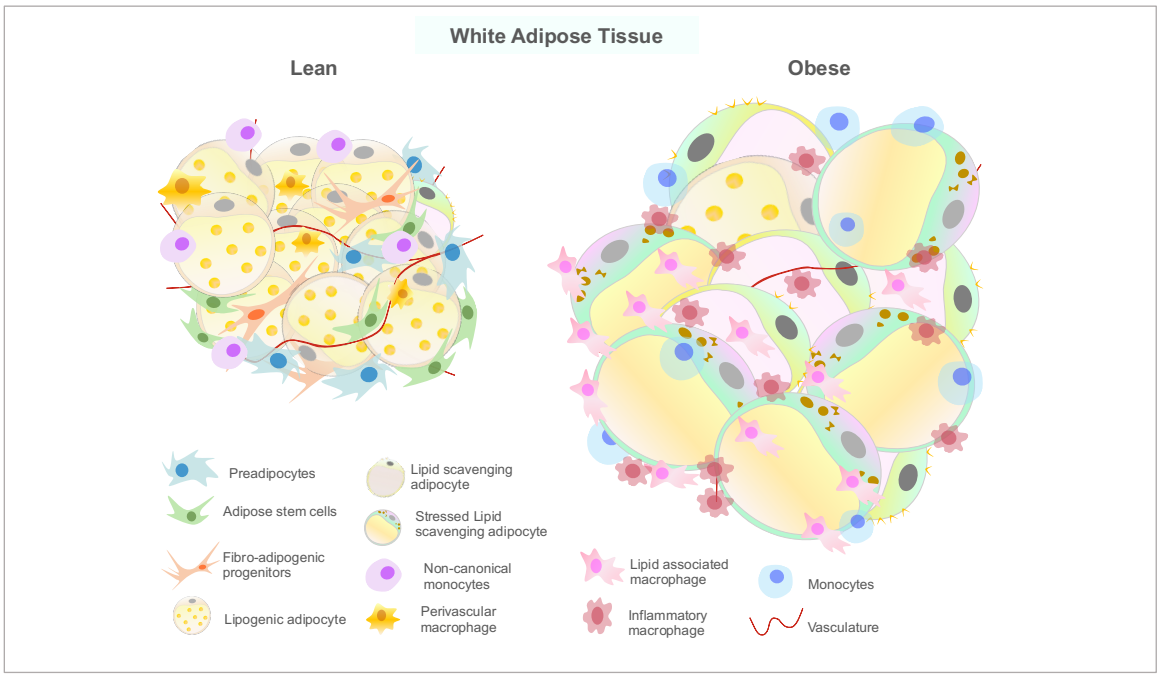

Figure 2.2 | **Cellular heterogeneity in white adipose tissue**

The cellular architecture within the white adipose tissue of both humans and mice is intricate, and this landscape undergoes significant changes in response to obesity. Among the adipogenic progenitor subpopulations, including Adipose stem cells, Fibro-adipogenic progenitors, and Preadipocytes, there is a notable reduction in the obese adipose tissue, leading to a substantial impairment of de novo adipogenesis. Furthermore, obesity also has a profound impact on the non-adipose cellular landscape. It is associated with a positive correlation with inflammatory macrophages, lipid-associated macrophages, and monocyte subpopulations, while concurrently resulting in a marked reduction in perivascular macrophages and non-canonical monocyte populations.

2.2.3 Dendritic cells

Dendritic cells (DCs) are pivotal in shaping adaptive immunity through their adeptness in antigen presentation (Soto et al., 2020). They share several surface markers with macrophages, including F4/80, CD11b, MHCII, C-X3-C motif chemokine receptor 1, and CD11c, though notably, they lack CD64 expression, setting them apart from macrophages. Adipose tissue DCs can be classified into two subtypes: CD11b−CD11c+ DCs and CD11b−CD11c+B220+ DCs (Soedono & Cho, 2021). Initially, studies suggested an increase in DC numbers within adipose tissue during obesity. However, subsequent research has shown that when adjusted for adipose tissue mass, DC numbers remain relatively constant in obesity (Cho et al., 2016). DCs detect antigens migrating from adipose tissue to the draining lymph nodes, thus orchestrating immune responses within the adipose tissue. Depleting CD11c-expressing cells, which include DCs, has been observed to protect against chronic inflammation and insulin resistance in diet-induced obesity in mice. It's essential to note that these effects may be attributed to the loss of CD11c+ inflammatory macrophages (Stefanovic-Racic et al., 2012). CCR7-deficient mice, characterized by reduced DC numbers in adipose tissue, exhibit reduced adipose tissue inflammation and insulin resistance (Patsouris et al., 2008). Chemerin, an adipokine upregulated in the circulation of obese individuals contributes DCs accumulation WAT causing IR (Ernst & Sinal, 2010). Moreover, under steady-state conditions, DCs in vWAT play a protective role by delaying the onset of obesity and adipose tissue inflammation. Specifically, the activation of the Wnt/β-catenin pathway and triggers IL-10 production. Additionally, activation of the PPARγ pathway suppresses their proinflammatory activation. Together, these effects postpone the initiation of inflammation and insulin resistance in mice subjected to a high-fat, high-sugar diet (Macdougall et al., 2018).

In both mouse and human WAT, two primary subpopulations of conventional dendritic cells was found. However, in humans, a more intricate classification of cDC2 subgroups has been proposed, based on distinct gene expression profiles. On the other hand, in mouse adipose tissue dendritic cells subcluster categorization relies on their activation state, particularly the expression of CCR7, and the presence of proliferation markers. Notably, lean mouse white adipose tissue is notably abundant in monocyte-derived dendritic cells (moDCs)(Maniyadath et al., 2023).

2.2.4 Lymphocytes

A pivotal aspect of lymphoid cell heterogeneity in adipose tissue is the presence of distinct subsets of lymphocytes. Among these subsets, T cells, B cells, and innate lymphoid cells (ILCs) have emerged as key players. Notably, T cells, including both CD4+ and CD8+ subsets, have garnered significant attention for their differential roles in adipose tissue inflammation and insulin resistance (Sonnenberg & Hepworth, 2019). CD4+ T helper cells can differentiate into various subsets, including Th1, Th2, Th17, and regulatory T cells (Tregs), each exerting specific effects on adipose tissue physiology. Th1 and Th17 cells have been implicated in promoting adipose tissue inflammation through the secretion of proinflammatory cytokines such as IFN-γ and IL-17, while Tregs have been associated with an anti-inflammatory, metabolic homeostatic role through IL-10 production (Croce et al., 2021; Q. Wang et al., 2021; S. Zhang et al., 2021). Evidence supporting the heterogeneity of lymphoid cells in adipose tissue is bolstered by comprehensive profiling techniques have revealed a vast diversity of lymphocyte subpopulations that occupy this tissue. Furthermore, lineage-tracing experiments have uncovered the existence of tissue-resident memory T cells within adipose tissue, suggesting a dynamic and long-lasting immune surveillance mechanism within this metabolic niche (Han et al., 2017). Another intriguing aspect of lymphoid cell heterogeneity in adipose tissue is the interaction between B cells and adipocytes. B cells have been shown to infiltrate adipose tissue, and their presence is often associated with the formation of tertiary lymphoid structures (TLSs). TLSs in adipose tissue are organized lymphoid aggregates resembling lymphoid organs, and they can serve as niches for immune cell interactions (Sato et al., 2023). B cell-derived antibodies, particularly IgG, have been implicated in modulating adipose tissue inflammation by binding to adipocyte antigens and activating complement cascades, contributing to local immune responses (Frasca & Blomberg, 2017). In addition to adaptive immune cells, innate lymphoid cells (ILCs) have emerged as a critical component of lymphoid cell heterogeneity in adipose tissue (Song et al., 2023). ILCs produce an array of cytokines, such as IFN-γ, IL-5, and IL-22, which can profoundly influence adipose tissue inflammation and metabolism. ILC2s, in particular, have been associated with the promotion of tissue homeostasis by secreting anti-inflammatory cytokines like IL-10 and IL-13 (Cautivo & Molofsky, 2016; Seillet & Jacquelot, 2019). The impact of lymphoid cell heterogeneity in adipose tissue extends beyond mere cellular composition (Ikutani & Nakae, 2022). Functional studies involving the depletion or modulation of specific lymphoid cell subsets in murine models have provided compelling evidence that these immune cells play pivotal roles in regulating adipose tissue inflammation, insulin sensitivity, and lipid metabolism. The comprehension of the diversity and adaptability of the lymphoid immune component residing within adipose tissue remains limited compared to other subsets of adipose tissue immune cells.

2.2.5 Endothelial cells

Endothelial cells within adipose tissues (ATs) exhibit notable heterogeneity, primarily categorized based on their anatomical location into arterial, venous, capillary, and lymphatic connections. Adipose ECs play a pivotal role in maintaining AT's physiological functions by regulating local blood flow and nutrient supply. ECs control permeability and chemokine recruitment during inflammation induced by obesity. ECs engage in paracrine communication with mature adipocytes and adipose stromal cells to uphold adipose tissue homeostasis. Recent advancements in single-cell sequencing of visceral AT from obese subjects have shed light on the diversity of adipose endothelial cells (AdECs). Notably, around 78% of vascular stromal cells in visceral AT were found to be $LYVE1^{+}$. While substantial progress has been made in understanding the types of AdECs in WAT, precise classification of AdECs in other fat depots remains an area where further research is needed to comprehensively decipher their roles and contributions to AT function and metabolism (Liao et al., 2022).

The intricate interplay between immune and non-immune stromal cells in WAT has profound implications for adipose tissue function and metabolic health. An imbalance in this intricate network can lead to chronic low-grade inflammation within adipose tissue, a hallmark of metabolic disorders associated with obesity, such as T2D. Ongoing research aimed at deciphering the roles of these distinct cell subsets within WAT continues to shed light on their contributions to adipose tissue physiology and metabolic health. Understanding the polarization of macrophages from pro-inflammatory to anti-inflammatory states is crucial for mitigating inflammation and improving metabolic health in obese individuals. Furthermore, exploring the roles of adipocyte progenitors and MSCs holds promise for regenerative medicine and novel therapeutic interventions, particularly in conditions characterized by adipose tissue dysfunction. Stromal cell heterogeneity in white adipose tissue encompasses a wide array of both immune and non-immune cell populations, each with its unique functions.

2.3 Obesity induced adipose tissue dysfunction causing inflammation and insulin resistance

Adipose tissue inflammation is a well-documented phenomenon characterized by a compelling connection between increased body fat (adiposity) and heightened inflammatory responses due to excessive caloric intake, substantiated by both animal and human research. Multiple studies utilizing immunocompromised mouse models reveal, the central role of inflammation in the emergence of insulin resistance following prolonged consumption of a Western-type diet that promotes obesity (Kawai et al., 2021). Adipose tissue has two types in humans, White and Brown adipose tissue. White adipose tissue (WAT) functions as the primary reservoir for long-term energy storage and is characterized by the presence of large unilocular white adipocytes. These cells store surplus metabolic energy in the form of triacylglycerides (TAGs) during anabolic conditions and release this stored

energy as free fatty acids (FFAs) to support peripheral tissues during catabolic states (Luo & Liu, 2016). WAT is distributed throughout the bodies of mammals, with major depots broadly categorized as subcutaneous (located beneath the skin) or intra-abdominal (found within the peritoneum, adjacent to internal organs). Additionally, numerous smaller depots can be identified in various locations, including bone marrow, subdermal areas, perivascular regions, epicardial spaces, and peri- and inter-muscular regions. In addition to its energy-storage function, WAT serves various non-metabolic roles, including providing thermal insulation and cushioning for internal organs. The second major type of adipose tissue in mammals is brown adipose tissue (BAT), which plays a critical role in thermogenesis. BAT is found in smaller depots at distinct anatomical sites, including anterior cervical, supraclavicular, interscapular, perirenal, and perivascular locations in both mice and humans. Brown adipocytes are distinguished by their multilocular lipid droplets, high mitochondrial content, and expression of uncoupling protein 1 (UCP1), a proton carrier in the inner mitochondrial membrane. UCP1, in conjunction with other futile energy cycling processes, enables brown adipocytes to dissipate excess energy as heat, serving as a metabolic sink. In adult humans, BAT depots typically constitute only 1%-2% of total adipose tissue. However, in small hibernating mammals or neonates, BAT can comprise up to 5% of the total body mass (Choe et al., 2016; P. Lee et al., 2013). A distinctive hallmark of this inflammatory process within expanding WAT is its persistence and chronic low-grade nature, which has been coined as mediators can influence IR either directly, by impacting insulin signaling, or indirectly, by triggering inflammatory pathways. The association between obesity and T2D has long been acknowledged, with obesity's primary contribution being its ability to exacerbate IR, a fundamental pathophysiological aspect of T2D (B. B. Kahn & Flier, 2000). IR manifests as a metabolic complication wherein the three major insulin-sensitive tissues, namely skeletal muscle, liver, and AT, progressively become less responsive to the actions of insulin. This decreased sensitivity is marked by substantial impairments in glucose uptake, glycogen synthesis, and to a lesser extent, glucose oxidation. To counterbalance IR, β-cells augment their insulin secretion, thereby restoring blood glucose levels to the normal range. However, as insulin sensitivity continues to decline, β-cells can become overworked, eventually leading to persistent hyperglycaemia and the development of the T2D (Zatterale et al., 2020).

Insulin, an anabolic hormone secreted by β-cells, plays a pivotal role not only in regulating carbohydrate metabolism but also in governing protein and lipid anabolism, cellular growth, and proliferation. The synthesis and release of insulin are stimulated by blood glucose concentrations, and its systemic effects stem from its interaction with cell membrane receptors, leading to the autophosphorylation of specific tyrosine residues. Subsequently, the activated insulin receptor recruits intracellular proteins, commonly referred to as IRSs. Downstream of IRS proteins, PI3K assumes a central role in mediating insulin's functions, primarily by activating PKB and protein kinase C cascades, which promote glucose uptake, facilitate glycogen synthesis, and inhibit hepatic gluconeogenesis.

Additionally, insulin signaling elicits mitogenic effects, primarily mediated by the PKB cascade and activation of the Ras/mitogen-activated protein kinase (MAPK) pathway (Ramalingam et al., 2013).

Both animal and human studies have pinpointed WAT as the central hub to relay intrinsic and extrinsic signals for the remodeling of adipose tissue during obesity (Weisberg et al., 2003). These ultimately converge on the activation of the multiple inflammatory signaling pathways such as JNK and NF-κB. The activation of these signaling pathways, in turn, amplifies the production of pro-inflammatory cytokines, endothelial adhesion molecules, and chemotactic mediators, all of which facilitate the infiltration of monocytes into adipose tissue and their differentiation into pro-inflammatory M1 macrophages. These infiltrating macrophages are responsible for generating and releasing numerous inflammatory mediators that contribute to local and systemic pro-inflammatory conditions while impairing insulin signalling. The actions of these cytokines are mediated through the stimulation of IκB kinase β (IKKβ) and JNK1, which are expressed in myeloid and insulin-targeted cells. JNK stands out as one of the most extensively studied signal transducers in obesity-related IR models. Once activated, JNK initiates the transcription of pro-inflammatory genes and hampers the insulin signaling pathway by phosphorylating IRS-1 at inhibitory serine-threonine sites, consequently reducing PI3K/PKB signaling. In the context of obesity, specifically in obese mice (such as ob/ob and diet-induced obesity models), JNK activity in adipose tissue is elevated compared to lean control mice. To investigate the role of Jnk1 in adipocytes, researchers have employed tissue-specific Jnk1-deficient mice, revealing that these mice are shielded from the development of IR when subjected to HFD. It's worth noting that this protective effect is tissue-specific, as Jnk1 deficiency in adipocytes does not affect muscle insulin sensitivity (Khalid et al., 2021; Liu et al., 2017; Yung & Giacca, 2020).

Obesity also triggers the activation of the NF-κB inflammatory pathway. Under normal physiological conditions, NF-κB proteins are sequestered in the cytoplasm of myeloid and insulin-sensitive cells by a family of inhibitors known as inhibitors of κB (IκBs). Activation of the IKK kinase complex induces the proteasomal degradation of IκBα, facilitating the nuclear translocation of NF-κB. This, in turn, leads to increased expression of several NF-κB target genes, including IL-6, TNFα, interferon-γ (IFN-γ), TGF-β, MCP-1, IL-1β, all of which contribute to the progression of IR (Baker et al., 2011; Hinz & Scheidereit, 2014). Notably, IKKβ deficiency in adipocytes completely prevents the expression of IL-6 and TNF-α induced by free fatty acids, while its activation suppresses the expression of anti-inflammatory cytokines like adiponectin and leptin. In the context of obesity, a phenomenon of significant scientific interest emerges as macrophages infiltrate AT, giving rise to the secretion of a myriad of pro-inflammatory cytokines. These potent signaling molecules exert their effects not only locally within the confines of AT, where they interact with adipocytes and resident immune cells such as neutrophils, B cells, and T cells but also extend their reach systemically, affecting the insulin sensitivity of vital metabolic tissues, notably the liver and skeletal muscles. Macrophages and other

sentinel immune cells engage in an intricate choreography of immune responses, detecting a spectrum of PAMPs or DAMPs through an extensive repertoire of pattern-recognition receptors, including TLRs and NLRs. The compelling body of evidence underscores the central role of NLRP3, the most extensively scrutinized member of the NLR family, in the context of obesity-related chronic inflammation and IR, particularly given its activation by DAMPs generated as a consequence of nutrient excess in obesity (Amarante-Mendes et al., 2018; Chait & den Hartigh, 2020; L. Chen et al., 2015; Rheinheimer et al., 2017). NLRP3, while widely expressed across various tissues and cell types, remains an enigma with regard to its precise location within adipose tissue compartments. Nonetheless, a striking revelation emanates from the immunostaining of adipose tissue sections harvested from obese mice, vividly portraying a pronounced co-localization of NLRP3 with the macrophage marker F4/80 within distinct crown-like structures. Once catapulted into action, NLRP3 orchestrates a remarkable interplay, interacting with procaspase-1 through an adaptive protein interface, ultimately culminating in the formation of the NLRP3 inflammasome. This pivotal cascade sets the stage for the processing and activation of caspase-1, the chief architect behind the maturation and secretion of vital inflammatory mediators, notably IL-1β and IL-18, by macrophages. Further substantiating its primacy, genetic studies involving the ablation of NLRP3 have revealed its indispensable role, as NLRP3 deficiency effectively curtails the activation of the inflammasome within adipose tissue, affording protection against diet-induced IR. Intriguingly, interventions such as caloric restriction and exercise, orchestrated to achieve weight loss in individuals grappling with obesity and T2D, have been observed to instigate a reduction in NLPR3 and IL-1β gene expression within abdominal subcutaneous adipose tissue, precipitating tangible enhancements in systemic insulin sensitivity (Cunha et al., 2010; Pavillard et al., 2017; Swanson et al., 2019; Vandanmagsar et al., 2011; Wu et al., 2020).

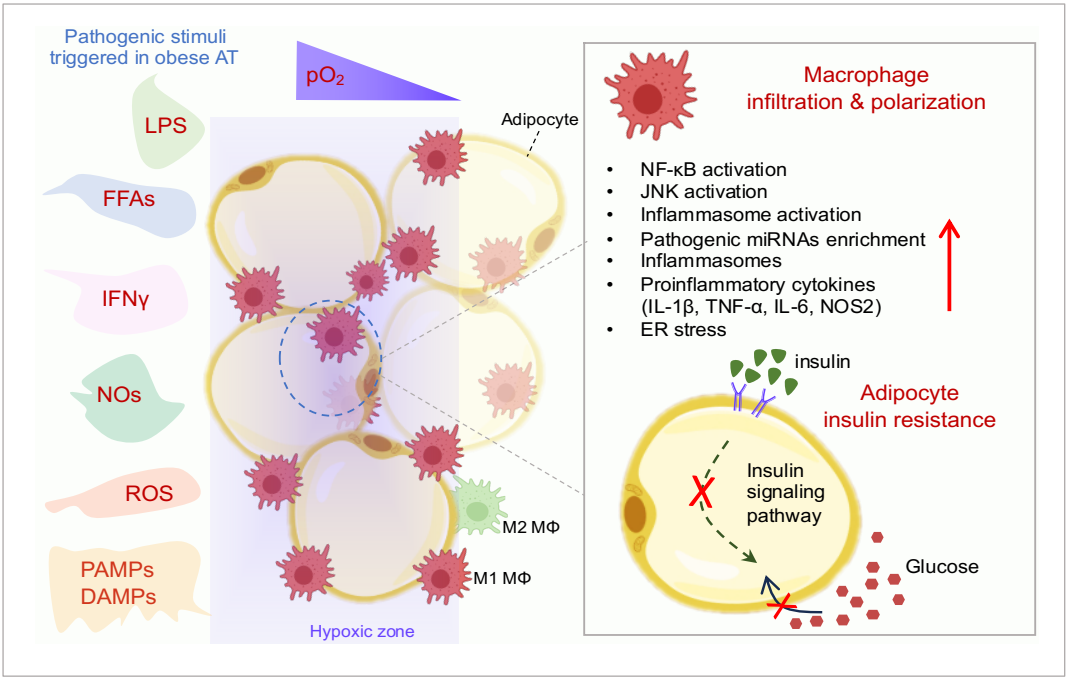

Figure 2.3 | **Obese pathogenic factors potentiate adipose tissue inflammation and insulin resistance.**

Obesity is associated with the triggering of multiple pathogenic stimuli in white adipose tissue (such as hypoxia, FFAs, LPS, Nos, ROS, PAMPs, DAMPs, etc.) that endorses immune cell migration, activating inflammatory signaling pathway, miRNA overexpression, macrophage polarization, inducing ER stress, lipotoxicity and disrupts insulin signaling pathway in adipocytes causing chronic inflammatory landscape followed by adipose tissue insulin resistance.

The role assumed by inflammasome-activated IL-1β assumes paramount importance as a keystone cytokine prominently featured in the repertoire of macrophage-produced signaling molecules. Its augmented production, notably in pancreatic islets and insulin-sensitive tissues, emerges as a pivotal scientific focus, bearing a direct association with T2D. IL-1β exerts a multifaceted impact on adipose tissue insulin sensitivity, wielding its influence by stifling insulin signaling, a phenomenon substantiated by studies showcasing its ability to attenuate insulin-stimulated glucose uptake and lipogenesis in both murine and human adipocytes (Donath & Shoelson, 2011; Eizirik & Mandrup-Poulsen, 2001; Gao et al., 2014; Hotamisligil et al., 1993; Mukherjee et al., 2013).

Obesity-induced adipose tissue hypoxia is a pivotal driver of adipose tissue inflammation and insulin resistance. In obesity, expanding adipocytes and compromised microcirculation lead to localized low oxygen levels. This hypoxic microenvironment triggers the activation of hypoxia-inducible factors (HIFs) and the release of pro-inflammatory cytokines within the adipose tissue. These cytokines, along with immune cell infiltration and dysregulated adipokine secretion, disrupt insulin signaling pathways, impair glucose uptake, and contribute to insulin resistance. Moreover, the systemic consequences of adipose tissue inflammation extend to distant organs, exacerbating metabolic dysfunction. The intricate interplay between adipose tissue hypoxia, inflammation, and insulin resistance underscores the complex pathophysiology of obesity-related metabolic disorders, highlighting the need for targeted therapeutic strategies (J. W. Lee et al., 2019; Lempesis et al., 2020; O'Rourke et al., 2011; Seo et al., 2019; Ye et al., 2007).

2.4 microRNAs regulating adipose tissue dysfunction

In the last decades, miRNAs have received substantial attention as potential players in pathophysiological conditions. These are a type of regulatory non-coding RNAs (ncRNAs), play regulatory roles at epigenetic, transcriptional, and post-transcriptional levels. These regulatory ncRNAs can be categorized based on their average size, with small non-coding RNAs (sncRNAs) comprising transcripts fewer than 200 nucleotides and long non-coding RNAs (lncRNAs) exceeding 200 nucleotides. Among the primary classes of small ncRNAs, microRNAs (miRNAs), small interfering RNAs (siRNAs), and piwi-interacting RNAs (piRNAs) are prominent. Nevertheless, certain ncRNAs

with variable lengths may simultaneously fall into two classifications. Examples include promoter-associated transcripts (PATs), enhancer RNAs (eRNAs), and circular RNAs (circRNAs). This multifaceted classification system highlights the diverse roles and characteristics of regulatory ncRNAs in governing gene expression across various biological processes.

miRNAs are an endogenous class of small noncoding RNA, which is found in tissues, serum, and body fluids with highly stable form. An increasing number of altered miRNA expressions were observed in the pathophysiological state of the diabetes. Detectability of those circulatory miRNAs is quite high in such cases. In obese patients, a list of tissue-specific differentially expressed miRNAs regulates various intracellular communications, critical for insulin signaling pathway, glucose uptake, release of cytokines, and inflammation that leads to insulin resistance. Circulatory miRNAs released from obese adipose tissue also have a strong association with the pathogenic state of diabetes. Obesity-related insulin resistance and T2D alter metabolic organs' physiology such as liver, skeletal muscles, and adipose tissue by facilitating chronic low-grade inflammation, mediated by activation or down-regulation of several microRNAs, directly affecting tissue metabolism (Chowdhury et al., 2013; Odegaard & Chawla, 2012; Thomou et al., 2017).

A list of overwhelming evidence in recent years suggests AT, a dynamic endocrine organ and a crucial immunological organ, is adversely affected during obesity. Overnutrition causes excess lipid accumulation that triggers chronic inflammation in AT which leads to insulin resistance. Excess accumulation of the WAT in the visceral fat pad causes secretion of angiotensinogen, adipsin, leptin, adiponectin, growth factors (IGF-1, PDGF, PAI-1), and cytokines (IL-6, IL-8, and TNF-α). Also, diet-induced obesity decreases the interstitial oxygen tension in obese adipose tissue of HFD mice. miRNAs are known as critical regulators of glucose uptake, insulin signaling pathway, lipid metabolism, and chronic inflammation (Dasgupta et al., 2011; Grant & Dixit, 2015; Guilherme et al., 2008; Seo et al., 2019; Trayhurn, 2013). Microarray study reveals that among all 373 miRNAs studied, 28 miRNAs were differentially expressed in differentiated 3T3-L1 adipocytes than pre-adipocytes. Interestingly, adipocytes from diet-induced obese mice express 35 different miRNAs when compared with adipocytes of lean individuals. Similarly, human obese WAT showcased numerous distinctly expressed miRNA profiles (P. Arner & Kulyté, 2015; Xie et al., 2009). However, the study on obesity-induced miRNAs involved with insulin resistance is still insufficient.

2.4.1 miRNA regulates AT insulin signaling pathway

Insulin resistance is ensured in obese adipose tissue by alteration of potential miRNAs, that are found to silence crucial factors and signaling molecules of insulin signaling pathway. Recently Arcidiacono et al, reported the overexpression of *miR-433*, *-520h*, *-153*, *-128*, *-579* and low expression of *miR-514*,

-520e, *-1275*, *-141*, *-17-5p*, *-132*, *-221*, *-184*, *-196*, *-518*, *-337* observed in the VAT of obese individuals. Among all, miR-128 exclusively participates in the regulation of insulin sensitivity by targeting insulin receptor(INSR). 3T3-L1 adipocytes exposed to 1%O_2 cause declined INSR mRNA and protein expression with increased *miR-128* level and miR-128 inhibition improves INSR expression in adipocytes (Arcidiacono et al., 2020). Binding of insulin to INSR triggers PI3K action which is crucial for PIP3 conversion and functional insulin signaling. miRNA microarray study revealed, that *miR-320* expression increases by fifty folds in insulin-resistant adipocytes that directly target p85 subunit of phosphatidylinositol 3-kinase (PI3K). Anti-*miR-320* oligos therapy surprisingly improves insulin sensitivity and glucose uptake in insulin-resistant cells (Ling et al., 2009). PI3K mediated phosphorylation of PIP2 and conversion into PIP3 negatively controlled by the phosphatase PTEN. While dual luciferase assay showed, *miR-26b* directly targets *PTEN*. It was reported that miR-26b level drops in the adipocytes of VAT in dietary obese mice and obese humans. Depleted expression of *miR-26b* proportionally cuts glucose uptake by inhibiting GLUT4 translocation to human mature adipocytes' plasma membrane (Xu et al., 2015). The downstream target of PI3K is Akt, a key player in transducing extracellular insulin signals into a wide range of action. Reportedly, the expression of *miR-29* paralogs (*miR-29a/b/c*) increased in adipose tissue of obese diabetic rats. Interestingly, overexpression of *miR-29* in 3T3-L1 adipocytes causes a severe imbalance of glucose uptake and IR by inhibiting Akt activation (Zhu & Leung, 2015). Obesity-induced IR also leads to a significant downregulation of *miR-181b*, which targets Pleckstrin homology domain leucine-rich repeat protein phosphatase (PHLLP) found to dephosphorylate Akt at Ser473. While PHLLP phosphatase silencing significantly improves insulin signaling and glucose homeostasis in epididymal WAT in *in-vivo* conditions (Sun et al., 2016). There is evidence that obesity increases the *miR-103* and *miR-107* expressions in fat tissue, which directly regulates insulin sensitivity in adipocytes by targeting *caveolin-1*, a key molecule for insulin receptor-mediated signaling, insulin secretion, and the development of IR (Trajkovski et al., 2011). Along with the PI3K-Akt signaling pathway, insulin activation is followed through MAPK activation. *miR-125* also overexpressed in adipose tissue of diabetic mice model causes adipose tissue dysfunction. Computational analysis showed it generates insulin resistance by potentially targeting the MAPK signaling pathway (Herrera et al., 2009).

2.4.2 miRNA regulates AT inflammation that linked with IR

Recent studies demonstrate microRNAs are critical players in regulating inflammation and phenotype switching in obese adipose tissue microenvironment. Reportedly, *miR-223* regulates myeloid cell-mediated adipose tissue inflammation and IR, specifically targeting *PKNOX*, essential for classical macrophage activation. They found *miR-223* level drops in the HFD model and *miR-223* KO mice showed increased PKNOX with the activation of M1 macrophage and enhanced migration inside AT and cause its inflammation. Dietary obesity also induces AT-specific overexpression of *miR-34a* and

is released by mature adipocytes in systemic circulation via paracrine manner through EVs. *miR-34* targets *KLF4*, a family member of the Zinc finger class of transcription factor, essentially regulates macrophage polarization and over over-activated in M2 type of macrophages. The suppression of M2 macrophage polarization by miR-34 acts as a leading factor in severe AT inflammation and insulin resistance (Pan et al., 2019; Zhuang et al., 2012).

Peroxisome proliferator-activated receptor-γ (PPARγ), a crucial nuclear receptor, regulates adipocyte development, and insulin sensitivity and most importantly determines IL-13 or IL-4 mediated polarization of macrophage into anti-inflammatory M2 phenotype. *miR-155*, *miR-27a,* and *miR-130b* found to target *PPARγ*, are overexpressed in obese AT. Inflamed adipose tissue macrophages (ATMs) release extracellular vesicles loaded with *miR-155* causing insulin resistance and glucose intolerance in DIO mice. While miRNAs loaded EVs treatment impairs insulin sensitivity in cultured adipocytes by reducing Akt phosphorylation. *miR-155* KO mice showed improved insulin sensitivity and glucose tolerance (Ying et al., 2017). AT-specific overexpression of *miR-27a* proportionally increases pro-inflammatory cytokine secretion along with stimulating macrophage infiltration that causes chronic inflammation and insulin resistance (Yao et al., 2017). qRT-PCR analysis showed upregulated expression of *miR-130b* in the macrophage population of obese AT that targets *PPAR-γ* and regulates glucose tolerance by alleviating alternative macrophage polarization (M. Zhang et al., 2016).

Adipose tissue inflammation is linked with overexpression of CCL2, which accumulates and attracts immune cells toward the adipose mass. *miR-193b* and *miR-126* negatively regulate *CCL2* expression by indirectly regulating via ETS1 or ARNT (activators of CCL2) and directly binds to its 3'UTR, respectively (E. Arner et al., 2012). The vicious events of oxidative stress, and inflammatory signaling are orchestrated in obesity and T2D by NAD^+-dependent deacetylase, SIRT1. Overwhelming evidence suggests, SIRT1 suppresses inflammation in AT and deacetylates NF-κB p65 subunit at K310 to inhibit downstream activation of inflammatory genes (Kitada et al., 2019). Upregulated *miR-221* in obese AT targets *SIRT1*, along with adiponectin receptor 1 (*ADIPOR1*), transcription factor v-ets erythroblastosis virus E26 oncogene homolog 1 (*ETS1*), that triggers inflammation. While silencing of *miR-221* improves insulin sensitivity and glucose uptake in fat cells (Meerson et al., 2013; Peng et al., 2018). another important tumor suppressor *miR-377* upregulated in DIO mice fat pad, specifically targets *SIRT1* and exerts chronic inflammation and insulin resistance (Peng et al., 2017). HFD gradually decreases thermogenic gene expression and induces visceralization of subcutaneous AT. Accumulated confirmations suggested, PRDM16, a master transcriptional regulator to stimulate SAT specifically the thermogenesis gene's activation. DIO results in SAT-specific gradual decrease of PRDM16 level with increased expression of *miR-149-3p* that targets *PRDM16*. Whereas, ablation of *miR-149-3p* in AT improves whole body insulin-sensitivity and lessens inflammatory effects (Zheng et al., 2019). High

serum FFA is closely associated with AT inflammation and IR Studies showed that inhibition of lipolysis in obese AT improves insulin sensitivity and glucose metabolism (Girousse et al., 2013). In lipolysis, a series of enzymatic hydrolysis reactions takes place, where adipose triglyceride lipase (ATGL) initiates by binding with its substrate triacylglycerol (TGA) leading to hydrolysis of ester bond as a result formation of DAG and one free fatty acid released. ATGL and its co-activator comparative gene identification 58(CGI-58) expression critically regulated by abdominal AT-specific *miR-124a*, which reduces lipolysis and accumulation of TG takes place (Das et al., 2015; Girousse et al., 2013; Mentzel et al., 2015). Stearoyl-Co-A desaturase-1 (Scd-1) is another crucial lipogenic enzyme that acts on monounsaturated fatty acid (mainly oleate (C18:1) and palmitoleate (C16:1)) synthesis. Disrupted Scd-1 results lessen adiposity, reduce weight gain, and improve insulin sensitivity. *Scd-1*, a functional target of *miR-378* and systemically administration of *miR-378* significantly prevents HFD-induced obesity in mice model by reducing WAT size; displayed improvement of GTT and ITT in comparison to WT HFD induced obese mice (Y. Zhang et al., 2016). Genetically obese mice displayed activation of *miR-335* in WAT which is associated with lipid metabolism (Nakanishi et al., 2009). *miR-425* remarkably increases in adipose tissues of obese mice, which is transcriptionally regulated by PPAR-γ and targets Mapk14/p38 of the MAPK family which negatively regulates adipogenesis and induces lipolysis(Qi et al., 2019). *miR-425* remarkably increases in adipose tissues of obese mice, which is transcriptionally regulated by PPAR-γ and targets Mapk14/p38 of the MAPK family which negatively regulates adipogenesis and induces lipolysis (Qi et al., 2019). Moreover, *miR-145* overexpression stimulates the release of pro-lipolytic cytokine, TNF-α and simultaneous overexpression of *miR-26a* and *let-7d* in human adipocytes significantly inhibits lipolysis (Lorente-Cebrián et al., 2014). Furthermore, obese females have low *miR-141* and *miR-520* expression that directly targets *RAB11A* and *YWHAG* (encodes 14-3-3 protein gamma), involved in glucose homeostasis, lipid metabolism (Capobianco et al., 2012). For the last decades, multiple tissue-specific miRNAs were reported as differentially expressed under obesity-induced pathophysiological conditions and detected in blood, serum, saliva, and other body fluids which can serve as reliable biomarkers of obesity and T2D. Meta-analyses study showed 16 stress-related miRNAs were dysregulated, among all, *miR-148b*, *miR-223*, *miR-130a*, *miR-19a*, *miR-26b*, and *miR-27b*, serve as possible T2D biomarkers (Liang et al., 2020). Overexpression of *miR-144-5p*, *let-7d*, *miR-34a*, and *miR-532-5p* positively correlates to IR in obese Europeans (Choi et al., 2019). The serum levels of *miR-10b* were found to be low during obesity and silence *PI3K* and transcription factor *FOXO1* (Parrizas et al., 2020). Alteration in 25 exosomal miRNAs due to dysregulation of glucose metabolism in T2D may play a role as a potential biomarker and therapeutic target for treating obesity-induced T2D (Kim et al., 2020). In addition to proving crucial biomarkers, miRNAs are extremely useful prognostic biomolecules for therapeutic/pharmacologic purposes. Further investigation in miRNA therapeutics are required to design stable, sensitive, and specific molecules.

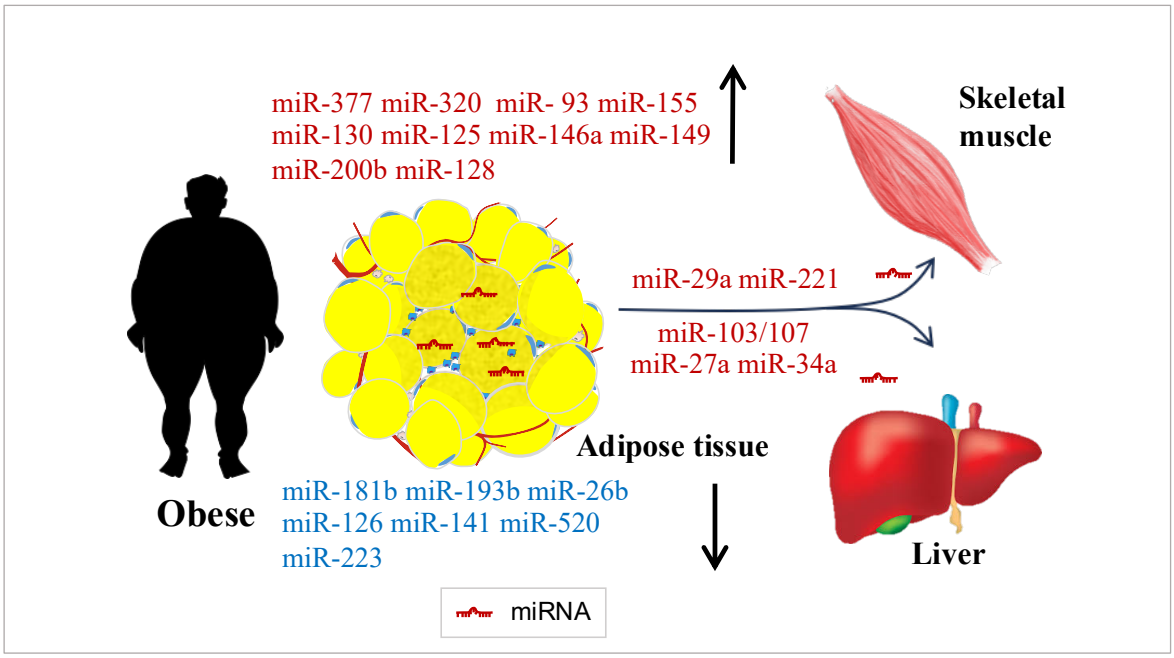

Figure 2.4| **Overview of miRNAs expression in AT under obesity**

Differential expression of miRNAs in adipose tissue and delivery in distal insulin responsive organ liver and skeletal muscle. miRNAs in red color font indicates upregulation and green color miRNAs indicates downregulation under obese condition. Adipose tissue-derived miRNAs miR-103/107, miR-27a, and miR-34a are secreted and shared with the liver which induces hepatic insulin resistance. Similarly, miR-29a and miR-221 upregulation are associated with skeletal muscle IR.

2.5 Extracellular vesicle-mediates AT dysfunction during obesity

Adipose tissue is acknowledged as the largest endocrine organ, releasing a range of bioactive molecules known as adipokines that exert profound effects on various physiological processes throughout the body. These adipokines influence metabolic regulation, inflammation, vascular function, immune modulation, reproductive health, cancer risk, and organ crosstalk. Beyond the realm of traditional secreted proteins, recent research has unveiled the remarkable role of adipose tissues in releasing extracellular vesicles that exert a profound influence on metabolic homeostasis. Adipocytes are responsible for secreting a diverse array of substances, encompassing adipokines, lipids, RNA molecules, and metabolites, all of which possess significant signaling capabilities. (Deng & Scherer, 2010; C. R. Kahn et al., 2019; Kita et al., 2019). The release of a specific subgroup of small extracellular vesicles (sEVs) known as exosomes is closely associated with cellular stress conditions. In cultured adipocytes, an increased release of sEVs has been observed in response to various stressors, including hypoxia, pro-inflammatory cytokines, and fatty acids. However, the precise molecular mechanisms responsible for initiating sEVs release during stress have not been fully elucidated. It is worth noting that the production of sEVs in response to palmitate is likely mediated by the generation of ceramide. Ceramides are well-known inducers of exosome release in a variety of cell types (Hu et al., 2023). Substantial presence of adipocyte-derived microRNAs within exosomes circulating in the bloodstream.

These microRNAs journey to the liver, where they enhance glucose tolerance while reducing hepatic FGF21 expression. Furthermore, exosomal communication between endothelial cells and adipocytes within adipose tissues was reported. Their meticulous isolation of extracellular vesicles from adipose tissue revealed the presence of proteins and lipids capable of modulating cellular signaling pathways, adding another layer to the complexity of adipose tissue communication. Additionally, exosomal microRNAs originating from adipose tissue macrophages play a crucial role in regulating whole-body glucose metabolism by modulating adipocyte functions. Adipocyte-secreted exosomal microRNA-34a, which hinders the polarization of M2 macrophages, thus promoting inflammation in obesity-induced adipose tissue. Collectively, these studies highlighting the intricate network of interorgan communication involving adipose tissue, liver, endothelial cells, macrophages, and beyond. Adipocytes release neutral lipids directly through exosomes, complementing the traditional lipolysis process that releases fatty acids and glycerol through neutral lipases(Crewe et al., 2018, 2021; Flaherty et al., 2019; Ying et al., 2017).

Adipose tissue-derived extracellular vesicles (Ad-EVs) exhibit a significant capacity to modulate the functions of various cell types inhabiting or infiltrating the adipose tissue milieu, including macrophages, cancer cells, endothelial cells, adipocyte progenitors, and fully differentiated adipocytes. Although the mechanistic intricacies governing these intercellular signaling events remain incompletely elucidated, the most extensively explored axis of communication occurs between adipocytes and macrophages. These studies have provided compelling evidence of the transfer of adipocyte-specific mRNAs, proteins, or adipocyte-associated membrane markers to macrophages. Early research underscored the functional significance of this intercellular exchange. EVs derived from the adipose tissue of genetically obese mice have been observed to internalize in circulating monocytes, prompting their differentiation into proinflammatory macrophages. Notably, injections of sEVs derived from obese adipose tissue were sufficient to induce whole-body glucose intolerance and insulin resistance.It is noteworthy that while the sEVs employed in this study were not exclusively adipocyte-specific, similar effects have been demonstrated using sEVs originating from cultured adipocytes. In these investigations, sEVs were isolated from mature primary adipocytes derived from obese mice or 3T3-L1 adipocytes subjected to in vitro differentiation to mimic the characteristics of the obese state, achieved through culture under high glucose and insulin conditions. Adipocyte-derived EVs were found to induce the migration and differentiation of monocytes into a proinflammatory M1-like state, both in vitro and in vivo. These effects are believed to be mediated through various mechanisms, including the involvement of RBP4, and miR-155, all of which have been reported as constituents of Ad-EVs.

Table 2.2

miRNA	Target mRNA (3' UTR)	Expression in obesity	Mechanism of action	Reference
miR-103 miR-107	CAVEOLIN-1	↑	Regulate insulin sensitivity.	(Trajkovski et al., 2011)
miR-124a	ATGL and CGI-58	-	Regulates lipolysis and triglyceride metabolism.	(Das et al., 2015)
miR-126	CCL2	↓	Regulates AT inflammation	(E. Arner et al., 2012)
miR-128	INSR	↑	Regulated by adipose tissue hypoxia and overexpression cause impairment of glucose homeostasis.	(Arcidiacono et al., 2020)
miR-130 & miR-130b	PPAR-γ	↑	Adipose tissue dysfunction and insulin resistance by regulating TNFα, NF-κB activation. Also induces IR by hindering M2 macrophage polarization.	(Heyn et al., 2020)
miR-141	RAB11A	↓	Controls glucose homeostasis	(Capobianco et al., 2012)
miR-149-3p	PRDM16	↑	Induces IR.	(Zheng et al., 2019)
miR-155	PPAR-γ	↑	EVs secreted by obese ATMs loaded with miR-155 cause IR and glucose intolerance.	(Guo et al., 2017)
miR-181b	Pleckstrin homology domain leucine-rich repeat protein phosphatase	↓	Regulates phosphatase activity leads to increase AKT phosphorylation at Serine 473 and improved EC insulin signaling.	(Sun et al., 2016)

miR-193b	ETS1 or ARNT (activators of CCL2)	↓	Regulates inflammation by controlling CCL2 and adiponectins production.	(E. Arner et al., 2012)
miR-223	PKNOX	↓	Regulates inflammation by controlling macrophage polarization and migration.	(Zhuang et al., 2012)
miR-26b	PTEN	↓	Modulates PTEN/PI3K/AKT pathway	(Xu et al., 2015)
miR-27a/b	PPAR-γ	↑	Regulates macrophage polarization, migration and chronic inflammation. Also regulates adipocytes differentiation, cause adipose tissue dysfunction	(Q. Lin et al., 2009; Yao et al., 2017)
miR-29a/b/c	Indirectly inhibits Akt activation	↑	Repress insulin-stimulated glucose uptake.	(Dalgaard et al., 2022)
miR-320	p85 subunit of PI3K	↑	Modulates insulin-PI3K signaling pathways.	(Ling et al., 2009)
miR-34a	KLF4	↑	Inhibits M2 macrophage polarization during obesity and promotes insulin resistance.	(Pan et al., 2019)
miR-377	SIRT-1	↑	Mediates chronic inflammation and insulin resistance.	(Peng et al., 2017)
miR-378	Scd-1	↑	Controls lipid metabolism	(Y. Zhang et al., 2016)
miR-425	MAPK signaling pathway	↑	May generate insulin resistance.	(Qi et al., 2019)
miR-520	YWHAG	↓	Involved in glucose homeostasis and lipid metabolism	(Capobianco et al., 2012)

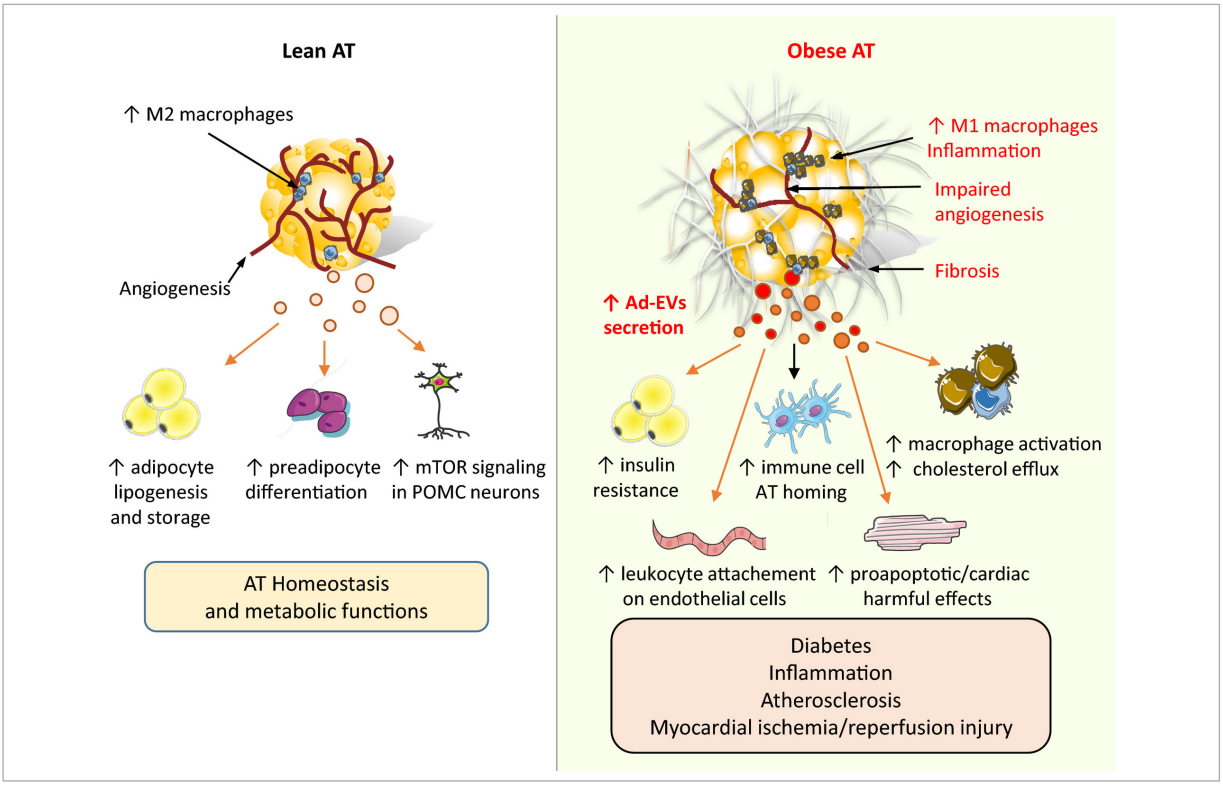

Figure 2.5 | **Adipose tissue-derived extracellular vesicles regulate obesity-induced pathogenesis**

Adipose tissue undergoes considerable remodeling as a result of obesity, which increases the production of EVs produced from adipose (Ad-EVs), and it is believed that the contents of these Ad-EVs reflect the pathophysiological state of their parent cells. Ad-EVs have the ability to transport their payload to a variety of recipient cells, aiding in the preservation of metabolic and AT homeostasis under normal circumstances. On the other hand, Ad-EVs produced from obese AT contribute to the development of metabolic dysfunction linked to obesity. The figure was **adopted** from Le Lay, Soazig, et al. (2021) FASEB BioAdvances, Volume: 3, Issue: 6, Pages: 407-419.

EVs have been shown to actively hinder the polarization of macrophages into the anti-inflammatory M2-like state by targeting Klf4 via miR-34a. Beyond macrophage activation, Ad-EVs also contribute to lipid accumulation within macrophages through the direct transfer of lipid droplets. The subsequent metabolism of these lipids within macrophages is closely associated with inflammation-induced insulin resistance. This process of EV-mediated communication extends reciprocally from macrophages to adipocytes, although research on this aspect remains relatively limited. EVs derived from macrophages exposed to LPS have been shown to propagate a proinflammatory gene signature within recipient adipocytes. Adipose tissue-derived extracellular vesicles enter the bloodstream, facilitating signaling in remote organs. Simultaneously, they induce insulin resistance in skeletal muscle and the liver. In response, the liver releases small EVs that stimulate lipid accumulation in adipose tissue (Pan et al., 2019; Yáñez-Mó et al., 2015; Ying et al., 2017; Zhuang et al., 2012).

2.6. Adipocyte senescence-mediated AT pathogenesis during obesity

Obesity induces alteration of the adipose tissue microenvironment associated with cellular heterogeneity involving massive infiltration of immune cell types along with the hypertrophy and hyperplasia of adipocytes leading to adipose tissue inflammation and senescence. Adipocyte senescence involves irreversible growth arrest in adipocytes associated with the secretion of various cytokines, chemokines, and extracellular matrix proteins that contribute to the development and progression of obesity-related complications, such as insulin resistance and T2D (Tchkonia et al., 2010). Recent studies revealed that premature cell senescence attributed to obese adipose tissue significantly diverges from aging-mediated cell senescence wherein mitochondrial dysfunction, DNA damage, and rapid mitogenic induction irreversibly inhibit cell cycle progression (Smith et al., 2021). Increased abundance of senescent adipose progenitor cells and endothelial cells were reported in obese adipose tissue of T2D patients. In addition to senescent progenitor cells, the magnitude of pro-senescent mature adipose tissue cells population also skyrocketed in obese T2D patients (Gustafson et al., 2022; Smith et al., 2021). Moreover, systemic hyperinsulinemia has been recently revealed as an activator of endoreplication by switching on cell cycle regulator protein cyclin D1 in mature human adipocytes which potentiates the induction of adipocyte death (Q. Li et al., 2021). Morbidly obese adipose tissue exhibits features of severe stress conditions including chronic inflammation, lipotoxicity, and oxidative stress, and these are the probable cause of adipocyte senescence (Manna & Jain, 2015). Unregulated adipocyte senescence is a key signature of obese adipose tissue which may contribute to the development of insulin resistance and T2D (Palmer et al., 2019).

The initial discovery of cellular senescence was made by Hayflick, which showed proliferating cells losing cell division ability by irreversible blockage of the cell cycle that leads to a nondividing state, now it is called replicative senescence and considered an essential physiological event, often associated with aging (Hayflick, 1965; Shay, 2016). Research in the field of obesity-associated adipocyte senescence, particularly in white adipose tissue has been done by multiple research groups over the last decade. Adipocyte death rapidly increased with obesity in rodents and humans, where the death toll hiked by 30 folds. Moreover, the number of adipocytes in epididymal adipose tissue decreased by approximately 80% in 16 weeks of high-fat-diet obese mice by rapid senescence (Cinti et al., 2005; Strissel et al., 2007). Dead adipocytes attract macrophages to scavenge the lipid droplets ultimately forming multinucleate giant cells, which are a hallmark of chronic inflammation and play role in the development of obesity-related metabolic disorders (Cinti et al., 2005). As the ‘mouse Ageing Cell Atlas’ uncovers aging associated with increased cell senescence in most of the tissue and organs that implicate lower number of functional cells with increased inflammation (Tabula Muris Consortium, 2020). Interestingly, obesity promotes pro-senescent cell accumulation in vWAT that contributes to the development of type 2 diabetes. Higher oxidative stress associated with the obese murine model as well

as obese type 2 diabetes individuals adipose tissue and promotes senescent phenotype including high β-galactosidase activity and secretion of TNF-α, IL-6, and CCL2 by rapid activation of p53 (Minamino et al., 2009). The adipose tissue senescence is also regulated by severe DNA damage and mediated by DNA polymerase η ablation in mice, followed by overexpression of p21, ATM, and p53. Moreover polymerase $\eta^{-/-}$ mice exacerbate body fat gain, accumulated senescent cells, and increased SASP profile (Y.-W. Chen et al., 2015). Systemic high glucose enforces premature senescence in vitro in endothelial cells, renal mesangial cells, adipose-derived stem cells (also known as preadipocytes or fat cell progenitors), and fibroblasts. Senescent preadipocytes are found in higher abundance in obese individuals compared to lean individuals of the same age, even in younger individuals and it contributes to declines in adipogenic and lipogenic potential, leading to age-related lipodystrophy, lipotoxicity, and inflammation (Smith et al., 2021). Moreover, the secretion of inflammatory cytokines from senescent preadipocytes, which is part of the senescence-associated secretory phenotype (SASP), creates a low-grade inflammatory state that can contribute to insulin resistance and the development of T2D (Gustafson et al., 2019). Furthermore, impaired adipose tissue function leads to an imbalance in lipid metabolism, resulting in ectopic lipid deposition in non-adipose tissues such as the liver or muscle exacerbating pathogenesis. Recently it was reported that postmitotic mature adipocytes can enter in cell cycle are able to synthesize DNA, and pass through the S phase, which enhances adipocyte's genetic enrichment as well as cell size increases and acts as endo-replicating cells (Q. Li et al., 2021). Whereas type 2 diabetes-associated hyperinsulinemia induces cell cycle progress and implicates senescent cell program in mature adipocytes. Adipose progenitor cells, as well as mature lipid-laden adipocytes, were characterized by increased senescence in comparison to lean individuals which may occur because of earlier evident hyperinsulinemia in obese T2D patients (Gustafson et al., 2019, 2022; Smith et al., 2021). Moreover, senescent cells play a causal role in obesity-related metabolic derangements and chronic inflammation, and emerging senolytic agents are found to selectively target and eliminate senescent cells (Palmer et al., 2015, 2019; Tchkonia et al., 2010).

In conclusion, the comprehensive review of the literature underscores the pivotal role of obesity-induced adipose tissue dysfunction, driven by a triad of factors: adipocyte senescence, miRNA-mediated inflammation, and insulin resistance. These interconnected mechanisms orchestrate significant adipose tissue remodeling, profoundly altering its cellular architecture. Understanding these intricate processes is imperative for unraveling the complexities of obesity-related health consequences and may hold the key to developing targeted interventions for improving metabolic health in the face of this growing global health challenge.

References

Amarante-Mendes, G. P., Adjemian, S., Branco, L. M., Zanetti, L. C., Weinlich, R., & Bortoluci, K. R. (2018). Pattern Recognition Receptors and the Host Cell Death Molecular Machinery. *Frontiers in Immunology*, *9*. https://www.frontiersin.org/articles/10.3389/fimmu.2018.02379

Arcidiacono, B., Chiefari, E., Foryst-Ludwig, A., Currò, G., Navarra, G., Brunetti, F. S., Mirabelli, M., Corigliano, D. M., Kintscher, U., Britti, D., Mollace, V., Foti, D. P., Goldfine, I. D., & Brunetti, A. (2020). Obesity-related hypoxia via miR-128 decreases insulin-receptor expression in human and mouse adipose tissue promoting systemic insulin resistance. *EBioMedicine*, *59*, 102912. https://doi.org/10.1016/j.ebiom.2020.102912

Arner, E., Mejhert, N., Kulyté, A., Balwierz, P. J., Pachkov, M., Cormont, M., Lorente-Cebrián, S., Ehrlund, A., Laurencikiene, J., Hedén, P., Dahlman-Wright, K., Tanti, J.-F., Hayashizaki, Y., Rydén, M., Dahlman, I., van Nimwegen, E., Daub, C. O., & Arner, P. (2012). Adipose Tissue MicroRNAs as Regulators of CCL2 Production in Human Obesity. *Diabetes*, *61*(8), 1986–1993. https://doi.org/10.2337/db11-1508

Arner, P., & Kulyté, A. (2015). MicroRNA regulatory networks in human adipose tissue and obesity. *Nature Reviews Endocrinology*, *11*(5), Article 5. https://doi.org/10.1038/nrendo.2015.25

Bäckdahl, J., Franzén, L., Massier, L., Li, Q., Jalkanen, J., Gao, H., Andersson, A., Bhalla, N., Thorell, A., Rydén, M., Ståhl, P. L., & Mejhert, N. (2021). Spatial mapping reveals human adipocyte subpopulations with distinct sensitivities to insulin. *Cell Metabolism*, *33*(9), 1869-1882.e6. https://doi.org/10.1016/j.cmet.2021.07.018

Baker, R. G., Hayden, M. S., & Ghosh, S. (2011). NF-κB, Inflammation, and Metabolic Disease. *Cell Metabolism*, *13*(1), 11–22. https://doi.org/10.1016/j.cmet.2010.12.008

Berg, A. H., & Scherer, P. E. (2005). Adipose Tissue, Inflammation, and Cardiovascular Disease. *Circulation Research*, *96*(9), 939–949. https://doi.org/10.1161/01.RES.0000163635.62927.34

Boutens, L., & Stienstra, R. (2016). Adipose tissue macrophages: Going off track during obesity. *Diabetologia*, *59*, 879–894. https://doi.org/10.1007/s00125-016-3904-9

Burl, R. B., Ramseyer, V. D., Rondini, E. A., Pique-Regi, R., Lee, Y.-H., & Granneman, J. G. (2018). Deconstructing Adipogenesis Induced by β3-Adrenergic Receptor Activation with Single-Cell Expression Profiling. *Cell Metabolism*, *28*(2), 300-309.e4. https://doi.org/10.1016/j.cmet.2018.05.025

Capobianco, V., Nardelli, C., Ferrigno, M., Iaffaldano, L., Pilone, V., Forestieri, P., Zambrano, N., & Sacchetti, L. (2012). miRNA and Protein Expression Profiles of VWAT Reveal miR-141/YWHAG and miR-520e/RAB11A as Two Potential miRNA/Protein Target Pairs Associated with Severe Obesity. *Journal of Proteome Research*, *11*(6), 3358–3369. https://doi.org/10.1021/pr300152z

Cautivo, K. M., & Molofsky, A. B. (2016). Regulation of metabolic health and adipose tissue function by group 2 innate lymphoid cells. *European Journal of Immunology*, *46*(6), 1315–1325. https://doi.org/10.1002/eji.201545562

Chait, A., & den Hartigh, L. J. (2020). Adipose Tissue Distribution, Inflammation and Its Metabolic Consequences, Including Diabetes and Cardiovascular Disease. *Frontiers in Cardiovascular Medicine*, *7*. https://www.frontiersin.org/articles/10.3389/fcvm.2020.00022

Chen, L., Chen, R., Wang, H., & Liang, F. (2015). Mechanisms Linking Inflammation to Insulin Resistance. *International Journal of Endocrinology*, *2015*, e508409. https://doi.org/10.1155/2015/508409

Chen, Y.-W., Harris, R. A., Hatahet, Z., & Chou, K. (2015). Ablation of XP-V gene causes adipose tissue senescence and metabolic abnormalities. *Proceedings of the National Academy of Sciences*, *112*(33). https://doi.org/10.1073/pnas.1506954112

Choe, S. S., Huh, J. Y., Hwang, I. J., Kim, J. I., & Kim, J. B. (2016). Adipose Tissue Remodeling: Its Role in Energy Metabolism and Metabolic Disorders. *Frontiers in Endocrinology*, *7*. https://www.frontiersin.org/articles/10.3389/fendo.2016.00030

Choi, H., Koh, H. W. L., Zhou, L., Cheng, H., Loh, T. P., Parvaresh Rizi, E., Toh, S. A., Ronnett, G. V., Huang, B. E., & Khoo, C. M. (2019). Plasma Protein and MicroRNA Biomarkers of Insulin Resistance: A Network-Based Integrative -Omics Analysis. *Frontiers in Physiology*, *10*. https://www.frontiersin.org/articles/10.3389/fphys.2019.00379

Chowdhury, D., Choi, Y. E., & Brault, M. E. (2013). Charity begins at home: Non-coding RNA functions in DNA repair. *Nature Reviews Molecular Cell Biology*, *14*(3), Article 3. https://doi.org/10.1038/nrm3523

Cinti, S., Mitchell, G., Barbatelli, G., Murano, I., Ceresi, E., Faloia, E., Wang, S., Fortier, M., Greenberg, A. S., & Obin, M. S. (2005). Adipocyte death defines macrophage localization and function in adipose

tissue of obese mice and humans. *Journal of Lipid Research*, *46*(11), 2347–2355. https://doi.org/10.1194/jlr.M500294-JLR200

Corvera, S. (2021). Cellular Heterogeneity in Adipose Tissues. *Annual Review of Physiology*, *83*(1), 257–278. https://doi.org/10.1146/annurev-physiol-031620-095446

Crewe, C., Funcke, J.-B., Li, S., Joffin, N., Gliniak, C. M., Ghaben, A. L., An, Y. A., Sadek, H. A., Gordillo, R., Akgul, Y., Chen, S., Samovski, D., Fischer-Posovszky, P., Kusminski, C. M., Klein, S., & Scherer, P. E. (2021). Extracellular vesicle-based interorgan transport of mitochondria from energetically stressed adipocytes. *Cell Metabolism*, *33*(9), 1853-1868.e11. https://doi.org/10.1016/j.cmet.2021.08.002

Crewe, C., Joffin, N., Rutkowski, J. M., Kim, M., Zhang, F., Towler, D. A., Gordillo, R., & Scherer, P. E. (2018). An Endothelial-to-Adipocyte Extracellular Vesicle Axis Governed by Metabolic State. *Cell*, *175*(3), 695-708.e13. https://doi.org/10.1016/j.cell.2018.09.005

Croce, S., Avanzini, M. A., Regalbuto, C., Cordaro, E., Vinci, F., Zuccotti, G., & Calcaterra, V. (2021). Adipose Tissue Immunomodulation and Treg/Th17 Imbalance in the Impaired Glucose Metabolism of Children with Obesity. *Children*, *8*(7), Article 7. https://doi.org/10.3390/children8070554

Cunha, T. M., Talbot, J., Pinto, L. G., Vieira, S. M., Souza, G. R., Guerrero, A. T., Sonego, F., Verri, W. A., Zamboni, D. S., Ferreira, S. H., & Cunha, F. Q. (2010). Caspase-1 is Involved in the Genesis of Inflammatory Hypernociception by Contributing to Peripheral IL-1β Maturation. *Molecular Pain*, *6*, 1744-8069-6–63. https://doi.org/10.1186/1744-8069-6-63

Dalgaard, L. T., Sørensen, A. E., Hardikar, A. A., & Joglekar, M. V. (2022). The microRNA-29 family: Role in metabolism and metabolic disease. *American Journal of Physiology-Cell Physiology*, *323*(2), C367–C377. https://doi.org/10.1152/ajpcell.00051.2022

Das, S. K., Stadelmeyer, E., Schauer, S., Schwarz, A., Strohmaier, H., Claudel, T., Zechner, R., Hoefler, G., & Vesely, P. W. (2015). Micro RNA-124a Regulates Lipolysis via Adipose Triglyceride Lipase and Comparative Gene Identification 58. *International Journal of Molecular Sciences*, *16*(4), Article 4. https://doi.org/10.3390/ijms16048555

Dasgupta, S., Bhattacharya, S., Maitra, S., Pal, D., Majumdar, S. S., Datta, A., & Bhattacharya, S. (2011). Mechanism of lipid induced insulin resistance: Activated PKCε is a key regulator. *Biochimica et Biophysica Acta (BBA) - Molecular Basis of Disease*, *1812*(4), 495–506. https://doi.org/10.1016/j.bbadis.2011.01.001

Deng, Y., & Scherer, P. E. (2010). Adipokines as novel biomarkers and regulators of the metabolic syndrome. *Annals of the New York Academy of Sciences*, *1212*, E1–E19. https://doi.org/10.1111/j.1749-6632.2010.05875.x

Donath, M. Y., & Shoelson, S. E. (2011). Type 2 diabetes as an inflammatory disease. *Nature Reviews Immunology*, *11*(2), Article 2. https://doi.org/10.1038/nri2925

Eizirik, D. L., & Mandrup-Poulsen, T. (2001). A choice of death – the signal-transduction of immune-mediated beta-cell apoptosis. *Diabetologia*, *44*(12), 2115–2133. https://doi.org/10.1007/s001250100021

Emont, M. P., Jacobs, C., Essene, A. L., Pant, D., Tenen, D., Colleluori, G., Di Vincenzo, A., Jørgensen, A. M., Dashti, H., Stefek, A., McGonagle, E., Strobel, S., Laber, S., Agrawal, S., Westcott, G. P., Kar, A., Veregge, M. L., Gulko, A., Srinivasan, H., … Rosen, E. D. (2022). A single-cell atlas of human and mouse white adipose tissue. *Nature*, *603*(7903), 926–933. https://doi.org/10.1038/s41586-022-04518-2

Ernst, M. C., & Sinal, C. J. (2010). Chemerin: At the crossroads of inflammation and obesity. *Trends in Endocrinology & Metabolism*, *21*(11), 660–667. https://doi.org/10.1016/j.tem.2010.08.001

Flaherty, S. E., Grijalva, A., Xu, X., Ables, E., Nomani, A., & Ferrante, A. W. (2019). A lipase-independent pathway of lipid release and immune modulation by adipocytes. *Science*, *363*(6430), 989–993. https://doi.org/10.1126/science.aaw2586

Frasca, D., & Blomberg, B. B. (2017). Adipose Tissue Inflammation Induces B Cell Inflammation and Decreases B Cell Function in Aging. *Frontiers in Immunology*, *8*. https://www.frontiersin.org/articles/10.3389/fimmu.2017.01003

Gao, D., Madi, M., Ding, C., Fok, M., Steele, T., Ford, C., Hunter, L., & Bing, C. (2014). Interleukin-1β mediates macrophage-induced impairment of insulin signaling in human primary adipocytes. *American Journal of Physiology-Endocrinology and Metabolism*, *307*(3), E289–E304. https://doi.org/10.1152/ajpendo.00430.2013

Girousse, A., Tavernier, G., Valle, C., Moro, C., Mejhert, N., Dinel, A.-L., Houssier, M., Roussel, B., Besse-Patin, A., Combes, M., Mir, L., Monbrun, L., Bézaire, V., Prunet-Marcassus, B., Waget, A., Vila, I., Caspar-Bauguil, S., Louche, K., Marques, M.-A., … Langin, D. (2013). Partial inhibition of adipose tissue

lipolysis improves glucose metabolism and insulin sensitivity without alteration of fat mass. *PLoS Biology*, *11*(2), e1001485. https://doi.org/10.1371/journal.pbio.1001485

Grant, R. W., & Dixit, V. D. (2015). Adipose tissue as an immunological organ: Adipose Tissue as an Immunological Organ. *Obesity*, *23*(3), 512–518. https://doi.org/10.1002/oby.21003

Guilherme, A., Virbasius, J. V., Puri, V., & Czech, M. P. (2008). Adipocyte dysfunctions linking obesity to insulin resistance and type 2 diabetes. *Nature Reviews Molecular Cell Biology*, *9*(5), Article 5. https://doi.org/10.1038/nrm2391

Gustafson, B., Nerstedt, A., & Smith, U. (2019). Reduced subcutaneous adipogenesis in human hypertrophic obesity is linked to senescent precursor cells. *Nature Communications*, *10*(1), 2757. https://doi.org/10.1038/s41467-019-10688-x

Gustafson, B., Nerstedt, A., Spinelli, R., Beguinot, F., & Smith, U. (2022). Type 2 Diabetes, Independent of Obesity and Age, Is Characterized by Senescent and Dysfunctional Mature Human Adipose Cells. *Diabetes*, *71*(11), 2372–2383. https://doi.org/10.2337/db22-0003

Han, S.-J., Glatman Zaretsky, A., Andrade-Oliveira, V., Collins, N., Dzutsev, A., Shaik, J., Morais da Fonseca, D., Harrison, O. J., Tamoutounour, S., Byrd, A. L., Smelkinson, M., Bouladoux, N., Bliska, J. B., Brenchley, J. M., Brodsky, I. E., & Belkaid, Y. (2017). White Adipose Tissue Is a Reservoir for Memory T Cells and Promotes Protective Memory Responses to Infection. *Immunity*, *47*(6), 1154-1168.e6. https://doi.org/10.1016/j.immuni.2017.11.009

Hayflick, L. (1965). The limited in vitro lifetime of human diploid cell strains. *Experimental Cell Research*, *37*(3), 614–636. https://doi.org/10.1016/0014-4827(65)90211-9

Hepler, C., & Gupta, R. K. (2017). The expanding problem of adipose depot remodeling and postnatal adipocyte progenitor recruitment. *Molecular and Cellular Endocrinology*, *445*, 95–108. https://doi.org/10.1016/j.mce.2016.10.011

Hepler, C., Shan, B., Zhang, Q., Henry, G. H., Shao, M., Vishvanath, L., Ghaben, A. L., Mobley, A. B., Strand, D., Hon, G. C., & Gupta, R. K. (2018). Identification of functionally distinct fibro-inflammatory and adipogenic stromal subpopulations in vWAT of adult mice. *eLife*, *7*, e39636. https://doi.org/10.7554/eLife.39636

Herrera, B. M., Lockstone, H. E., Taylor, J. M., Wills, Q. F., Kaisaki, P. J., Barrett, A., Camps, C., Fernandez, C., Ragoussis, J., Gauguier, D., McCarthy, M. I., & Lindgren, C. M. (2009). MicroRNA-125a is over-expressed in insulin target tissues in a spontaneous rat model of Type 2 Diabetes. *BMC Medical Genomics*, *2*(1), 54. https://doi.org/10.1186/1755-8794-2-54

Heyn, G. S., Corrêa, L. H., & Magalhães, K. G. (2020). The Impact of Adipose Tissue–Derived miRNAs in Metabolic Syndrome, Obesity, and Cancer. *Frontiers in Endocrinology*, *11*. https://www.frontiersin.org/articles/10.3389/fendo.2020.563816

Hildreth, A. D., Ma, F., Wong, Y. Y., Sun, R., Pellegrini, M., & O'Sullivan, T. E. (2021). Single-cell sequencing of human white adipose tissue identifies new cell states in health and obesity. *Nature Immunology*, *22*(5), 639–653. https://doi.org/10.1038/s41590-021-00922-4

Hinz, M., & Scheidereit, C. (2014). The IκB kinase complex in NF-κB regulation and beyond. *EMBO Reports*, *15*(1), 46–61. https://doi.org/10.1002/embr.201337983

Hotamisligil, G. S., Shargill, N. S., & Spiegelman, B. M. (1993). Adipose Expression of Tumor Necrosis Factor-α: Direct Role in Obesity-Linked Insulin Resistance. *Science*, *259*(5091), 87–91. https://doi.org/10.1126/science.7678183

Hu, S., Hu, Y., & Yan, W. (2023). Extracellular vesicle-mediated interorgan communication in metabolic diseases. *Trends in Endocrinology & Metabolism*, *34*(9), 571–582. https://doi.org/10.1016/j.tem.2023.06.002

Ikutani, M., & Nakae, S. (2022). Heterogeneity of Group 2 Innate Lymphoid Cells Defines Their Pleiotropic Roles in Cancer, Obesity, and Cardiovascular Diseases. *Frontiers in Immunology*, *13*. https://www.frontiersin.org/articles/10.3389/fimmu.2022.939378

Jaitin, D. A., Adlung, L., Thaiss, C. A., Weiner, A., Li, B., Descamps, H., Lundgren, P., Bleriot, C., Liu, Z., Deczkowska, A., Keren-Shaul, H., David, E., Zmora, N., Eldar, S. M., Lubezky, N., Shibolet, O., Hill, D. A., Lazar, M. A., Colonna, M., … Amit, I. (2019). Lipid-Associated Macrophages Control Metabolic Homeostasis in a Trem2-Dependent Manner. *Cell*, *178*(3), 686-698.e14. https://doi.org/10.1016/j.cell.2019.05.054

Jiang, Y., Berry, D. C., Tang, W., & Graff, J. M. (2014). Independent Stem Cell Lineages Regulate Adipose Organogenesis and Adipose Homeostasis. *Cell Reports*, *9*(3), 1007–1022. https://doi.org/10.1016/j.celrep.2014.09.049

Jung, U. J., & Choi, M.-S. (2014). Obesity and Its Metabolic Complications: The Role of Adipokines and the Relationship between Obesity, Inflammation, Insulin Resistance, Dyslipidemia and Nonalcoholic Fatty Liver Disease. *International Journal of Molecular Sciences*, *15*(4), 6184–6223. https://doi.org/10.3390/ijms15046184

Kahn, B. B., & Flier, J. S. (2000). Obesity and insulin resistance. *The Journal of Clinical Investigation*, *106*(4), 473–481. https://doi.org/10.1172/JCI10842

Kahn, C. R., Wang, G., & Lee, K. Y. (2019). Altered adipose tissue and adipocyte function in the pathogenesis of metabolic syndrome. *The Journal of Clinical Investigation*, *129*(10), 3990–4000. https://doi.org/10.1172/JCI129187

Kawai, T., Autieri, M. V., & Scalia, R. (2021). Adipose tissue inflammation and metabolic dysfunction in obesity. *American Journal of Physiology-Cell Physiology*, *320*(3), C375–C391. https://doi.org/10.1152/ajpcell.00379.2020

Khalid, M., Alkaabi, J., Khan, M. A. B., & Adem, A. (2021). Insulin Signal Transduction Perturbations in Insulin Resistance. *International Journal of Molecular Sciences*, *22*(16), Article 16. https://doi.org/10.3390/ijms22168590

Khan, Mohd. P., Singh, A. K., Joharapurkar, A. A., Yadav, M., Shree, S., Kumar, H., Gurjar, A., Mishra, J. S., Tiwari, M. C., Nagar, G. K., Kumar, S., Ramachandran, R., Sharan, A., Jain, M. R., Trivedi, A. K., Maurya, R., Godbole, M. M., Gayen, J. R., Sanyal, S., & Chattopadhyay, N. (2015). Pathophysiological Mechanism of Bone Loss in Type 2 Diabetes Involves Inverse Regulation of Osteoblast Function by PGC-1α and Skeletal Muscle Atrogenes: AdipoR1 as a Potential Target for Reversing Diabetes-Induced Osteopenia. *Diabetes*, *64*(7), 2609–2623. https://doi.org/10.2337/db14-1611

Khan, S., Chan, Y. T., Revelo, X. S., & Winer, D. A. (2020). The Immune Landscape of VWAT During Obesity and Aging. *Frontiers in Endocrinology*, *11*. https://www.frontiersin.org/articles/10.3389/fendo.2020.00267

Kim, H., Bae, Y.-U., Lee, H., Kim, H., Jeon, J. S., Noh, H., Han, D. C., Byun, D. W., Kim, S. H., Park, H. K., Ryu, S., & Kwon, S. H. (2020). Effect of diabetes on exosomal miRNA profile in patients with obesity. *BMJ Open Diabetes Research and Care*, *8*(1), e001403. https://doi.org/10.1136/bmjdrc-2020-001403

Kita, S., Maeda, N., & Shimomura, I. (2019). Interorgan communication by exosomes, adipose tissue, and adiponectin in metabolic syndrome. *The Journal of Clinical Investigation*, *129*(10), 4041–4049. https://doi.org/10.1172/JCI129193

Kitada, M., Ogura, Y., Monno, I., & Koya, D. (2019). Sirtuins and Type 2 Diabetes: Role in Inflammation, Oxidative Stress, and Mitochondrial Function. *Frontiers in Endocrinology*, *10*. https://www.frontiersin.org/articles/10.3389/fendo.2019.00187

Lee, J. W., Ko, J., Ju, C., & Eltzschig, H. K. (2019). Hypoxia signaling in human diseases and therapeutic targets. *Experimental & Molecular Medicine*, *51*(6), Article 6. https://doi.org/10.1038/s12276-019-0235-1

Lee, P., Swarbrick, M. M., & Ho, K. K. Y. (2013). Brown Adipose Tissue in Adult Humans: A Metabolic Renaissance. *Endocrine Reviews*, *34*(3), 413–438. https://doi.org/10.1210/er.2012-1081

Lempesis, I. G., van Meijel, R. L. J., Manolopoulos, K. N., & Goossens, G. H. (2020). Oxygenation of adipose tissue: A human perspective. *Acta Physiologica*, *228*(1), e13298. https://doi.org/10.1111/apha.13298

Li, C., Menoret, A., Farragher, C., Ouyang, Z., Bonin, C., Holvoet, P., Vella, A. T., & Zhou, B. (2019). Single-cell transcriptomics–based MacSpectrum reveals macrophage activation signatures in diseases. *JCI Insight*, *4*(10). https://doi.org/10.1172/jci.insight.126453

Li, Q., Hagberg, C. E., Silva Cascales, H., Lang, S., Hyvönen, M. T., Salehzadeh, F., Chen, P., Alexandersson, I., Terezaki, E., Harms, M. J., Kutschke, M., Arifen, N., Krämer, N., Aouadi, M., Knibbe, C., Boucher, J., Thorell, A., & Spalding, K. L. (2021). Obesity and hyperinsulinemia drive adipocytes to activate a cell cycle program and senesce. *Nature Medicine*, *27*(11), Article 11. https://doi.org/10.1038/s41591-021-01501-8

Liang, Y.-Z., Li, J.-J.-H., Xiao, H.-B., He, Y., Zhang, L., & Yan, Y.-X. (2020). Identification of stress-related microRNA biomarkers in type 2 diabetes mellitus: A systematic review and meta-analysis. *Journal of Diabetes*, *12*(9), 633–644. https://doi.org/10.1111/1753-0407.12643

Liao, Z.-Z., Ran, L., Qi, X.-Y., Wang, Y.-D., Wang, Y.-Y., Yang, J., Liu, J.-H., & Xiao, X.-H. (2022). Adipose endothelial cells mastering adipose tissues metabolic fate. *Adipocyte*, *11*(1), 108–119. https://doi.org/10.1080/21623945.2022.2028372

Lin, Q., Gao, Z., Alarcon, R. M., Ye, J., & Yun, Z. (2009). A role of miR-27 in the regulation of adipogenesis. *The FEBS Journal*, *276*(8), 2348–2358. https://doi.org/10.1111/j.1742-4658.2009.06967.x

Lin, X., & Li, H. (2021). Obesity: Epidemiology, Pathophysiology, and Therapeutics. *Frontiers in Endocrinology*, *12*. https://www.frontiersin.org/articles/10.3389/fendo.2021.706978

Ling, H.-Y., Ou, H.-S., Feng, S.-D., Zhang, X.-Y., Tuo, Q.-H., Chen, L.-X., Zhu, B.-Y., Gao, Z.-P., Tang, C.-K., Yin, W.-D., Zhang, L., & Liao, D.-F. (2009). CHANGES IN microRNA (miR) PROFILE AND EFFECTS OF miR-320 IN INSULIN-RESISTANT 3T3-L1 ADIPOCYTES. *Clinical and Experimental Pharmacology and Physiology*, *36*(9), e32–e39. https://doi.org/10.1111/j.1440-1681.2009.05207.x

Liu, T., Zhang, L., Joo, D., & Sun, S.-C. (2017). NF-κB signaling in inflammation. *Signal Transduction and Targeted Therapy*, *2*(1), Article 1. https://doi.org/10.1038/sigtrans.2017.23

Lorente-Cebrián, S., Mejhert, N., Kulyté, A., Laurencikiene, J., Åström, G., Hedén, P., Rydén, M., & Arner, P. (2014). MicroRNAs Regulate Human Adipocyte Lipolysis: Effects of miR-145 Are Linked to TNF-α. *PLOS ONE*, *9*(1), e86800. https://doi.org/10.1371/journal.pone.0086800

Luo, L., & Liu, M. (2016). Adipose tissue in control of metabolism. *Journal of Endocrinology*, *231*(3), R77–R99. https://doi.org/10.1530/JOE-16-0211

Macdougall, C. E., Wood, E. G., Loschko, J., Scagliotti, V., Cassidy, F. C., Robinson, M. E., Feldhahn, N., Castellano, L., Voisin, M.-B., Marelli-Berg, F., Gaston-Massuet, C., Charalambous, M., & Longhi, M. P. (2018). VWAT Immune Homeostasis Is Regulated by the Crosstalk between Adipocytes and Dendritic Cell Subsets. *Cell Metabolism*, *27*(3), 588-601.e4. https://doi.org/10.1016/j.cmet.2018.02.007

Maniyadath, B., Zhang, Q., Gupta, R. K., & Mandrup, S. (2023). Adipose tissue at single-cell resolution. *Cell Metabolism*, *35*(3), 386–413. https://doi.org/10.1016/j.cmet.2023.02.002

Manna, P., & Jain, S. K. (2015). Obesity, Oxidative Stress, Adipose Tissue Dysfunction, and the Associated Health Risks: Causes and Therapeutic Strategies. *Metabolic Syndrome and Related Disorders*, *13*(10), 423–444. https://doi.org/10.1089/met.2015.0095

Massier, L., Jalkanen, J., Elmastas, M., Zhong, J., Wang, T., Nono Nankam, P. A., Frendo-Cumbo, S., Bäckdahl, J., Subramanian, N., Sekine, T., Kerr, A. G., Tseng, B. T. P., Laurencikiene, J., Buggert, M., Lourda, M., Kublickiene, K., Bhalla, N., Andersson, A., Valsesia, A., … Mejhert, N. (2023). An integrated single cell and spatial transcriptomic map of human white adipose tissue. *Nature Communications*, *14*(1), 1438. https://doi.org/10.1038/s41467-023-36983-2

Meerson, A., Traurig, M., Ossowski, V., Fleming, J. M., Mullins, M., & Baier, L. J. (2013). Human adipose microRNA-221 is upregulated in obesity and affects fat metabolism downstream of leptin and TNF-α. *Diabetologia*, *56*(9), 1971–1979. https://doi.org/10.1007/s00125-013-2950-9

Mentzel, C. M. J., Anthon, C., Jacobsen, M. J., Karlskov-Mortensen, P., Bruun, C. S., Jørgensen, C. B., Gorodkin, J., Cirera, S., & Fredholm, M. (2015). Gender and Obesity Specific MicroRNA Expression in Adipose Tissue from Lean and Obese Pigs. *PLOS ONE*, *10*(7), e0131650. https://doi.org/10.1371/journal.pone.0131650

Minamino, T., Orimo, M., Shimizu, I., Kunieda, T., Yokoyama, M., Ito, T., Nojima, A., Nabetani, A., Oike, Y., Matsubara, H., Ishikawa, F., & Komuro, I. (2009). A crucial role for adipose tissue p53 in the regulation of insulin resistance. *Nature Medicine*, *15*(9), 1082–1087. https://doi.org/10.1038/nm.2014

Mukherjee, B., Hossain, C. M., Mondal, L., Paul, P., & Ghosh, M. K. (2013). Obesity and Insulin Resistance: An Abridged Molecular Correlation. *Lipid Insights*, *6*, LPI.S10805. https://doi.org/10.4137/LPI.S10805

Nahmgoong, H., Jeon, Y. G., Park, E. S., Choi, Y. H., Han, S. M., Park, J., Ji, Y., Sohn, J. H., Han, J. S., Kim, Y. Y., Hwang, I., Lee, Y. K., Huh, J. Y., Choe, S. S., Oh, T. J., Choi, S. H., Kim, J. K., & Kim, J. B. (2022). Distinct properties of adipose stem cell subpopulations determine fat depot-specific characteristics. *Cell Metabolism*, *34*(3), 458-472.e6. https://doi.org/10.1016/j.cmet.2021.11.014

Nakanishi, N., Nakagawa, Y., Tokushige, N., Aoki, N., Matsuzaka, T., Ishii, K., Yahagi, N., Kobayashi, K., Yatoh, S., Takahashi, A., Suzuki, H., Urayama, O., Yamada, N., & Shimano, H. (2009). The up-regulation of microRNA-335 is associated with lipid metabolism in liver and white adipose tissue of genetically obese mice. *Biochemical and Biophysical Research Communications*, *385*(4), 492–496. https://doi.org/10.1016/j.bbrc.2009.05.058

Odegaard, J. I., & Chawla, A. (2012). Connecting Type 1 and Type 2 Diabetes through Innate Immunity. *Cold Spring Harbor Perspectives in Medicine*, *2*(3), a007724. https://doi.org/10.1101/cshperspect.a007724

O'Rourke, R. W., White, A. E., Metcalf, M. D., Olivas, A. S., Mitra, P., Larison, W. G., Cheang, E. C., Varlamov, O., Corless, C. L., Roberts, C. T., & Marks, D. L. (2011). Hypoxia-induced inflammatory

cytokine secretion in human adipose tissue stromovascular cells. *Diabetologia*, *54*(6), 1480–1490. https://doi.org/10.1007/s00125-011-2103-y

Palmer, A. K., Tchkonia, T., LeBrasseur, N. K., Chini, E. N., Xu, M., & Kirkland, J. L. (2015). Cellular Senescence in Type 2 Diabetes: A Therapeutic Opportunity. *Diabetes*, *64*(7), 2289–2298. https://doi.org/10.2337/db14-1820

Palmer, A. K., Xu, M., Zhu, Y., Pirtskhalava, T., Weivoda, M. M., Hachfeld, C. M., Prata, L. G., van Dijk, T. H., Verkade, E., Casaclang-Verzosa, G., Johnson, K. O., Cubro, H., Doornebal, E. J., Ogrodnik, M., Jurk, D., Jensen, M. D., Chini, E. N., Miller, J. D., Matveyenko, A., … Kirkland, J. L. (2019). Targeting senescent cells alleviates obesity-induced metabolic dysfunction. *Aging Cell*, *18*(3), e12950. https://doi.org/10.1111/acel.12950

Pan, Y., Hui, X., Hoo, R. L. C., Ye, D., Chan, C. Y. C., Feng, T., Wang, Y., Lam, K. S. L., & Xu, A. (2019). Adipocyte-secreted exosomal microRNA-34a inhibits M2 macrophage polarization to promote obesity-induced adipose inflammation. *The Journal of Clinical Investigation*, *129*(2), 834–849. https://doi.org/10.1172/JCI123069

Parrizas, M., Mundet, X., Castaño, C., Canivell, S., Cos, X., Brugnara, L., Giráldez-García, C., Regidor, E., Mata-Cases, M., Franch-Nadal, J., & Novials, A. (2020). miR-10b and miR-223-3p in serum microvesicles signal progression from prediabetes to type 2 diabetes. *Journal of Endocrinological Investigation*, *43*(4), 451–459. https://doi.org/10.1007/s40618-019-01129-z

Patsouris, D., Li, P.-P., Thapar, D., Chapman, J., Olefsky, J. M., & Neels, J. G. (2008). Ablation of CD11c-Positive Cells Normalizes Insulin Sensitivity in Obese Insulin Resistant Animals. *Cell Metabolism*, *8*(4), 301–309. https://doi.org/10.1016/j.cmet.2008.08.015

Pavillard, L. E., Cañadas-Lozano, D., Alcocer-Gómez, E., Marín-Aguilar, F., Pereira, S., Robertson, A. A. B., Muntané, J., Ryffel, B., Cooper, M. A., Quiles, J. L., Bullón, P., Ruiz-Cabello, J., & Cordero, M. D. (2017). NLRP3-inflammasome inhibition prevents high fat and high sugar diets-induced heart damage through autophagy induction. *Oncotarget*, *8*(59), 99740–99756. https://doi.org/10.18632/oncotarget.20763

Peng, J., Wu, Y., Deng, Z., Zhou, Y., Song, T., Yang, Y., Zhang, X., Xu, T., Xia, M., Cai, A., Liu, Z., & Peng, J. (2017). MiR-377 promotes white adipose tissue inflammation and decreases insulin sensitivity in obesity via suppression of sirtuin-1 (SIRT1). *Oncotarget*, *8*(41), 70550–70563. https://doi.org/10.18632/oncotarget.19742

Peng, J., Zhou, Y., Deng, Z., Zhang, H., Wu, Y., Song, T., Yang, Y., Wei, H., & Peng, J. (2018). miR-221 negatively regulates inflammation and insulin sensitivity in white adipose tissue by repression of sirtuin-1 (SIRT1). *Journal of Cellular Biochemistry*, *119*(8), 6418–6428. https://doi.org/10.1002/jcb.26589

Poirier, P., Giles, T. D., Bray, G. A., Hong, Y., Stern, J. S., Pi-Sunyer, F. X., & Eckel, R. H. (2006). Obesity and Cardiovascular Disease: Pathophysiology, Evaluation, and Effect of Weight Loss: An Update of the 1997 American Heart Association Scientific Statement on Obesity and Heart Disease From the Obesity Committee of the Council on Nutrition, Physical Activity, and Metabolism. *Circulation*, *113*(6), 898–918. https://doi.org/10.1161/CIRCULATIONAHA.106.171016

Qi, R., Wang, J., Wang, Q., Qiu, X., Yang, F., Liu, Z., & Huang, J. (2019). MicroRNA-425 controls lipogenesis and lipolysis in adipocytes. *Biochimica et Biophysica Acta (BBA) - Molecular and Cell Biology of Lipids*, *1864*(5), 744–755. https://doi.org/10.1016/j.bbalip.2019.02.007

Ramalingam, L., Oh, E., & Thurmond, D. C. (2013). Novel roles for insulin receptor (IR) in adipocytes and skeletal muscle cells via new and unexpected substrates. *Cellular and Molecular Life Sciences*, *70*(16), 2815–2834. https://doi.org/10.1007/s00018-012-1176-1

Rheinheimer, J., Souza, B. M. de, Cardoso, N. S., Bauer, A. C., & Crispim, D. (2017). Current role of the NLRP3 inflammasome on obesity and insulin resistance: A systematic review. *Metabolism - Clinical and Experimental*, *74*, 1–9. https://doi.org/10.1016/j.metabol.2017.06.002

Sárvári, A. K., Van Hauwaert, E. L., Markussen, L. K., Gammelmark, E., Marcher, A.-B., Ebbesen, M. F., Nielsen, R., Brewer, J. R., Madsen, J. G. S., & Mandrup, S. (2021). Plasticity of Epididymal Adipose Tissue in Response to Diet-Induced Obesity at Single-Nucleus Resolution. *Cell Metabolism*, *33*(2), 437-453.e5. https://doi.org/10.1016/j.cmet.2020.12.004

Sato, Y., Silina, K., van den Broek, M., Hirahara, K., & Yanagita, M. (2023). The roles of tertiary lymphoid structures in chronic diseases. *Nature Reviews Nephrology*, *19*(8), Article 8. https://doi.org/10.1038/s41581-023-00706-z

Seillet, C., & Jacquelot, N. (2019). Sensing of physiological regulators by innate lymphoid cells. *Cellular & Molecular Immunology*, *16*(5), Article 5. https://doi.org/10.1038/s41423-019-0217-1

Seo, J. B., Riopel, M., Cabrales, P., Huh, J. Y., Bandyopadhyay, G. K., Andreyev, A. Yu., Murphy, A. N., Beeman, S. C., Smith, G. I., Klein, S., Lee, Y. S., & Olefsky, J. M. (2019). Knockdown of Ant2 Reduces Adipocyte Hypoxia And Improves Insulin Resistance in Obesity. *Nature Metabolism*, *1*(1), 86–97. https://doi.org/10.1038/s42255-018-0003-x

Shay, J. W. (2016). Role of Telomeres and Telomerase in Aging and Cancer. *Cancer Discovery*, *6*(6), 584–593. https://doi.org/10.1158/2159-8290.CD-16-0062

Silva, H. M., Báfica, A., Rodrigues-Luiz, G. F., Chi, J., Santos, P. d'Emery A., Reis, B. S., Hoytema van Konijnenburg, D. P., Crane, A., Arifa, R. D. N., Martin, P., Mendes, D. A. G. B., Mansur, D. S., Torres, V. J., Cadwell, K., Cohen, P., Mucida, D., & Lafaille, J. J. (2019). Vasculature-associated fat macrophages readily adapt to inflammatory and metabolic challenges. *Journal of Experimental Medicine*, *216*(4), 786–806. https://doi.org/10.1084/jem.20181049

Smith, U., Li, Q., Rydén, M., & Spalding, K. L. (2021). Cellular senescence and its role in white adipose tissue. *International Journal of Obesity*, *45*(5), Article 5. https://doi.org/10.1038/s41366-021-00757-x

Song, P., Cao, K., Mao, Y., Ai, S., Sun, F., Hu, Q., Liu, S., Wang, M., Lu, X., Guan, W., & Shen, X. (2023). Tissue specific imprinting on innate lymphoid cells during homeostasis and disease process revealed by integrative inference of single-cell transcriptomics. *Frontiers in Immunology*, *14*. https://www.frontiersin.org/articles/10.3389/fimmu.2023.1127413

Sonnenberg, G. F., & Hepworth, M. R. (2019). Functional interactions between innate lymphoid cells and adaptive immunity. *Nature Reviews Immunology*, *19*(10), Article 10. https://doi.org/10.1038/s41577-019-0194-8

Stefanovic-Racic, M., Yang, X., Turner, M. S., Mantell, B. S., Stolz, D. B., Sumpter, T. L., Sipula, I. J., Dedousis, N., Scott, D. K., Morel, P. A., Thomson, A. W., & O'Doherty, R. M. (2012). Dendritic Cells Promote Macrophage Infiltration and Comprise a Substantial Proportion of Obesity-Associated Increases in CD11c+ Cells in Adipose Tissue and Liver. *Diabetes*, *61*(9), 2330–2339. https://doi.org/10.2337/db11-1523

Strissel, K. J., Stancheva, Z., Miyoshi, H., Perfield, J. W., DeFuria, J., Jick, Z., Greenberg, A. S., & Obin, M. S. (2007). Adipocyte death, adipose tissue remodeling, and obesity complications. *Diabetes*, *56*(12), 2910–2918. https://doi.org/10.2337/db07-0767

Sun, X., Lin, J., Zhang, Y., Kang, S., Belkin, N., Wara, A. K., Icli, B., Hamburg, N. M., Li, D., & Feinberg, M. W. (2016). MicroRNA-181b Improves Glucose Homeostasis and Insulin Sensitivity by Regulating Endothelial Function in White Adipose Tissue. *Circulation Research*, *118*(5), 810–821. https://doi.org/10.1161/CIRCRESAHA.115.308166

Swanson, K. V., Deng, M., & Ting, J. P.-Y. (2019). The NLRP3 inflammasome: Molecular activation and regulation to therapeutics. *Nature Reviews Immunology*, *19*(8), Article 8. https://doi.org/10.1038/s41577-019-0165-0

Tabula Muris Consortium. (2020). A single-cell transcriptomic atlas characterizes ageing tissues in the mouse. *Nature*, *583*(7817), 590–595. https://doi.org/10.1038/s41586-020-2496-1

Tchkonia, T., Morbeck, D. E., Von Zglinicki, T., Van Deursen, J., Lustgarten, J., Scrable, H., Khosla, S., Jensen, M. D., & Kirkland, J. L. (2010). Fat tissue, aging, and cellular senescence. *Aging Cell*, *9*(5), 667–684. https://doi.org/10.1111/j.1474-9726.2010.00608.x

Thomou, T., Mori, M. A., Dreyfuss, J. M., Konishi, M., Sakaguchi, M., Wolfrum, C., Rao, T. N., Winnay, J. N., Garcia-Martin, R., Grinspoon, S. K., Gorden, P., & Kahn, C. R. (2017). Adipose-derived circulating miRNAs regulate gene expression in other tissues. *Nature*, *542*(7642), Article 7642. https://doi.org/10.1038/nature21365

Trajkovski, M., Hausser, J., Soutschek, J., Bhat, B., Akin, A., Zavolan, M., Heim, M. H., & Stoffel, M. (2011). MicroRNAs 103 and 107 regulate insulin sensitivity. *Nature*, *474*(7353), 649–653. https://doi.org/10.1038/nature10112

Trayhurn, P. (2013). Hypoxia and Adipose Tissue Function and Dysfunction in Obesity. *Physiological Reviews*, *93*(1), 1–21. https://doi.org/10.1152/physrev.00017.2012

Vandanmagsar, B., Youm, Y.-H., Ravussin, A., Galgani, J. E., Stadler, K., Mynatt, R. L., Ravussin, E., Stephens, J. M., & Dixit, V. D. (2011). The NLRP3 inflammasome instigates obesity-induced inflammation and insulin resistance. *Nature Medicine*, *17*(2), Article 2. https://doi.org/10.1038/nm.2279

Vijay, J., Gauthier, M.-F., Biswell, R. L., Louiselle, D. A., Johnston, J. J., Cheung, W. A., Belden, B., Pramatarova, A., Biertho, L., Gibson, M., Simon, M.-M., Djambazian, H., Staffa, A., Bourque, G., Laitinen, A., Nystedt, J., Vohl, M.-C., Fraser, J. D., Pastinen, T., … Grundberg, E. (2020). Single-cell

analysis of human adipose tissue identifies depot- and disease-specific cell types. *Nature Metabolism*, *2*(1), Article 1. https://doi.org/10.1038/s42255-019-0152-6

Wang, Q. A., Tao, C., Gupta, R. K., & Scherer, P. E. (2013). Tracking adipogenesis during white adipose tissue development, expansion and regeneration. *Nature Medicine*, *19*(10), Article 10. https://doi.org/10.1038/nm.3324

Wang, Q., Wang, Y., & Xu, D. (2021). The roles of T cells in obese adipose tissue inflammation. *Adipocyte*, *10*(1), 435–445. https://doi.org/10.1080/21623945.2021.1965314

Weisberg, S. P., McCann, D., Desai, M., Rosenbaum, M., Leibel, R. L., & Ferrante, A. W. (2003). Obesity is associated with macrophage accumulation in adipose tissue. *The Journal of Clinical Investigation*, *112*(12), 1796–1808. https://doi.org/10.1172/JCI19246

Wu, K. K.-L., Cheung, S. W.-M., & Cheng, K. K.-Y. (2020). NLRP3 Inflammasome Activation in Adipose Tissues and Its Implications on Metabolic Diseases. *International Journal of Molecular Sciences*, *21*(11), 4184. https://doi.org/10.3390/ijms21114184

Xie, H., Lim, B., & Lodish, H. F. (2009). MicroRNAs Induced During Adipogenesis that Accelerate Fat Cell Development Are Downregulated in Obesity. *Diabetes*, *58*(5), 1050–1057. https://doi.org/10.2337/db08-1299

Xu, G., Ji, C., Song, G., Zhao, C., Shi, C., Song, L., Chen, L., Yang, L., Huang, F., Pang, L., Zhang, N., Zhao, Y., & Guo, X. (2015). MiR-26b modulates insulin sensitivity in adipocytes by interrupting the PTEN/PI3K/AKT pathway. *International Journal of Obesity*, *39*(10), Article 10. https://doi.org/10.1038/ijo.2015.95

Yáñez-Mó, M., Siljander, P. R. -M., Andreu, Z., Bedina Zavec, A., Borràs, F. E., Buzas, E. I., Buzas, K., Casal, E., Cappello, F., Carvalho, J., Colás, E., Cordeiro-da Silva, A., Fais, S., Falcon-Perez, J. M., Ghobrial, I. M., Giebel, B., Gimona, M., Graner, M., Gursel, I., … De Wever, O. (2015). Biological properties of extracellular vesicles and their physiological functions. *Journal of Extracellular Vesicles*, *4*(1), 27066. https://doi.org/10.3402/jev.v4.27066

Yao, F., Yu, Y., Feng, L., Li, J., Zhang, M., Lan, X., Yan, X., Liu, Y., Guan, F., Zhang, M., & Chen, L. (2017). Adipogenic miR-27a in adipose tissue upregulates macrophage activation via inhibiting PPARγ of insulin resistance induced by high-fat diet-associated obesity. *Experimental Cell Research*, *355*(2), 105–112. https://doi.org/10.1016/j.yexcr.2017.03.060

Ye, J., Gao, Z., Yin, J., & He, Q. (2007). Hypoxia is a potential risk factor for chronic inflammation and adiponectin reduction in adipose tissue of ob/ob and dietary obese mice. *American Journal of Physiology-Endocrinology and Metabolism*, *293*(4), E1118–E1128. https://doi.org/10.1152/ajpendo.00435.2007

Ying, W., Riopel, M., Bandyopadhyay, G., Dong, Y., Birmingham, A., Seo, J. B., Ofrecio, J. M., Wollam, J., Hernandez-Carretero, A., Fu, W., Li, P., & Olefsky, J. M. (2017). Adipose Tissue Macrophage-Derived Exosomal miRNAs Can Modulate In Vivo and In Vitro Insulin Sensitivity. *Cell*, *171*(2), 372-384.e12. https://doi.org/10.1016/j.cell.2017.08.035

Yung, J. H. M., & Giacca, A. (2020). Role of c-Jun N-terminal Kinase (JNK) in Obesity and Type 2 Diabetes. *Cells*, *9*(3), Article 3. https://doi.org/10.3390/cells9030706

Zatterale, F., Longo, M., Naderi, J., Raciti, G. A., Desiderio, A., Miele, C., & Beguinot, F. (2020). Chronic Adipose Tissue Inflammation Linking Obesity to Insulin Resistance and Type 2 Diabetes. *Frontiers in Physiology*, *10*. https://www.frontiersin.org/articles/10.3389/fphys.2019.01607

Zhang, M., Zhou, Z., Wang, J., & Li, S. (2016). MiR-130b promotes obesity associated adipose tissue inflammation and insulin resistance in diabetes mice through alleviating M2 macrophage polarization via repression of PPAR-γ. *Immunology Letters*, *180*, 1–8. https://doi.org/10.1016/j.imlet.2016.10.004

Zhang, S., Gang, X., Yang, S., Cui, M., Sun, L., Li, Z., & Wang, G. (2021). The Alterations in and the Role of the Th17/Treg Balance in Metabolic Diseases. *Frontiers in Immunology*, *12*. https://www.frontiersin.org/articles/10.3389/fimmu.2021.678355

Zhang, Y., Li, C., Li, H., Song, Y., Zhao, Y., Zhai, L., Wang, H., Zhong, R., Tang, H., & Zhu, D. (2016). miR-378 Activates the Pyruvate-PEP Futile Cycle and Enhances Lipolysis to Ameliorate Obesity in Mice. *EBioMedicine*, *5*, 93–104. https://doi.org/10.1016/j.ebiom.2016.01.035

Zheng, S., Guo, S., Sun, G., Shi, Y., Wei, Z., Tang, Y., He, F., Shi, C., Dai, P., Chong, H., Samuelson, I., Zen, K., Zhang, C.-Y., Zhang, Y., Li, J., & Jiang, X. (2019). Gain of Metabolic Benefit with Ablation of miR-149-3p from Subcutaneous Adipose Tissue in Diet-Induced Obese Mice. *Molecular Therapy - Nucleic Acids*, *18*, 194–203. https://doi.org/10.1016/j.omtn.2019.07.024

Zhu, H., & Leung, S. W. (2015). Identification of microRNA biomarkers in type 2 diabetes: A meta-analysis of controlled profiling studies. *Diabetologia*, *58*(5), 900–911. https://doi.org/10.1007/s00125-015-3510-2

Zhuang, G., Meng, C., Guo, X., Cheruku, P. S., Shi, L., Xu, H., Li, H., Wang, G., Evans, A. R., Safe, S., Wu, C., & Zhou, B. (2012). A Novel Regulator of Macrophage Activation. *Circulation*, *125*(23), 2892–2903. https://doi.org/10.1161/CIRCULATIONAHA.111.087817

Chapter 3 | miR-210-3p promotes Adipose Tissue Macrophage Inflammation in Obesity

3.1 Background

Increased accumulation of body fat in obesity is considered the highest risk factor for the development of several metabolic diseases including IR and T2D (Hotamisligil et al., 1995; Qatanani & Lazar, 2007; Xu et al., 2003). Excess storage of fat inside the adipocytes leads to the formation of hypertrophied adipocytes which by releasing higher levels of circulatory free fatty acids (FFAs) induce a state of chronic low-grade inflammation in adipocytes and adipose tissue macrophages (ATMs) resulting in the onset of obesity-induced adipose tissue inflammation. Obesity-induced enhancement of FFAs is accompanied by the reduction of adipose tissue vascularisation creating a zone deprived of adequate oxygen and nutrients. Accumulating evidence revealed a considerable drop in partial pressure of oxygen (pO_2) referred to as hypoxia in the subcutaneous and vWAT of obese diabetic patients as compared to lean non-diabetic subjects. It has been shown that adipose tissue hypoxia plays a major role in adipose tissue inflammation and insulin resistance during the state of chronic obesity. Hypoxic adipocytes promote adipose tissue inflammation by secreting various proinflammatory cytokines and chemokines. The inflammatory chemokines such as CCL2/MCP1 aggravate the adipose tissue inflammation by heightened infiltration of macrophages and its polarization towards the M1 phenotype as evident in the obese adipose tissue of patients and mice (Blüher, 2016; Fuster et al., 2016; Pasarica et al., 2009; Ye et al., 2007).

Exploring the involvement of non-coding RNAs particularly microRNAs in the obese hypoxic adipose tissue, it appeared that *miR-210* is a well-known hypoxia-inducible miRNA. Recent shreds of evidence have shown that diabetic patients as well as diabetic animal models have abnormally high levels of *miR-210.* In clinical studies, elevated level of *miR-210* has been detected in both adolescent T1D and T2D patients. From these above facts, we are interested in investigating any potential role of *miR-210-3p* in ATMs for causing obesity-induced chronic low-grade inflammation (Amr et al., 2018; Chan et al., 2012; Liu et al., 2021; Osipova et al., 2014).

Although the lone effects of palmitate or hypoxia on adipocyte function and insulin resistance have been well studied, however, the combined impact of high lipid content along with hypoxia on ATM inflammation has not been clearly understood yet. In this study, we have found that the obese hypoxic AT*env* stimulates the increased expression of *miR-210-3p* in the ATMs that provoked inflammation and its polarization towards the M1 phenotype via the SOCS-1/NF-κB pathway. Suppression of *miR-210-3p* markedly attenuated adipose tissue inflammation with the improvement of insulin sensitivity. Therefore, targeting ATM-specific *miR-210-3p* could be an excellent strategy to regulate obesity

induced adipose tissue inflammation for the management of IR and T2D (Pasarica et al., 2009; Wang et al., 2007).

3.2 Results

3.2.1 Obesity-associated hypoxic state of adipose tissue microenvironment potentiates increased expression of *miR-210-3p* in ATMs

Investigating pathophysiological adipose tissue microenvironment (AT*env*) of obese diabetic state, we have found a marked induction of hypoxia and lipid accumulation in the vWAT (VAT) of obese T2D patients and high fat diet-induced (HFD) obese diabetic mice model (**Fig. 3.1K**) as evident from the HIF1α levels (**Fig. 3.1A-B and Fig. 3.1M**) and lipid staining (Oil red-O and BODIPY F16) (**Fig. 3.1A-B and Fig. 3.1L**) in comparison with their control counterparts. This was further confirmed by the significant enhancement of TG levels in the VAT of obese diabetic patients and HFD mice (**Fig. 3.1C**) along with the lowering of oxygen tension indicated by Image-iT green hypoxia staining in the VAT of HFD mice (**Fig. 3.1D**) as compared to controls. These results indicate the dyslipidemic and hypoxic state of obese diabetic AT*env*. We also noticed a significant accumulation of macrophage population in the VAT of obese diabetic patients and HFD mice model as indicated by CD68 and F4/80 staining (**Fig. 3.1E,F**) which coincided with the inflammatory landscape as evident from the increased level of iNOS over ARG1 (**Fig. 3.1E,F**) and various proinflammatory cytokines gene expression (**Fig. 1O**).

Since adipose tissue macrophages (ATMs) play a crucial role in obesity-associated chronic inflammation and insulin resistance, therefore, we are interested in exploring the involvement of specific microRNAs (miRNAs) therein. To investigate the specific hypoxia-induced miRNAs in the ATMs of obese diabetic AT*env*, we searched existing literature and considered a GEO database (GSE97652) that comprised a miRNA dataset of ATM-derived exosomes (ATM-Exos) obtained from lean and obese mice. We reanalyzed the dataset and filtered out the primary miRNAs associated with hypoxic conditions**.** Interestingly, the volcano plot derived from the DESeq2 analysis of the GSE97652 dataset (**Fig. 3.1G**) showed six differentially expressed hypoxia-regulated miRNAs (*miR-210-5p, miR-210-3p, miR-27a-5p, miR-27b-5p, miR-101b-5p, and miR-128-1-5p*) in ATM-Exos of the obese mouse as compared to lean one. Data showcased in **Fig. 3.1H** shows read count distribution boxplots for these miRNAs in the ATM-Exos of lean and obese mice. Among these miRNAs, *miR-210-3p* exhibited maximum induction of ~4-fold increase in obese mice in comparison to lean controls (**Fig. 3.1I**). This finding encouraged us to examine the *miR-210-3p* level in the ATMs of obese diabetic patients, and HFD-induced diabetic mouse model. As expected, we observed a profound increase of *miR-210-3p* a higher level of *miR-210-3p* is a key signature in the ATMs of the pathophysiological obese diabetic condition(**Fig. 3.1J**).

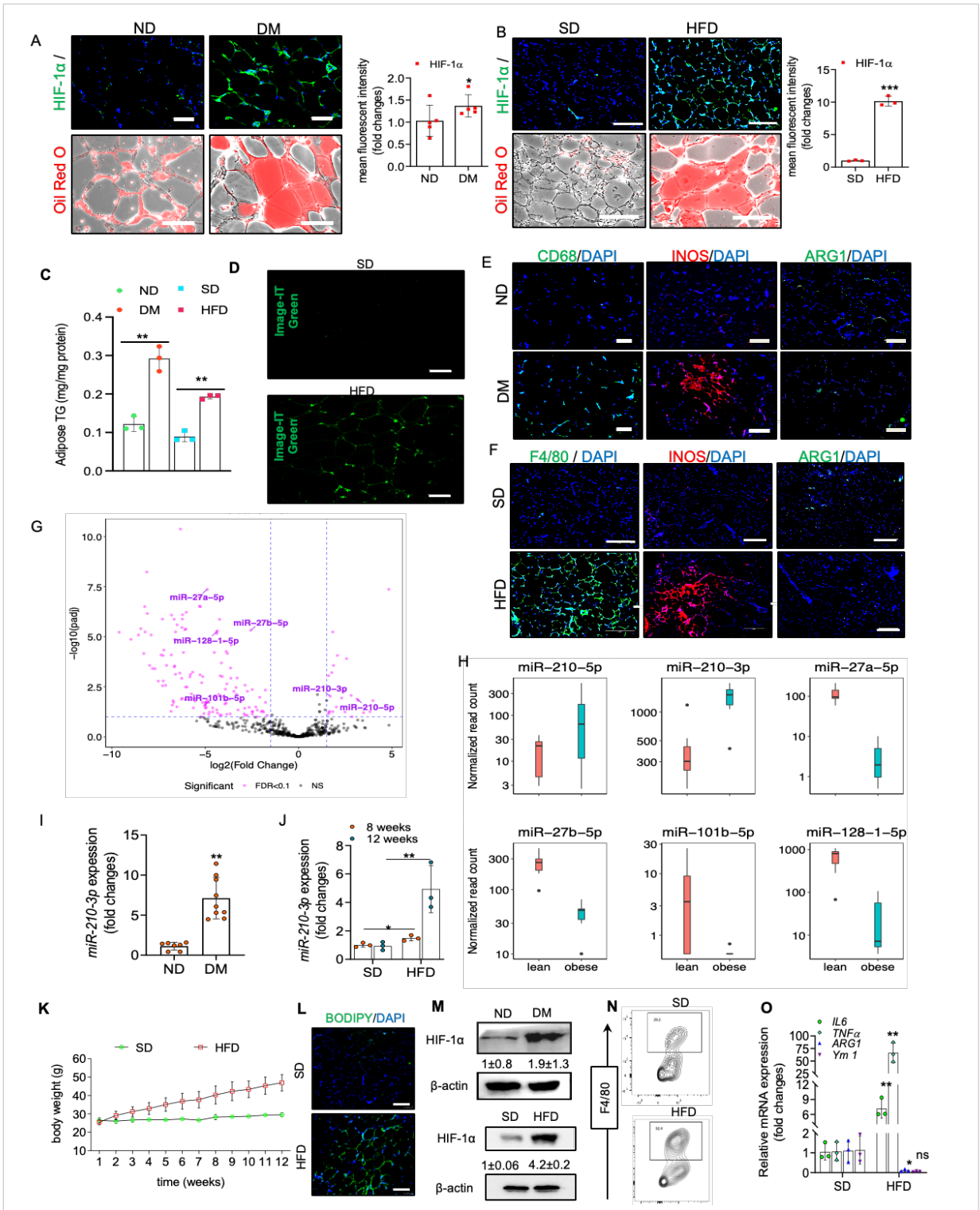

Figure 3.1 | **Lipid-rich low oxygen tension in obese AT*env* potentiates high *miR-210-3p* expression in ATMs.**

(A-B) Representative images of human (A) and mice (B) VAT sections with HIF1α immunohistochemical staining or Oil red O staining with quantification data; Scale bar, 100µm. n=5, *p<0.05; for patients sample and Scale bar,200µm. n=3, for mice ***p<0.001 (student's t-test). (C) VAT Triglyceride level was measured in patients (ND and DM) and mice (SD and HFD) (D) Image-IT green hypoxia staining of VAT sections of SD and HFD mice. Scale bar size, 100µm.(E) Immunohistochemical analysis of CD68, iNOS, and ARG1 in ND and obese diabetic (DM) patients VAT and its quantification analyses. Scale bar, 100µm. (F) Representative images of SD and HFD

mice VAT sections with F4/80, iNOS and ARG1 immunohistochemical staining. Scale bar, 200µm. (G) Volcano plot derived from the DESeq2 analysis of GSE97652 dataset indicates miRNAs differential expressed between obese and lean samples. Y-axis denotes -log10 of p-adjusted values obtained from the DESeq2 pipeline, and log2 fold changes are plotted on the X-axis. Red dots indicate significant miRNAs that passed certain criteria filters (FDR < 0.1 and |log2FC| >1.5), while black dots are considered non-significant. Annotated miRNAs with purple text are of special interest. (H) Read count distribution boxplots for five miRNAs of interest overlapped with differentially expressed miRNAs. Y-axis indicates normalized read counts on the log10 scale. The X-axis indicates two different levels of condition for mice. (I) Quantitative RT-PCR analyses of *miR-210-3p* in ATMs of ND and DM patients. n=7-9, **p<0.01(J) Relative expression of *miR-210-3p* in F4/80+ sorted ATMs from vWAT from SD and HFD mice of 8 weeks, 12 weeks. n=3,***p<0.001. (K) Body weight of C57BL/6 mice fed with SD or HFD for 12 weeks and body weight was measured. (L) Immunofluorescence images showing BODIPY staining and quantification of mean fluorescence intensity in the adipose tissue section of SD and HFD mice. scale bar, 150µm. (M) HIF-1α protein expression was analyzed in the SVF of control (ND) and DM patients VAT and in ATMs of SD and HFD mice VAT. (N) Flow cytometry analyses of F4/80+ macrophages in SVF of SD and HFD VAT. (O) qRT-PCR analyses showed the expression of inflammatory cytokines (*IL6*, *TNF-a*, *ARG1*, *Ym1*) in F4/80+ ATMs from SD and HFD mice.

3.2.2 Inhibition of *miR-210-3p* protects HL-induced macrophage inflammation and its polarization

Since ATMs are the main source of inflammatory cytokine production in the obesity-induced inflamed adipose tissue and that caused its dysfunction (Martin, 2011), we, therefore, questioned how increased expression of *miR-210-3p* in obese AT*env* governed the ATM inflammation and adipocyte dysfunction. To explore this, we first set up an *in-vitro* condition where RAW 264.7 macrophages were co-incubated with 1%O_2 and 0.75mM palmitate for different time periods to simulate the pathophysiological condition of obese AT*env* and analysed *miR-210-3p* expression. Co-exposure of both hypoxia and lipid (HL) significantly increased the *miR-210-3p* and HIF1α levels at 16h in RAW 264.7 cells (**Fig. 3.2A and Fig. 3.2M,N).** Hypoxia and lipid alone stimulation augment *miR-210-3p* expression in macrophages but the co-exposure of both hypoxia and palmitate potentiates *miR-210-3p* expression in macrophages to a greater extent (**Fig. 3.2B**). Moreover, HL co-exposure notably stimulates various pro-inflammatory cytokines gene expression (**Fig. 3.2C**) as compared to the lone effect of hypoxia or lipid (**Fig. 3.2O**). Immunofluorescence staining of iNOS and ARG1 further confirmed that co-exposure of HL soared the iNOS levels in concomitance with the reduction of ARG1 levels in RAW 264.7 macrophages (**Fig. 3.2D and Fig. 3.2P-R**).

For a better understanding of the inflammatory nature of HL-treated macrophages, we examined the expression profile of 21 different inflammatory genes and found a significant upregulation of *NOS2*, *TNF-α*, *CXCL5*, *IL6*, *CCL2*, *IL1β*, *CD80*, *CD86*, *MHCII*, and *CCR2* gene expression and downregulation of *IL10*, *IL4*, *Ym1*, *CD206*, *CD163* gene expressions (**Fig. 3.2E**) which depicting M1 macrophage phenotype. Furthermore, a significant enhancement of proinflammatory cytokines gene expression was observed due to HL in IL4 induced M2 macrophages (**Fig. 3.2S**) suggesting M2 to M1

polarization shift. For more clarification, we have performed flow cytometric analysis of M1 (CD80) and M2 (CD206) phenotypic markers. A massive induction of $CD80^{+}CD206^{-}$ population (~80 fold) was noticed in HL-treated RAW264.7 cells as compared to control (**Fig. 3.2T**). For further validation, we have isolated ATMs ($CD11b^{+}CD64^{+}$) from VAT of non-diabetic and obese diabetic subjects and analysed CD80 (M1) and CD163 (M2) surface markers. Sorted ATMs of obese diabetic patients displayed an enhanced level of M1 over the M2 marker by expressing high CD80 and low CD163 (**Fig. 3.2U**). Similarly, high CD80 with low CD206 was observed in $F4/80^{+}$ ATM populations of HFD mice as compared to SD mice (**Fig. 3.2V**). All these results indicate that the obese hypoxic state of AT*env* influence macrophages' M1 state with a higher level of *miR-210-3p* expression, suggesting a possible link of *miR-210-3p* with obesity-induced adipose tissue inflammation.

To investigate the direct effect of *miR-210* on macrophage M1 polarization and inflammation, RAW264.7 macrophages were transfected with *miR-210-3p* mimic or inhibitor in the absence and presence of HL microenvironment followed by the analysis of M1/M2 populations through flow cytometry. Interestingly, *miR-210-3p* inhibition significantly reduced CD80(M1) levels along with the induction of CD206(M2) in HL-treated macrophages (**Fig. 3.2F and Fig. 3.2W**). Concomitantly, we noticed suppression of proinflammatory cytokines genes (*TNF-α*, *iNOS*, and *IL6*) expression along with the upregulation of anti-inflammatory cytokines genes (*IL4*, *IL13*, and *Ym1*) expression in *miR-210-3p* inhibited HL-treated macrophages (**Fig. 3.2G**). ELISA analysis further confirmed higher levels of IL6 and TNF-α cytokine secretion from the HL-stimulated macrophages, and this was significantly prevented in the presence of *miR-210-3p* inhibitor as compared to the control inhibitor (**Fig. 3.2H**). Since *miR-210-3p* inhibited macrophages are protected from HL-induced inflammation, iNOS and ARG1 levels remain unaltered under the HL microenvironment (**Fig. 3.2I**).

On the contrary, introducing *miR-210-3p* mimic markedly upregulates the CD80 level in macrophages in absence of HL stimulation (**Fig. 3.2J**). Furthermore, induction of proinflammatory gene expression along with the reduction of anti-inflammatory *Ym1* gene expression (**Fig. 3.2K**) coincided with the increased levels of iNOS and subdued levels of ARG1 (**Fig. 3.2L**) were observed in *miR-210-3p* mimic transfected cells. Since obese adipose tissue has a profound accumulation of macrophages which releases a considerable amount of *miR-210-3p* in the exosomes, we are therefore interested to see the impact of *miR-210-3p* in nearby adipocytes. For this, miR-210-3p mimic was transfected in 3T3-L1 adipocytes and found thatmiR-210-3p mimic significantly increased NF-κB activation, as well as upregulation of proinflammatory cytokines (*iNOS*, *MCP1*) gene expression without any notable alteration of anti-inflammatory cytokines (*IL4*, *IL10*) gene expression (**Fig. S3.2X,Y**). These results vowed a direct role of *miR-210-3p* in ATM and adipocyte inflammation favouring a state of inflamed adipose tissue that facilitates macrophage polarity switching toward the M1 proinflammatory phenotype.

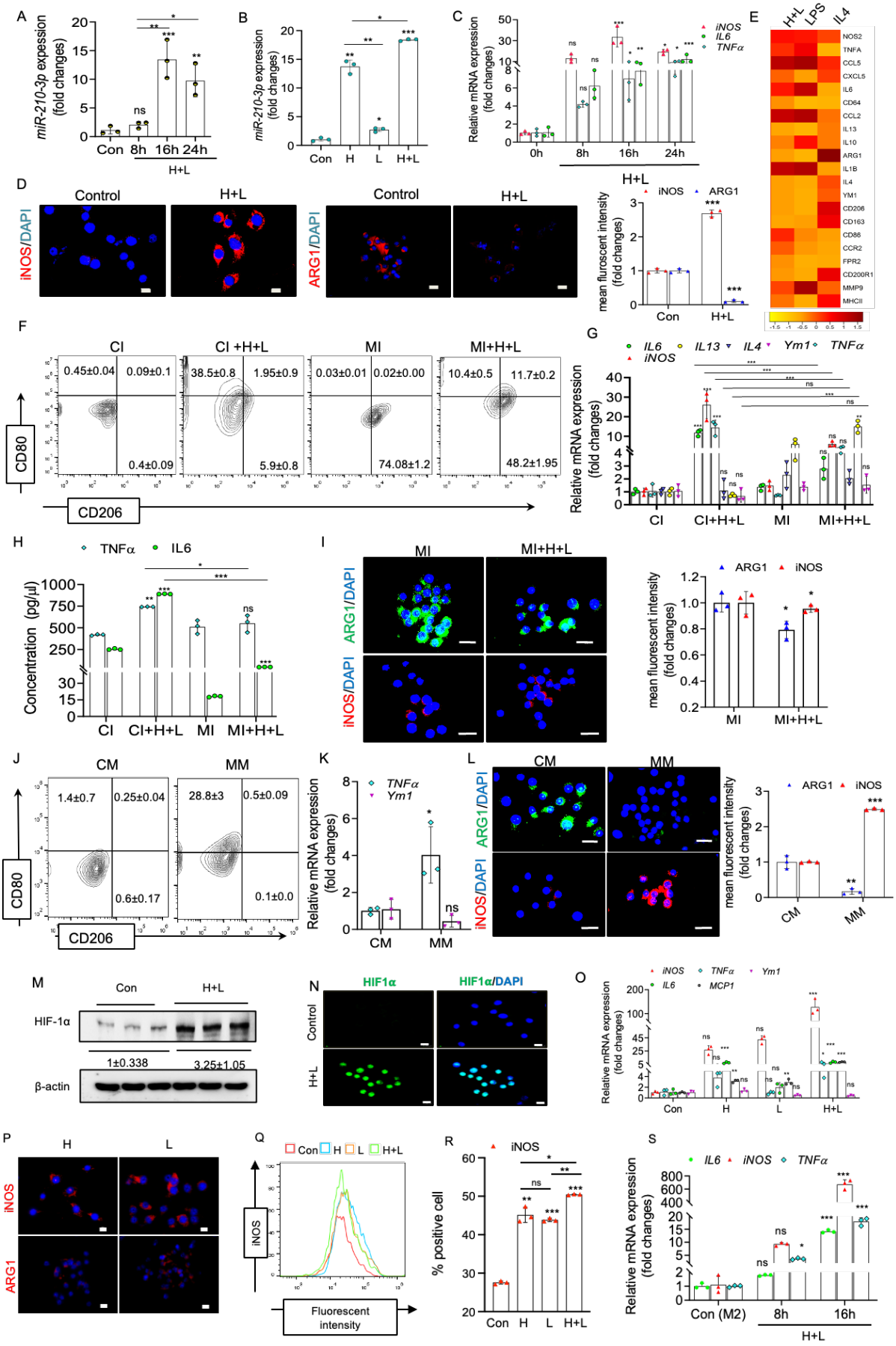
A
miR-210-3p expression (fold changes)
Con 8h 16h 24h
H+L
B
miR-210-3p expression (fold changes)
Con H L H+L
C
Relative mRNA expression (fold changes)
iNOS IL6 TNFα
0h 8h 16h 24h
E
H+L LPS IL4
NOS2 TNFA CCL5 CXCL5 IL6 CD64 CCL2 IL13 IL10 ARG1 IL1B IL4 YM1 CD206 CD163 CD86 CCR2 FPR2 CD200R1 MMP9 MHCII
D
Control H+L Control H+L
iNOS/DAPI ARG1/DAPI
H+L
iNOS ARG1
mean fluroscent intensity (fold changes)
Con H+L
F
CI CI +H+L MI MI+H+L
0.45±0.04 0.09±0.1 0.4±0.09
38.5±0.8 1.95±0.9 5.9±0.8
0.03±0.01 0.02±0.00 74.08±1.2
10.4±0.5 11.7±0.2 48.2±1.95
CD80
CD206
G
IL6 IL13 IL4 Ym1 TNFα iNOS
Relative mRNA expression (fold changes)
CI CI+H+L MI MI+H+L
H
TNFα IL6
Concentration (pg/μl)
CI CI+H+L MI MI+H+L
I
MI MI+H+L
ARG1/DAPI iNOS/DAPI
ARG1 iNOS
mean fluorescent intensity (fold changes)
MI MI+H+L
J
CM MM
1.4±0.7 0.25±0.04 0.6±0.17
28.8±3 0.5±0.09 0.1±0.0
CD80
CD206
K
TNFα Ym1
Relative mRNA expression (fold changes)
CM MM
L
CM MM
ARG1/DAPI iNOS/DAPI
ARG1 iNOS
mean fluorescent intensity (fold changes)
CM MM
M
Con H+L
HIF-1α
1±0.338 3.25±1.05
β-actin
N
HIF1α HIF1α/DAPI
Control H+L
O
iNOS TNFα Ym1 IL6 MCP1
Relative mRNA expression (fold changes)
Con H L H+L
P
H L
iNOS ARG1
Q
Con H L H+L
iNOS
Fluorescent intensity
R
iNOS
% positive cell
Con H L H+L
S
IL6 iNOS TNFα
Relative mRNA expression (fold changes)
Con (M2) 8h 16h
H+L

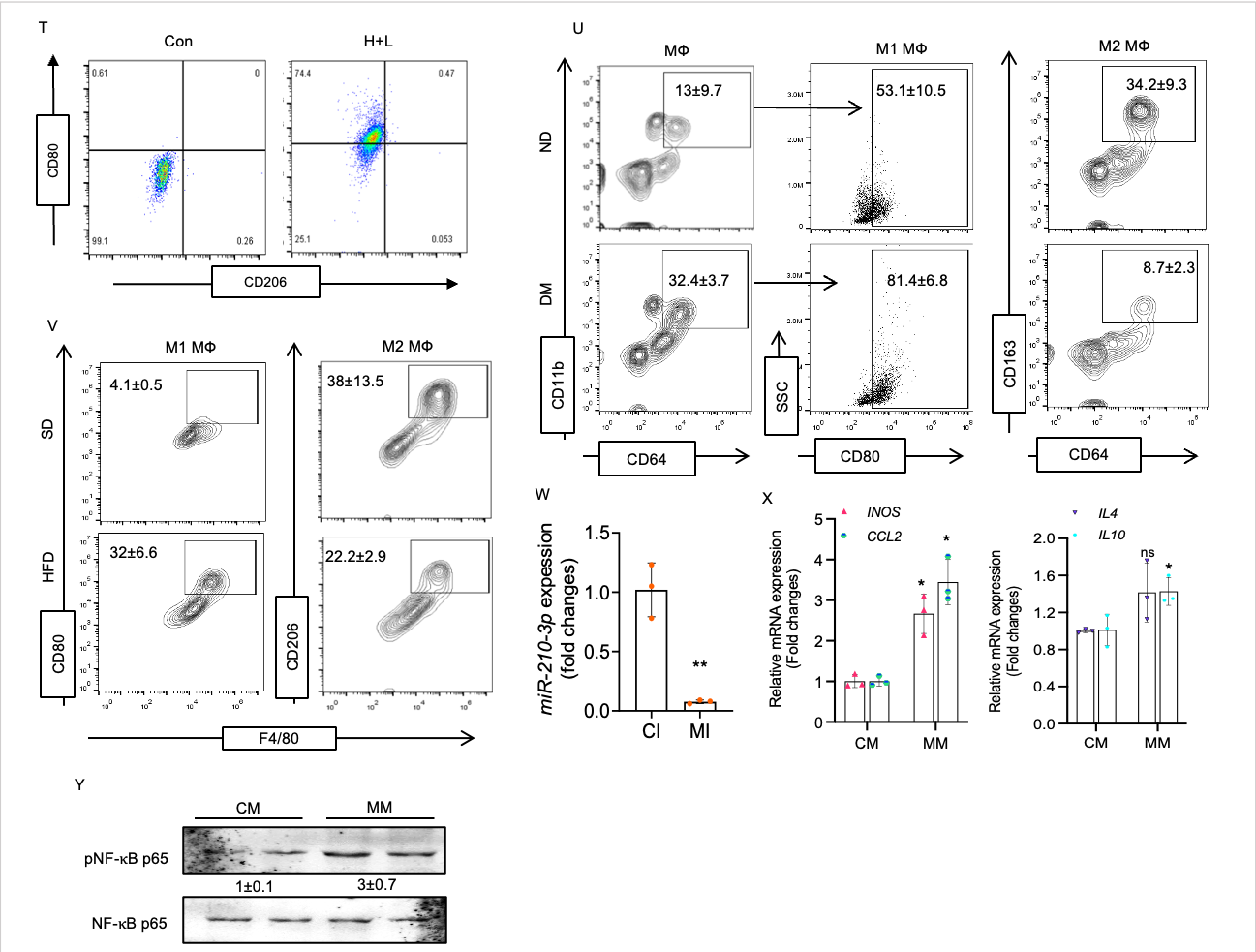

Figure 3.2 |**Chronic obese AT*env* promotes ATMs skewing towards M1**

(A-B) qRT-PCR analyses of *miR-210-3p* expression in RAW264.7 murine macrophages, co-incubated with hypoxia(H) and lipid(L) for different time periods (A) and treated with hypoxia or lipid alone or in combination of hypoxia and lipid for 16 hours (B). n=3, *p<0.05, **p<0.01, ***p<0.001 or ns.(C) Relative mRNA expression of proinflammatory cytokines *iNOS*, *IL6*, and *TNF-α* in HL co-stimulated macrophages for different time periods (8,16, 24 hours) n=3, *p<0.05, **p<0.01, ***p<0.001 or ns. (D) Immunofluorescence analysis of iNOS (left panel) and ARG1 (right panel) expression with quantification analyses in murine macrophages co-treated with or without HL. DAPI was used for nuclear staining. Scale bar, 10μM. n=3, ***p<0.001. (E) Quantitative RT-PCR analyses of different pro-inflammatory and anti-inflammatory markers in HL treated macrophages for 16 hours. LPS and IL4 treatment were considered as positive control for M1 and M2 phenotype macrophage respectively. (F) Flow cytometry analyses for CD80 and CD206 in control inhibitor (CI) or *miR-210-3p* inhibitor (MI) treated mouse macrophages co-incubated with or without HL. n=3, **p<0.01 (G) Quantitative RT-PCR analyses of proinflammatory cytokines (*iNOS*, *TNF-α*, *IL6)* and anti-inflammatory cytokines (*Ym1*, *IL4*, *IL13*) in CI or MI treated mouse macrophages co-incubated with or without HL. n=3, **p<0.01, ***p<0.001 or ns. (H) Quantification of extracellular release of IL6 and TNF-α in CI or MI treated mouse macrophages co-incubated with or without HL. n=3, *p<0.05, **p<0.01, ***p<0.001 or ns. (I) Immunofluorescence analysis of iNOS and ARG1 expression (left panel) in CI or MI-treated macrophages co-incubated with or without HL and quantification analyses (right panel). DAPI was used for nuclear staining. scale bar, 20μM. n=3, *p<0.05 (J) Flow cytometry analyses for CD80 and CD206 in control mimic (CM) or *miR-210-3p* mimic (MM) treated macrophages. (K) Relative gene expression of *TNF-α* and *Ym1* in CM or MM treated macrophages. n=3, *p<0.05 or ns. (L) Immunofluorescence analysis (left) of iNOS and ARG1 expression in CM or MM treated macrophages

and quantification analyses (right). DAPI was used for nuclear staining. scale bar 20µm. n=3, *p<0.05 or **p<0.01. (M) Immunoblot analyses showed HIF-1α expression in RAW264.7 macrophage co-treated with or without hypoxia and lipid. (N) Immunofluorescence monograph depicts HIF-1α (green) expression and nuclear localization in RAW 264.7 macrophages in the presence or absence of HL. Colocalization quantification was performed using pearson coefficient. scale bar size, 10µM. (O) mRNA expression analysis of pro-inflammatory (*IL6*, *iNOS*, *TNFa*, *MCP1*) and anti-inflammatory cytokine (*Ym1*) in RAW264.7 macrophages under different conditions. (P) Immunofluorescence analyses of iNOS and ARG1 in RAW 264.7 macrophages exposed to hypoxia or lipid individually. scale bar size, 10µm. (Q,R) Flow cytometry analysis for iNOS in macrophage cells under different conditions and quantification analyses. (S) Quantitative RT-PCR analyses of proinflammatory cytokines (*iNOS*, *TNFa*, *IL6*) in mouse macrophage differentiated into M2 phenotype then co-incubated with hypoxia and lipid for different time periods. (T) Flow cytometry analysis of $CD80^+$ and $CD206^+$ expression in RAW264.7 macrophages under hypoxia and lipid co-exposure. (U) Flow cytometry analysis for $CD11b^+/CD64^+$, $CD80^+$, $CD64^+/CD163^+$ positive cells from single cell suspension of stromal vascular fraction isolated from VAT of control (ND) and obese diabetic patients (DM). (V) Flow cytometry analysis for $F4/80^+/CD80^+$, $F4/80^+/CD206^+$ positive cells from single cell suspension of stromal vascular fraction isolated from VAT of SD and HFD mice. (W) qRT-PCR analyses of *miR-210-3p* expression in murine macrophages transfected with control inhibitor (CI) and miR-210-3p inhibitor (MI). (X) qRT-PCR analyses showed relative mRNA expression of proinflammatory genes *iNOS*, *MCP1* and anti-inflammatory genes *IL4, IL10* in adipocytes transfected control mimic (CM) and miR-210-3p mimic MM. (Y) Western blot analyses showed expression of phosphorylated NF-κB in whole cell lysate from adipocytes transfected with control mimic (CM) and miR-210-3p mimic (MM).

3.2.3 *miR-210-3p* drives obesity-induced ATM inflammation by targeting the SOCS1/NF-κB pathway

To investigate the underlying mechanism of *miR-210-3p* involvement in obesity-induced ATMs inflammation, we have searched for the putative targets of *miR-210-3p* that can potentially regulate inflammatory pathways. We have found that SOCS1 could be a potential target of *miR-210-3p* as indicated by the miRWalk miRNA target prediction database (**Fig. 3.3K**), and that may be involved in the impairment of NF-κB signalling. The nucleotide sequence of *SOCS1* 3′-UTR are conserved in the transcript sequence of human and mice that critically offers the binding site of *miR-210-3p* (**Fig. 3.3A**). We have used *RNAhybrid* webserver to predict the minimum free energy (mfe) for the interaction of different SOCS1 mRNA transcripts with *miR-210-3p*. The *miR-210-3p* sequence complementary to 3′-UTR of *SOCS1* forms a hybrid sequence having minimum free energy of -32.2 kcal/mol (mouse *SOCS1* transcript) and -31.7 kcal/mol (human *SOCS1* transcript) (**Fig. 3.3L**). To validate the binding of *miR-210-3p* with 3′-UTR of *SOCS1*, we have performed a luciferase reporter assay with wild-type and mutant *SOCS1* 3′-UTR. HL co-exposure significantly inhibits luciferase activity in wild-type *SOCS1* 3′-UTR transfected cells, however, such effect was compromised in cells transfected with mutated *SOCS1* 3′UTRs (**Fig. 3.3B**) indicating a direct interaction of *miR-210-3p* with *SOCS1* 3′UTR in the pathophysiological condition. We then examined the *SOCS1* expression and observed a significant reduction of its level in the SVF of adipose tissue of obese diabetic patients as compared to lean non-diabetic subjects (**Fig. 3.3C,D**). Among the members of the SOCS family, only SOCS1 acts as a ubiquitin ligase, that is capable to interact with NF-κBp65 through its SOCS box domain which leads

to polyubiquitination and proteasomal degradation of NF-κBp65 resulting in termination of NF-κB inducible gene expressions (Love et al., 2014). We, therefore, analyzed the SOCS1 mediated NF-κB activation in pathophysiological conditions. Western blot analysis showcased a significant reduction of SOCS1 expression along with the enhanced levels of phospho-NF-κB in the adipose tissue SVF of obese diabetic patients as compared to lean non-diabetic subjects (**Fig. 3.3E**). This was also evident from HL-treated RAW264.7 cells, exhibiting a time-dependent enhancement of NF-κB activation (**Fig. 3.3M**) and its increased nuclear translocation (**Fig. 3.3N,O**). To examine the role of macrophage-specific SOCS1 in macrophage inflammation, we silenced SOCS1 in RAW264.7 cells using siRNA (**Fig. 3.3P**) and incubated them in the absence or presence of HL stimulation. Silencing of SOCS1 significantly increased NF-κB activation whereas, co-stimulation of HL in SOCS1 silenced cells further aggravated NF-κB activation (**Fig. 3.3Q**). Furthermore, to exclude the possibility of other targets of miR-210-3p which could contribute to the suppression of NF-κB signaling, we analyzed RelA (p65 subunit of NF-κB) interacting partners using the EMBL INACT server (www.ebi.ac.uk/intact/search). Each of the RelA interacting partners was searched against the 16853 *mmu-miR-210-3p* target genes identified through miRWALK database search (**Fig. 3.3S,T**) and found that *BRD4*, *NF-κBIB*, *SOCS1*, *CUL2*, *COMMD1*, *XPO1*, and *MYOCD* are predicted targets of *mmu-miR-210-3p*, out of which *SOCS1*, *NF-κBIB*, *CUL2*, *COMMD1*, and *MYOCD* are negative regulators of NF-κB. To find out the most efficient target of *miR-210-3p* that can potentially inhibit NF-κB under lipid-rich hypoxic conditions, we evaluated the expression of these selected candidate genes in control mimic and *miR-210-3p* mimic transfected macrophages and observed a profound decline of *SOCS1* gene expression (~70 %) as compared to other candidate genes in *miR-210-3p* mimic transfected cells (**Fig. 3.3U**).

To decipher the direct role of *miR-210-3p* on SOCS1 mediated NF-κB activation in the ATMs, *miR-210-3p* mimic transfected cells were examined and found a significant downregulation of *SOCS1* gene and protein expression in concomitance with the upregulation of NF-κB activation (**Fig. 3.3V,W**). Also, we have analysed the SOCS1 and NF-κB activation in control and *miR-210-3p* inhibitor transfected RAW264.7 macrophages co-treated with HL. Exposure of HL strikingly reduced SOCS1 expression which coincided with the increased level of phospho-NF-κB and its nuclear translocation; however, such attributes were significantly attenuated in *miR-210-3p* inhibitor transfected cells (**Fig. 3.3F-H**). Moreover, to assess whether the SOCS1 inhibitory effect on NF-κB activation is mediated through the proteasomal degradation of phospho-NF-κB, we transfected macrophages with control or *miR-210-3p* inhibitor in the absence or presence of a proteasome inhibitor, MG-132 and treated with HL. Our finding demonstrated that MG-132 treatment notably protects NF-κB p65 phosphorylation-dependent proteasomal degradation in macrophages transfected with *miR-210-3p* inhibitor (**Fig. 3I**). Moreover, a higher level of phospho-NF-κB and its nuclear localization was fanned when *miR-210-3p* mimic transfected cells were treated with MG-132 (**Fig. 3.3X**). Since obesity-induced inflammatory milieu in

the adipose tissue is known to be associated with the impairment of insulin sensitivity (Curat et al., 2006), we co-cultured 3T3-L1 adipocytes with macrophages transfected with a control inhibitor or *miR-210-3p* inhibitor in the absence or presence of HL stimulation. Interestingly, attenuation of adipocytes' insulin sensitivity in response to its co-culture with HL-incubated macrophages was markedly prevented when transfected with *miR-210-3p* inhibitor (**Fig. 3.3J**). Since higher enrichment of *miR-210-3p* was evident from ATM-derived exosome, therefore, we analysed the paracrine and endocrine action of *miR-210-3p* on the insulin sensitivity of 3T3-L1 adipocytes and C2C12 myotubes. Interestingly, we have found that delivery of *miR-210-3p* mimic significantly attenuates insulin sensitivity in 3T3-L1 adipocytes and C2C12 myotubes as evident from the reduction of 2-NBDG uptake study (**Fig. 3.Y,Z**). All these results suggest that *miR-210-3p* plays a key role in obesity-induced ATMs inflammation by targeting the SOCS1/NF-κB pathway and it could also influence the adipocyte's insulin sensitivity.

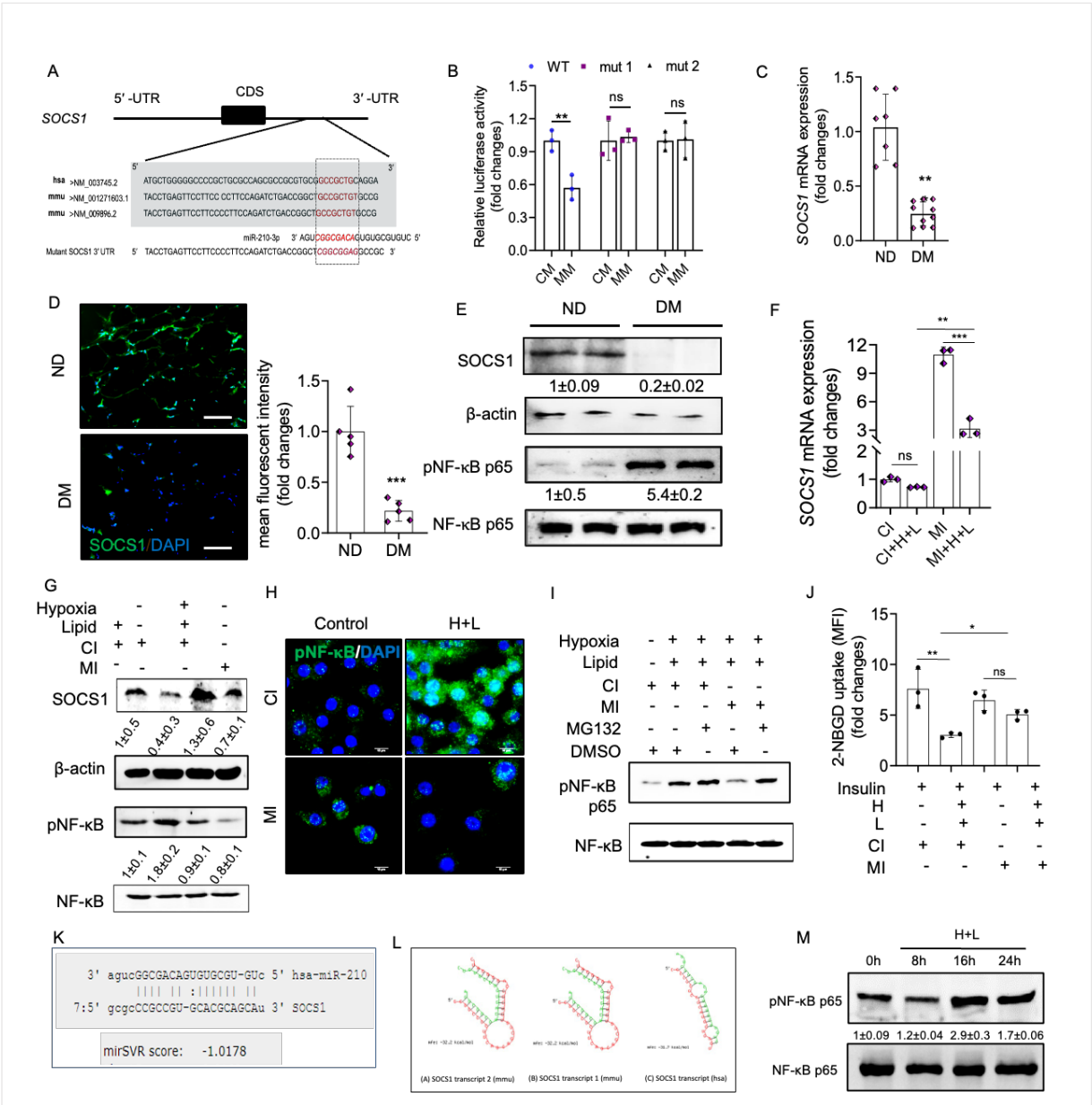

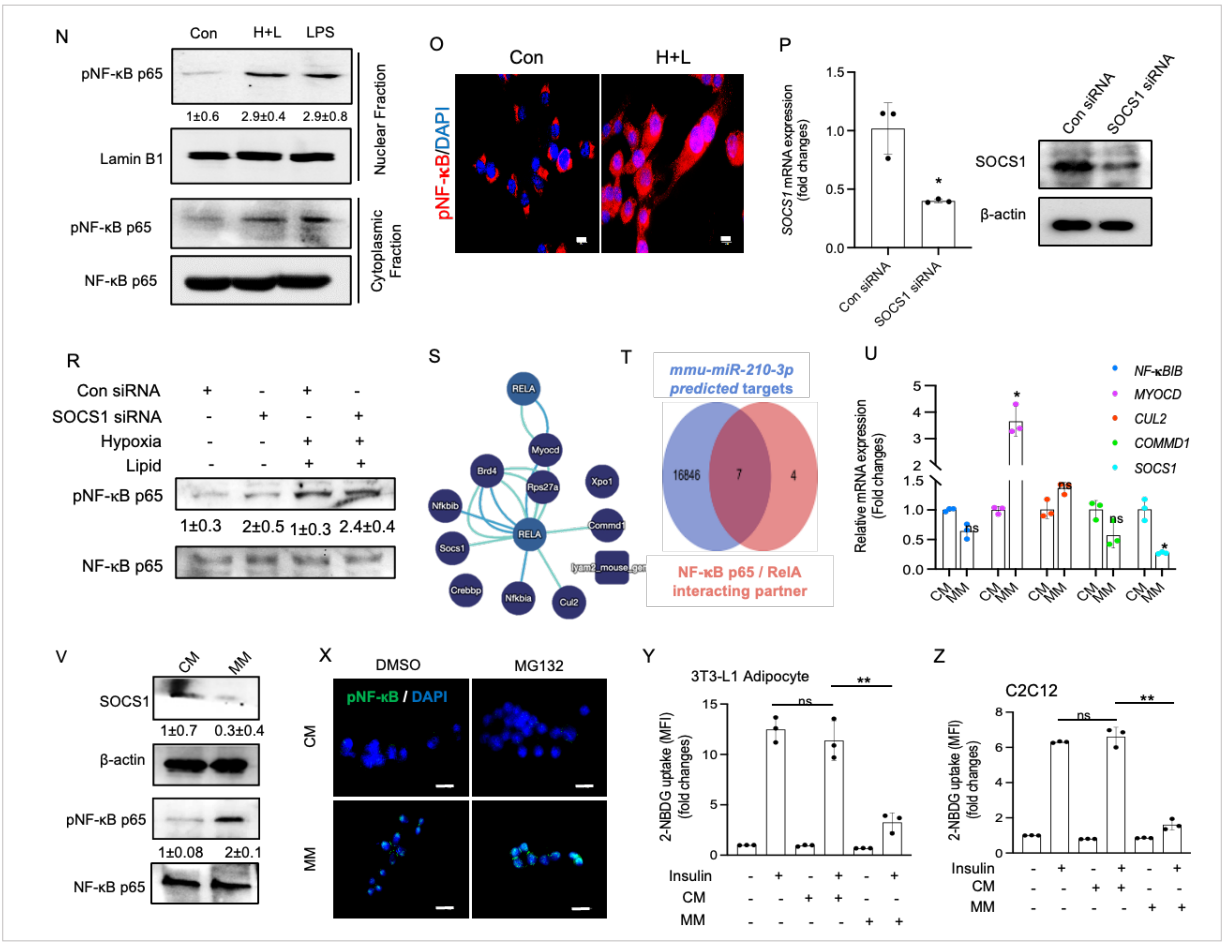

Figure 3.3 | ***miR-210-3p* derives obesity-induced ATM polarization and inflammation by targeting the SOCS1-NF-κB pathway**

(A) Putative conserved binding site of SOCS1 with *miR-210-3p* and seed sequence of *miR-210-3p* and mutated 3′ UTR site of SOCS1. (B) Luciferase activity in RAW264.7 macrophages co-transfected with WT or mutated (mut1 and mut 2) SOCS1 plasmid constructs and CM or MM. n=3, **p<0.01. (C) Relative mRNA expression of *SOCS1* in stromal vascular fractions of control (ND) and obese diabetic (DM) patients. n=7-10, ***p<0.001. (D) Immunohistochemical staining (left panel) of SOCS1 in adipose tissue section of human VAT and quantification analyses (right panel). Scale bar, 100μM. n=5, ***p<0.001 (student's t-test). (E) Western blot analyses of SOCS1 and phosphorylated NF-κB in the cellular lysate of stromal vascular fractions isolated from VAT of control (ND) and obese diabetic (DM) human subjects. (F-G) CI or MI treated macrophages co-incubated with or without HL are considered for mRNA expression analyses of *SOCS1* (F) and western blot analyses of SOCS1, phosphorylated NF-κB p65 (G). n=3, **p<0.01, ***p<0.001 or ns. (H) Immunofluorescence analysis (left panel) showing nuclear localization and expression of phospho-NF-κB in CI or MI treated macrophages co-incubated with or without HL and quantification analyses (right panel). Scale bar, 10μM. n=3, *p<0.05, ***p<0.001. (I) Immunoblotting analyses of phosphorylated NF-κB in control and *miR-210-3p* inhibited macrophages treated with or without HL and MG132. DMSO was used as vehicle control. (J) Glucose uptake assay performed in 3T3-L1 adipocytes cocultured (transwell) with CI or MI transfected macrophages in the presence or absence of HL. n=3, *p<0.05, **p<0.01. (K,L) Database (microRNA.org) searching result showing the interaction of miR-210-3p with human SOCS1 mRNA (K) and RNAhybrid webserver was used to predict the minimum free energy (mfe) of different mouse SOCS1 mRNA transcripts and miRNA-210-3p interactions (L). (M) Phosphorylated NF-κB expression was quantified by performing western blot analyses in murine macrophages co-exposed to hypoxia and lipid for different time periods. (N) Western blot analyses showed expression of phosphorylated NF-κB p65 in nuclear fraction and cytoplasmic fraction of RAW264.7 macrophages,

co-incubated with hypoxia and lipid. LPS exposure counted as positive control for NF-κB activation. (O) Immunofluorescence analyses and mean fluorescence intensity quantification of phospho NF-κB p65 in hypoxia and lipid combined exposed macrophages. DAPI was used for nuclear staining. Scale bar size, 10μm. (P,Q) mRNA expression analysis (P) and western blot analyses (Q) showed reduced expression of SOCS1 in SOCS1 siRNA transfected macrophages. (R) Immunoblot analyses of phosphorylated NF-κB p65 in control siRNA or SOCS1 siRNA transfected macrophage co-incubated with or without hypoxia and lipid. (S) Rel A (p65 subunit of NF-**κ**B) interacting partner in EMBL INACT server. (T) Overlapping pie diagram showed selected negative regulators of NF-κB p65 and miR-210-3p target molecule as per the miRWALK database search. (U) qRT-PCR analyses of MYOCD, CUL2, COMMD1, NF-κBIB and SOCS1 in control mimic and miR-210-3p mimic transfected macrophages. (V) Control mimic and miR-210-3p mimic transfected macrophages are considered for protein expression of SOCS1, phospho NF-κB p65. (W) Immunofluorescence analyses of phosphorylated NF-κB p65 in control mimic and miR-210-3p mimic transfected murine macrophages treated with or without MG132. DMSO was used as vehicle control. (X,Y) Glucose uptake assay was performed in CM and MM transfected adipocytes (X), and C2C12 (Y).

3.2.4 Anti-*miR-210-3p* delivery rescued obesity-induced ATM inflammation

To inspect the therapeutic potential of *miR-210-3p* inhibitor in the rescue of obesity-induced adipose tissue inflammation and insulin resistance, we administered control LNA or anti-*miR-210-3p* LNA directly to the VAT of HFD mice (**Fig. 3.4A**) and validated their efficacy by analysing *miR-210-3p* expression (**Fig.3.4L**). Also, we have estimated the body weight and food intake for the entire 7 days of post-surgery (**Fig. 3.4M,N**) to examine the post-surgery recovery of mice. On day 7, adipose tissue was harvested for immunofluorescence analysis of F4/80, CD163, iNOS, and ARG1. A profound increase in the anti-inflammatory $CD163^{+}F4/80^{+}$ macrophage population was observed in the HFD adipose tissue injected with anti-*miR-210-3p* LNA (**Fig. 3.4B**). Similarly, reduced level of iNOS and enhanced level of ARG1 was also witnessed in the anti-*miR-210-3p* LNA delivered adipose tissue of HFD mice (**Fig. 3.4C**). Moreover, we have collected the ATMs from these mice on day 7 and analysed for ATM polarization and inflammation. Anti-*miR-210-3p* LNA administered HFD mice exhibited an abundance of M2 ($F4/80^{+}CD206^{+}$) over M1 ($F4/80^{+}CD80^{+}$) ATM population (**Fig. 3.4D**) with a notable reduction of proinflammatory (*iNOS*, and *IL6*) over anti-inflammatory (*IL13*, and *Ym1*) cytokines gene expression (**Fig. 3.4E**) as compared to control LNA injected HFD mice. To exclude the contributions of other cell types in adipose tissue in response to anti-*miR-210-3p* LNA treatment, we have checked *miR-210-3p* and SOCS1 expression in the adipocytes isolated from control LNA and anti-*miR-210-3p* LNA injected mice. We found that *miR-210-3p* expression was reduced in isolated adipocytes of anti-*miR-210-3p* LNA administered mice but not significantly compared with control (**Fig. 3.4O**). Also, adipocytes' SOCS1 expression and inflammatory cytokines levels were not significantly altered in response to anti-*miR-210-3p* LNA administration (**Fig. 3.4P,Q**). These results suggest that adipocytes' contribution has not been substantial for altering adipose tissue inflammatory state upon anti-*miR-210-3p* LNA treatment, rather it depicts the exclusive role of *miR-210-3p* in ATMs inflammation and therefore ATM-specific inhibition of *miR-210-3p* would be beneficial to improve the inflammatory setting of obese adipose tissue.

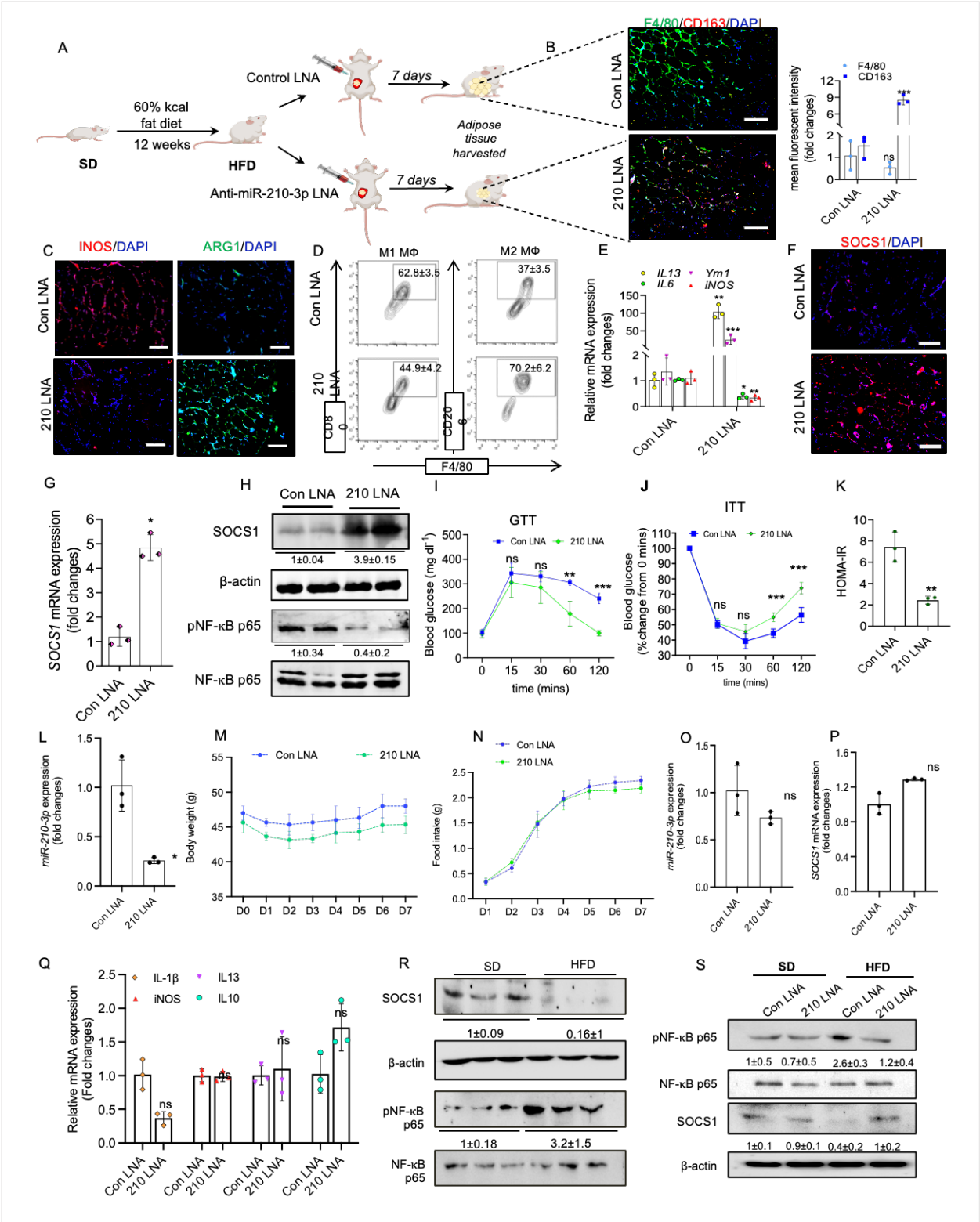

Figure 3.4| Anti-miR-210-3p LNA delivery rescues obesity-induced ATM inflammation and insulin resistance

(A) Schematic diagram showing the development of HFD (DIO) mice model and adipose tissue-specific delivery of control LNA or anti-miR-210-3p LNA. (B,C) Representative images of VAT sections showing immunohistochemical staining along with quantification analyses of F4/80 and CD163 (B) iNOS or ARG1 (C) in control LNA and anti-miR-210-3p LNA injected HFD mice. Scale

bar, 200μm. n=3, ***p<0.001 or ns. (D) Flow cytometry analyses for F4/80$^+$ CD80$^+$ and F4/80$^+$ CD206$^+$ positive cells in the stromal vascular fraction of control LNA or anti-miR-210-3p LNA injected HFD mice VAT. n=3, **p<0.01, ***p<0.001 (E) Relative gene expression of proinflammatory cytokines (IL6, iNOS) and anti-inflammatory cytokine (IL13, Ym1) in sorted ATMs from control LNA or anti-miR-210-3p LNA injected HFD mice. n=3, *p<0.05, **p<0.01, ***p<0.001. (F) SOCS1 protein expression was analyzed and quantified by performing immunohistochemical staining of VAT of control LNA or anti-miR-210-3p LNA injected HFD mice (left) with quantification analyses (right). Scale bar, 200μM. n=3, ***p<0.001. (G) Quantitative RT-PCR analyses of SOCS1 mRNA in the ATMs of control LNA or anti-miR-210-3p LNA injected HFD mice. n=3, *p<0.05. (H) Western blot analysis was performed to measure phosphorylated NF-κB and SOCS1 protein expression in the ATMs of control LNA or anti-miR-210-3p LNA injected HFD mice. n=3, **p<0.01, ***p<0.001. (L) qRT-PCR analyses showed miR-210-3p expression in ATMs isolated from control inhibitor LNA and miR-210-3p inhibitor LNA injected adipose tissue. (M, N) Body weight and daily food intake data in HFD mice undergo surgical procedures to administer control inhibitor LNA and anti-miR-210-3p LNA. (O-Q) qPCR analyses showed miR-210-3p, SOCS1, inflammatory cytokines IL-1β, iNOS, IL13, and IL10 mRNA expression in adipocytes isolated from control inhibitor LNA and anti-miR-210-3p LNA injected adipose tissue of HFD mice. (R) Western blot analyses of SOCS1 and phospho NF-κB p65 in ATMs isolated from SD and HFD VAT. (S) Immunoblot analyses of phospho NF-κB p65 and SOCS1 in ATMs isolated from control inhibitor LNA and miR-210-3p inhibitor LNA injected adipose tissue of SD and HFD groups. *p<0.05 **p<0.01 ***p<0.001 or ns.

As we have found that *miR-210-3p* promotes NF-κB activation-dependent inflammation in RAW 264.7 macrophages by targeting the SOCS1/NF-κB pathway (**Fig. 3.3**), therefore, we examined the level of SOCS1 expression and NF-κB activation in the adipose tissue of SD and HFD mice (**Fig. 3.4R**). Immunofluorescence analysis showed a profound induction of SOCS1 in the VAT of HFD mice treated with anti-*miR-210-3p* LNA (**Fig. 3.4F**). Upregulation of *SOCS1* expression (**Fig. 3.4G-H**) coincided with the subdued levels of phospho-NF-κB p65 (**Fig. 3.4H**) in the ATMs of anti-*miR-210-3p* LNA administered HFD mice. However, NF-κB p65 activation and SOCS1 expression have not been altered significantly in SD mice treated with anti-*miR-210-3p* LNA or control LNA (**Fig. 3.4S**). These results suggest that the application of anti-*miR-210-3p* LNA could be beneficial to rescue from obesity-induced inflammation.

3.3 Discussion

Alteration of adipose tissue microenvironment (ATenv) is an important feature in obesity that is characterized by the adipose tissue expansion along with the increased infiltration and activation of immune cells, particularly macrophages. Compelling evidence shows that the obesity-associated hypertrophic expansion of visceral adipocytes leads to the deprivation of oxygen resulting in adipose tissue hypoxia. Moreover, adipose tissue hypoxia positively correlated with the increased rate of necrotic adipocytes (crown-like structure) which, by secreting various chemoattractants and related proteins, strongly influenced macrophage recruitment and its polarization towards a pro-inflammatory

state in hypertrophic adipose tissue (Lee & Lee, 2014; Lorente-Cebrián et al., 2019; Strebovsky et al., 2011; Surmi & Hasty, 2008).

Studies from the last decades majorly focussed on the role of either increased lipid level or deprived oxygen tension on adipose tissue dysfunction and provide evidence that both of these phenomena caused criminalable offense on the onset of adipose tissue inflammation that leads to insulin resistance and T2D. In reality, both lipid burden and hypoxia coincided in obese conditions due to the hypertrophied adipocytes and poor vasculature creating a unique pathophysiological ATenv. We also noticed the coexistence of lipid burden and hypoxia in the vWAT of obese diabetic patients and mice models. Therefore, we weighted both lipid and hypoxic insults on ATMs to understand their synergic effect and the underlying mechanism of adipose tissue inflammation and insulin resistance. Increased accumulation of ATMs in the VAT of diabetic patients or mice exhibited proinflammatory features which coincided with the results of an in-vitro model of RAW264.7 macrophages co-stimulated with HL. These findings distinctly depict that obesity-associated ATenv strongly correlated with ATMs inflammation (Cifarelli et al., 2020; Ye, 2009; Zatterale et al., 2020).
Several recent studies have revealed that non-coding RNAs, particularly microRNAs (miRNAs), play a key role in the regulation of inflammatory responses. To decipher the involvement of specific miRNAs on macrophage inflammation in the obese ATenv, we first explored a GEO dataset of miRNAs profile in ATMs-derived exosomes (ATM-Exo) isolated from the vWAT of lean and obese mice. Reanalysis of GEO dataset GSE97652 in the context of hypoxia gives six differentially expressed miRNAs -miR-210-5p, miR-210-3p, miR-27a-5p, miR-27b-5p, miR-101b-5p, and miR-128-1-5p, out of which miR-210-3p showed profound increase in the ATM-Exo of obese mice as compared to lean one. This is also evident in the ATMs of obese diabetic patients and HFD fed mice of our study. This observation intrigued us to examine the role of miR-210-3p in ATMs inflammation and insulin resistance (Zheng et al., 2015).

During obesity, different immune cell types accumulate in adipose tissue, and among them, macrophages are the most abundant in nature and constitute up to 40% of all cell types. Obesity-associated inflamed adipose tissue is characterized by an increased ratio of M1 proinflammatory to M2 anti-inflammatory phenotypic state of ATMs which is considered as a major source of different pro-inflammatory mediators responsible for adipocyte dysfunction and insulin resistance. Investigating the involvement of miR-210-3p on macrophage polarization and inflammation, we used miR-210-3p mimic and inhibitor transfected cells and treated without or with a hypoxic lipid environment. While miR-210-3p mimic notably enhanced the M1 polarization with the secretion of pro-inflammatory cytokines in the absence of any treatment; the miR-210-3p inhibitor rescues HL mediated M1 polarization and inflammation by favouring M2 polarization state with increased anti-inflammatory cytokines. To investigate the molecular target of miR-210-3p in the regulation of macrophage

inflammation, different miRNA analysis tools were employed. In searching for the putative target of miR-210-3p, we have found suppressor of cytokine signalling-1 (SOCS1) is one of the targets of miR-210-3p. The SCOS1 3′UTR luciferase assay confirmed that miR-210-3p directly binds at 3′UTR of SCOS1. Since SOCS1 is known to regulate the NF-κB inflammatory pathway by proteasomal degradation of activated NF-κB p65, we, therefore, compared the SOCS1 expression and NF-κB activation in the ATMs of diabetic patients and HFD mice. Pathophysiological obese ATenv stimulates miR-210-3p expression in ATMs and promotes NF-κB inflammatory signalling by downregulating SOCS1 expression. However, it will be interesting to see the impact of miR-210-3p on other cell types of adipose tissue. A plethora of studies highlighted that inflamed adipose tissue microenvironment negatively correlated with insulin sensitivity. HL treated RAW264.7 macrophages when co-cultured with adipocytes, we observed a significant impairment of insulin-stimulated glucose uptake in adipocytes, however, such effect was compromised when macrophages were transfected with miR-210-3p inhibitor. All these observations encouraged us to evaluate the therapeutic potential of miR-210-3p inhibitor on adipose tissue inflammation and insulin resistance in-vivo. Direct administration of anti-miR-210-3p LNA into the VAT of HFD-induced diabetic mice exhibited a lower level of F4/80+ sorted ATMs which coincided with a lower level of CD80 and a higher level of CD206+ macrophage phenotypic markers. Moreover, anti-miR-210-3p LNA delivery remarkably increased SOCS1 levels in HFD mice which coincided with the attenuation of NF-κB activation as compared to control LNA-treated HFD mice. As suppression of adipose tissue inflammation is known to be associated with improvement of insulin sensitivity it will be interesting to investigate if ATM specific miR-210-3p ablation can restore obesity induced insulin resistance. It suggests, an in-depth study will be required to understand the role of ATM-derived miR-210-3p in improving adipocytes' insulin sensitivity (O'Connell et al., 2012; Snodgrass et al., 2016; Thomas & Apovian, 2017; Yin et al., 2009).

In conclusion, our study revealed that miR-210-3p plays a crucial role in ATM polarization and inflammation under the influence of lipid-enriched hypoxic microenvironment of obese adipose tissue. However, the inclusion of more sample sizes of patients will strengthen the results. Moreover, the use of macrophage-specific miR-210-3p knockout and SOCS1 knock-in mouse models will provide firm and compelling evidence about the vital role of miR-210-3p and SOCS1. Altogether these shreds of evidence will authenticate and fortify the conclusive statement. Hence, targeted inhibition of miR-210-3p could be beneficial for the management of obesity-induced adipose tissue inflammation in type 2 diabetic patients.

3.4 Materials and Methods

3.4.1 Reagents and antibodies

All tissue culture materials were purchased from Life Technologies/Gibco, and Nunc, Grand Island, NY; and Corning, NY. Description of all the antibodies including catalog numbers and the dilutions used in different experiments presented in **Table A**. We purchased Dual-Luciferase Reporter Assay System (cat. no. #E1910) from Promega, Madison, WI; Vectashield anti-fade mounting medium with DAPI (cat. no. #H-1500) from Vector Laboratories, Burlingame, CA.; QuickChange Lightning Multi Site-Directed Mutagenesis Kit (cat. no. #210515) from Agilent Technologies, Santa Clara, CA; Glucose Uptake Cell-Based Assay Kit (cat. no. #600470) from Cayman, Ann Arbor, MI; *mir*Vana™ miRNA Isolation Kit (cat. no. #AM1560), Lipofectamine™ LTX reagent with PLUS™ reagent (cat. no. #15338100), Lipofectamine™ RNAiMAX Transfection Reagent (cat. no. #13778-075), and NP40 Cell lysis buffer (cat. no. #FNN0021) from Invitrogen, Thermo-Scientific, Grand Island, NY; Pierce™BCA Protein Assay Kit (cat. no. #23227), and Halt™ Protease and Phosphatase Inhibitor Cocktail (cat. no. #78441) from Thermo Scientific, Waltham, MA, USA;Clarity™ Western ECL Substrate (cat. no. #1705060), and iScript Reverse Transcription Supermix (cat. no. #1708891) from Bio-Rad Laboratories, Hercules, CA; PVDF membranes (cat. no. #548IPVH00010) from Merck, Darmstadt, Germany; PowerUp™ SYBR™ Green Master Mix (cat. no. #A25742) from Applied Biosystems, Thermo-Scientific, Grand Island, NY; TaqMan™ MicroRNA Reverse Transcription Kit (Cat. no.: #4366596), TaqMan™ Multiplex Master Mix (Cat. no.: #4461881) from Applied Biosystems, Waltham, MA; We purchased miRIDIAN miRNA miRNAmmu-miR-210-3p mimic (cat.no. #C-310570-05-0005, sequence: CUGUGCGUGUGACAGCGGCUGAaccession no.: MIMAT0000658), miRIDIAN miRNA hairpin mimic negative control (cat. no. #CN-001000-01-05, accession no.:MIMAT0000039), miRIDIAN miRNA hsa-miR-210-3p hairpin inhibitor (cat. no. #IH-310570-07-0005, sequence: GACACGCACACUGUCGCCGACU, accession no.:MIMAT0000267), and miRIDIAN miRNA hairpin inhibitor negative control (cat. no. #IN-001005-01-05, accession no.: MIMAT0000039) from GE Dharmacon, Lafayette, CO. The miRNA specific primers for miR-210-3p (cat. no.: #4427975; assay ID-000512), and U6 sn RNA (cat. no. #4427975; assay ID-001973) were procured from Applied Biosystems, Foster City, CA. We have procured con siRNA(sc-37007) and SOCS-1 siRNA(m) (sc-40997) from Santa Cruz Biotechnology, Inc. Image-iT™ Green Hypoxia Reagent (cat. no. I14833) was procured from Invitrogen, Thermo-Scientific, Grand Island, NY. Different gene-specific primers were procured from Integrated DNA Technologies, India, and the sequence details are presented in **Table B**.

3.4.2 Mice models and treatments

Wild-type C57BL/6J male mice aged 4-5 weeks and weighed 18-22 g were procured from the IISER Mohali animal facility and kept in the NIPER Mohali animal house facility for 5-6 days in 12 light/dark cycle at 23 ± 2ºC with relative humidity 55 ± 5% and fed with normal pellet diet (standard diet, SD) and water ad libitum. For the development of diet-induced obese diabetic model, C57BL/6J mice were fed with high fat diet (HFD) pellets (D12492, Research Diet Inc., New Brunswick, NJ) having 60% kcal of fat for 12 weeks. All other mice were fed with SD pellets that provide 10% kcal of fat for 12 weeks. All experimental animals have free access to sterilized water and food. The blood glucose level has been measured regularly with Accu-Chek glucometer (Roche). Mice fed with HFD diet for 12 weeks were considered for anti-miR-210-3p LNA delivery. Briefly, mice were anaesthetized by low-dose isoflurane inhalation as per standard recommendations. We then created a small incision on the abdominal site and take out the omental fat pads from the abdominal cavity. A total of 100 nM miRCURY LNA miRNA Power Inhibitor (anti)mmu-miR-210-3p (Gene Globe ID-YI04103147-DDA, Qiagen, Germantown, MD) was injected in 5 different sites of each side of the abdominal omental fat pad. 100 nM of miRCURY LNA Control Inhibitor (Gene Globe ID-YI00199006-ADA; Qiagen, Germantown, MD) was injected similarly on the 5 different sites on each side of the abdominal omental fat pad of the control HFD group. The skin layer was stitched carefully using Ethicon absorbable surgical suture (Johnson & Johnson, USA). We determined glucose tolerance test (GTT) by measuring blood glucose level before and after oral gavages of 1 g glucose/kg body weight at the indicated time points. Similarly, insulin tolerance test (ITT) was performed by injecting 1 IU insulin/kg. Mice were then sacrificed and omental adipose tissue was collected. For the FACS study, adipose tissue was immediately processed for experiments. SD and HFD mice were administered with 250nM of Image IT green dye/mice in the tail vein (*intravenous*) and after 2 hours of injection vWATs were harvested in a dark place. Immediately after collection, tissues were snap frozen in OCT (Leica Biosystems) for cryosectioning and imaging. All animal experiments were performed following the guidelines prescribed by and with the approval of the Institutional Animal Ethics Committee (IAEC) NIPER Mohali, Punjab (Project no.: IAEC/19/37-ext1).

3.4.3 Human subjects

A total of 13 men and 17 women have participated in this study. The study population was categorized into two groups based on BMI and blood glucose level. Study subjects having BMI 18–25 kg m^{-2} with fasting blood glucose level <85 were considered as lean non-diabetic group (n=16) whereas patients with BMI >30 kg m^{-2} and fasting blood glucose level>120 were considered as an obese diabetic group (n=14) as presented in the **Table C**. In this study, surgically dissected vWAT samples were collected from the patients who were admitted to the Dayanand Medical College & Hospital, Ludhiana, Punjab, and underwent abdominal surgery. The study protocol for the use of human blood and tissue samples

was approved by the Institute Ethics Committee (IEC), Dayanand Medical College & Hospital, Ludhiana, Punjab (Protocol no.: DMCH/R&D/2021/64; IEC No.: 2021-658). We have obtained written informed consent from all participants in this study.

3.4.4 Cell culture and treatments

RAW264.7 macrophage, C2C12 myoblast cells were obtained from National Centre for Cell Science (NCCS), Pune, India, and cultured in DMEM (Gibco™/Life Technologies, cat. no. #11995073) supplemented with 10% FBS (Gibco™/Life Technologies, cat. no. #10082147) and 1% Penicillin-Streptomycin Solution (Gibco™/Life Technologies, cat. no. #15140122) at 37°C in a humidified atmosphere with 5% CO_2. We have procured 3T3-L1 preadipocyte (Cat. no. CL-173) cell line from ATCC and cultured it in ATCC-formulated Dulbecco's Modified Eagle's Medium (Cat. No. 30-2002), supplemented with 10% Bovine Calf Serum (Cat. No. ATCC 30-2030) and 1% Penicillin-Streptomycin Solution. To differentiate preadipocytes into mature adipocytes we followed a chemically-induced differentiation protocol provided by ATCC. Briefly, Preadipocytes were seeded with a density of$8 x10^4$ cells in each well of 6 well plates having preadipocyte expansion medium (contains DMEM, 10% BCS and 1% Penicillin-Streptomycin) until it achieves 100% confluency. The media was changed after full confluency and continued with preadipocyte expansion medium for another 48 hours. Now the existing growth media was removed and differentiation media (consisting of DMEM, 10% FBS, 1.0 µM Dexamethasone, 0.5 mM IBMX, 1.0 µg/mL Insulin) was added for 48 hours. The differentiation media was replaced with adipocyte maintenance media (consisting of DMEM, 10% FBS, 1.0 µg/mL Insulin) for 72 hours until visible lipid accumulation was observed. We incubated macrophages and other mentioned cells with fixed concentration of palmitate (0.75mM) and were exposed to hypoxia conditions (1% O_2, and 5% CO_2) for different time periods in the Heracell™ VIOS 160i incubator (Thermo Scientific). We performed primary cell culture with adipose tissue macrophages(ATMs) isolated from the vWAT of lean and obese mice using BD FACS Aria Cell Sorter (Franklin Lakes, New Jersey; USA). The ATMs were cultured in RPMI 1640 (Gibco™/ Life Technologies, cat. no. #A1049101) supplemented with 10% FBS and 1% Penicillin-Streptomycin Solution at 37°C in a humidified atmosphere with 5% CO_2. The ATMs were used in different treatment conditions. All treatments were given in serum and antibiotics-free media.

We have prepared 50mM Palmitate for the in-vitro treatment followed by Pal et al., 2012. Briefly, 135mg Palmitate was dissolved in 200µl of absolute alcohol and kept at room temperature for overnight to evaporate excess ethanol. 10ml of DMEM containing 1% FBS and 0.2gm of BSA was added to the palmitate and mixed well, followed by incubating at 60°C until the palmitate is dissolved completely. We have filtered the using 0.4µm filter before treating the cell.

3.4.5 miR-210-3p mimic/inhibitor transfection

For transfection of miR-210-3p mimic/inhibitor and their respective control mimic/inhibitor, Lipofectamine^{TM}RNAiMAX transfection reagent (Invitrogen) was used according to the manufacturer's protocol. Briefly, RAW264.7 macrophages were seeded ($0.1x10^6$ cells/well) in a 12-well plate in an antibiotic-free complete growth medium for 24 h before transfection. For each well, 50 nM of miR-210-3p mimic/control mimic (miRIDIAN miRNA mmu-miR-210-3p mimic/miRIDIAN miRNA hairpin mimic negative control) or 100 nM of miR-210-3p inhibitor/control inhibitor (miRIDIAN miRNA mmu-miR-210-3p hairpin inhibitor/miRIDIAN miRNA hairpin inhibitor negative control) and Lipofectamine RNAiMAX reagent was added separately into the Opti-MEM serum-free medium (Thermo Scientific). Both these solutions were mixed and incubated for 5 min. The transfection mixture was added to the cells containing complete growth medium and incubated for 48 h. After 48 h of transfection, cells were washed; fresh complete growth medium was added and used for different treatments. Above mentioned culture and transfection

3.4.6 Transwell co-culture and glucose uptake assay

RAW264.7 macrophages (0.5×10^5 cells/well) were cultured on transwell cell culture insert (0.4-µm pore size, Corning) transfected with control mimic/inhibitor or miR-210-3p mimic/inhibitor in absence or presence of hypoxia (1% O_2) and lipid (palmitate, 0.75 mM) microenvironment for 16 h. On termination of incubations, cells were washed several times with PBS to remove the residual palmitate, if any, and placed on a 24 well plate containing 3T3-L1 adipocytes (0.5×10^5 cells/well) serum-starved overnight in Kreb's Ringer Bicarbonate Buffer (Cat. No. #TL-1097; HiMedia Laboratories, Mumbai, India) supplemented with 0.2% BSA and incubated for 6 h. After 6 h, the 3T3-L1 adipocytes were utilized for glucose uptake assay using a Glucose Uptake Cell-Based Assay Kit (Cayman Chemicals, Item No. 600470) following the manufacturer's instruction. Briefly, insulin (100 nM) was added to the control and treated adipocytes and incubated for 30 min. Fluorescent labelled glucose analogue 2-NBDG was added to each of the incubations for 10 min before the termination of the experiment. Cells were then lysed and fluorescent intensity was measured by a Microplate Reader (BMG Labtech Allmendgrün 8, 77799 Ortenberg, Germany).

3.4.7 Site directed mutagenesis

Wild-type SOCS1 3′-UTR plasmid construct was used as template for the generation of mutated SOCS1 3′-UTR plasmids by using QuickChange Lightning Multi Site-Directed Mutagenesis Kit following the manufacturer's protocol. Primers used to generate the mutated SOCS1 3′-UTR plasmids were designed with the help of Quik Change Primer Design Program available online at www.agilent.com/genomics/qcpd. Primer sequences used for mutated SOCS1 3′-UTR plasmids construction are listed in **Table B**

3.4.8 SOCS1 3'-UTR luciferase reporter assay

RAW264.7 macrophages were co-transfected with 500 ng of Wild-type or mutated SOCS1 3′-UTR plasmid and with either control mimic or *miR-210-3p* mimic, or control or *miR-210-3p* inhibitor (GE Dharmacon, Lafayette, CO) using Lipofectamine LTX/Plus Reagent (Invitrogen) for 48h in a 24 well plate. Cells were then treated without or with palmitate (0.75 mM) and 1% O_2. On termination of incubations, cells were lysed, and luciferase activity was determined using Dual Luciferase Reporter Assay System (Promega) in GloMax Navigator Microplate Luminometer (Promega, Madison, Wisconsin, USA) following the manufacturer's protocol. Data normalization was achieved by co-transfecting cells with Renilla plasmid (10 ng). Relative luciferase activity was plotted as a ratio of firefly to Renilla luciferase activity.

3.4.9 Flow cytometry

Control and treated RAW264.7 macrophages and primary ATMs isolated from the vWAT of humans or mice were harvested, centrifuged at 350 g for 5 min, and washed with PBS. The cell pellets were re-suspended in cell staining buffer (PBS containing 0.2% FBS and 0.09% $NaNO_3$) and blocked with TruStainFcX™ (Fcγ blocker, mouse anti-CD16/32 antibody, BioLegend) for 15 min at 4°C. Cells were then stained with fluorochrome-labelled primary antibodies against F4/80 (anti-mouse), CD80 (anti-mouse/anti-human), CD206 (anti-mouse), CD64 (anti-human), CD163 (anti-human), CD11b (anti-human/ anti-mouse) (BioLegend) for 1h on ice. Cells were then washed twice with chilled PBS, re-suspended in cell staining buffer, and analysed in a Flow cytometer (BD Accuri C6+, BD Biosciences, San Jose, CA) using FlowJo™ v10.6.1 software.

3.4.10 Immunocytochemistry

Cells grown on a sterile glass coverslip for overnight were incubated without or with palmitate (0.75 mM) and hypoxia (1% O_2) condition for 16h. On termination of incubations, cells were washed in PBS and fixed with ice-cold methanol for 5 min. For intracellular staining, cells were permeabilized with 0.25% TritonX-100 in PBS for 10 min at room temperature. Cells were blocked with 1% BSA in PBS containing 0.1% Tween-20 for 30 min at room temperature and incubated with primary antibodies for 1 h in room temperature. Cells were then washed with ice-cold PBS thrice for 5 min each, followed by the incubation with fluorescence-conjugated secondary antibodies for 1h room temperature in the dark. Before mounting on a glass slide, cells were washed thrice for 5 min each with ice-cold PBS. Coverslips were mounted onto glass slides using anti-fade mounting medium with DAPI. Cellular images were captured by an inverted fluorescent microscope (Leica DMi8, Germany) and image analysis was performed using LAS X software. Fluorescence intensity was quantified using ImageJ software (1.48v, NIH, USA).

3.4.11 Immunofluorescence

Adipose tissue samples collected from human subjects and mice models immediately washed in sterile saline and then placed in Neutral buffer formalin (10%) for overnight fixation at 4°C. After fixation, adipose tissue were embedded in OCT (optimal cutting temperature compound, Sigma) and frozen in -30°C to -60°C followed by cryosections using Cryotome (Leica CM 1860, Leica Biosystem, Wetzlar, Germany). Immunostaining was performed on tissue cryosections using specific antibodies. Briefly, tissue cryosections (10 μm) were placed in gelatin coated glass slides, fixed in ice-cold methanol for 5 min, blocked with 5% BSA containing blocking buffer, and incubated with specific primary antibodies for 1h in room temperature. After washing, signal was visualized by subsequent incubation with fluorescence-conjugated appropriate secondary antibodies and counter-stained with anti-fade mounting medium containing DAPI. Images were captured by a fluorescence microscope (Leica DMi8, Germany) and analysis was performed using LASX software.

3.4.12 Oil Red O staining

Fresh frozen adipose tissues (collected from patients and mice) were cryo-sectioned into 10μM thick slices and placed in membrane coated glass slides. The sections were air dried for 45 min and fixed in chilled formalin for 10 mins. Then fixed samples were air dried for 30 min in room temperature and gently rinsed with distilled water. The sections were air dried and absolute propylene glycol added for 5 mins and stained with prewarmed oil red o solution for 10 min in 60˚C oven. Then the section containing slides were differentiated in 85% propylene glycol for 3 mins. The slides were rinsed 2 times with distilled water and stained with haematoxylin for 30 sec. Then running tap water was used to wash the stained sections and mounted using glycerine. Images were captured by a fluorescence microscope (Leica DMi8, Germany) and analysis was performed using LASX software.

3.4.13 H&E staining and imaging

Cryo-sectioning of the tissues was performed, as previously described in this manuscript. These tissue sections were placed on gelatin-coated glass slides and subjected to regressive staining using the following steps: 100% alcohol was passed over the sections for 20 seconds, repeated twice; followed by 90% alcohol for 20 seconds, repeated twice; 80% alcohol for 20 seconds; 70% alcohol for 20 seconds; 50% alcohol for 20 seconds. Subsequently, the slides were rinsed with dH2O for 1 minute. Next, the slides were incubated in Hematoxylin (Harris) for 3 minutes, followed by a 2-minute water rinse. The slides were then dipped three times in a 0.3% acetic acid-containing alcohol solution, rinsed in dH2O, and further dipped several times in 0.3% ammonium water, inducing bluing upon rinsing in water. Afterward, the slides were passed through 80% alcohol for 20 seconds, followed by staining with 2% Eosin for 30 seconds. To remove excess staining, the sections were washed with 95% alcohol for 20 seconds, repeated twice, and then with 100% alcohol for 20 seconds. Finally, the slides

underwent a few brief dips in xylene before mounting using DPX solution. Subsequently, the H&E stained slides were examined using a Leica DMi8 microscope for imaging.

3.4.14 RNA extraction and Quantitative PCR

Total RNA was extracted from the cells by TRIzol (Invitrogen) and quantified using NanoDrop™ OneC spectrophotometer (NanoDrop Technologies, Thermo Scientific, Waltham, MA USA). RNA (100 ng) was then treated with DNase I and reverse transcribed using the iScript™ cDNA Synthesis Kit (Bio-Rad, Hercules, California, USA). We used PowerUp™ SYBR™ Green Master Mix (Applied Biosystems) to perform real time quantitative PCR in QuantStudio™ 5 Real-Time PCR System (Applied Biosystems, Waltham, Massachusetts, USA) using gene specific primers. microRNA was isolated from the cells using *mir*Vana™ miRNA Isolation Kit (Ambion, Thermo Scientific) following manufacturer's protocol and microRNA specific cDNA synthesis was performed using TaqMan™ MicroRNA Reverse Transcription Kit (Applied Biosystems). TaqMan™ Multiplex Master Mix (Applied Biosystems) was used to perform real-time quantitative PCR for miRNA with specific miRNA primers of miR-210-3p and U6 sn RNA (Applied Biosystems). mRNA and miRNA expression were normalized to β-actin and U6 snRNA, respectively, following the $^{\Delta\Delta}$CT method. Mean $^{\Delta}$Ct value was transformed to relative expression or fold change by $2^{\Delta\Delta CT}$ and average fold change value was calculated.

3.4.15 Immunoblotting

Control and treated cells were lysed in NP40 cell lysis buffer (Invitrogen) supplemented with the Halt protease and phosphatase inhibitor cocktail (Thermo Scientific), centrifuged at 13,0000 rpm for 10 min at 4°C. Protein concentrations of cell lysates were determined by the BCA Protein Assay Kit (Pierce) following manufactures' guideline. Cell lysates (50 µg of protein) were resolved on 10% SDS–PAGE and transferred on to PVDF membranes (GE Healthcare Biosciences) with the help of Turbo Blotting System (Bio-Rad Laboratories). Membranes were first blocked with 5% BSA in TBS (Tris-buffered saline) buffer for 1h followed by the overnight incubation with primary antibodies in a rotating shaker at 4°C. The membranes were then washed three times with TBST (TBS containing 0.1% Tween 20) buffer for 10 min intervals and incubated with peroxidise conjugated specific secondary antibodies for 2 h at room temperature. Membranes were then washed three times with TBST for 10 min intervals and subjected to Clarity™ Western ECL Substrate (Bio-Rad, Hercules, California, USA) incubation for 5 min at room temperature. Protein bands were visualized in Chemidoc XRS+ System (Bio-Rad Laboratories, Hercules, California, USA) using Image Lab Software.

3.4.16 Enzyme-linked immunosorbent assay (ELISA)

We measured IL6 and TNF-α cytokine levels in the cell culture medium of control and treated cells using mouse IL-6 (cat. no. #431307) and TNF- α (cat no. #430907) ELISA kits (BioLegend, San Diego, CA) following manufacturer's instructions. We measured insulin levels in the cell culture medium of control and treated cells using mouse ELISA kits (Elabscience) following the manufacturer's instructions.

3.4.17 Fluorescence-activated cell sorting (FACS)

VWATs collected from human and mice were rinsed in sterile PBS, chopped into small pieces and then digested in Hanks' Balanced Salt Solution containing collagenase type II (2 mg/ml), glucose (5.5 mM), and 4% BSA (fatty acid-free) for 45 min at 37ºC water bath shaker. The enzymatic activity was then neutralized by the addition of serum and the digestion mixture was passed through a cell strainer (pore size: 70 µm).. The isolated cell suspension was subjected to centrifugation at 2000 rpm for 10 min. Cell pellet was washed twice with ice-cold PBS and the cells were sorted for F4/80+ (anti-mouse) or CD68+ (anti-human) antibody for the collection of adipose tissue macrophages.

3.4.18 miRNA transcriptomic analysis

miRNA sequencing dataset of adipose tissue macrophage derived exosomes (ATM-Exos), obtained from lean and obese mice (GSE97652, n=7 in each group) were downloaded from the Gene Expression Omnibus database. miRNA-Seq reads were quality-assessed by 'FastQC' toolkit. Further, Illumina 3′ small RNA sequencing adapter was clipped by the' cutadapt' tool from the sequencing libraries. Trimmed short sequencing reads were subsequently aligned by 'bowtie' to the mouse reference genome (GRCm38) using prebuilt genomic indices, downloaded from Illuminai Genomes collection site. 'feature Counts' from the Subread package was used to calculate per-miRNA count across all the samples (43; 44). miRNA with very low read counts (*i.e.,* sum of read counts < 5 across all samples) were excluded from further analysis. DESeq2 package was employed to identify differentially expressed miRNAs between obese vs lean conditions in R Bioconductor. miRNAs with log2(foldchange) of 1.5 and FDR < 0.1 were considered as significant expression changes between contrasting conditions. Volcano plot and boxplots of normalized read-counts for corresponding miRNAs of specific interest were plotted using the'ggplot2' package in R.

3.4.19 Statistical analysis

All data analyses were performed using GraphPad Prism software (v.8.0; GraphPad Software, Inc., La Jolla, CA). Data represented as mean ± S.D. The student's *t*-test or ANOVA (one way or two way) were used to determine statistical significance, and the p-value indicated significance. A level of $p<0.05$ was considered significant.

References

Amr, K., Abdelmawgoud, H., Ali, Z., Shehata, S., & Raslan, H. (2018). Potential value of circulating microRNA-126 and microRNA-210 as biomarkers for type 2 diabetes with coronary artery disease. *British Journal of Biomedical Science*, *75*(2), 82–87. https://doi.org/10.1080/09674845.2017.1402404

Blüher, M. (2016). Adipose tissue inflammation: A cause or consequence of obesity-related insulin resistance? *Clinical Science*, *130*(18), 1603–1614. https://doi.org/10.1042/CS20160005

Chan, Y. C., Banerjee, J., Choi, S. Y., & Sen, C. K. (2012). miR-210: The Master Hypoxamir. *Microcirculation*, *19*(3), 215–223. https://doi.org/10.1111/j.1549-8719.2011.00154.x

Cifarelli, V., Beeman, S. C., Smith, G. I., Yoshino, J., Morozov, D., Beals, J. W., Kayser, B. D., Watrous, J. D., Jain, M., Patterson, B. W., & Klein, S. (2020). Decreased adipose tissue oxygenation associates with insulin resistance in individuals with obesity. *The Journal of Clinical Investigation*, *130*(12), 6688–6699. https://doi.org/10.1172/JCI141828

Curat, C. A., Wegner, V., Sengenès, C., Miranville, A., Tonus, C., Busse, R., & Bouloumié, A. (2006). Macrophages in human vWAT: Increased accumulation in obesity and a source of resistin and visfatin. *Diabetologia*, *49*(4), 744–747. https://doi.org/10.1007/s00125-006-0173-z

Fuster, J. J., Ouchi, N., Gokce, N., & Walsh, K. (2016). Obesity-Induced Changes in Adipose Tissue Microenvironment and Their Impact on Cardiovascular Disease. *Circulation Research*, *118*(11), 1786–1807. https://doi.org/10.1161/CIRCRESAHA.115.306885

Hotamisligil, G. S., Arner, P., Caro, J. F., Atkinson, R. L., & Spiegelman, B. M. (1995). Increased adipose tissue expression of tumor necrosis factor-alpha in human obesity and insulin resistance. *The Journal of Clinical Investigation*, *95*(5), 2409–2415. https://doi.org/10.1172/JCI117936

Lee, B.-C., & Lee, J. (2014). Cellular and molecular players in adipose tissue inflammation in the development of obesity-induced insulin resistance. *Biochimica et Biophysica Acta (BBA) - Molecular Basis of Disease*, *1842*(3), 446–462. https://doi.org/10.1016/j.bbadis.2013.05.017

Liu, H., Chen, C., Zeng, J., Zhao, Z., & Hu, Q. (2021). MicroRNA-210-3p is transcriptionally upregulated by hypoxia induction and thus promoting EMT and chemoresistance in glioma cells. *PLOS ONE*, *16*(7), e0253522. https://doi.org/10.1371/journal.pone.0253522

Lorente-Cebrián, S., González-Muniesa, P., Milagro, F. I., & Martínez, J. A. (2019). MicroRNAs and other non-coding RNAs in adipose tissue and obesity: Emerging roles as biomarkers and therapeutic targets. *Clinical Science*, *133*(1), 23–40. https://doi.org/10.1042/CS20180890

Love, M. I., Huber, W., & Anders, S. (2014). Moderated estimation of fold change and dispersion for RNA-seq data with DESeq2. *Genome Biology*, *15*(12), 550. https://doi.org/10.1186/s13059-014-0550-8

Martin, M. (2011). Cutadapt removes adapter sequences from high-throughput sequencing reads. *EMBnet.Journal*, *17*(1), Article 1. https://doi.org/10.14806/ej.17.1.200

O'Connell, R. M., Rao, D. S., & Baltimore, D. (2012). microRNA Regulation of Inflammatory Responses. *Annual Review of Immunology*, *30*(1), 295–312. https://doi.org/10.1146/annurev-immunol-020711-075013

Osipova, J., Fischer, D.-C., Dangwal, S., Volkmann, I., Widera, C., Schwarz, K., Lorenzen, J. M., Schreiver, C., Jacoby, U., Heimhalt, M., Thum, T., & Haffner, D. (2014). Diabetes-Associated MicroRNAs in Pediatric Patients With Type 1 Diabetes Mellitus: A Cross-Sectional Cohort Study. *The Journal of Clinical Endocrinology & Metabolism*, *99*(9), E1661–E1665. https://doi.org/10.1210/jc.2013-3868

Pasarica, M., Sereda, O. R., Redman, L. M., Albarado, D. C., Hymel, D. T., Roan, L. E., Rood, J. C., Burk, D. H., & Smith, S. R. (2009). Reduced Adipose Tissue Oxygenation in Human Obesity: Evidence for Rarefaction, Macrophage Chemotaxis, and Inflammation Without an Angiogenic Response. *Diabetes*, *58*(3), 718–725. https://doi.org/10.2337/db08-1098

Qatanani, M., & Lazar, M. A. (2007). Mechanisms of obesity-associated insulin resistance: Many choices on the menu. *Genes & Development*, *21*(12), 1443–1455. https://doi.org/10.1101/gad.1550907

Snodgrass, R. G., Boß, M., Zezina, E., Weigert, A., Dehne, N., Fleming, I., Brüne, B., & Namgaladze, D. (2016). Hypoxia Potentiates Palmitate-induced Pro-inflammatory Activation of Primary Human

Macrophages*. *Journal of Biological Chemistry*, *291*(1), 413–424. https://doi.org/10.1074/jbc.M115.686709

Strebovsky, J., Walker, P., Lang, R., & Dalpke, A. H. (2011). Suppressor of cytokine signaling 1 (SOCS1) limits NFκB signaling by decreasing p65 stability within the cell nucleus. *The FASEB Journal*, *25*(3), 863–874. https://doi.org/10.1096/fj.10-170597

Surmi, B., & Hasty, A. (2008). Macrophage infiltration into adipose tissue: Initiation, propagation and remodeling. *Future Lipidology*, *3*(5), 545–556. https://doi.org/10.2217/17460875.3.5.545

Thomas, D., & Apovian, C. (2017). Macrophage functions in lean and obese adipose tissue. *Metabolism*, *72*, 120–143. https://doi.org/10.1016/j.metabol.2017.04.005

Wang, B., Wood, I. S., & Trayhurn, P. (2007). Dysregulation of the expression and secretion of inflammation-related adipokines by hypoxia in human adipocytes. *Pflügers Archiv - European Journal of Physiology*, *455*(3), 479–492. https://doi.org/10.1007/s00424-007-0301-8

Xu, H., Barnes, G. T., Yang, Q., Tan, G., Yang, D., Chou, C. J., Sole, J., Nichols, A., Ross, J. S., Tartaglia, L. A., & Chen, H. (2003). Chronic inflammation in fat plays a crucial role in the development of obesity-related insulin resistance. *The Journal of Clinical Investigation*, *112*(12), 1821–1830. https://doi.org/10.1172/JCI19451

Ye, J. (2009). Emerging role of adipose tissue hypoxia in obesity and insulin resistance. *International Journal of Obesity*, *33*(1), Article 1. https://doi.org/10.1038/ijo.2008.229

Ye, J., Gao, Z., Yin, J., & He, Q. (2007). Hypoxia is a potential risk factor for chronic inflammation and adiponectin reduction in adipose tissue of ob/ob and dietary obese mice. *American Journal of Physiology-Endocrinology and Metabolism*, *293*(4), E1118–E1128. https://doi.org/10.1152/ajpendo.00435.2007

Yin, J., Gao, Z., He, Q., Zhou, D., Guo, Z., & Ye, J. (2009). Role of hypoxia in obesity-induced disorders of glucose and lipid metabolism in adipose tissue. *American Journal of Physiology-Endocrinology and Metabolism*, *296*(2), E333–E342. https://doi.org/10.1152/ajpendo.90760.2008

Zatterale, F., Longo, M., Naderi, J., Raciti, G. A., Desiderio, A., Miele, C., & Beguinot, F. (2020). Chronic Adipose Tissue Inflammation Linking Obesity to Insulin Resistance and Type 2 Diabetes. *Frontiers in Physiology*, *10*. https://www.frontiersin.org/articles/10.3389/fphys.2019.01607

Zheng, C., Yang, Q., Xu, C., Shou, P., Cao, J., Jiang, M., Chen, Q., Cao, G., Han, Y., Li, F., Cao, W., Zhang, L., Zhang, L., Shi, Y., & Wang, Y. (2015). CD11b regulates obesity-induced insulin resistance via limiting alternative activation and proliferation of adipose tissue macrophages. *Proceedings of the National Academy of Sciences*, *112*(52), E7239–E7248. https://doi.org/10.1073/pnas.1500396113

Chapter 4 |

Obese adipose tissue macrophage-derived miR-210 disrupts systemic insulin sensitivity by GLUT4 silencing

4.1 Background

Chronic obesity has emerged as a global epidemic of multifactorial poor health conditions with increasing risk of various metabolic disorders, including insulin resistance (IR) and type 2 diabetes (T2D) (Hruby & Hu, 2015). The obesity-associated systemic metabolic dysfunction influences cross-talk between cells in adipose tissue microenvironment (AT*env*) that critically regulates chronic low-grade inflammation in adipose tissue (Grant & Dixit, 2015; Reilly & Saltiel, 2017). Despite extensive research efforts, effective therapeutic interventions targeting obesity-related metabolic dysregulation remain a pressing need.

Adipose tissue (AT) undergoes significant transformations during obesity, leading to the establishment of a unique lipid-rich hypoxic AT*env* (Goossens et al., 2011; Ye, 2009). The pathophysiological AT*env* accelerates infiltration of immune cells, particularly monocytes which differentiate into adipose tissue macrophages (ATMs)and switch their polarity from anti-inflammatory to proinflammatory state that aggravates AT inflammation and IR by activating NF-κB pathway (McNelis & Olefsky, 2014; Pal et al., 2012). Recent single-cell transcriptomic dataset analyses revealed that ATMs of obese individuals primarily comprised of *Trem2*$^{+}$lipid-associated macrophages (LAMs), CD9^{+} macrophages, and other inflammatory macrophages (IMs) (Hill et al., 2018; Jaitin et al., 2019; Maniyadath et al., 2023) which are causally linked with chronic AT inflammation and IR (Chakarov et al., 2022).

Extracellular vesicles (EVs)are small membrane-bound vesicles secreted by the cells comprising exosomes (30-120 nm) and microvesicles (150-1000 nm), that transfer a wide range of biomolecules to exert their biological functions (Jeppesen et al., 2023). Research in this direction demonstrated that EVs play a key role in the exchange of organelles and various biomolecules including microRNAs (miRNAs) (Crewe et al., 2018, 2021; Pan et al., 2019). A recent report showed that obese ATMs secreted exosomes containing miR-155 contribute to insulin resistance by targeting PPARγ, a regulator of adipogenesis and an indirect participant in the insulin signaling pathway (Ying et al., 2017). Moreover, adipose tissue-derived exosomal miR-27b is distributed in vascular endothelial cells which potentiates atherogenesis by silencing PPARγ (Tang et al., 2023).

To date, no evidence suggests that hypoxia-induced miRNAs (hypoxamiRs) originating from obese ATMs could have the potential to directly target insulin signaling pathway molecules exerting systemic insulin resistance. The present study elucidated, for the first time, the direct involvement of obese

ATMs-derived hypoxia-induced miR-210-3p on the impairment of systemic insulin sensitivity and glucose homeostasis through the silencing of an insulin signaling pathway molecule, GLUT4. ATMs dispense *miR-210-3p* to neighboring adipocytes through EVs in the lipid-rich hypoxic AT*env*, which causes IR and glucose intolerance by targeting GLUT4 expression. We also found that miR-210-3p-enriched EVs, secreted from obese ATMs, notably inhibit insulin sensitivity in the skeletal muscle cells and hepatocytes via endocrine actions. Delivering Dicer-silenced *miR-210-3p*-enriched EVs is sufficient to impair insulin sensitivity in lean mice. In addition, the delivery of anti-miR-210-3p LNA into the VAT notably rescued obese HFD mice from systemic glucose intolerance and IR. Therefore, specific inhibition of miR-210-3p in ATMs and/or the delivery of anti-miR-210-3p to insulin target cells could serve as novel therapeutic approaches for the management of obese-induced insulin resistance.

4.2 Results

4.2.1 Obese ATMs-derived extracellular vesicles (EVs) bestow miR-210-3p to adipocytes

To investigate the quantum of preadipocyte and macrophage populations in obese vWAT (VAT), we have stained tissue sections with the F4/80 (macrophage marker) and Pref-1 (preadipocyte marker). An increased accumulation of macrophages coincides with the reduction of preadipocyte pool in the VAT of high-fat diet (HFD)-fed mice as compared to standard diet (StndD)-fed mice (**Fig. 4.1A, B**). Reanalysis of the publicly available single nuclei sequencing dataset of VAT from lean and obese human subjects as well as StndD and HFD mice (GSE176171) (Emont et al., 2022), revealed a significant increase in adipose tissue macrophages (ATMs) both in the VAT samples of obese human (**Fig. 4.1C,D**) and HFD mice (**Fig. 4.1E,F**). We recently reported that ATMs of obese VAT profoundly expressed *miR-210-3p* (Patra et al., 2023). However, the specific action of *miR-210-3p* on adipocytes in obese *ATenv* for inducing insulin resistance has not yet been explored. Comparative expression analysis demonstrated significant high expression of*miR-210-3p* in macrophages compared to preadipocytes and adipocytes, in the obese subject and HFD mice in contrast to lean control counterparts. (**Fig. 4.1R,S**). A similar trend was also observed in 3T3-L1 preadipocytes, adipocytes, and RAW264.7 macrophages when exposed to both hypoxia (H, 1% O_2) and lipid (L, 0.75mM Palmitate) for 16 hours (**Fig. 4.1T**). All these observations suggest that ATMs, which constitute a major pool in the SVF, serve as a key cellular source of *miR-210-3p*.

To examine the fate of ATMs-derived miR-210-3p, we first explored the ATMs released extracellular vesicles (EVs), as recent studies indicated that ATMs-derived EVs bolster systemic inflammation and insulin resistance (Salomon et al., 2022; Ying et al., 2017). The TEM imaging of VAT from HFD (16 weeks) mice demonstrated massive amounts of EVs are present within the ATMs and also blebbed out from its membrane (**Fig. 4.1G**). In addition, bone marrow-derived macrophages (BMDMs) exposed to

hypoxia (H, 1% O_2) and lipid (L, 0.75 mM), similar to pathophysiological obese AT*env*, increased the size of EVs (216.8±54.3 nM) as compared to EVs of control untreated cells (175.1±51.8 nM) (**Fig. 4.1H, I**). The nanoparticle tracking analyses (NTA) demonstrated the average mode size was increased along with the particle density (**Fig. 4.1J**). To comprehend the fusion of ATMs-derived EVs with adipocytes in pathophysiological condition, we performed *in-vitro* coculture of Vibrant DiO-labelled RAW264.1 macrophages on the upper boyden chamber (transwell 0.4µM membrane), with differentiated 3T3-L1 adipocytes, in the lower chamber. Interestingly, fluorescence imaging of Oil red-O-stained mature adipocytes showed notable uptake of Vibrant DiO dye indicating possible delivery of macrophage-specific EVs to the adipocytes (**Fig. 4.1K**). However, to examine the carriage of *miR-210-3p* from macrophage EVs to adipocytes, we cocultured FAM-conjugated *miR-210-3p* mimic transfected macrophages with differentiated 3T3-L1 adipocytes. Fluorescence imaging displayed that majority of Oil red-O-stained mature adipocytes were FAM positive (**Fig. 4.1L**) suggesting the delivery of macrophage-originated *miR-210-3p* into the mature adipocytes via the EVs. The isolated EVs from the cell culture supernatant, animal serum, and patient serum were confirmed by the presence of an EV-specific marker CD63 with a profound increase in the abundance of EVs secreted from H+L treated macrophages, and in the serum of HFD mice, and T2D patients (**Fig.4.1M**). For further validation, we performed qPCR analyses of *miR-210-3p* level in the EVs. Our finding showed that *miR-210-3p* expression was considerably increased by approximately 60-folds in the EVs of H+L treated macrophages as compared to the control (**Fig. 4.1N**). Similarly, *ex-vivo* culture of ATMs, isolated from the omental fat pads of StndD and HFD mice, demonstrated a significant upregulation of *miR-210-3p* in the EVs of HFD mice (**Fig. 4.1O**). Moreover, the magnitude of *miR-210-3p*levels in the systemic circulation was detected by extracting serum EVs from StndD and HFD mice as well as from lean non-diabetic and obese T2D patients. We found that *miR-210-3p* levels were upregulated by approximately 6.9 folds and 7.5 folds, respectively, in HFD mice and obese T2D patients (**Fig. 4.1P, Q**).

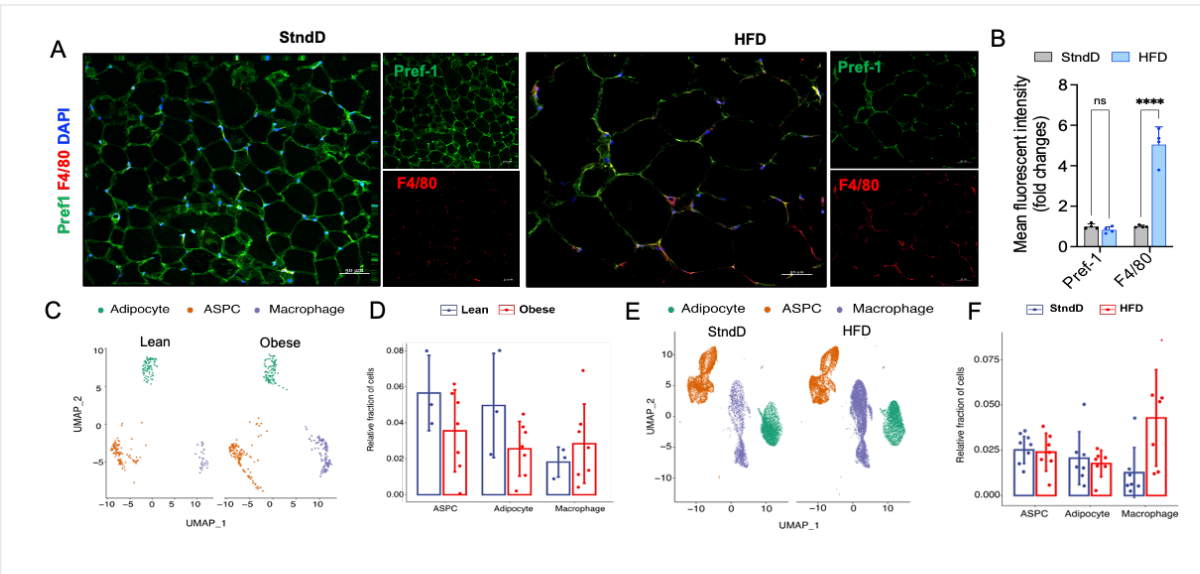

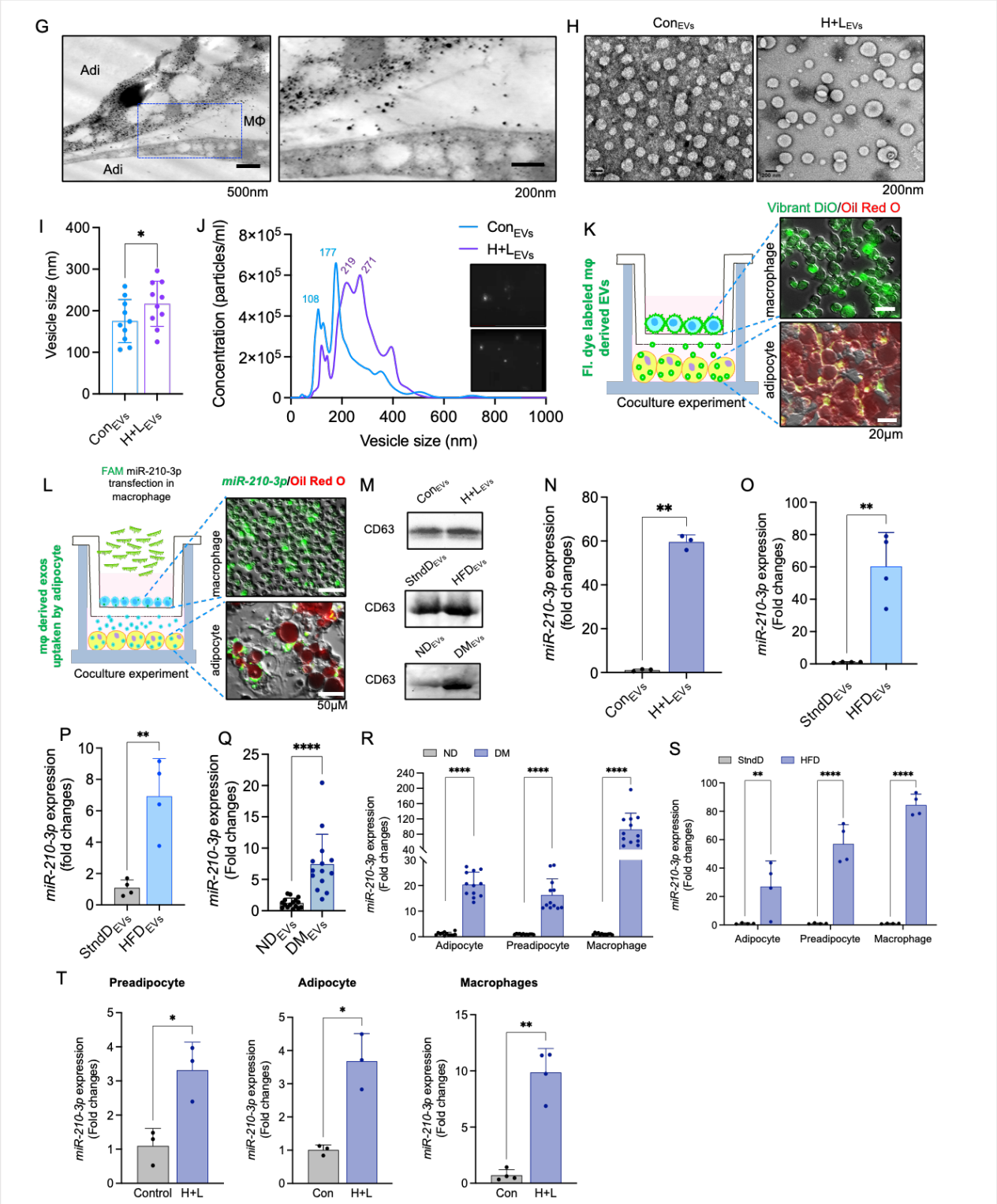

Figure 4.1 | **Obese ATMs-derived extracellular vesicles (EVs) bestow miR-210-3p to adipocytes**

A and *B*: Representative immunofluorescence staining of F4/80 (red), Pref1 (green) with DAPI counterstaining in the VAT section of StndD and HFD-fed mice followed by confocal microscopy (A) and quantification analyses (B) Scale bar, 50μm. *C* and *D*: Uniform manifold approximation and projection (UMAP) of adipose progenitor cells, mature adipocytes, and macrophages from the reanalysis of publicly available sn-Seq data, sequenced all cells of VAT in healthy and obese individuals followed by quantification of the projected cells. *E* and *F*: Uniform manifold approximation

and projection (UMAP), and relative fraction of adipose progenitor cells (ASPC), mature adipocytes, and macrophages from the reanalysis of publicly available sn-Seq data, sequenced all cells of VAT in StndD and HFD fed mice followed by quantification of the projected cells. *G:*Representative images showing ATM (MΦ) releases extracellular vesicles (EVs) uptake by adipocytes (Adi) in the obese AT*env*. Transmission electron microscopic (TEM) images of VAT section of the obese HFD mice. *H* and *I*: TEM images of EVs isolated from primary culture of mouse BMDM cotreated with H + L and mean size quantification **P*<0.05. *J*: Visualization of control and H + L treated macrophage released EVs on NanoSight LM10 with size analysis. *K*: Representative image showing Vibrant DiO staining in macrophages cocultured with 3T3-L1 adipocytes in transwell setup. Adipocytes were stained with oil red o dye. Scale bar: 50µm. *L*: Representative image showing FAM conjugated miR-210-3p mimic transfected macrophages cocultured with 3T3-L1 adipocytes in transwell setup and fluorescence imaging showed the presence of *miR-210-3p*-FAM to adipocyte. Adipocytes were stained with oil redo dye. Scale bar: 50µm. *M*: Western blot analysis showing CD63 expression in EVs isolated from control and H + L co-incubated macrophage culture supernatant, EVs isolated from StndD or HFD mice serum, and ND or DM patients' serum. *N*: *miR-210-3p* expression analyses in control and H + L incubated macrophage-secreted EVs (n=3) ***P*<0.01. *O*: qRT-PCR analyses of *miR-210-3p* in EVs isolated from the primary culture of sorted F4/80+ ATMs from VAT of StndD and HFD mice (n=4) ***P*<0.01. *P* and *Q*: *miR-210-3p* expression in the serum-containing EVs isolated from the serum of StnD and HFD mice (P) (n=4) ***P*<0.01; ND and DM individuals (Q) (n=14-16) *****P*<0.0001. R: qRT-PCR analyses of miR-210-3p in the preadipocytes, adipocytes, and macrophages isolated from VAT of ND and DM human patients. (n= 14-16) ****P<0.000. S: qRT-PCR analyses of miR-210-3p in the preadipocytes, adipocytes, and macrophages isolated from VAT of StndD and HFD mice. (n=4) **P<0.01, ****P<0.000. T: miR-210-3p expression in the in-vitro cultured murine preadipocyte, adipocyte, and macrophage in the presence or absence of hypoxia and lipid. (n=3) *P<0.05; **P<0.01.

4.2.2 miR-210-3p enriched EVs of obese ATMs promote glucose intolerance and insulin resistance

To examine the efficacy of *miR-210-3p*-enriched EVs on the impairment of insulin sensitivity; we isolated EVs from the macrophages at normal (con) or lipid-rich hypoxic (H+L) condition, then incubated them with the differentiated 3T3-L1 adipocytes for 16 hours. A significant reduction of glucose uptake by adipocytes was noticed in response to EVs of H+L condition, as indicated by the 2-NBDG uptake (**Fig. 4.2A**). Moreover, analysis of insulin signaling pathway molecules activation revealed a considerable impairment of Akt activation and downregulation of GLUT4 expression in adipocytes treated with *miR-210-3p*-enriched EVs of H+L condition (**Fig. 4.2B**). These results suggest that EVs secreted from H+L-treated macrophages which encompass higher levels of *miR-210-3p* markedly attenuate insulin sensitivity in adipocytes. To further validate the role of macrophage-derived *miR-210-3p*-loaded EVs on adipocytes' insulin action, *miR-210-3p* mimic or control mimic transfected to macrophages and were co-cultured with adipocytes. We observed a notable declination of insulin-stimulated 2-NBDG uptake and Akt activation in adipocytes in response to *miR-210-3p* mimic transfected macrophages (**Fig. 4.2C,D**). Several reports evidenced EV miRNAs secreted from ATMs govern the pathophysiology of metabolic diseases (Akbar et al., 2019; Wang et al., 2020; Ying et al., 2017). Therefore, to nullify the involvement of other miRNA species in the EVs of *miR-210-3p* mimic transfected macrophages on the induction of adipocytes insulin resistance, we first silenced DICER expression in macrophages by siRNA followed by the delivery of control mimic LNA or *miR-210-3p*

mimic LNA. The knockdown of DICER expression was validated by RT-qPCR analysis (**Fig.4.2Q**). As expected, the gene expression analyses revealed a striking reduction of other miRNA's like *miR-27a-3p*, *miR-126*, and *miR-200b-3p* expression, with the increased level of *miR-210-3p* in the EVs isolated from DICER-silenced miR-210-3p mimic transfected macrophages (**Fig.4.2R,S**). The EVs isolated from these cells, when incubated with 3T3-L1 adipocytes, a significant reduction of 2-NBDG uptake was observed (**Fig. 4.2E**) suggesting the potential role of macrophage EVs-associated *miR-210-3p* in the impairment of insulin-stimulated glucose uptake in adipocytes. For *in-vivo* validation, we have administered Vibrant DiO-labelled EVs isolated from the DICER-silenced macrophages transfected with control or *miR-210-3p* mimic LNAs to C57BL/6 lean mice by intravenous injection ($2x10^6$ particles/ mice) once every 3 days for 20 days (**Fig. 4.2F**). The considerable accumulation of Vibrant Dio-labelled EVs (**Fig. 4.2T**) with a profound increase of *miR-210-3p* levels (**Fig. 4.2U**) was noticed in the VAT, skeletal muscle, and liver, without any significant alteration of body mass (**Fig. 4.2V**). Moreover, mice administered with labelled EVs exhibited impaired glucose- and insulin-tolerance indicated by GTT and ITT analyses (**Fig. 4.2G,H**). Furthermore, HOMA-IR analysis demonstrated a significant induction of insulin resistance (**Fig. 4.2I**). At the molecular level, impairment of Akt activation in the VAT, skeletal muscle, and liver of these mice as compared to the control group (**Fig. 4.2J,K**). All these results indicate that *in-vivo* delivery of *miR-210-3p*-loaded EVs promotes glucose intolerance and insulin resistance in mice through the paracrine and endocrine actions on the VAT, skeletal muscle, and liver. For direct evidence, we administered the FAM-conjugated control or *miR-210-3p* mimic LNAs in lean mice through intravenous injections for 6times in 21 days with regular intervals (**Fig. 4.2L**). The localization and increased abundance of *miR-210-3p*was noticed in the VAT, skeletal muscle, and liver of labelled miR-210-3p LNA administered mice as indicated by fluorescence imaging and RT-qPCR analysis, respectively with no change in body weight (**Fig. 4.2W-Y**). Systemic glucose homeostasis and insulin responsiveness were disturbed in these mice (**Fig. 4.2M,N**). These observations are corroborated by the impairment of Akt activation in the VAT, skeletal muscle, and liver (**Fig. 4.2O,P**). Collectively, all these results suggest that macrophage EVs-derived *miR-210-3p* localized into the insulin target tissue and confers systemic glucose intolerance and insulin resistance.

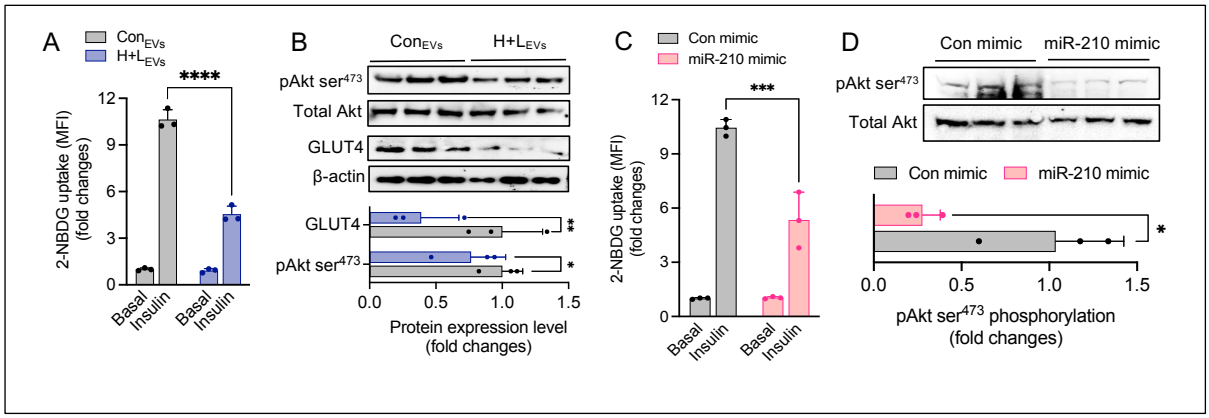

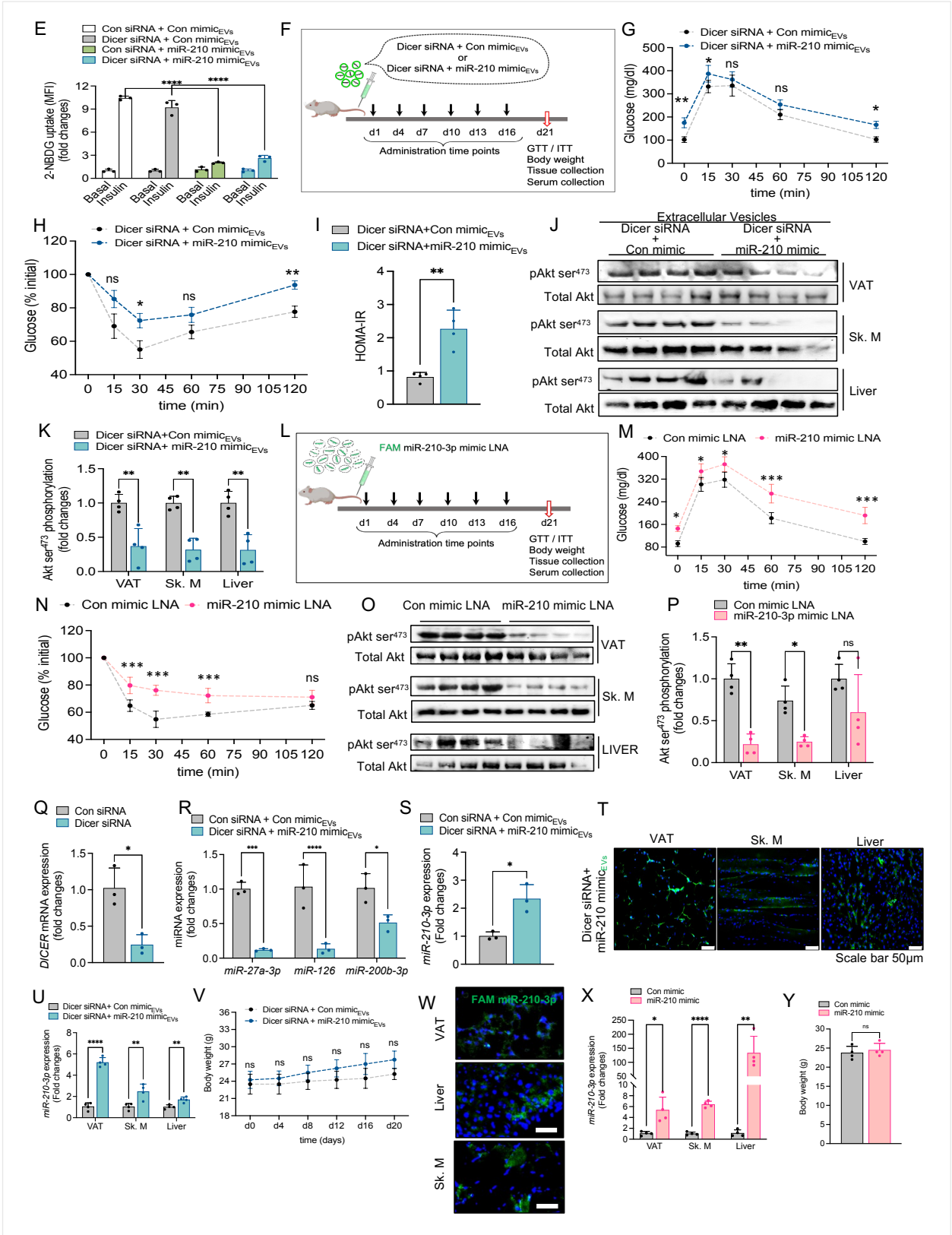

Figure 4.2 |**miR-210-3p-enriched EVs of obese ATMs promote glucose intolerance and insulin resistance**

A: Insulin-stimulated glucose uptake was monitored by measuring 2-NBDG in the cell lysate of adipocytes, incubated with control and H+L treated BMDM released EVs. (n=3) ****P<0.0001 *B*: Western blot analysis showed Akt ser^{473} phosphorylation and GLUT4 protein expression in adipocyte

exposed with control or H+L incubated BMDM EVs. (n=3). *C*: Glucose uptake in the presence or absence of insulin stimulation in Control mimic or *miR-210-3p* mimic transfected adipocytes. (n=3) ***P<0.001 *D*: Western blot analysis showed Akt ser^{473} phosphorylation in adipocyte transfected with Control mimic and miR-210-3p mimic. (n=3). *E:* Glucose uptake assay under the presence or absence of insulin stimulation in adipocytes cocultured with Dicer silenced macrophage transfected with Control mimic or miR-210-3p mimic. (n=3) ****P<0.0001 *F*: Schematic diagram showing Standard diet fed mice administered with EVs isolated from Dicer silenced macrophages transfected with control mimic and miR-210-3p mimic via an intravenous route with a regular interval for 21 days before termination of the experiment. *G-I*: Glucose tolerance test (GTT) (*G*), insulin tolerance test (ITT) (*H*), and HOMA-IR (*I)* analyses were performed in StndD fed mice injected with EVs isolated from DICER silenced macrophage transfected with control mimic LNA or miR-210-3p mimic LNA (n = 4). *P<0.05, **P<0.01, ns- non-significant. *J* and *K*: Western blot analyses of Akt ser^{473} phosphorylation (*J*) and quantification analyses (*K*) in VAT, Sk. M, and liver in StndD mice administered with EVs, isolated from DICER silenced macrophage transfected with Control mimic LNA or miR-210-3p mimic LNA via the intravenous route in regular intervals for 21 days; **P<0.01two-way ANOVA. *L*: Schematic diagram showing control mimic or miR-210-3p mimic LNA intravenous injection in regular intervals for 21 days in C57BL/6 mice. *M* and *N*: GTT (*M*) and ITT (*N*) were performed in StndD mice administered with control mimic LNA and miR-210-3p mimic LNA with each 3-day interval in the period of 21 days. (n=4). *P<0.05, **P<0.01, ***P<0.001, *O* and *P*: Western blot analyses Akt ser^{473} phosphorylation in VAT, Sk. M, and liver in StndD mice administered Control mimic LNA or miR-210-3p mimic LNA via the intravenous route in regular intervals for 21 days and quantification analyses (n = 4). *P< 0.05, **P<0.01, ns non-significant. *Q*: qRT-PCR analyses of DICER mRNA expression in BMDMs transfected with control siRNA and DICER siRNA (n=3) *P<0.05. *R,S*: miR-27a-3p, miR-126, miR-200b-3p and miR-210-3p expression in EVs isolated from DICER silenced BMDMs transfected with control mimic and miR-210-3p. (n=3) *P<0.05, ***P<0.001, ****P<0.0001. *T*: Fluorescence images of histological sections showing fluorochrome-labeled EVs presence in the AT, liver, and Sk. M of StnD mice. Scale bar 50µm. U: miR-210-3p expression in VAT, Sk. M and Liver in StnD mice administered with DICER silenced BMDMs EVs having control mimic or miR-210-3p mimic LNA via the intravenous route in regular intervals for 21 days. (n=4) **P<0.01, ***P<0.001. *V*: Body weight measurement in StnD mice administered with DICER silenced macrophage EVs having control mimic or miR-210-3p mimic LNA via the intravenous route in regular intervals for 21 days. (n=4). *W*: Fluorescence images of histological sections showing miR-210-3p presence in VAT, liver, and Sk. M of StnD mice administered FAM conjugated miR-210-3p mimic LNA encapsulated with invivofectamine^{TM} via the intravenous route in regular intervals for 21 days. Scale bar 50µm. *X*: miR-210-3p expression in VAT, Sk. M, and Liver in StnD mice administered control mimic or miR-210-3p mimic LNA via the intravenous route in regular intervals for 21 days. (n=4) *P<0.05, **P<0.01, ****P<0.0001. *Y*: Body weight of mice administered FAM conjugated control mimic LNA and miR-210-3p mimic LNA, measured before sacrifice. (n=4). Data are expressed as means ± SD; n= 3-5

4.2.3 Suppression of GLUT4 expression by the direct interaction with miR-210-3p potentiates insulin resistance

To investigate any direct role of *miR-210-3p* in the insulin signaling pathway, we have searched putative binding sites of *miR-210-3p* on the insulin signaling pathway molecules. Analysis of miRWALK database search revealed that there are multiple molecular targets of *miR-210-3p* including *GLUT4*, *INSR*, and *IRS1/2/4* that display a critical seed sequence necessary for *miR-210-3p* binding (**Fig. 4.3A and 4.3P**). We have validated this by transfecting the control mimic or miR-210-3p mimic to adipocytes. *miR-210-3p* mimic significantly silenced the mRNA expression of GLUT4 as compared to others (**Fig. 4.3Q-R**). Moreover, we also measured the minimum free energy (-31.5 kCal/mol) required for the interaction between *GLUT4* 3′UTR and *miR-210-3p* by using RNAhybrid webserver

(**Fig. 4.3B**). However, to confirm the binding of *GLUT4* 3′UTR with *miR-210-3p*, we performed the *GLUT4* 3′UTR luciferase reporter assay. For this, wild-type (WT)- or mutated (MUT)- *GLUT4* 3′UTR luciferase plasmid was co-transfected with control mimic or *miR-210-3p* mimic in 3T3-L1 adipocytes. The *miR-210-3p* mimic delivery significantly repressed WT-*GLUT4* 3′UTR luciferase activity in comparison to control mimic transfected cells, whereas, MUT-*GLUT4* luciferase activity was not compromised in *miR-210-3p* mimic transfected cells (**Fig. 4.3C**) indicating a direct involvement of *miR-210-3p* binding with *GLUT4* 3′UTR. In addition, analysis of GLUT4 protein expression in *miR-210-3p*mimic transfected 3T3-L1 cells demonstrated a considerable reduction of cellular GLUT4 level as indicated by immunoblotting (**Fig. 4.3D,E**), and immunofluorescence analyses (**Fig. 4.3F,G**). Moreover, the reduction of cellular GLUT4 level in response to *miR-210-3p* mimic transfection was also observed in C2C12 skeletal muscle cells (**Fig. 4.3H,I**). Next, we administered *miR-210-3p* mimic LNA in C57BL/6 lean mice to evaluate its efficacy on the impairment of GLUT4 expression in insulin target tissue. A striking reduction of *GLUT4* mRNA (**Fig. 4.3J**) and protein (**Fig. 4.3K,L**) expressions were noticed in the VAT, skeletal muscle, and liver of *miR-210-3p* mimic LNA-administered mice. Interestingly, H&E staining and GLUT4 immunostaining of the VAT displayed an increase in adipocyte size which coincided with subdued expression of GLUT4 in *miR-210-3p* mimic LNA administered mice (**Fig. 4.3S-U**). To decipher the role of macrophage-derived *miR-210-3p*-enriched EVs in GLUT4 expression, we incubated adipocytes with EVs isolated from control or *miR-210-3p* mimic transfected DICER-silenced macrophages. A significant reduction of GLUT4 protein expression was observed in adipocytes when treated with the EVs of DICER-silenced *miR-210-3p* mimic transfected BMDMs (**Fig. 4.3V**). Administration of these EVs in lean mice exhibited adipocyte hypertrophy (**Fig. 4.3W**) with a notable decrease in GLUT4 gene and protein expression in the VAT, skeletal muscle, and liver (**Fig. 4.3M-O and X**). Taken together, these results showed that GLUT4 serves as a key molecular target of *miR-210-3p* for affecting insulin sensitivity.

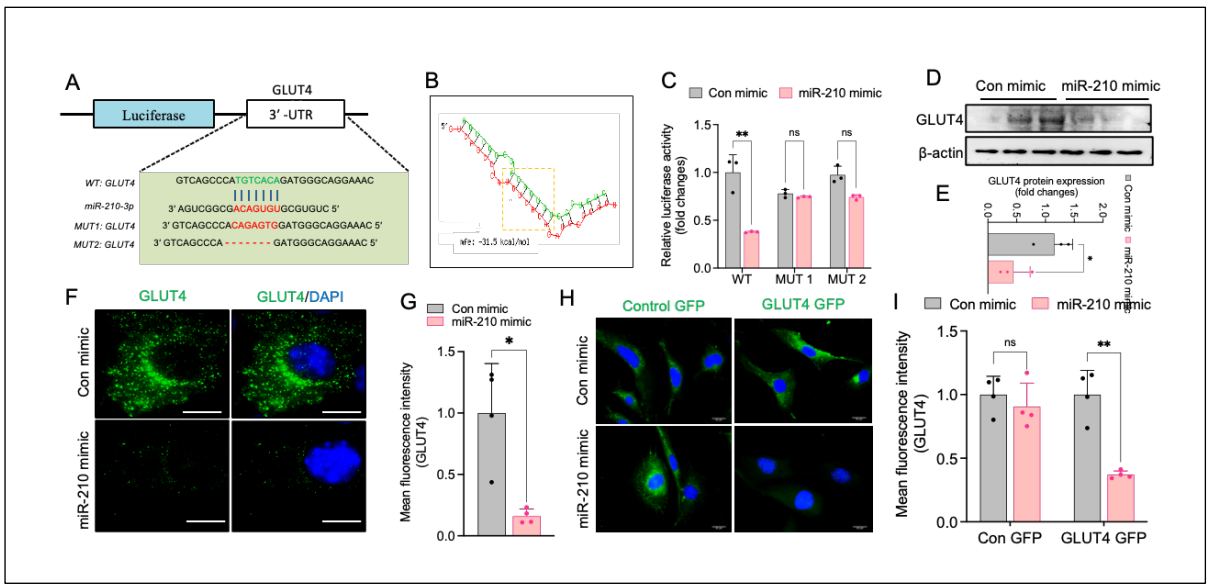

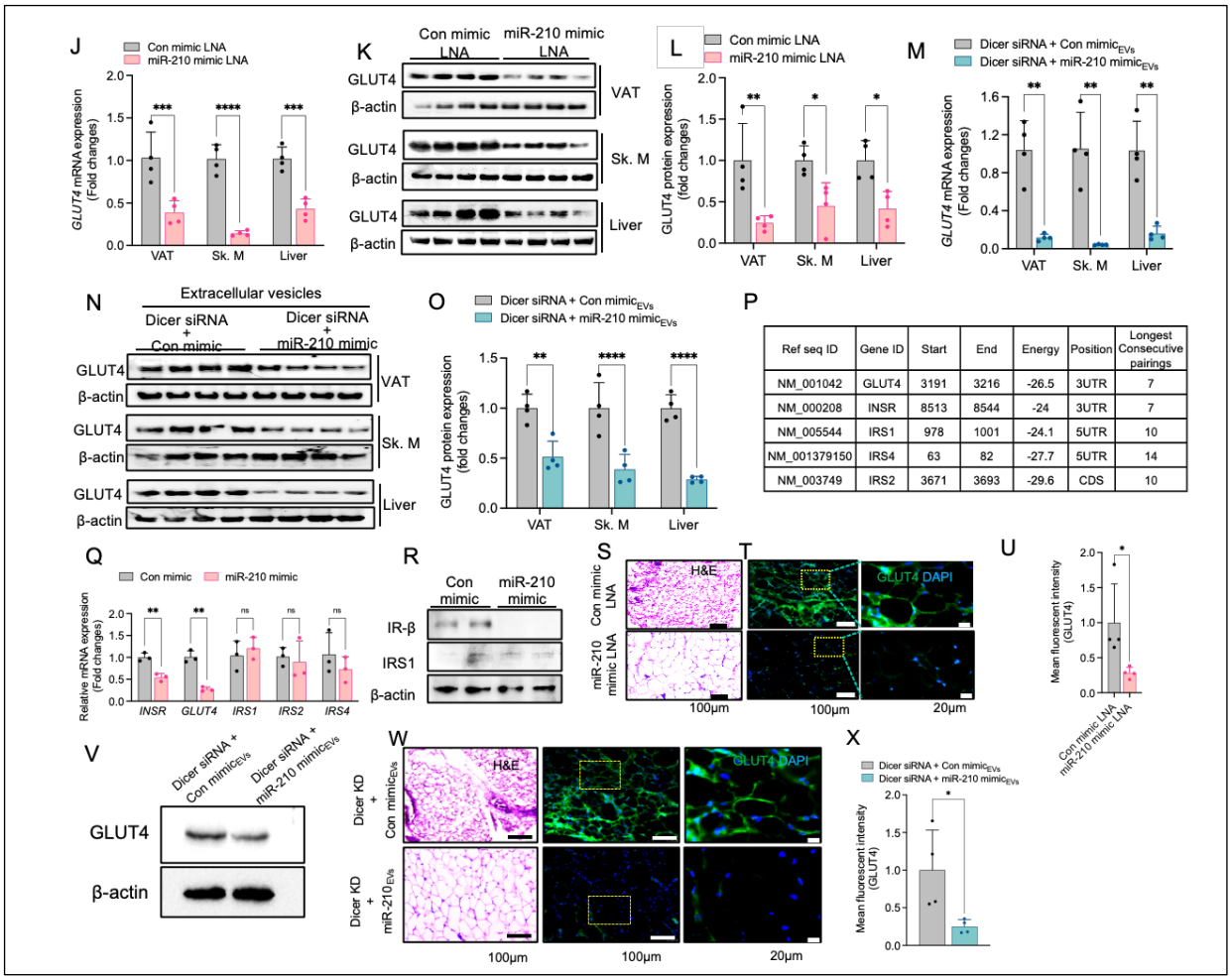

Figure 4.3 | **Suppression of GLUT4 expression by the direct interaction with miR-210-3p potentiates insulin resistance**.

A: Putative conserved binding site of GLUT4 with *miR-210-3p* and seed sequence of *miR-210-3p* and mutated 3′-UTR sites of GLUT4. *B*: RNAhybrid webserver was used to predict the minimum free energy (mfe) of *GLUT4* mRNA transcripts and *miRNA-210-3p* interactions. *C*: Luciferase activity in Preadipocytes co-transfected with WT or mutated (mut1 and mut 2) GLUT4 plasmid constructs and control mimic or miR-210-3p mimic (n = 3). ***P*<0.01. *D*, *E*: GLUT4 protein expression measured by performing western blotting (D) and quantification analyses (E) in adipocytes transfected with control mimic and miR-210-3p mimic (n=3). ***P*<0.01. *F* and *G*: GLUT4 immunofluorescence imaging (F) and quantification analyses (G) in adipocytes transfected with control mimic and miR-210-3p mimic (n=3). ***P*<0.01. *H,I*: Immunofluorescence image showing GLUT4 migration in murine myoblast cells transfected with control mimic or miR-210-3p mimic (H) and Quantification analysis (I). ***P*<0.01, ns= not significant. *J*-L: qRT-PCR analyses (J), Immunoblotting, and quantification analyses (K and L) of *GLUT4* mRNA expression in StndD mice injected with control mimic LNA or miR-210-3p mimic LNA via the intravenous route in regular intervals for 21 days. (n=4).***P*<0.01, ****P*<0.001, *****P*<0.0001. *M-O*: *GLUT4* mRNA expression analyses (M), western blotting, and quantification analyses (N and O) in VAT, Liver, and Sk.M in StndD mice administered with DICER silenced macrophage exosomes having control mimic LNA or miR-210-3p mimic LNA via the intravenous route in regular intervals for 21 days. (n=4) ***P*<0.01, ****P*<0.001, *****P*<0.0001. P: miRNA target prediction analyses using miRWALK database search analysis showed miR-210-3p targets for insulin signaling pathways molecule. Q: mRNA expression analyses of predicted targets INSR, GLUT4, IRS1, IRS2, IRS4 in adipocytes transfected with control mimic or miR-210-3p mimic. (n=3) *P<0.05, **P<0.01. R: Western blotting analyses of IR-β, IRS1 in adipocytes transfected with control mimic or miR-210-3p mimic. S-U: VAT sectioning, H&E staining followed by brightfield imaging (S), and

immunofluorescence imaging staining GLUT4 (T) followed by quantification analyses of control mimic LNA or miR-210-3p mimic LNA. Quantification analyses (U). V: Immunoblotting analyses and quantification of GLUT4 in adipocytes treated with EVs from DICER silenced macrophages transfected with control mimic or miR-210-3p mimic. Quantification analyses. W,X: VAT sectioning, H&E staining followed by brightfield imaging, and immunofluorescence imaging staining GLUT4, quantification analyses (W) in StnD mice administered with DICER silenced and control mimic or miR-210-3p mimic co-transfected macrophage EVs administered via the intravenous route in regular intervals. Quantification analyses. (X) (n=4) *P<0.05. Data are expressed as means ± SD; n= 3-4.

4.2.4 miR-210-3p inhibition rescues DIO mice from glucose intolerance and insulin resistance

To examine the therapeutic potential of anti-miR-210-3p in the rescue of obesity-induced impairment of insulin resistance, we delivered invivofectamine^{TM} encapsulated FAM-labeled control inhibitor LNA or miR-210-3p inhibitor LNA at the VAT of HFD-fed obese mice for 14 days followed by the collection of serum and tissue samples (**Fig. 4.4A**). The HFD mice exhibited a substantial decrease in GLUT4 expression and Akt activation in the VAT, skeletal muscle, and liver, as compared to StndD mice (**Fig. 4.4O-T**). The validation of FAM-labeled miR-210-3p inhibitor LNA accumulation was observed in the VAT, skeletal muscle, and liver (**Fig. 4.4U**) correspond to diminished adipocyte hypertrophy in the VAT (**Fig. 4.4B**) of miR-210-3p inhibitor LNA administered HFD mice. Administration of miR-210-3p inhibitor LNA in the VAT of HFD mice notably increased GLUT4 abundance and Akt activation in the VAT (**Fig. 4.4C-G**), skeletal muscle (**Fig. 4.4V,W)**, and liver(**Fig. 4.4X,Y**) which coincided with a subdued level of miR-210-3p in the vWAT, ATM released EVs, and the circulatory EVs in serum(**Fig. 4.4H-J**) with a significant reduction in body weight (**Fig. 4.4K**). All these results suggest that miR-210-3p inhibitor LNA-enriched EVs delivered to the VAT, skeletal muscle, and liver improve insulin sensitivity. However, a future study is needed to establish the correlation of miR-210-3p inhibitor delivery with the reduction of body mass in mice. Moreover, VAT-specific delivery of miR-210-3p inhibitor significantly restored systemic glucose tolerance and insulin sensitivity in HFD mice as indicated by GTT, ITT, and HOMA-IR analyses (**Fig. 4.4L-N**). Altogether,

our studies suggest miR-210-3p as a strong therapeutic candidate for the management of obesity-induced insulin resistance and T2D.

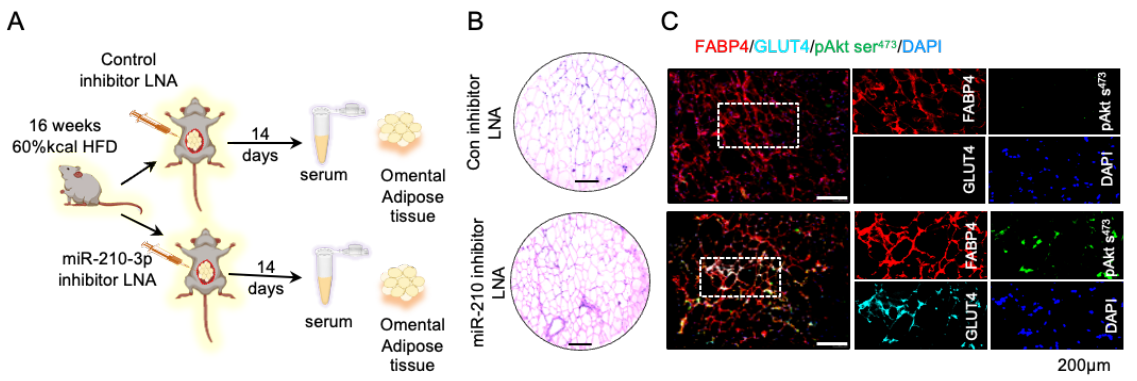

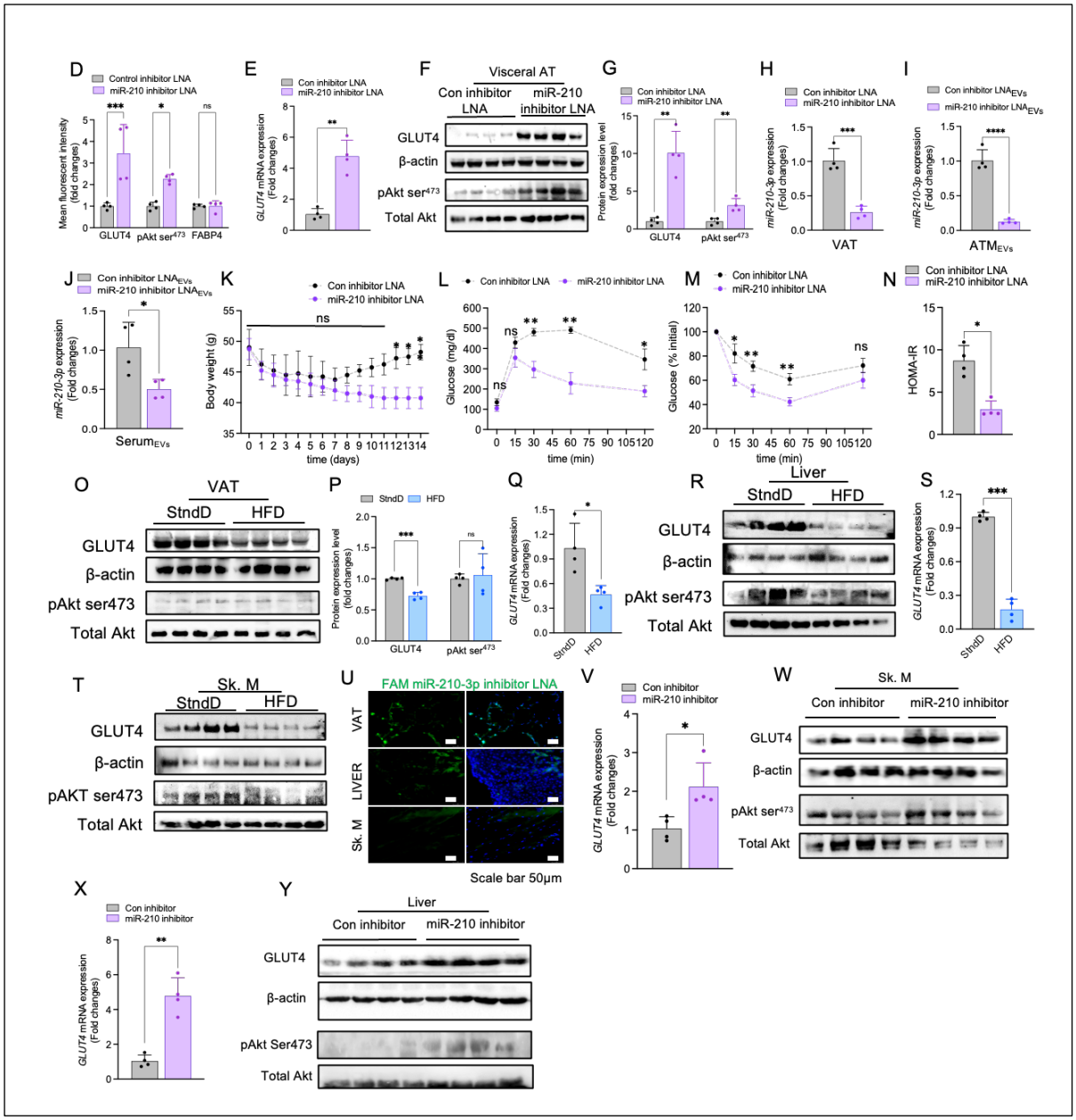

Figure 4.4 | **Suppression of GLUT4 expression by the direct interaction with miR-210-3p potentiates insulin resistance**.

A: Schematic diagram showing control inhibitor LNA or miR-210 inhibitor LNA administration in the VAT of 12 weeks HFD mice. *B*: H&E staining of VAT section of control inhibitor LNA or miR-210 inhibitor LNA treated HFD mice. *C,D*: Immunofluorescence imaging (C) and fluorescent intensity quantification analyses (D) of GLUT4(cyan), pAkt ser^{473}(green), and FABP4(red) in the VAT section of control inhibitor LNA and miR-210 inhibitor administered HFD mice. (n=4) *P<0.05, ***P<0.001. *E,F*: Western blotting (E) and quantification analyses (F) of GLUT4 and pAkt ser^{473} phosphorylation in VAT of control inhibitor LNA or miR-210 inhibitor LNA treated HFD mice. *G*: *GLUT4* mRNA expression in VAT of control inhibitor LNA or miR-210 inhibitor LNA treated HFD mice. (n=4). **P<0.01. *H*: *miR-210-3p* expression in the VAT of control inhibitor LNA or miR-210 inhibitor LNA mice. (n=4). **P<0.01. *I*: *miR-210-3p* expression in the ATM-derived EVs isolated from VAT of control inhibitor or miR-210-3p inhibitor LNA administered HFD mice. (n=4) ****P<0.0001. *J: miR-210-3p* expression in the EVs isolated from the serum of Control inhibitor LNA and miR-210-3p inhibitor LNA administered HFD mice(n = 4). *P<0.05. *K*: Body weight of HFD mice administered with control inhibitor LNA or miR-210-3p inhibitor LNA in the VAT for 14 days. (n=4) *P<0.05,

**P<0.01, ns= not significant. *L-N*: GTT (L), ITT (M), and HOMA-IR (N) analyses were performed in HFD mice injected with control inhibitor LNA or miR-210 inhibitor LNA (n=4). *P<0.05, **P<0.01. *O-Q*: Western blotting and quantification analyses showing GLUT4, phosphorylated AKT ser473, and mRNA expression of GLUT4 in the VAT of StndD and HFD mice. (n=4) ***P<0.001; *P<0.01. *R,S*: Western blotting showing GLUT4, phosphorylated AKT ser473, and mRNA expression of GLUT4 in the liver of StndD and HFD mice. (n=4) **P<0.01.*T*: Western blotting and quantification analyses showing GLUT4, phosphorylated AKT ser473 expression in the skeletal muscle of StndD and HFD mice. (n=4) **P<0.01; **P<0.01. *U*: Fluorescence imaging showing the presence of FAM conjugated miR-210-3p inhibitor in the histological sections of VAT, liver, and skeletal muscle from HFD mice administered with miR-210-3p inhibitor. *V,W*: GLUT4 mRNA expression analyses (V) Immunoblotting analyses of GLUT4 and pAkt ser473 phosphorylation (W) in skeletal muscle of control inhibitor LNA or miR-210 inhibitor LNA treated HFD mice. (n=4). *P<0.05. *X,Y*: qRT-PCR analyses of GLUT4 mRNA expression analyses (X) and Immunoblot analyses of GLUT4 and phosphorylated AKT (Y) in the liver of control inhibitor or miR-210-3p inhibitor administered HFD mice. **P<0.01.

4.3 Discussion

Obesity-induced pathophysiological AT*env* influences massive ATM infiltration and alteration of their polarity towards proinflammatory state influencing chronic AT inflammation and insulin resistance (Boutens & Stienstra, 2016; Patra et al., 2023). It has been shown that the alteration of miRNAs profile in the obese adipose tissue is critically associated with the modulation of insulin signaling pathway. Reportedly, miR-128, miR-103, miR-107, and miR-26b were found to be altered in obese AT*env* which directly regulate the key signaling molecules of insulin signaling pathway and implement insulin resistance (Arcidiacono et al., 2020; Trajkovski et al., 2011; Xu et al., 2015). Among these miRNAs, miR-128 specifically increased in adipocytes under hypoxic conditions which attenuates adipocytes insulin sensitivity by the suppression of insulin receptor (INSR) expression (Arcidiacono et al., 2020). These studies primarily focus on adipose tissue biology and its insulin sensitivity, however, the participation of these miRNAs in the different insulin-responsive cells and systemic insulin resistance has not been explored.

The miRNAs are often packaged and delivered in many organs through extracellular vesicles (EVs) (György et al., 2015; Jeppesen et al., 2023). ATMs secrete varied sizes of EVs, including exomeres, exosomes, and microvesicles that contribute to adipose tissue dysfunction(Huang & Xu, 2021; Wang et al., 2020; Ying et al., 2017). Recently it has been shown that lean insulin-sensitive mice readily develop systemic insulin resistance and glucose intolerance when treated with ATMs-derived exosomes (Exos) from obese mice, whereas, the opposite effect was observed in obese insulin-resistant mice with improved insulin sensitivity when administered to ATMs-derived Exos (Ying et al., 2017, 2021). Analysis of ATMs-derived Exos from obese mice revealed that miR-155 is among the major differentially expressed miRNAs, responsible for the promotion of glucose intolerance through the suppression of PPARγ(Ying et al., 2017). The role of pathophysiologic lipid-rich and hypoxic AT*env* on the cross-talk between ATMs and neighboring adipocytes with the specific involvement of ATMs-

derived hypoxamiR-enriched EVs has not yet been explored. Also, specific miRNA-enriched EVs that could directly target insulin signaling pathway molecules have not been revealed. In our previous study, we identified that *miR-210-3p* level has been greatly increased in the ATMs of obese mice that critically regulate inflammation by targeting the SOCS1-NF-kB pathway (Patra et al., 2023). In this study, we have shown that obesity-induced lipid-enriched hypoxic AT*env* navigates the pathogenesis of insulin resistance and glucose intolerance by inducing ATMs to release and transfer *miR-210-3p*-loaded EVs to insulin target cells such as adipocytes, skeletal muscle cells, and hepatocytes through paracrine and endocrine actions. EVs isolated from the serum of obese T2D patients and HFD mice are highly enriched with *miR-210-3p* as compared to the lean non-diabetic subject or StndD mice.

Examining the exclusive role of miR-210-3p in the ATMs-derived EVs of obese T2D mice on the suppression of insulin signaling, we have performed many experiments which evidenced EVs isolated from miR-210-3p transfected DICER-silenced BMDMs when administrated to StndD mice, it promotes glucose intolerance and insulin insensitivity in them by reducing GLUT4 expression and Akt activation in the VAT, skeletal muscle, and liver. This observation nullifies the involvement of other ATMs-derived EV-borne miRNAs in obesity-induced insulin resistance. However, to investigate the direct effect of miR-210-3p in regulating cellular insulin sensitivity, glucose uptake was monitored in adipocytes transfected with the miR-210-3p mimics. A significant loss of insulin-stimulated glucose uptake in adipocytes was noticed in response to miR-210-3p mimic delivery clarifying the direct participation of miR-210-3p on insulin resistance. Following bioinformatic database search analyses, in-vitro cell culture experiment with 3T3-L1 adipocytes, transfected with miR-210-3p mimic, showed down expression of INSR, and GLUT4 mRNAs, which involved in insulin-signaling pathway (Saltiel, 2021), suggesting miR-210-3p might directly target multiple molecules of the insulin-signaling pathway, but extensive studies required to prove it. Since miR-210-3p has higher efficiency in silencing the GLUT4 molecule, we performed luciferase assay that evidenced *miR-210-3p* directly bound to the 3′UTR of *GLUT4* mRNA and silenced their expression in adipocytes, skeletal muscle cells, and hepatocytes, thus lowering cellular insulin responsiveness and glucose uptake. Moreover, delivery of lipid nanoparticle (invivofectamine)-encapsulated miR-210-3p LNA in lean mice notably augments metabolic dysfunction as indicated by the impairment of glucose- and insulin-tolerance test, which, coupled with the significant loss of GLUT4 expression and Akt activation in the VAT, skeletal muscle, and liver. This study revealed a novel action of obese ATM-derived EV-loadedmiR-210-3p in contributing to insulin resistance in lean mice, which potentially links with glucose intolerance. Intervention study was performed to assess the therapeutic potential of anti-miR-210-3p (miR-210-3p inhibitor LNA) by delivering it to the VAT of HFD mice, and to our surprise, we found that *anti-miR-210-3p* administration conducive to the amelioration of metabolic health with improved glucose tolerance and insulin sensitivity. *Anti-miR-210-3p* administered mice depict enhanced GLUT4

expression and Akt activation not only in the VAT (distant from the injection site) but also in the liver and skeletal muscle. Thus, *miR-210-3p* inhibition in the VAT may be a potent therapeutic strategy to combat obesity-induced systemic glucose intolerance and insulin resistance. However, further studies on ATM-specific *miR-210-3p* deficient animal models will provide direct evidence of *miR-210-3p* role in the understanding of disease progression and therefore it could be considered a limiting point of this study.

In summary, our findings demonstrated that ATMs-secreted *miR-210-3p*-enriched EVs from obese mice have the potential to induce systemic glucose intolerance and insulin resistance in lean mice by directly hindering insulin signaling pathway. In contrast, the VAT-specific delivery of *anti-miR-210-3p* LNA rescues obese HFD mice from the pathophysiological systemic glucose intolerance state by improving insulin sensitivity in target tissues. Thus, our study posits *anti-miR-210-3p* as a novel therapeutic candidate for managing insulin resistance and T2D.

4.4 Materials and Methods

4.4.1 Reagents and antibodies

All tissue culture materials were purchased from Life Technologies/Gibco, Nunc; Grand Island, NY; and Corning, NY. Description of all the antibodies including catalogue numbers, and the dilutions used in different experiments was given in **Table A.** We purchased Firefly Luciferase Reporter Assay System (cat. no. #E1500) from Promega, Madison, WI; QuickChange Lightning Multi Site-Directed Mutagenesis Kit (cat. no. #210515) from Agilent Technologies, Santa Clara, CA; XbaI (cat. no. R0145S) and SalI (cat. no. R3138S) restriction enzymes, T4 DNA Ligase enzyme (cat. no. M0202S) were procured from NEB, Ipswich, MA, USA. EV isolation kit from cell culture media and serum (ExoQuick-TC ULTRA and ExoQuick ULTRA respectively) were purchased from System Biosciences, Embarcadero Way Palo Alto, CA; 5' FAM conjugated miRCURY miR-210-3p mimic LNA (GeneGlobe ID: YM00470861-AGB; cat.no. 339174; 5'CUGUGCGUGUGACAGCGGCUGA), miRCURY control mimic LNA (GeneGlobe ID: YM00479902-AGA; cat. no. 339174; 5'UCACCGGGUGUAAAUCAGCUUG),miRCURY miR-210-3p mimic LNA (GeneGlobe ID: YM00470861-AGA, cat. no. 339174), 3' FAM conjugated mmu-miR-210-3p miRCURY LNA miRNA Inhibitor (GeneGlobe ID: YI04103147-DDC; catalog no. 339131), and miRCURY LNA miRNA Inhibitor Control (GeneGlobe ID: YI00199006-DDA; cat no. 339136) were procured from QIAGEN, Germantown, MD. The miRNA specific primers for miR-210-3p (cat. no.: #4427975; assay ID-000512), miR-200b-3p (cat. no.: #4427975; assay ID-002251), miR-27a-3p (cat. no.: #4427975; assay ID-000408), miR-126 (cat. no.:4427975 #; assay ID-000451), and U6 snRNA (cat. no.: #4427975; assay ID-001973) were procured from Applied Biosystems, Foster City, CA. Different gene-specific

primers were procured from Integrated DNA Technologies, India, and the sequence details were presented in **Table B.**

4.4.2 Mice models and treatments

Wild-type C57BL/6J male mice were considered for generating diet-induced obese mice model as described in Section 3.4.2. We have evaluated the role of *miR-210-3p* on the development of insulin resistance by administering nanoparticle encapsulated control mimic or FAM conjugated miR-210-3p mimic (2.5mg/kg bw) in tail-vein of lean StndD-fed mice for 6 times in the span of 21 days. The dose for each injection was 5nmole of mimic/mice. In the termination of experiments, we harvested VAT, liver, and skeletal muscle to visualize the presence of fluorescent conjugated mimic.

To decipher the role miR-210-3p loaded EVs of 8 weeks aged C57BL/6J mice fed with Standard-diet were intravenously administered with BMDMs derived extracellular vesicles (2 x 10^6 EVs per animal) particles with an interval of 3 days for 21 days (total 6 times). To isolate EVs BMDMs were co-transfected with Dicer siRNA and control mimic or Dicer siRNA and miR-210-3p mimic followed by the collection of conditioned media and EVs isolation. To monitor the in-vivo trafficking of EVs, BMDMs were stained with Vibrant DiO (Invitrogen) prior to EVs isolation. Fluorescent-labeled EVs were isolated, purified, and administered through tail-vein injection in mice. The confirmation was done by taking out biopsies of VAT, Liver, and skeletal muscles.

We measured the body weight of the animals on a regular basis and determined the glucose tolerance test (GTT) by measuring blood glucose levels before and after oral gavages of 1 g glucose/kg bw at the indicated time points before the termination of all of the animal experiments. Similarly, insulin tolerance test (ITT) was performed by injecting 1 IU insulin/kg bw. For histochemistry analyses, a small portion of harvested tissues were freshly frozen followed by cryosectioning.

All animal experiments were performed following the guidelines prescribed by and with the approval of the Institutional Animal Ethics Committee (IAEC) NIPER Mohali, Punjab.

4.4.3 Human subjects

As described in Section 3.4.3

4.4.4 Cell culture and treatments

3T3-L1 cells procured from ATCC (cat. no. ATCCL-173), were cultured in growth medium, containing DMEM (Gibco^{TM}/Life Technologies, cat. no. #11995073) supplemented with 10% BCS (ATCC; cat. no. ATCC30-2030) and 1% Penicillin-Streptomycin Solution (Gibco^{TM}/Life Technologies, cat. no. #15140122). 3T3-L1 preadipocytes were differentiated into adipocytes following chemically induced differentiation protocol of ATCC, such as medium containing DMEM with high glucose, HI- FBS, 1.0 µM Dexamethasone, 0.5 mM IBMX, and 1.0 µg/mL Insulin were

added upon full confluency. Later on, differentiation medium replaced by Adipocyte maintenance medium containing DMEM with high glucose, 10% HI- FBS, and 1.0 µg/mL Insulin. HepG2, hepatocyte cells were procured from NCCS, Pune, India and cultured in Minimum Essential Medium (ATCC, Cat. No. 30-2003), supplemented with 10% HI-FBS (Gibco™/Life Technologies, cat. no. #10082147) and 1% Penicillin-Streptomycin Solution (Gibco™/Life Technologies, cat. no. #15140122). C2C12 myoblasts cells were procured from ATCC, and cultured in Dulbecco's Modified Eagle's Medium (Catalog No. 30-2002), supplemented with 10% HI-FBS (Gibco™/Life Technologies, cat. no. #10082147) and 1% Penicillin-Streptomycin Solution (Gibco™/Life Technologies, cat. no. #15140122). RAW264.7 macrophage cells were obtained from National Centre for Cell Science (NCCS), Pune, India, and cultured in DMEM (Gibco™/Life Technologies, cat. no. #11995073) supplemented with 10% FBS (Gibco™/Life Technologies, cat. no. #10082147) and 1% Penicillin-Streptomycin Solution (Gibco™/Life Technologies, cat. no. #15140122) at 37°C in humidified atmosphere with 5% CO_2. We incubated RAW264.7macrophages with fixed concentration of palmitate (0.75mM) and exposed them to hypoxia condition (1% O_2, and 5% CO_2) for different time periods in the Heracell™ VIOS 160i incubator (Thermo Scientific).

To culture bone marrow-derived macrophages (BMDMs), we surgically removed the femur and tibia from 8-10 weeks C57BL/6J mice in a sterile environment and flushed out bone marrow cells, and differentiated into BMDM following literature (Toda et al., 2021). Briefly, epiphyses from bone marrow were removed and were gently washed with 2 ml of PBS, 2-3 times. The bone marrow cells were collected in a 50 ml tube followed by centrifuge at 200xg for 5 mins at 4°C. Cell pellets were resuspended with chilled RBC lysis solution for 5 mins followed by centrifuge at 200xg for 5 mins at 4°C. The BM cell pellet was further resuspended in a growth media (DMEM high glucose with 10% HI-FBS, 1% Pen-Strep) containing 1ng/ml mouse M-CSF1 recombinant protein (Gibco, cat. no. PMC2044) and passed through a 100µM sterile cell strainer to remove debris and macroparticles. Cells were seeded in a 6-well plate with 0.5 x 10^6 cells per well and 3 x 10^6 cells in 100 mm dish, cultured for 6 days prior to further experiments.

We cultured adipose tissue macrophages (F4/80+), sorted from the stromal vascular fraction (SVF), which was isolated from the vWAT of lean and obese mice following Collagenase I digestion. The sorting of macrophages was performed in BD FACS Aria Cell Sorter (Franklin Lakes, New Jersey; USA). The macrophages were cultured in RPMI 1640 (Gibco™/ Life Technologies, cat. no. #A1049101) supplemented with 10% FBS and 1% Penicillin-Streptomycin Solution at 37°C in a humidified atmosphere with 5% CO_2 for prior to isolation of EVs released from these cells. All treatments were given in serum and antibiotics-free media and EVs isolation from these cultures was performed in cells having fresh serum and antibiotics-free media, changed at least 16 hours prior to termination of the experiment.

4.4.5 Extracellular vesicle experiments

Isolation and Characterization The macrophage (BMDMs or RAW264.7) cultured media was collected for Extracellular vesicle isolation. After 48 hours of transfection experiments, the complete media was replaced with serum and antibiotics-free media and kept for 16 hours for EVs isolation using EV isolation kit (ExoQuick-TC ULTRA). Prior to initiating isolation process, the conditioned media were centrifuged at 3000x g for 15 minutes and the supernatant was transferred to a fresh tube to remove cells and debris. We have isolated EVs from serum samples of both humans and mice using the ExoQuick ULTRA kit following manufacturer's protocol.

Nanoparticle Tracking Analyses

After isolation and purification of EVs, it was subjected to concentration and size analyses using Nanosight LM10 NTA analyses these vesicles using (Malvern Instruments, Westborough, MA).

Transmission Electron Microscopy

We measured the size of EVs by performing Transmission Electron Microscopy. Briefly, the purified EVs were fixed using 2% paraformaldehyde for 5 minutes at room temperature. 5-7ul of exosomal suspension was loaded onto the carbon-coated copper grid and incubated for 1 min, followed by staining using 2% of uranyl acetate solution on the surface of the EM grid by syringe. The excess staining solution was removed using filter paper & rinsed the grid with a drop of water & then the grid was subjected to drying for 30 mins & then examined by using transmission electron microscopy (Model TF-20), FEI, at NIPER, S.A.S Nagar, Punjab.

RNA and Protein isolation from EVs

EVs isolated from cell culture media or serum with a particle number of 3 $x10^6$ – 5 x 10^6 were considered for miRNA isolation and $1x10^7$ – $1x10^8$ EVs were considered for protein isolation using total exosome RNA and protein isolation kit (Invitrogen cat. no. 4478545) following manufacturers protocol.

4.4.6 Transmission Electron microscopy of Tissue sections

The experiment was performed following the protocol reported earlier (Pant et al., 2023). Briefly, a small portion of adipose tissue was subjected to fixation using 2.5% phosphate-buffered glutaraldehyde for at least 1 hr at room temperature, followed by post-fixation using 1% osmium tetraoxide for 1hr. The samples are subsequently washed using phosphate buffer saline to remove the traces of osmium tetraoxide. The samples were dehydrated in ethanol, followed by propylene oxide, and then embedded in epoxy resin. The samples were sectioned using the glass knife and contrast stained using 4% uranyl

acetate. These thin sections were placed on the copper grid & then were examined by using transmission electron microscopy (Model TF-20), FEI, at NIPER, S.A.S Nagar, Punjab, India.

4.4.7 miR-210-3p mimic transfection: As described in section 3.4.5

4.4.8 Transwell co-culture experiment: As described in section 3.4.6**.** Here, Macrophages were seeded on the trans-well culture insert and stained with Vibrant DiO (Invitrogen) for 24 hours followed by changing media and transfer to a new well having mature adipocyte. The cells in this co-culture setup have been co-exposed to a hypoxic environment along with lipid induction for 16 hours and were considered for microscopy.

4.4.9 Glucose uptake assay: As described in section 3.4.6

4.4.10 Cloning of GLUT4 3'UTR

The GLUT4 3'UTR region was PCR amplified from the genomic DNA of human PBMC using specific cloning primers. The cloning primers were designed using the Takara Bio cloning primer design tool (https://www.takarabio.com/learning-centers/cloning/primer-design-and-other-tools) for targeted amplification of GLUT4 3'UTR region flanked by XbaI and SalI restriction sites. The forward primer contained the XbaI site and the reverse primer contained the SalI site and the sequence details are provided in **Table B**. The PCR amplification of the GLUT4 3'UTR region was performed with a melting temperature (Tm) of 70°C. After 35 cycles of PCR reaction, we confirmed the presence of a band of approximately 1.35 kb in agarose gel electrophoresis that specifies targeted amplification GLUT4 3'UTR region. The target band representing the GLUT4 3'UTR region was subjected to gel purification using the GeneJET Gel Extraction Kit following the manufacturer's instructions. For the construction of the GLUT4 3'UTR-luciferase plasmid, we used pGL3-Myb-3'UTR-luciferase vector (cat. no. #25798, Addgene) (Navarro et al., 2009) as the backbone. We performed restriction digestion of the pGL3-Myb-3'UTR-luciferase vector using XbaI and SalI enzymes for the removal of the Myb-3'UTR region from the vector. For this, 1 µg plasmid was digested by 20 units of each restriction enzyme and incubated for 45 minutes at room temperature followed by the heat-inactivation at 65˚C for 15 mins. The digested reaction mixture was run on 0.8% agarose gel electrophoresis and the target band representing pGL3-luciferase plasmid was subjected to gel extraction. The concentration of the purified plasmid was measured and used for the ligation with purified GLUT4 3'UTR region flanked by XbaI and SalI sites for creating GLUT4 3'UTR-luciferase plasmid. For ligation, 100 ng of the purified pGL3-luciferase plasmid was incubated with 74.2 ng of the purified GLUT4 3'UTR region in the presence of T4 DNA ligase at room temperature for 15 mins following manufacturers' protocol. The ratio of insert to vector DNA was maintained at 3:1, as calculated using the NEBio Calculator. Subsequently, the ligation mixture was transformed into DH5α competent cells and plated on agar

plates containing ampicillin (50 μg/ml). After transformation, single colonies were picked and inoculated in LB Broth for 6-8 h at 37°C for plasmid amplification. Plasmids were then isolated for further experiments.

4.4.11 Site directed mutagenesis

Wild-type GLUT4 3′-UTR plasmid construct was used as template for the generation of mutated GLUT4 3′-UTR plasmids by using QuickChange Lightning Multi Site-Directed Mutagenesis Kit following manufacture's protocol. Primers used to generate the mutated GLUT4 3′-UTR plasmids were designed with the help of QuikChange Primer Design Program available online at www.agilent.com/genomics/qcpd. Primer sequences used for mutated GLUT41 3′-UTR plasmids construction are listed in **Table B**.

4.4.12 GLUT4 3'-UTR luciferase reporter assay

3T3-L1 adipocytes were co-transfected with 500 ng of Wild-type or mutated GLUT4 3′-UTR plasmid and with either control mimic or miR-210-3p mimic (Dharmacon, Lafayette, CO) using Lipofectamine LTX/Plus Reagent (Invitrogen) for 48h in a 24 well plate. Upon termination of treatment, adipocytes were lysed, and luciferase activity was determined using Luciferase Reporter Assay System (Promega) in GloMax Navigator Microplate Luminometer (Promega, Madison, Wisconsin, USA) following the manufacturer's protocol.

4.4.13 Immunocytochemistry: As described in section 3.4.10

4.4.14 Oil-red O staining: As described in section 3.4.12

4.4.15 Immunostaining and Confocal microscopy

Adipose tissue samples collected from human subjects and mice models were immediately washed in sterile saline and then placed in Neutral buffer formalin (10%) for overnight fixation at 4°C. After fixation, adipose tissues were passed through increasing concentration of sucrose solution (10%, 15%, 20%) followed by embedded in OCT (optimal cutting temperature compound, Sigma) and frozen at -60°C followed by cryosections using Cryotome with internal temperature less than -25°C (Leica CM 1860, Leica Biosystem, Wetzlar, Germany). Immunostaining was performed on tissue cryosections using specific antibodies. Briefly, tissue cryosections (10 μm) were placed in gelatin-coated glass slides, fixed in ice-cold methanol for 5 min, blocked with 5% BSA containing blocking buffer, and incubated with specific primary antibodies for 1 h at room temperature. After washing, signal was visualized by subsequent incubation with fluorescence-conjugated appropriate secondary antibodies and counter-stained with anti-fade mounting medium containing DAPI. Images were captured by a Confocal microscope (LSM 880 Carl Zeiss, Germany) and analysis was performed using Zen software.

4.4.16 H&E staining and imaging: As described in section 3.4.13

4.4.17 RNA extraction and Quantitative PCR: As described in section 3.4.14

4.4.18 Immunoblotting: As described in section 3.4.15

4.4.19 Enzyme-linked immunosorbent assay (ELISA): As described in section 3.4.16

4.4.20 Flow cytometry: As described in section 3.4.9

4.4.21 Reanalyses of publicly available snSeq dataset

Human white adipose tissue single cell dataset was used for the analysis (Emont et al., 2022). The RDS file obtained by the authors was loaded into R, processed using Seurat package (Emont et al., 2022). We considered the following criteria to filter the cells: firstly cells originated from OAT tissue only, second being BMI as defining criteria of obese condition (lean: BMI <25 and obese: BMI >30), and thirdly, selected only ASPC, adipocytes, and macrophage cells. Seurat was used to visualize the UMAP projection of the cells and split by obese condition. Additionally, we calculated the proportion of each of the three cell types (ASPC, adipocytes, macrophages) for lean and obese conditions and all the OAT samples. For the mouse dataset (Emont et al., 2022) objects were directly imported in R and handled using Seurat. Mouse dataset was filtered to contain only three cell types, ASPC, adipocyte, and macrophages We calculated the cell proportion of each cell type obtained from HFD and Chow (projected as 'StndD') diet-fed mouse.

4.4.22 Statistical analyses: As described in section 3.4.19

References

Akbar, N., Azzimato, V., Choudhury, R. P., & Aouadi, M. (2019). Extracellular vesicles in metabolic disease. *Diabetologia*, *62*(12), 2179–2187. https://doi.org/10.1007/s00125-019-05014-5

Arcidiacono, B., Chiefari, E., Foryst-Ludwig, A., Currò, G., Navarra, G., Brunetti, F. S., Mirabelli, M., Corigliano, D. M., Kintscher, U., Britti, D., Mollace, V., Foti, D. P., Goldfine, I. D., & Brunetti, A. (2020). Obesity-related hypoxia via miR-128 decreases insulin-receptor expression in human and mouse adipose tissue promoting systemic insulin resistance. *EBioMedicine*, *59*, 102912. https://doi.org/10.1016/j.ebiom.2020.102912

Arora, L., Patra, D., Roy, S., Nanda, S., Singh, N., Verma, A. K., Chakraborti, A., Dasgupta, S., & Pal, D. (n.d.). Hypoxia-induced miR-210-3p expression in lung adenocarcinoma potentiates tumor development by regulating CCL2-mediated monocyte infiltration. *Molecular Oncology*, *n/a*(n/a). https://doi.org/10.1002/1878-0261.13260

Boutens, L., & Stienstra, R. (2016). Adipose tissue macrophages: Going off track during obesity. *Diabetologia*, *59*, 879–894. https://doi.org/10.1007/s00125-016-3904-9

Butler, A., Hoffman, P., Smibert, P., Papalexi, E., & Satija, R. (2018). Integrating single-cell transcriptomic data across different conditions, technologies, and species. *Nature Biotechnology*, *36*(5), Article 5. https://doi.org/10.1038/nbt.4096

Crewe, C., Funcke, J.-B., Li, S., Joffin, N., Gliniak, C. M., Ghaben, A. L., An, Y. A., Sadek, H. A., Gordillo, R., Akgul, Y., Chen, S., Samovski, D., Fischer-Posovszky, P., Kusminski, C. M., Klein, S., & Scherer, P. E. (2021). Extracellular vesicle-based interorgan transport of mitochondria from energetically stressed adipocytes. *Cell Metabolism*, *33*(9), 1853-1868.e11. https://doi.org/10.1016/j.cmet.2021.08.002

Crewe, C., Joffin, N., Rutkowski, J. M., Kim, M., Zhang, F., Towler, D. A., Gordillo, R., & Scherer, P. E. (2018). An Endothelial-to-Adipocyte Extracellular Vesicle Axis Governed by Metabolic State. *Cell*, *175*(3), 695-708.e13. https://doi.org/10.1016/j.cell.2018.09.005

Emont, M. P., Jacobs, C., Essene, A. L., Pant, D., Tenen, D., Colleluori, G., Di Vincenzo, A., Jørgensen, A. M., Dashti, H., Stefek, A., McGonagle, E., Strobel, S., Laber, S., Agrawal, S., Westcott, G. P., Kar, A., Veregge, M. L., Gulko, A., Srinivasan, H., … Rosen, E. D. (2022). A single-cell atlas of human and mouse white adipose tissue. *Nature*, *603*(7903), 926–933. https://doi.org/10.1038/s41586-022-04518-2

Goossens, G. H., Bizzarri, A., Venteclef, N., Essers, Y., Cleutjens, J. P., Konings, E., Jocken, J. W. E., Čajlaković, M., Ribitsch, V., Clément, K., & Blaak, E. E. (2011). Increased Adipose Tissue Oxygen Tension in Obese Compared With Lean Men Is Accompanied by Insulin Resistance, Impaired Adipose Tissue Capillarization, and Inflammation. *Circulation*, *124*(1), 67–76. https://doi.org/10.1161/CIRCULATIONAHA.111.027813

Grant, R. W., & Dixit, V. D. (2015). Adipose tissue as an immunological organ: Adipose Tissue as an Immunological Organ. *Obesity*, *23*(3), 512–518. https://doi.org/10.1002/oby.21003

György, B., Hung, M. E., Breakefield, X. O., & Leonard, J. N. (2015). Therapeutic Applications of Extracellular Vesicles: Clinical Promise and Open Questions. *Annual Review of Pharmacology and Toxicology*, *55*(1), 439–464. https://doi.org/10.1146/annurev-pharmtox-010814-124630

Hill, D. A., Lim, H.-W., Kim, Y. H., Ho, W. Y., Foong, Y. H., Nelson, V. L., Nguyen, H. C. B., Chegireddy, K., Kim, J., Habertheuer, A., Vallabhajosyula, P., Kambayashi, T., Won, K.-J., & Lazar, M. A. (2018). Distinct macrophage populations direct inflammatory versus physiological changes in adipose tissue. *Proceedings of the National Academy of Sciences*, *115*(22). https://doi.org/10.1073/pnas.1802611115

Hruby, A., & Hu, F. B. (2015). The Epidemiology of Obesity: A Big Picture. *PharmacoEconomics*, *33*(7), 673–689. https://doi.org/10.1007/s40273-014-0243-x

Huang, Z., & Xu, A. (2021). Adipose Extracellular Vesicles in Intercellular and Inter-Organ Crosstalk in Metabolic Health and Diseases. *Frontiers in Immunology*, *12*. https://www.frontiersin.org/articles/10.3389/fimmu.2021.608680

Jaitin, D. A., Adlung, L., Thaiss, C. A., Weiner, A., Li, B., Descamps, H., Lundgren, P., Bleriot, C., Liu, Z., Deczkowska, A., Keren-Shaul, H., David, E., Zmora, N., Eldar, S. M., Lubezky, N., Shibolet, O., Hill, D. A., Lazar, M. A., Colonna, M., … Amit, I. (2019). Lipid-Associated Macrophages

Control Metabolic Homeostasis in a Trem2-Dependent Manner. *Cell*, *178*(3), 686-698.e14. https://doi.org/10.1016/j.cell.2019.05.054

Jeppesen, D. K., Zhang, Q., Franklin, J. L., & Coffey, R. J. (2023). Extracellular vesicles and nanoparticles: Emerging complexities. *Trends in Cell Biology*, *33*(8), 667–681. https://doi.org/10.1016/j.tcb.2023.01.002

Maniyadath, B., Zhang, Q., Gupta, R. K., & Mandrup, S. (2023). Adipose tissue at single-cell resolution. *Cell Metabolism*, *35*(3), 386–413. https://doi.org/10.1016/j.cmet.2023.02.002

McNelis, J. C., & Olefsky, J. M. (2014). Macrophages, Immunity, and Metabolic Disease. *Immunity*, *41*(1), 36–48. https://doi.org/10.1016/j.immuni.2014.05.010

Navarro, F., Gutman, D., Meire, E., Cáceres, M., Rigoutsos, I., Bentwich, Z., & Lieberman, J. (2009). miR-34a contributes to megakaryocytic differentiation of K562 cells independently of p53. *Blood*, *114*(10), 2181–2192. https://doi.org/10.1182/blood-2009-02-205062

Pan, Y., Hui, X., Hoo, R. L. C., Ye, D., Chan, C. Y. C., Feng, T., Wang, Y., Lam, K. S. L., & Xu, A. (2019). Adipocyte-secreted exosomal microRNA-34a inhibits M2 macrophage polarization to promote obesity-induced adipose inflammation. *Journal of Clinical Investigation*, *129*(2), 834–849. https://doi.org/10.1172/JCI123069

Patra, D., Roy, S., Arora, L., Kabeer, S. W., Singh, S., Dey, U., Banerjee, D., Sinha, A., Dasgupta, S., Tikoo, K., Kumar, A., & Pal, D. (2023). miR-210-3p Promotes Obesity-Induced Adipose Tissue Inflammation and Insulin Resistance by Targeting SOCS1-Mediated NF-κB Pathway. *Diabetes*, *72*(3), 375–388. https://doi.org/10.2337/db22-0284

Reilly, S. M., & Saltiel, A. R. (2017). Adapting to obesity with adipose tissue inflammation. *Nature Reviews Endocrinology*, *13*(11), Article 11. https://doi.org/10.1038/nrendo.2017.90

Salomon, C., Das, S., Erdbrügger, U., Kalluri, R., Kiang Lim, S., Olefsky, J. M., Rice, G. E., Sahoo, S., Andy Tao, W., Vader, P., Wang, Q., & Weaver, A. M. (2022). Extracellular Vesicles and Their Emerging Roles as Cellular Messengers in Endocrinology: An Endocrine Society Scientific Statement. *Endocrine Reviews*, *43*(3), 441–468. https://doi.org/10.1210/endrev/bnac009

Saltiel, A. R. (2021). Insulin signaling in health and disease. *The Journal of Clinical Investigation*, *131*(1). https://doi.org/10.1172/JCI142241

Tang, Y., Yang, L.-J., Liu, H., Song, Y.-J., Yang, Q.-Q., Liu, Y., Qian, S.-W., & Tang, Q.-Q. (2023). Exosomal miR-27b-3p secreted by visceral adipocytes contributes to endothelial inflammation and atherogenesis. *Cell Reports*, *42*(1), 111948. https://doi.org/10.1016/j.celrep.2022.111948

Toda, G., Yamauchi, T., Kadowaki, T., & Ueki, K. (2021). Preparation and culture of bone marrow-derived macrophages from mice for functional analysis. *STAR Protocols*, *2*(1), 100246. https://doi.org/10.1016/j.xpro.2020.100246

Trajkovski, M., Hausser, J., Soutschek, J., Bhat, B., Akin, A., Zavolan, M., Heim, M. H., & Stoffel, M. (2011). MicroRNAs 103 and 107 regulate insulin sensitivity. *Nature*, *474*(7353), 649–653. https://doi.org/10.1038/nature10112

Wang, Y., Zhao, M., Liu, S., Guo, J., Lu, Y., Cheng, J., & Liu, J. (2020). Macrophage-derived extracellular vesicles: Diverse mediators of pathology and therapeutics in multiple diseases. *Cell Death & Disease*, *11*(10), Article 10. https://doi.org/10.1038/s41419-020-03127-z

Xu, G., Ji, C., Song, G., Zhao, C., Shi, C., Song, L., Chen, L., Yang, L., Huang, F., Pang, L., Zhang, N., Zhao, Y., & Guo, X. (2015). MiR-26b modulates insulin sensitivity in adipocytes by interrupting the PTEN/PI3K/AKT pathway. *International Journal of Obesity*, *39*(10), Article 10. https://doi.org/10.1038/ijo.2015.95

Ye, J. (2009). Emerging role of adipose tissue hypoxia in obesity and insulin resistance. *International Journal of Obesity*, *33*(1), Article 1. https://doi.org/10.1038/ijo.2008.229

Ying, W., Gao, H., Dos Reis, F. C. G., Bandyopadhyay, G., Ofrecio, J. M., Luo, Z., Ji, Y., Jin, Z., Ly, C., & Olefsky, J. M. (2021). MiR-690, an exosomal-derived miRNA from M2-polarized macrophages, improves insulin sensitivity in obese mice. *Cell Metabolism*, *33*(4), 781-790.e5. https://doi.org/10.1016/j.cmet.2020.12.019

Ying, W., Riopel, M., Bandyopadhyay, G., Dong, Y., Birmingham, A., Seo, J. B., Ofrecio, J. M., Wollam, J., Hernandez-Carretero, A., Fu, W., Li, P., & Olefsky, J. M. (2017). Adipose Tissue Macrophage-Derived Exosomal miRNAs Can Modulate In Vivo and In Vitro Insulin Sensitivity. *Cell*, *171*(2), 372-384.e12. https://doi.org/10.1016/j.cell.2017.08.035

Chapter 5 |

Obese adipose tissue microenvironment-induced nuclear FetuinA that promotes adipocyte senescence

5.1 Background

Obesity is an aetiological factor considered the hallmark of severe metabolic disorders including insulin resistance and T2D (B. B. Kahn & Flier, 2000; S. E. Kahn et al., 2006). The colossal expansion of adipose tissue, mainly due to the hypertrophic growth of adipocytes, in obese subjects has coincided with the hypoxic and lipid-enriched microenvironment of adipose tissue (AT*env*) which is causally linked to the remodeling and dysfunction of adipocytes (Fuster et al., 2016; Hosogai et al., 2007; Seo et al., 2019). Previous reports indicated that increased circulatory levels of fetuin-A (also known as alpha-2 heremans schmid glycoprotein, AHSG), a member of the cystatin superfamily of cysteine protease inhibitors, positively correlated with obesity progression (Trepanowski et al., 2015) and obesity-related metabolic disorders including T2D (Kröger et al., 2018). Although fetuin-A (FetA) is mainly secreted from hepatocytes(Mukhopadhyay et al., 2014), however, its secretion can also be influenced by other cell types including adipocytes during obesity (Chatterjee et al., 2013). Obesity-induced higher level of circulatory FetA is linked with the chronic low-grade inflammation of adipose tissue by recruiting macrophages and stimulating NF-κB-dependent signalling through direct binding with the toll-like receptor 4 (TLR4) (Pal et al., 2012). It has also been shown that increased systemic FetA level markedly inhibits the insulin signalling pathway by abrogating receptor tyrosine kinase activity for the autophosphorylation of its tyrosine residues and insulin receptor substrate-1 (IRS-1) which results in insulin resistance (Mathews et al., 2000; Srinivas et al., 1993). In addition, epidemiological studies highlighted that the higher level of circulatory FetA is critically linked with the incidence of T2D in aged individual irrespective of their sex or race (Ix et al., 2012). Recent reports also suggest the involvement of adipose tissue dysfunction mainly due to the promotion of adipocyte senescence (Gustafson et al., 2019; Smith et al., 2021; Tchkonia et al., 2010). Although a plethora of studies highlighted the increased abundance of circulating FetA compromised the adipose tissue function, however, till date, intracellular FetA distribution and its role in adipocyte senescence have not been explored. In this context, several cell types such as liver, bone, brain, heart, and adipose tissue have demonstrated senescence-associated dysfunctions causing age- or obesity-related diseases including non-alcoholic fatty liver disease, osteoporosis, cardiovascular diseases, and T2D(Palmer, Gustafson, et al., 2019; Palmer, Xu, et al., 2019). Moreover, while the appearance of senescent pancreatic β-cells is associated with the impairment of glucose homeostasis, the clearance of these cells and recovery of β-cell function improves blood glucose levels (Aguayo-Mazzucato et al., 2019;

Aguayo-Mazzucato & Midha, 2019). In obese individuals and more pronounced those with T2D, a large population of mature and fully differentiated adipocytes manifested the signs of cellular senescence and dysfunction (Gustafson et al., 2019)**.** Recent insights into adipocyte senescence revealed that obesity-associated hypertrophic expansion of adipocytes is critically linked with its dysfunction and characterized by the induction of an inflammatory state which coincided with the reduction of insulin sensitivity and lipid storage capacity (Palmer, Gustafson, et al., 2019). Adipocyte senescence also impairs the adipogenic potential and proliferation of resident progenitor cells (Nerstedt & Smith, 2023). Research advancement in this field suggests that the removal of senescent cells or attenuation of SASP could serve as promising therapeutic strategies to regain or improve adipocyte function including insulin sensitivity. Therefore, understanding of pathophysiological obese AT*env* on adipocyte senescence and the involvement of intracellular FetA therein would provide a key link in connecting the association of adipocyte senescence with T2D.

5.2 Results

5.2.1 Nuclear localization of fetuin-A (fetA) in adipocytes of obese adipose tissue

We examined the distribution of intracellular FetA in vWAT of lean nondiabetic, and obese T2D patients. Immunofluorescence analyses of vWAT tissue sections revealed an increased abundance of FetA in obese T2D patients as compared to lean nondiabetic subjects (**Fig. 5.1A)**. To our surprise, we noticed a massive level of nuclear FetA in the vWAT of obese T2D patients as indicated by the higher co-localization of FetA and DAPI stained nucleus (**Fig. 5.1B**) suggesting obese adipose tissue microenvironment (AT*env*) might be responsible for nuclear accumulation of FetA. Consistent with this, FetA protein level was significantly higher in the nuclear fraction as compared to cytosolic fraction of isolated adipocytes from obese T2D patients (**Fig. 5.1C**). To apprehend whether hypoxic lipid-enriched (HL) microenvironment of obese adipose tissue could be accountable for the nuclear accumulation of FetA, we incubated differentiated 3T3-L1 adipocytes with 0.75 mM palmitate under hypoxic conditions (1% O_2) followed by the isolation of cytosolic and nuclear fractions and subjected to immunoblot analyses of FetA. A significant enhancement of FetA protein level was observed both in cytosolic and nuclear fractions of HL-treated adipocytes, however, the nuclear abundance of FetA was more intense than cytosolic content (**Fig. 5.1D**). Consistently, immunofluorescence analysis also demonstrated the nuclear enrichment of FetA in adipocytes exposed to HL stimulation (**Fig. 5.1E, F).** Furthermore, immunostaining was performed on the isolated nuclei which exhibited notable increase in nuclear localization of FetA in HL-exposed adipocytes (**Fig. 5.1G, H**). However, pre-treatment of adipocytes with a nuclear transport inhibitor, ivermectin, markedly inhibited HL-induced nuclear accumulation of FetA (**Fig. 5.1I,J**). All these results suggest that pathophysiological obese AT*env* promotes the nuclear abundance of FetA in adipocytes.

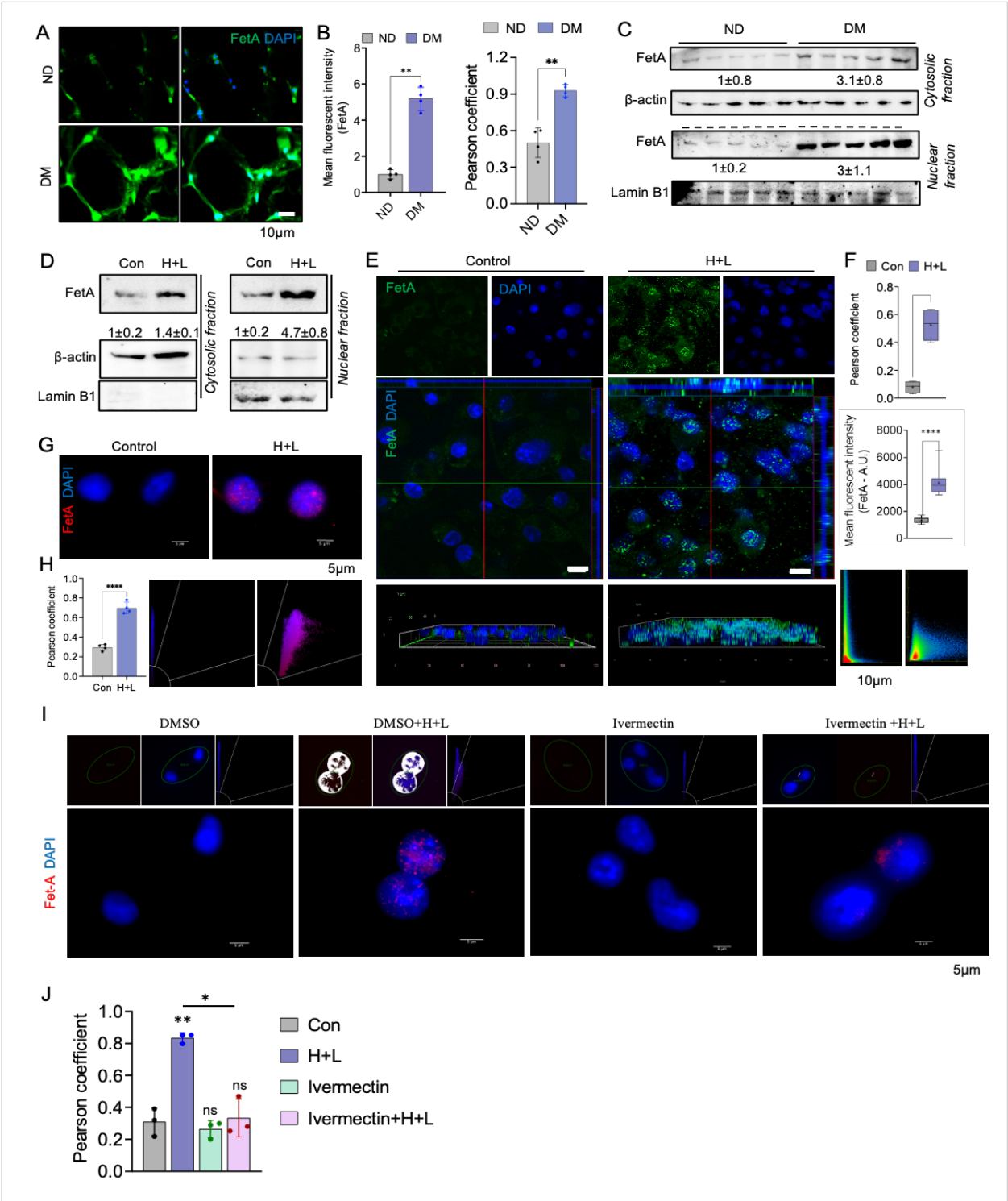

Figure 5.1 | **Nuclear localization of fetuin-A (FetA) in adipocytes of obese adipose tissue**

A: Immunofluorescence analyses of Fetuin-A in histological sections of VAT of lean, non-diabetic, and obese-diabetic individuals. *B*: Quantification of mean fluorescent intensity and colocalization was presented through the Pearson coefficient showed nuclear localization of Fetuin-A in tissue sections. *C*: Immunoblotting and quantification analyses of Fetuin-A in cytosolic lysate and nuclear lysate of adipocytes isolated from the VAT of ND, and DM individuals. β-actin was loading control for cytosolic proteins and Lamin B1 was loading control for nuclear proteins. *D*: Immunoblotting and quantification analyses of Fetuin-A in cytosolic lysate and nuclear lysate of 3T3-L1 adipocytes incubated with palmitate for 16 hours under H+L condition. β-actin was loading control for cytosolic proteins and

Lamin B1 was loading control for nuclear proteins. *E*: Confocal imaging of fetuin-A in adipocytes co-treated with or without H+L. *F*: Quantification of mean fluorescent intensity and nuclear localization of fetuin-A was quantified by measuring Pearson's correlation coefficient. *G*: Immunofluorescence imaging showing Fetuin-A expression in isolated nuclei from control and H+L treated adipocytes. *H*: Colocalization of fetuin-A in nuclei was quantified following pearson's correlation coefficient. *I*: Immunofluorescence staining and imaging analysis showing expression of Fetuin-A in nuclei isolated from adipocyte treated with either DMSO or ivermectin followed by H+L treatment. *J*: Pearson coefficient analysis for determining colocalization.

5.2.2 Hypoxia-inducible factor-1α regulates the nuclear migration of FetA

In HL-exposed adipocytes, a significant enhancement of FetA and HIF-1α interaction was noticed irrespective of whether immunoprecipitated with either anti-FetA or anti-HIF-1α antibodies followed by the immunoblotting with corresponding counter-antibodies (**Fig. 5.2A**). Similar observations were made from the isolated adipocytes of obese T2D patients and diet-induced mice models of obesity (**Fig. 5.2M,N**). To ensure that HIF-1α is critical for the nuclear translocation of FetA in obese adipocytes, 3T3-L1 adipocytes were transfected with HIF-1α siRNA in the presence or absence of HL stimulation and compared the results with their respective controls. Co-immunoprecipitation study revealed that nuclear migration of FetA was significantly attenuated in the HIF-1α silenced adipocytes even in the presence of HL incubations (**Fig. 5.2B**).

Immunofluorescence staining of FetA further corroborated the evidence that nuclear localization of FetA was considerably reduced in HIF-1α ablated adipocytes exposed to HL stimulation (**Fig. 5.2C,D and Fig. 5.2O,P**). A striking abolition of FetA-associated HIF-1α was noticed in the nuclear lysates of HIF-1α silenced adipocytes that were exposed to HL conditions (**Fig. 5.2E**). Next, we examined the effect of HIF-1α overexpression on the nuclear migration of FetA in adipocytes in the absence of HL stimulation. The forced expression of HIF-1α markedly increased the nuclear FetA level in adipocytes (**Fig. 5.2F**) and its interaction with HIF-1α (**Fig. 5.2G**). These results suggest the obligatory requirement of HIF-1α in HL-induced nuclear migration of FetA. We then silenced the FetA in HIF-1α overexpressed cells to explore whether the localization pattern of HIF-1α has been influenced by FetA level. HIF-1α overexpression notably enhanced the FetA protein level, which is expected as recent reports showed that HIF-1α promotes FetA gene expression (Rudloff et al., 2021). However, FetA silencing was unable to restrict the nuclear migration of HIF-1α (**Fig. 5.2H, I**) suggesting that HIF-1 α nuclear translocation is independent of cellular FetA level.

To explore the direct physical interaction of Fetuin-A and HIF-1α, the pull-down assay and surface plasmon resonance (SPR) analyses were performed. For pull-down assay, HEK293 cells were co-transfected with HIF-1α -HA and FetA-His (**Fig. 5.2Q**) plasmids followed by the immunoprecipitation of nuclear lysate with anti-his or anti-HA antibodies and then probed with anti-HIF-1α or anti-FetA antibodies, respectively. Data demonstrated a strong interaction between HIF-1α -HA and FetA-His proteins in the nuclear fraction upon their forced co-expression without any environmental stimuli (**Fig. 5.2J**). In SPR analyses, we first flowed the varied concentrations of HIF-1α (analyte) over the Histidine-tagged FetA (ligand) immobilized nitrilotriacetic acid (NTA) sensor chip surface. The SPR sensorgram displayed a concentration-dependent binding of HIF-1α to FetA with higher binding affinity between them as represented by the equilibrium dissociation constant (K_D) value is $1.19x10^{-8}$ M (**Fig. 5.2K and Fig. 5.2R**). To confirm the interaction nature, increasing concentrations of FetA (analyte) were then passed over the HIF-1α (ligand) coated CM5 sensor chip surface. A similar pattern of concentration-dependent enhancement of high affinity binding between FetA and HIF-1α ($K_D = 2.34x10^{-8}$ M) was observed (**Fig. 5.2K and Fig. 5.2R**). All these results suggest a strong biophysical protein-protein interaction between FetA and HIF-1α under pathophysiological AT*env* and their association is necessary for the nuclear localization of FetA. To investigate the specific molecular signatures of FeA and HIF-1α that could participate in their interaction, we collected the 3D structure of these proteins from the AlphaFold Protein Structure Database (EMBL-EBI)(Jumper et al., 2021) and performed FetA-HIF-1α interaction analysis using the ClusPro web server (Desta et al., 2020). We identified the key amino acid residues of FetA that are pivotal for its interaction with HIF-1α (**Fig. 5.2L**). The present study decisively revealed the nuclear accumulation of FetA, with the help of HIF-1α, in the lipid-enriched hypoxic state of adipocytes in obese adipose tissue.

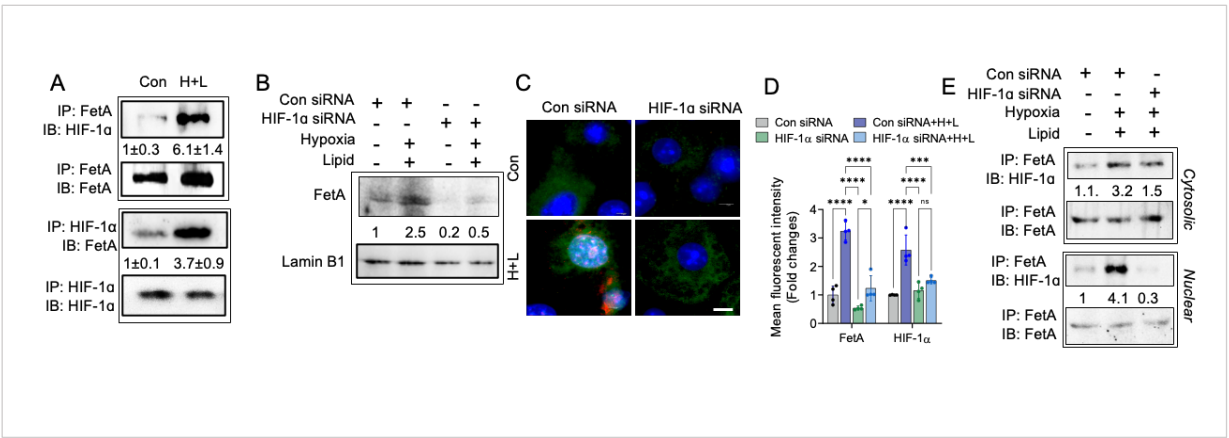

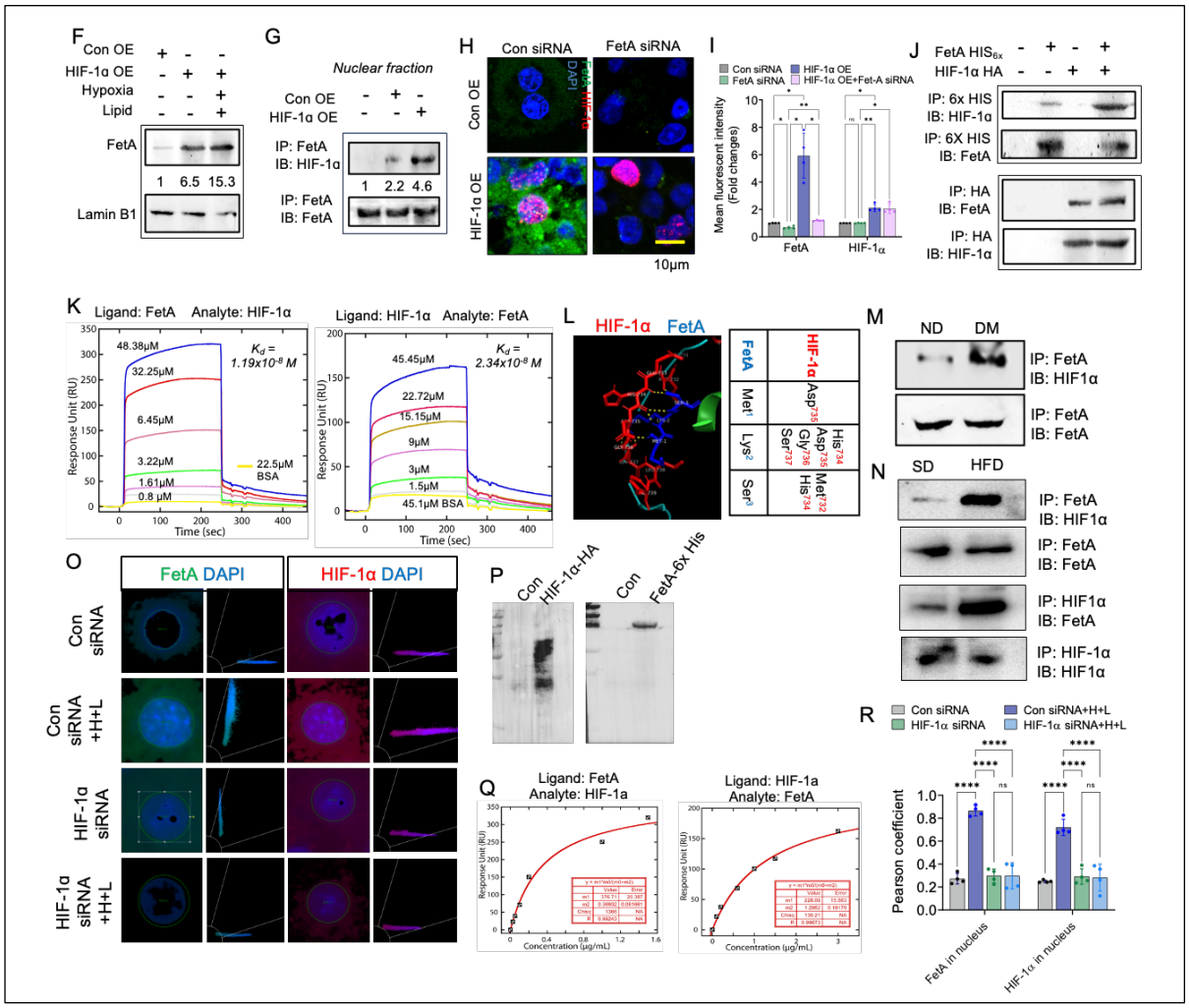

Figure 5.2 | **Hypoxia-inducible factor-1α facilitates nuclear migration of fetuin-A**

A: Western blot analyses of coimmunoprecipitation study showcasing Fetuin-A interaction with HIF-1α in control and H+L treated adipocytes. *B*: Western blot and quantification analyses demonstrating fetuin-A protein expression in the nuclear lysate of Control siRNA or HIF-1α siRNA transfected adipocytes co-treated with or without H+L. *C*: Immunofluorescence analyses revealing nuclear colocalization of fetuin-A and HIF-1α in adipocytes transfected with control siRNA or HIF-1α siRNA in the presence or absence of H+L. *D*: Quantification of Fetuin-A and HIF-1α mean fluorescent intensity (as fold changes) and the colocalization was measured by Pearson's correlation coefficient. *E*: Western blotting analyses of fetA and HIF-1α on immunoprecipitated samples using HIF-1α and FetA antibodies from control siRNA and HIF-1α siRNA transfected adipocyte's cytosolic lysate and nuclear lysate. *F*: Western blotting analyses of Fetuin-A in adipocytes transfected with HIF-1α OE plasmid in the presence or absence of H+L. *G*: Immunoblot analyses of FetA on HIF-1α immunoprecipitated samples from the nuclear lysate of adipocytes, transfected with control overexpression and HIF-1α overexpression plasmid. *H,I*: Immunofluorescence study showing Fetuin-A nuclear localization in adipocytes transfected with HIF-1α overexpression plasmid and/or Fetuin-A siRNA. **I:** Mean fluorescent intensity was noted and plotted for fetA and HIF-1α. *J*: Western blot analyses HIF-1α and FetA on the immunoprecipitation samples from adipocytes, precipitated using anti His antibody and anti-HA antibody. Adipocytes were transfected with HA-tagged HIF-1α plasmid, 6x His tagged FetA plasmid independently or together. *K*: SPR analyses demonstrating representative sensorgrams obtained by flowing described concentration of HIF-1α (left) where FetA acts as ligand and different concentration of FetA flowed (right) HIF-1α as ligand. BSA protein was used as a negative control protein. *L*: Molecular model predicts multiple active binding site (stretch) of human

HIF-1α (Red) and human FetA (Blue). *M*: Western blotting of HIF-1α in FetA immunoprecipitation samples from the ND and DM patients adipocytes, revealing HIF-1α and FetA interaction. *N*: Western blotting of HIF-1α in FetA immunoprecipitated samples from the adipocytes isolated from SD and HFD VAT, revealing HIF-1α and FetA interaction. *O,P*: Pearson coefficient revealing colocalization of FetA and HIF-1α in the nucleus of adipocytes transfected with control siRNA and HIF-1α siRNA and co-incubated with or without H+L. *Q*: Immunoblot analyzing demonstrating HIF-1α overexpression and FetA overexpression in adipocytes. *R*: Concentration-dependent response units (RU) of analytes. Experimental set up was FetA as ligand and HIF-1α as analyte (up) HIF-1α as ligand and FetA as analyte (below). BSA protein was used as a control protein.

5.2.3 Nuclear FetA induces adipocyte senescence and its' inhibition protects from senescence-induced pathogenesis

The SABG staining evinced a considerable enhancement of adipocyte senescence in HL-treated adipocytes as compared to the control (**Fig. 5.3O**). Since cellular senescence is implicated by the induction of various gene expressions that are related to the senescence-associated secretory phenotype (SASP)(Kumari & Jat, 2021), we evaluated these gene expressions by RT-qPCR analyses. We observed a heightened expression of SASP markers such as *β-gal*, *PAI-1*, *P53*, *P21*, *TNF-α*, *MMP3*, *CCL20*, *IL-8*, *FAS*, *TIMP2*, and *CCND1* in HL-treated adipocytes (**Fig. 5.3P**) which altogether supports the hypothesis that obese AT*env* activates senescence in mature adipocytes. Further, confocal imaging of HL-treated adipocytes displayed that enrichment of nuclear FetA coincided with the elevated level of β-gal expression (**Fig. 5.3Q**). To elucidate the function of nuclear FetA in adipocyte senescence, we executed a *gain-of-function* study by transfecting adipocytes with FetA and HIF-1α overexpression plasmids either individually or in combination. The FetA and HIF-1α co-transfected cells showcased a striking increase in nuclear FetA level was coincided with the significant increment of *β-gal*, *TNF-α*, *IL-6*, and *MMP3* expression (**Fig. 5.3A,B**). Interestingly, overexpression of FetA alone has not been enough to promote adipocyte senescence (**Fig. 5.3A, B**), emphasizing the importance of HIF-1α -mediated nuclear transport of FetA on the induction of senescence in obese adipocytes. The SABG assay result further correlated with our observations as SABG staining intensity was markedly augmented in FetA and HIF-1α overexpressed adipocytes (**Fig. 5.3C**). To get a clear picture of the senescent landscape in mature adipocytes in an obese state, we co-transfected FetA and HIF-1α plasmids in adipocytes and scanned the expression profile of SASP marker genes. The RT-qPCR analyses illustrated a profound elevation of SASP markers (*β-gal*, *PAI-1*, *IL-6*, *CCL2*, *MMP3*, *TIMP2*, *CCL20, CCND1, FAS*, *P21*, and *P53*) gene expression in FetA and HIF-1α plasmid co-transfected cells (**Fig. 5.3D**).

Further, *loss-of-function* of FetA was employed by transfecting the adipocytes with the FetA anti-sense oligonucleotides (ASO) to unravel its importance in adipose senescence. The FetA-ASO transfected adipocytes (**Fig. 5.3R,S**) exhibited a notable inhibition of HL-induced SABG activity (**Fig. 5.3E**) and SASP marker genes (*β-gal*, *PAI-1*, *CXCL-10*, *MMP3*, *IL-8*, *TIMP2*, *CCL20,* and *CCND1*) expression (**Fig. 5.3F**). We also observed that FetA or HIF-1α silenced adipocytes were unable to increase β-gal expression even after the overexpression of their binding partner HIF-1α or FetA, respectively (**Fig. 5.3T,U**). Collectively, these observations indicate the importance of HIF-1α -mediated nuclear migration of FetA in adipocyte senescence during obese conditions. However, future studies with selective inhibition of FetA nuclear migration will strengthen the role of nuclear FetA in the induction of senescence in obese adipocytes.

To comprehend the pathophysiological relevance of nuclear FetA in adipocyte senescence, we developed obese mice model by feeding with high-fat diet for 16 weeks and then administered Control inhibitor morpholino or FetA inhibitor morpholino at regular intervals for 14 days. A significant silencing of FetA was observed in the vWAT of obese animals (**Fig. 5.3G and 5.3V**) along with a considerable reduction in the intensity of SABG staining (**Fig. 5.3H**). Moreover, SASP marker expressions were also significantly reduced in the adipocytes, isolated from the vWAT of FetA ablated obese mice and the cryosection of vWAT (**Fig. 5.3I-K**). Interestingly, we observed a significant decrease in the body weight of FetA-silenced animals along with reduced fasting blood glucose levels (**Fig. 5.3L,M**). However, H&E analyses exhibit nonsignificant alterations in the physical appearance of vWAT (**Fig. 5.3N**).

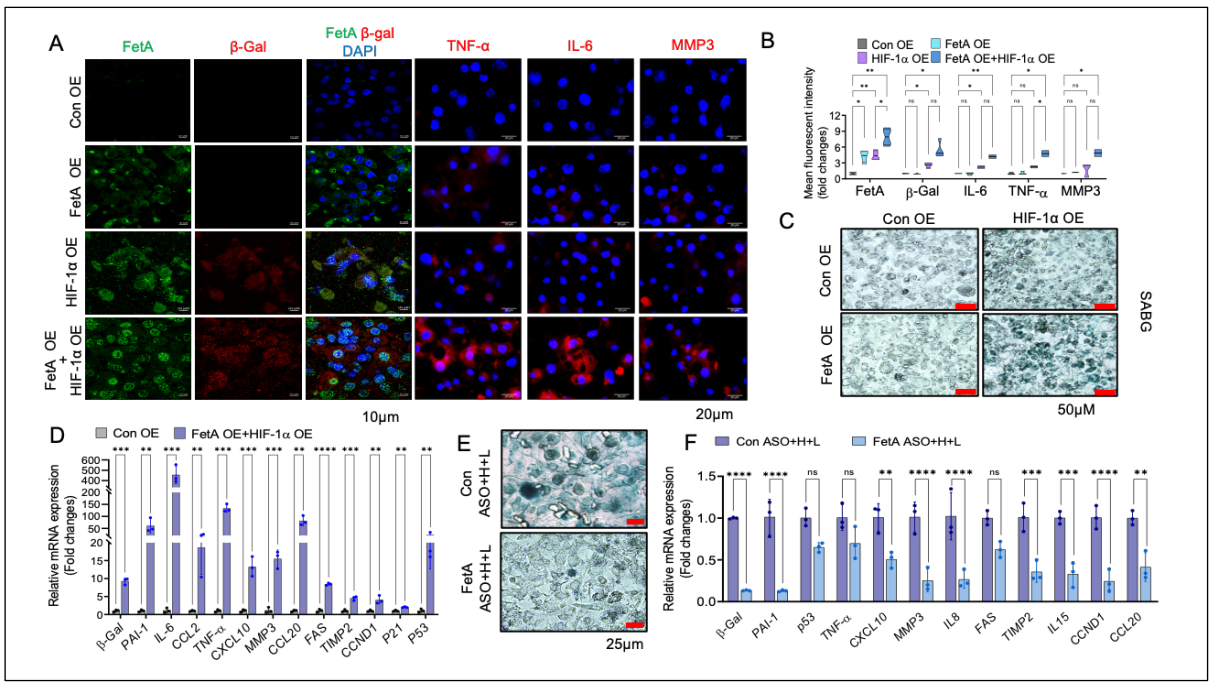

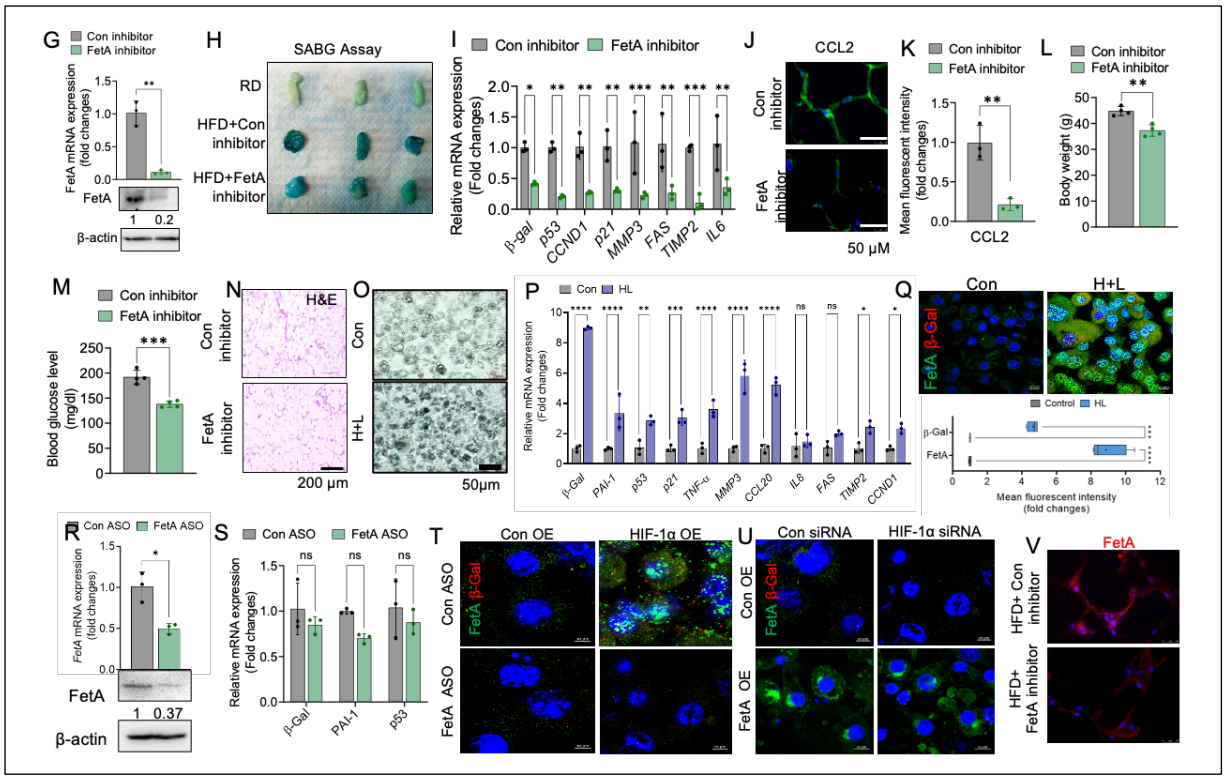

Figure 5.3 | **Nuclear fetuin-A induces adipocyte senescence**

A: Immunofluorescence study was performed using Confocal microscopy exhibits expression of SASP markers β-gal, IL-6, TNF-α, MMP3 (red) and FetA (green) in adipocytes transfected with HIF-1α and Fetuin-A overexpression plasmids independently and combinatorically. *B*: Mean fluorescent intensity quantification analyses of β-galactosidase, IL-6, TNF-α, CCL2, and FetA. *C*: Senescence-associated β-galactosidase (SA-β-gal) staining and imaging analyses in adipocytes transfected with HIF-1α and Fetuin-A overexpression plasmids independently and in combination. *D*: qRT-PCR analyses of SASP genes expression in adipocytes co-transfected with HIF-1α and Fetuin-A overexpression plasmids compared to control plasmid and data presented as fold changes. *E*: SA-β-gal staining of control and FetA silenced adipocytes treated with H+L, demonstrating of blue precipitate formation, which is the mark of senescent cells (scale bar size 50 μm). *F*: mRNA expression analyses by performing qRT-PCR for SASP markers in control and Fetuin-A silenced adipocytes incubated with H+L showing senescence associates gene expression occurs in the pathophysiological condition in FetA nuclear localization dependent manner. *G*: qRT-PCR analyses and western blotting analyses showing FetA expression in the vWAT of HFD animals administered with control inhibitor or FetA inhibitor. *H*: Representative images visually exhibit SA-β-gal staining and intensity pattern in the vWAT samples of RD, HFD+Control inhibitor morpholino, and HFD+FetA inhibitor morpholino. (n=3) *I*: qRT-PCR analyses of SASP marker genes on adipocytes isolated from vWAT of HFD animals injected with control or fetuin-A inhibitor morpholino. *J*: Immunostaining of CCL2 and fluorescence imaging on the cryosection of vWAT and *K*: quantification analyses. *L,M*: measurement of body weight, in gram (L) and fasting blood glucose level (M) of control inhibitor morpholino and fetuin-A inhibitor morpholino administered mice. *N*: H&E staining and brightfield microscopic imaging of vWAT cryosection of control inhibitor morpholino and fetuin-A inhibitor morpholino administered mice. Scale bar size 200μm. *O*: SA-β-Gal staining on adipocytes treated with or without H+L and blue color formation indicates activation of β-Galactosidase. *P*: qRT-PCR analyses of senescent-associated genes in the adipocytes treated with or without H+L. *Q*: Immunofluorescence analysis of FetA, β-Galactocidase in the control and H+L treated adipocytes. *R*: FetA mRNA expression analyses and western blotting analyses in the adipocytes transfected with control ASO and FetA ASO. *S*: qRT-PCR analyses of β-Gal, PAI-1, p53 genes in the control and FetA silenced adipocytes. *T*: Immunofluorescence staining

and confocal imaging analyses of adipocytes transfected with HIF-1α overexpression plasmid, FetA ASO, and in combination to demonstrate the expression of FetA, β-Galactocidase. *U*: Immunofluorescence staining and confocal imaging analyses of adipocytes transfected with HIF-1α siRNA, FetA overexpression plasmid alone or together to study FetA, β-Galactocidase expression. *V*: Immunofluorescence staining and imaging analyses of FetA in the cryosections of VAT from HFD mice administered with control inhibitor or FetA inhibitor and mean fluorescent intensity quantification analyses.

5.3 Discussion

FetA ablated mice are known to be resistant to weight gain on a high-fat diet and exhibit improved insulin sensitivity. FetA gene is mapped to the 3q27 region of the human genome, a well-established T2D and metabolic syndrome susceptibility locus. We have previously shown that obesity induces the expression and secretion of a FetA from hepatocytes and adipocytes (Chatterjee et al., 2013; Dasgupta et al., 2010) that plays a crucial role in the induction of insulin resistance and T2D (Mori et al., 2006), however, its intracellular localization and function in obesity is obscure. Consistent with earlier knowledge we found lipid-rich hypoxic environment induces FetA synthesis, interestingly we observed high nuclear localization of fetuin-A in adipocytes which positively correlates with adipocyte dysfunction. Since FetA lacks any known putative nuclear localization signal (NLS) conferring for its ability to nuclear migration, therefore, it would be intriguing to investigate the mechanism of FetA nuclear translocation in adipocytes under obese AT*env*. For examining the potential candidates that could possibly be responsible for the nuclear migration of FetA in adipocytes under AT*env*, we found novel role of hypoxia-inducible factor 1a (HIF-1α), a highly elevated molecule in adipocytes at obese ATenv, as we recently reported that obese AT*env* potentiates adipose tissue inflammation and insulin resistance by the activation of HIF-1α (Patra et al., 2023). HIF-1α belongs to the family that includes oxygen-sensitive HIF-1α, -2α, and -3α which forms heterodimer with a constitutively expressed non-oxygen responsive HIF-1α subunit of the PAS family (PER, AHR, ARNT, and SIM) (Weidemann & Johnson, 2008). In normoxic conditions, HIF-1α rapidly degraded by the action of prolyl hydroxylase domain (PHD) containing enzymes which cause hydroxylation of proline residues present in the oxygen-dependent death domain (ODDD). The hydroxylation of proline residues in HIF-1α helps the recognition and binding with E3 ubiquitin ligase complex, the von Hippel–Lindau tumor suppressor protein (pVHL), which leads to HIF-1α degradation. During hypoxic conditions, propyl hydroxylation of HIF-1α was inhibited which resulted in its accumulation and nuclear localization followed by the dimerization with HIF-1α. The HIF-1α /HIF-1α heterodimer binds to the core pentanucleotide sequence (RCGTG) present in the hypoxia response elements (HREs) of target genes and governs their expression (Greer et al., 2012; Majmundar et al., 2010; Weidemann & Johnson, 2008). Previous reports demonstrated that FetA is an evolutionarily conserved target gene of HIF-1α (Rudloff et al., 2021) and the increased level of systemic FetA is causally linked with adipose tissue inflammation and

macrophage polarization which is mainly responsible for insulin resistance and T2D, intrauterine growth restriction, fibrosis, and calcification (Rudloff et al., 2021).

The coimmunoprecipitation analysis astonished us having a possible association between FetA and HIF-1α in AT*env* condition. SPR analyses confirms the strong physical interaction of Fetuin-A with HIF-1α, and also bioinformatic tools analyses confirms the same by identifying the key amino acid residues of FetA that are pivotal for its interaction with HIF-1α. However, site directed mutational analyses on FetA will help us to confirm the necessary residues for this linkage and might be playing vital role in the nuclear migration of FetA.

After intriguing discovery of FetA mobilization in the adipocyte nucleus with the help of HIF-1a during obesity, we are then interested in examining its role in adipocyte functionality. Recent reports highlighted that adipocytes undergo a senescence phase with the progression of obesity as well as in aging (Gustafson et al., 2022; Li et al., 2021; Tchkonia et al., 2010). To understand the mature adipocytes senescence machinery under AT*env*, we observed increasing senescence-associated β-galactosidase (SABG) activity in adipocytes residing in obese pathogenic environment with augmented release of SASP markers. Adipocyte-specific overexpression of FetA and HIF-1α activates senescence independent of pathogenic environment which clearly justifies the significance of nuclear fetA in senescence, whereas, silencing of FetA abrogates senescence in adipocytes both in-vitro and in-vivo models of obesity. Direct intervention of fetA inhibitor in obese animals unravels fetA inhibition and protects adipocyte senescence in vWAT along with improving blood glucose levels and reducing bodyweight. In conclusion, our study uncover a novel mechanism for the development of adipose tissue dysfunction in obesity by highlighting the participation of nuclear FetA, through its association with HIF-1a, triggering adipocyte senescence.

The global epidemic of obesity harms millions of life each year, there is the utmost requirement to understand the molecular mechanism of pathogenesis for developing novel therapeutics, therapeutic targets as well as new strategies. Senescent cells are detrimental to physiological function, animal studies revealed an increase of senescent cells by 0.3% severely deteriorates the physical function of animals, and the application of sentolytics improves adipose tissue function both in animals and clinical settings (Xu et al., 2018). Here, we delve how obese pathogenic environment cause adipocyte senescence contributes to metabolic disorder and opens up a new horizon for obesity management.

5.4. Materials and methods

5.4.1 Reagents and antibodies

All tissue culture materials were purchased from Life Technologies/Gibco, Nunc; Grand Island, NY; and Corning, NY. Description of all the antibodies including catalog numbers, and the dilutions used

in different experiments were given in **Table A.** HIF-1α overexpression plasmids; HA-HIF1alpha-pcDNA3 was a gift from William Kaelin, Addgene plasmid # 18949 ; http://n2t.net/addgene:18949; RRID:Addgene_18949), pCAG-HIF1 alpha was a gift from Connie Cepko (Addgene plasmid # 21101; http://n2t.net/addgene: 21101; RRID:Addgene_21101), PBS/pU6- HIF1 alpha RNAi plasmid 1 was a gift from Connie Cepko (Addgene plasmid # 21103; http://n2t.net/addgene:21103; RRID: Addgene_21103), AHSG-bio-His was a gift from Gavin Wright (Addgene plasmid # 52175; http://n2t.net/addgene:52175; RRID:Addgene_52175). We have procured recombinant human HIF-1alpha (cat. No. CSB-RP129074h) from Causabio Technology (Houston, TX, USA). NP40 lysis buffer (cat. no. #FNN0021), Pierce BCA Protein Assay Kit (cat. no. 23227) and Halt Protease and Phosphatase Inhibitor Cocktail (cat.no. #78440) were purchased from Invitrogen (Thermo-Scientific, Grand Island, USA). Clarity Western ECL Blotting Detection Reagent (cat. no. #1705060) and precision plus protein dual-color standards (cat. no. #161-0374) were purchased from Bio-Rad Laboratories (Hercules, CA, USA). Clarity Western ECL Substrate (cat. no. 1705060) and iScript Reverse Transcription Supermix (cat. no. 1708891) from Bio-Rad Laboratories (Hercules, CA); polyvinylidene fluoride membranes (cat. no. 548IPVH00010), Ivermectin (Cat. No. I8898) from Merck (Darm- stadt, Germany); PowerUp SYBR Green Master Mix (cat. no. A25742); Ready to use X-Gal solution (cat no. R0941) was procured from Applied Biosystems, Thermo Fisher Scientific. VECTASHIELD Antifade Mounting Medium with DAPI (cat. no. H-1500) from Vector Laboratories (Burlingame, CA). Fetuin-A siRNA (sc-39443) was procured from Santa Cruz Biotechnology (Dallas, TX, USA). All primers were synthesized from IDT (Coralville, Iowa, USA) and sequences were presented in **Table B**. EpiQuick^{TM} Nuclear extraction kit (Cat. No. #OP-0002) was procured for EPIGENTEK (Farmingdale, NY, USA). Desalting columns packed with Sephadex G-25 resin (cat. No. PD-10) and NHS-activated Sepharose 4 Fast Flow matrix were procured from Cytiva (Marlborough, MA, USA). Empty gravity column (BB-EGC01) procured from Biobharati Life Sciences (Kolkata, WB, India). Tris, Glycine, Sodium Chloride, Sodium acetate, and other chemicals were procured from Sigma-Adrich (St. Louis, Missouri, USA).

5.4.2 Cell culture and transfection

As described earlier in sections 3.4.4 and 4.4.4. 3T3-L1 cells were cultured and differentiated into adipocytes. For transfection of Control siRNA, HIF-1α siRNA, control overexpression plasmid, HIF-1α OE plasmid, Fetuin-A siRNA, Fetuin-A overexpression plasmid we have used Lipofectamine LTX/Plus Reagent (Invitrogen) for 48h in a 24 well plate according to the manufacturer's protocol. Briefly, 3T3-L1 adipocytes(differentiated), HEK293 cells were cultured in a 6-well plate in an antibiotic-free complete growth medium prior to transfection. For each well, 5µg of siRNA or overexpression plasmid in Lipofectamine LTX/Plus reagent was prepared separately by mixing in OptiMEM serum-reduced media (Gibco) and incubated for 5 min. The transfection reagent cocktail

containing media was added to the cells containing OptiMEM serum-reduced media and incubated for 4h followed by the addition of antibiotic-free complete growth media. After 48 h of transfection, cells were washed; a fresh complete growth medium was added and used for different treatments.

5.4.3 Mice experiments

As described earlier in Section 3.4.2. Mice fed with the HFD diet for 12 weeks were considered for Fetuin-A inhibitor administration. Control inhibitor or Fetuin-A inhibitor (2.5mg/kg bw) was administered in the tail-vein of HFD mice, 3 times in the span of 14 days. On day 14, animals were utilized for different experiments. We procured (5′-AAGACCAGGGACTTCATGGTTGCTC-3′; accession code: NM_013465.1) and it's control VMOs from Gene Tools to generate FetA silencing in animals.

5.4.4 Clinical samples As described earlier in Section 3.4.3 and data presented in **Table C**.

5.4.5 Adipocyte nuclei isolation and staining

Dish containing adipocytes were washed twice with DPBS and 1 ml of chilled ethanol was added for 5 minutes and discarded. Adipocytes were washed with PBS again and 1ml chilled hypotonic lysis solution was added (20mM HEPES pH 7.5, 5mM Sodium chloride, 0.4%NP-40, Proteases Phosphatase inhibitor cocktail). Cells were scraped thoroughly, followed by passing it through 26 gauge needle for few times. The cell suspension was centrifuged at 600 x g for 20 minutes at 4°C to pellet down the nuclei. A supernatant containing cytoplasmic lysate was removed and nuclei pellet was washed 2-3 times with the hypotonic lysis solution. Nuclei pellets were resuspended in 0.2% triton X-100 containing PBS and incubated for 5 minutes followed by incubation with 3% BSA solution for 15 minutes. Primary antibody incubation for 1 hour followed by washing with PBS containing 0.1 % Tween-20 (PBST) solution and secondary antibody incubation was performed. Nuclei suspension was washed and 100nM DAPI solution was added for 2 minutes followed by a washing. Nuclei were suspended in PBS and glycerol was added to it. It was spread in a coated glass slide for fluorescent imaging.

5.4.6 Nuclear protein isolation

5-6x10^6 adipocytes were considered for nuclear protein isolation using a nuclear protein extraction kit- EpiQuick Nuclear Extraction Kit I (cat. No. OP-0002) following manufacturer protocol.

5.4.7 Co-immunoprecipitation

An immunoprecipitation study was performed on the adipocytes isolated from VAT of humans, mice, and in-vitro cultures of adipocytes. Approximately 5-6x10^6 adipocytes from tissue and 3x10^6 3T3-L1 adipocytes were considered total protein isolation. 3T3-L1 Adipocytes were differentiated in a 60 mm dish having a density of 3x10^6 and were considered for the Co-IP study. After completion of treatments, adipocytes were washed with chilled DPBS and lysed using freshly prepared lysis buffer followed by total protein isolation and quantification. Similarly, total protein was isolated and quantified from the adipocytes of the tissue sample. A total of 200 µg proteins suspended in were incubated with 3µg of HIF-1α or Fetuin-A, overnight at 4°C using a rotating mixture platform. The immunocomplex was precipitated by incubating with protein-A magnetic beads (sure beads, BioRad) for 2 hours. Protein-A bound immunocomplex was pulled down using a magnetic rack and washed with 0.1% Tween 20 containing DPBS. This washing and magnetic pulldown step was performed thrice. The pulled proteins complex was added with 4x reducing laemmlli sample buffer and boiled for 5 minutes followed by placing the tubes to remove magnetic beads and collection of supernatant. The isolated supernatant was run in SDS PAGE followed by immunoblotting analyses.

5.4.8 SPR analysis

The surface plasmon resonance (SPR) analysis was performed to measure the binding affinity between FET and HIF-1α protein. The measurements were performed using a Biacore-X100 instrument using a CM5 chip (GE Healthcare). All the measurements were performed using 20 mM HEPES buffer containing 150 mM NaCl, pH 7.3 at 25 °C. The surface of the CM5 sensor chip was coated (flow rate 10 µl/min) with anti-His-antibody as the target proteins contain His_{6x} tag. The anti-His-antibody capture level was 7000 response units (RU). One of the proteins (His-tag) was then immobilized on the antibody-coated surface as a ligand, and the other protein (without His-tag) was then passed over the surface as an analyte and vice versa. BSA was chosen as a control protein. The sensorgrams were analyzed to investigate the corresponding equilibrium dissociation constant (K_D) of the protein-protein interaction.

5.4.9 Protein-protein docking analyses

The protein (HIF1a & Fetuin A) structures were sourced from the European Bioinformatics Institute's AlphaFold Protein Structure Database (EMBL-EBI) (Jumper et al., 2021). These

structures were subsequently prepared using PyMol (PyMOL v2.5 - Incentive Product, Schrodinger, LLC). Then the protein-protein interaction study analysis was performed by ClusPro, a web server utilizing the PIPER rigid-body docking method. This process involves initially sampling all translational and rotational orientations of a ligand-protein concerning a receptor protein. Subsequently, it employs the fast Fourier transform (FFT) correlation approach, utilizing knowledge-based or statistical potentials as the scoring function. This allows it to organize the samples and select the most suitable model for the complex (Desta et al., 2020; Jumper et al., 2021; Kozakov et al., 2017; Vajda et al., 2017; Xia et al., 2016). The ClusPro server conducts three computational steps: 1) Rigid-body docking: It samples an extensive number of conformations, numbering in the billions. 2) Root-mean-square deviation (r.m.s.d.)-based clustering: This identifies the largest clusters among the 1000 lowest-energy structures, representing the most probable complex models. 3) Refinement: Selected structures undergo energy minimization. The efficiency of this method lies in its ability to efficiently calculate energy functions using FFTs. This allows it to thoroughly sample countless conformations of the interacting proteins, evaluating energies at each grid point. Consequently, ClusPro can perform protein docking without prior knowledge of the complex's structure. Later the obtained results underwent analysis and refinement through PyMol.

5.4.10 Senescence-associated beta-galactosidase (SABG) assay

SABG assay was performed following a published protocol (Dimri et. al, 1995) with slight modification. Briefly, adipocytes were washed twice with DPBS, followed by the addition of a fixative solution having 0.2% glutaraldehyde and 2% formaldehyde in PBS and incubated in RT for 5 minutes. Cells were washed with PBS 3 times and freshly prepared SA-βG staining solution for 8 hours in 37°C humidified chamber without having a supply of CO_2.

5.4.11 Immunofluorescence staining and Confocal microscopy: As described earlier in section 4.4.15

5.4.12 Oil-red O staining: As described earlier in section 3.4.12

5.4.13 H&E staining and imaging: As described earlier in section 3.4.13

5.4.14 RNA Extraction and Quantitative PCR: As described earlier in section 3.4.14

5.4.15 Immunoblotting: As described earlier in section 3.4.15

5.4.16 Statistical analyses

Data represented as mean ± SD. Student's *t*-test, two-way ANOVA was used to determine statistical significance, and a p-value at the level of $p<0.05$ was considered significant. Student's t-test was used for the comparisons among two groups and two-way ANOVA analyses were considered for calculating significance when comparing multiple groups. All data analyses were performed using GraphPad Prism software (v.8.0; GraphPad Software, Inc., La Jolla, CA).

References

Aguayo-Mazzucato, C., Andle, J., Lee, T. B., Midha, A., Talemal, L., Chipashvili, V., Hollister-Lock, J., Deursen, J. van, Weir, G., & Bonner-Weir, S. (2019). Acceleration of β Cell Aging Determines Diabetes and Senolysis Improves Disease Outcomes. *Cell Metabolism*, *30*(1), 129-142.e4. https://doi.org/10.1016/j.cmet.2019.05.006

Aguayo-Mazzucato, C., & Midha, A. (2019). β-cell senescence in type 2 diabetes. *Aging (Albany NY)*, *11*(22), 9967–9968. https://doi.org/10.18632/aging.102502

Dasgupta, S., Bhattacharya, S., Biswas, A., Majumdar, S. S., Mukhopadhyay, S., Ray, S., & Bhattacharya, S. (2010). NF-κB mediates lipid-induced fetuin-A expression in hepatocytes that impairs adipocyte function effecting insulin resistance. *Biochemical Journal*, *429*(3), 451–462. https://doi.org/10.1042/BJ20100330

Desta, I. T., Porter, K. A., Xia, B., Kozakov, D., & Vajda, S. (2020). Performance and Its Limits in Rigid Body Protein-Protein Docking. *Structure*, *28*(9), 1071-1081.e3. https://doi.org/10.1016/j.str.2020.06.006

Dimri, G. P., Lee, X., Basile, G., Acosta, M., Scott, G., Roskelley, C., Medrano, E. E., Linskens, M., Rubelj, I., & Pereira-Smith, O. (1995). A biomarker that identifies senescent human cells in culture and in aging skin in vivo. *Proceedings of the National Academy of Sciences*, *92*(20), 9363–9367. https://doi.org/10.1073/pnas.92.20.9363

Fuster, J. J., Ouchi, N., Gokce, N., & Walsh, K. (2016). Obesity-Induced Changes in Adipose Tissue Microenvironment and Their Impact on Cardiovascular Disease. *Circulation Research*, *118*(11), 1786–1807. https://doi.org/10.1161/CIRCRESAHA.115.306885

Greer, S. N., Metcalf, J. L., Wang, Y., & Ohh, M. (2012). The updated biology of hypoxia-inducible factor. *The EMBO Journal*, *31*(11), 2448–2460. https://doi.org/10.1038/emboj.2012.125

Gustafson, B., Nerstedt, A., & Smith, U. (2019). Reduced subcutaneous adipogenesis in human hypertrophic obesity is linked to senescent precursor cells. *Nature Communications*, *10*(1), 2757. https://doi.org/10.1038/s41467-019-10688-x

Hosogai, N., Fukuhara, A., Oshima, K., Miyata, Y., Tanaka, S., Segawa, K., Furukawa, S., Tochino, Y., Komuro, R., Matsuda, M., & Shimomura, I. (2007). Adipose Tissue Hypoxia in Obesity and Its Impact on Adipocytokine Dysregulation. *Diabetes*, *56*(4), 901–911. https://doi.org/10.2337/db06-0911

Ix, J. H., Biggs, M. L., Mukamal, K. J., Kizer, J. R., Zieman, S. J., Siscovick, D. S., Mozaffarian, D., Jensen, M. K., Nelson, L., Ruderman, N., & Djousse, L. (2012). Association of Fetuin-A With Incident Diabetes Mellitus in Community-Living Older Adults. *Circulation*, *125*(19), 2316–2322. https://doi.org/10.1161/CIRCULATIONAHA.111.072751

Johnson, A. M. F., & Olefsky, J. M. (2013). The Origins and Drivers of Insulin Resistance. *Cell*, *152*(4), 673–684. https://doi.org/10.1016/j.cell.2013.01.041

Jumper, J., Evans, R., Pritzel, A., Green, T., Figurnov, M., Ronneberger, O., Tunyasuvunakool, K., Bates, R., Žídek, A., Potapenko, A., Bridgland, A., Meyer, C., Kohl, S. A. A., Ballard, A. J., Cowie, A., Romera-Paredes, B., Nikolov, S., Jain, R., Adler, J., … Hassabis, D. (2021). Highly accurate

protein structure prediction with AlphaFold. *Nature*, *596*(7873), Article 7873. https://doi.org/10.1038/s41586-021-03819-2

Kahn, B. B., & Flier, J. S. (2000). Obesity and insulin resistance. *The Journal of Clinical Investigation*, *106*(4), 473–481. https://doi.org/10.1172/JCI10842

Kahn, S. E., Hull, R. L., & Utzschneider, K. M. (2006). Mechanisms linking obesity to insulin resistance and type 2 diabetes. *Nature*, *444*(7121), Article 7121. https://doi.org/10.1038/nature05482

Kozakov, D., Hall, D. R., Xia, B., Porter, K. A., Padhorny, D., Yueh, C., Beglov, D., & Vajda, S. (2017). The ClusPro web server for protein–protein docking. *Nature Protocols*, *12*(2), Article 2. https://doi.org/10.1038/nprot.2016.169

Kröger, J., Meidtner, K., Stefan, N., Guevara, M., Kerrison, N. D., Ardanaz, E., Aune, D., Boeing, H., Dorronsoro, M., Dow, C., Fagherazzi, G., Franks, P. W., Freisling, H., Gunter, M. J., Huerta, J. M., Kaaks, R., Key, T. J., Khaw, K. T., Krogh, V., … Wareham, N. J. (2018). Circulating Fetuin-A and Risk of Type 2 Diabetes: A Mendelian Randomization Analysis. *Diabetes*, *67*(6), 1200–1205. https://doi.org/10.2337/db17-1268

Kumari, R., & Jat, P. (2021). Mechanisms of Cellular Senescence: Cell Cycle Arrest and Senescence Associated Secretory Phenotype. *Frontiers in Cell and Developmental Biology*, *9*. https://www.frontiersin.org/articles/10.3389/fcell.2021.645593

Majmundar, A. J., Wong, W. J., & Simon, M. C. (2010). Hypoxia-Inducible Factors and the Response to Hypoxic Stress. *Molecular Cell*, *40*(2), 294–309. https://doi.org/10.1016/j.molcel.2010.09.022

Mathews, S. T., Chellam, N., Srinivas, P. R., Cintron, V. J., Leon, M. A., Goustin, A. S., & Grunberger, G. (2000). A2-HSG, a specific inhibitor of insulin receptor autophosphorylation, interacts with the insulin receptor. *Molecular and Cellular Endocrinology*, *164*(1), 87–98. https://doi.org/10.1016/S0303-7207(00)00237-9

Mathews, S. T., Rakhade, S., Zhou, X., Parker, G. C., Coscina, D. V., & Grunberger, G. (2006). Fetuin-null mice are protected against obesity and insulin resistance associated with aging. *Biochemical and Biophysical Research Communications*, *350*(2), 437–443. https://doi.org/10.1016/j.bbrc.2006.09.071

Mathews, S. T., Singh, G. P., Ranalletta, M., Cintron, V. J., Qiang, X., Goustin, A. S., Jen, K.-L. C., Charron, M. J., Jahnen-Dechent, W., & Grunberger, G. (2002). Improved Insulin Sensitivity and Resistance to Weight Gain in Mice Null for the Ahsg Gene. *Diabetes*, *51*(8), 2450–2458. https://doi.org/10.2337/diabetes.51.8.2450

Mori, K., Emoto, M., Yokoyama, H., Araki, T., Teramura, M., Koyama, H., Shoji, T., Inaba, M., & Nishizawa, Y. (2006). Association of Serum Fetuin-A With Insulin Resistance in Type 2 Diabetic and Nondiabetic Subjects. *Diabetes Care*, *29*(2), 468. https://doi.org/10.2337/diacare.29.02.06.dc05-1484

Mukhopadhyay, S., Mondal, S. A., Kumar, M., & Dutta, D. (2014). Proinflammatory and Antiinflammatory Attributes of Fetu Iv-A: A Novel Hepatokine Modulating Cardiovascular and Glycemic Outcomes in Metabolic Syndrome. *Endocrine Practice*, *20*(12), 1345–1351. https://doi.org/10.4158/EP14421.RA

Nerstedt, A., & Smith, U. (2023). The impact of cellular senescence in human adipose tissue. *Journal of Cell Communication and Signaling*, *17*(3), 563–573. https://doi.org/10.1007/s12079-023-00769-4

Palmer, A. K., Gustafson, B., Kirkland, J. L., & Smith, U. (2019). Cellular senescence: At the nexus between ageing and diabetes. *Diabetologia*, *62*(10), 1835–1841. https://doi.org/10.1007/s00125-019-4934-x

Qatanani, M., & Lazar, M. A. (2007). Mechanisms of obesity-associated insulin resistance: Many choices on the menu. *Genes & Development*, *21*(12), 1443–1455. https://doi.org/10.1101/gad.1550907

Rudloff, S., Janot, M., Rodriguez, S., Dessalle, K., Jahnen-Dechent, W., & Huynh-Do, U. (2021). Fetuin-A is a HIF target that safeguards tissue integrity during hypoxic stress. *Nature Communications*, *12*(1), Article 1. https://doi.org/10.1038/s41467-020-20832-7

Seo, J. B., Riopel, M., Cabrales, P., Huh, J. Y., Bandyopadhyay, G. K., Andreyev, A. Yu., Murphy, A. N., Beeman, S. C., Smith, G. I., Klein, S., Lee, Y. S., & Olefsky, J. M. (2019). Knockdown of Ant2

Reduces Adipocyte Hypoxia And Improves Insulin Resistance in Obesity. *Nature Metabolism*, *1*(1), 86–97. https://doi.org/10.1038/s42255-018-0003-x

Smith, U., Li, Q., Rydén, M., & Spalding, K. L. (2021). Cellular senescence and its role in white adipose tissue. *International Journal of Obesity*, *45*(5), Article 5. https://doi.org/10.1038/s41366-021-00757-x

Spinelli, R., Baboota, R. K., Gogg, S., Beguinot, F., Blüher, M., Nerstedt, A., & Smith, U. (2023). Increased cell senescence in human metabolic disorders. *The Journal of Clinical Investigation*, *133*(12). https://doi.org/10.1172/JCI169922

Srinivas, P. R., Wagner, A. S., Reddy, L. V., Deutsch, D. D., Leon, M. A., Goustin, A. S., & Grunberger, G. (1993). Serum alpha 2-HS-glycoprotein is an inhibitor of the human insulin receptor at the tyrosine kinase level. *Molecular Endocrinology*, *7*(11), 1445–1455. https://doi.org/10.1210/mend.7.11.7906861

Trepanowski, J. F., Mey, J., & Varady, K. A. (2015). Fetuin-A: A novel link between obesity and related complications. *International Journal of Obesity*, *39*(5), Article 5. https://doi.org/10.1038/ijo.2014.203

Vajda, S., Yueh, C., Beglov, D., Bohnuud, T., Mottarella, S. E., Xia, B., Hall, D. R., & Kozakov, D. (2017). New additions to the ClusPro server motivated by CAPRI. *Proteins: Structure, Function, and Bioinformatics*, *85*(3), 435–444. https://doi.org/10.1002/prot.25219

Van Deursen, & M, J. (2014). The role of senescent cells in ageing. *Nature*, *509*(7501), Article 7501. https://doi.org/10.1038/nature13193

von Loeffelholz, C., Horn, P., Birkenfeld, A. L., Claus, R. A., Metzing, B. U., Döcke, S., Jahreis, G., Heller, R., Hoppe, S., Stockmann, M., Lock, J. F., Rieger, A., Weickert, M. O., Settmacher, U., Rauchfuß, F., Pfeiffer, A. F. H., Bauer, M., & Sponholz, C. (2016). Fetuin A is a Predictor of Liver Fat in Preoperative Patients with Nonalcoholic Fatty Liver Disease. *Journal of Investigative Surgery*, *29*(5), 266–274. https://doi.org/10.3109/08941939.2016.1149640

Weidemann, A., & Johnson, R. S. (2008). Biology of HIF-1α. *Cell Death & Differentiation*, *15*(4), Article 4. https://doi.org/10.1038/cdd.2008.12

Wiley, C. D., & Campisi, J. (2021). The metabolic roots of senescence: Mechanisms and opportunities for intervention. *Nature Metabolism*, *3*(10), Article 10. https://doi.org/10.1038/s42255-021-00483-8

Xia, B., Vajda, S., & Kozakov, D. (2016). Accounting for pairwise distance restraints in FFT-based protein–protein docking. *Bioinformatics*, *32*(21), 3342–3344. https://doi.org/10.1093/bioinformatics/btw306

Xu, M., Pirtskhalava, T., Farr, J. N., Weigand, B. M., Palmer, A. K., Weivoda, M. M., Inman, C. L., Ogrodnik, M. B., Hachfeld, C. M., Fraser, D. G., Onken, J. L., Johnson, K. O., Verzosa, G. C., Langhi, L. G. P., Weigl, M., Giorgadze, N., LeBrasseur, N. K., Miller, J. D., Jurk, D., … Kirkland, J. L. (2018). Senolytics improve physical function and increase lifespan in old age. *Nature Medicine*, *24*(8), Article 8. https://doi.org/10.1038/s41591-018-0092-9

Chapter 6 | Summary

6.1 Highlights

In this thesis, compelling evidence has been presented supporting the role of obesity-induced lipid-rich hypoxic adipose tissue microenvironment (ATenv) in the dysfunction of adipose tissue macrophages (ATMs) and adipocytes governing pathophysiological chronic inflammatory state and type 2 diabetes (T2D). This study has provided novel insight on the involvement of specific miRNAs in obese ATenv for the impairment of metabolic functions particularly insulin sensitivity and glucose homeostasis. The following key findings have emerged from this study were highlighted:

1. The present investigation revealed that obese ATenv cause a substantial polarization of ATMs toward proinflammatory M1 phenotype by modulating miRNA-based epigenetic signature in both obese diabetic mouse models and patient samples as compared to their respective control counterparts.

2. The study identified colossal increase of a key hypoxamir miR-210-3p in the ATMs of obese pathophysiological ATenv which critically involved in skewing macrophage M1 phenotype by targeting SOCS1-NF-κB pathway.

3. Administration of miR-210-3p mimic in lean mice markedly induced proinflammatory phenotype in ATMs by activating the NF-κB inflammatory signaling pathway.

4. The direct delivery of anti-miR-210-3p in the adipose tissue of obese mice notably reduced the inflammatory burden which coincided with the alteration of ATMs phenotype toward an anti-inflammatory state by normalizing SOCS1 levels.

5. Furthermore, obese ATMs also promotes the massive release of miR-210-3p-enriched extracellular vesicles (EVs) in disseminating the pathophysiological effect in both paracrine and endocrine manners.

6. Delivery of EVs-loaded with miR-210-3p significantly induced insulin resistance in lean mice by directly targeting multiple insulin pathway molecules, such as GLUT4 and INSR, disrupting the cellular glucose uptake.

7. Moreover, anti-miR-210-3p administration considerably improved the glycemic status of obese, insulin-resistant mice which accompanied with the enhanced levels of insulin signaling pathway molecules phospho-AKT and GLUT4.

8. Further investigation of obesity-associated pathophysiological ATenv on adipocyte function, the present study also discovered fetuin-A (FetA), a well-documented hepatokine, acts as a nuclear protein in obese adipocytes which regulates its senescence, contributing to the development of insulin resistance and chronic inflammation.

9. The nuclear migration of FetA in obese adipocytes has been facilitated by its direct interaction with HIF-1α, a major hypoxia-induced transcription factor, promoting adipocyte senescence and thus suggesting its critical role in the progression of obesity-induced insulin resistance.

10. Furthermore, inhibition of FetA expression in obese mice strikingly reduced the senescent phenotype of adipocytes, emphasizing the significance of FetA as a novel target in the development of therapeutics against obesity-associated adipose tissue dysfunction and insulin resistance.

6.2 Conclusions

This comprehensive study has unveiled critical understanding on the role of obesity-induced lipid-rich hypoxic adipose tissue microenvironment (ATenv) on the metabolic health of individuals. The findings from this study have implications in our understanding of obesity-related pathophysiology and potential therapeutic interventions. It has been found that obese ATenv exerts a profound influence on various cell types within adipose tissue, notably adipocytes and macrophages, promoting a proinflammatory state and contributing to adipose tissue dysfunction. Importantly, these effects extend beyond adipose tissue, adversely impacting insulin-responsive organs like the liver and skeletal muscle. The identification of hypoxamiR-210-3p in the adipose tissue macrophages (ATMs) of obese ATenv as a key player in skewing macrophage polarity towards proinflammatory M1 phenotype and inducing insulin resistance in insulin target cells suggesting it could serve as potential molecular target for future therapeutic interventions against obesity-induced insulin resistance and T2D. However, in-depth studies will be required using transgenic ATMs-specific miR-210-3p ablated mice and extensive preclinical studies with miR-210-3p inhibitor for harnessing applicability of miR-210-3p as novel target and development of therapeutics. Moreover, the present investigation also unravelled a novel role ~~for~~ of nuclear fetuin-A in adipocyte senescence during obese ATenv and thus providing a deeper understanding of metabolic dysfunction in obesity. The manipulation of nuclear fetuin-A levels in obese adipocytes may serve as a promising avenue for future therapeutic development against obesity-induced adipocyte senescence and T2D.

In summary, the findings presented in this study underscore the intricate and multifaceted nature of obesity-related metabolic disturbances. It emphasized the need for a holistic approach to combat the adverse effects of obesity on adipose tissue and insulin-responsive organs, offering potential strategies to alleviate chronic inflammation and insulin resistance, ultimately contributing to the management of metabolic dysfunction. Thus, findings of this study open new avenues for research and hold promise for the development of novel therapeutic interventions in the battle against obesity-associated metabolic dysfunction.

However, inclusion of more sample size of patients will strengthen the results and macrophage-specific miR-210-3p knock-out mice model will provide firm and compelling evidence about the interaction of miR-210-3p with SOCS1 and GLUT4, altogether these shreds of evidence will authenticate and fortify the conclusive statement. Inclusion of adipocyte specific Fetuin-A knock-out mice model will also provide crucial evidence for the origin and role of nuclear fetuin-A in adipocyte senescence contributing white adipose tissue dysfunction.

6.3 Future perspectives

The contribution of the obese adipose tissue microenvironment (AT*env*) to insulin resistance is exceedingly promising and holds great importance in the field of metabolic health. The findings presented in this thesis provide a solid foundation for future investigations and potential clinical applications. Here, we highlight the importance of the present findings and outlined the key future perspectives:

1. By understanding the role of obese AT*env* particularly focussing on higher lipid level and low oxygen tension in adipose tissue inflammation, senescence, and insulin resistance, the present study raises many questions for researchers to consider other environmental factors like adipose resident microbiome and other epigenetic alterations like histone and DNA modifications in obese adipose tissue for the modulation of adipogenesis, lipigenesis, and lipolysis events.

2. Future examination of obese AT*env* on different insulin-responsive organs will imply the importance of early intervention to mitigate ATenv effect on the prevention and/or rescue from the onset of insulin resistance and related metabolic disorders.

3. The identification of miR-210-3p as key player in obesity-induced adipocyte dysfunction and insulin resistance may lead to the discovery of novel biomarkers that can predict an individual's susceptibility to metabolic dysfunction. Such biomarkers could be useful for early diagnosis and risk stratification of obesity-induced metabolic diseases.

4. Future investigation need to perform to understand the mechanistic role of nuclear fetuin-A in senescence markers expression in adipocytes and suppression of fetuin-A nuclear migration in rescuing adipocyte dysfunction and insulin resistance.

5. Investigating the long-term effects of interventions targeting AT*env* will be crucial. It's essential to assess not only their immediate impacts but also their sustainability and potential side effects over extended periods. Beyond therapeutic approaches, future research should also focus on preventive strategies. Understanding how lifestyle modifications, such as diet and exercise, influence AT*env* and subsequent insulin resistance will be critical in designing effective prevention programs.

6. As these findings become integrated into clinical practice, patient education and awareness about the importance of obesity-associated AT*env* in insulin resistance should be emphasized. Empowering individuals with knowledge about lifestyle changes and potential treatments will be vital.

In conclusion, the discoveries made in this thesis regarding the role of obese ATenv in inflammation, senescence, and insulin resistance represent a significant advancement in our understanding of metabolic disorders associated with obesity. The future prospects of this research are poised to revolutionize the field of metabolic medicine by offering novel therapeutic strategies, personalized interventions, and improved outcomes for individuals struggling with obesity-related insulin resistance and its complications. These discoveries have the potential to make a substantial impact on public health by addressing critical aspects of the global obesity epidemic-associated metabolic diseases.

Table A | Antibody

Antibody	Dilution	Company	Catalog No.
Phospho-NF-κBp65 (S-536)	1:1000 for ICC 1:2000 for WB	Abcam	#ab86299
SOCS1	1:100 for IHC 1:1000 for WB	Invitrogen	#38-5200
iNOS	1:400 for ICC 1:400 for IHC 1:1500 for FC	Cell Signaling Technology	#13120
Arginase 1	1:50 for ICC 1:400 for IHC	Cell Signaling Technology	#93668
Anti-Mouse IgG (Alexa Fluor 488 conjugated)	1:1000 for ICC 1:1000 for IHC	Cell Signaling Technology	#4408
Anti-Mouse IgG (Alexa Fluor 594 conjugated)	2μg/ml for ICC	Invitrogen	#A-11032
Anti-Rabbit IgG (Alexa Fluor 488 conjugated)	5μg/ml for ICC 1:500 for IHC	Invitrogen	#A-11034
Anti-Rabbit IgG (Alexa Fluor 568 conjugated)	2μg/ml for ICC 2μg/ml for IHC	Invitrogen	#A-1101
HIF1α	10μg/ml for IHC	Abcam	#ab16066
F4/80	1:50 for IHC	Santa Cruz Biotechnology	#sc-377009
CD68	1μg/ml for IHC	Abcam	#ab125212
PE anti-mouse CD80	0.5μg/million cells for FC	BioLegend	#104707
FITC anti-mouse CD80	1μg/million cells for FC	BioLegend	#104705
APC anti-mouse CD206 (MMR)	0.5μg/million cells for FC	BioLegend	#141707
PE anti-mouse F4/80	1μg/million cells for FC	BioLegend	#123110
PE anti-human CD80	5μl/million cells for FC	BioLegend	#305207
APC anti-human CD163	5μl/million cells for FC	BioLegend	#326510
FITC anti-human CD64	5μl/million cells for FC	BioLegend	#305006
APC anti-mouse/human CD11b	0.25μg/million cells for FC	BioLegend	#101212
PE anti-human CD68 Antibody	5μl/million cells for FC	BioLegend	#333807
TruStainFcX™ (anti-mouse CD16/32)	0.1μg/million cells for FC	BioLegend	#101319
NF-κB p65	2μg/ml for WB	Invitrogen	#PA1-186
HRP conjugated Anti-Mouse IgG antibody	1:20000 for WB	Sigma-Aldrich	#A9044

HRP conjugated Anti-Rabbit IgG antibody	1:20000 for WB	Sigma-Aldrich	#A9169
β-actin	1:1000 for WB	Invitrogen	#AM4302
Akt phospho Ser 473	1:1000 for WB	Cell Signaling Technology	#9271
GLUT4	1:1000 for WB 1:200 for ICC 1:200 for IHC	Cell Signaling Technology	#2213
Akt	1:1000 for WB	BD Biosciences	610860
Insulin Receptor β	1:1000 for WB	Cell Signaling Technology	#3025
IRS1	1:500 for WB	Santa Cruz Biotechnology	sc-8038
Pref1	1:400 for IF	Abcam	ab119930
CD63	1:1000 for WB	Abclonal	A19023
FABP4	1:200 for IF	Cell Signaling Technology	#50699
F4/80	5µg/ml for IF	Abcam	ab6640
Anti-Mouse IgG (Alexa Fluor 647 conjugated)	2µg/ml for ICC	Invitrogen	# A-21235
Anti-Goat IgG (Alexa Fluor 594 conjugated)	2µg/ml for IHC	Invitrogen	# A-11058
Fetuin-A	1:1000 for WB 1: 50 for IP	Cell Signaling Technology	#5258
Fetuin-A	1:1000 for WB	R&D System	MAB1563
Fetuin-A	1:1000 for WB 1:100 for IF 1:150 for IP	Santacruz Biotechnology	SC-166531
HA	1:100 for IP 1:1000 for WB	BioBharati LifeScience	#BB-AB0050
6x-His	1:100 for IP 1:1000 for WB	BioBharati LifeScience	#BB-AB0010
HIF-1α	1:1000 for WB 1: 100 for IF	ABclonal	A11945
Lamin B1	1:1000 for WB	ABclonal	A16909
GLB1	1:100 for IF	Affinity Biosciences	#DF3842
CCL2	1:100 for IF	Santacruz Biotechnology	SC-32771
TNF-α	1:200 for IF	Cell Signaling Technology	#3707
IL-6	1:100 for IF	Invitrogen	MA5-23698
MMP3	1:200 for IF	Invitrogen	PA5-119639

Table B | Primer sequence

Mouse Primers		
Gene	**Foward (5'-3')**	**Reverse (5'-3')**
SOCS1	CAACGGAACTGCTTCTTCGC	AGCTCGAAAAGGCAGTCGAA
IL1B	TGCCACCTTTTGACAGTGATG	GAAGGTCCACGGGAAAGACA
CD163	TGCTCAGGAAACCAATCCCA	ACCTCCACTCTTCCAGCG
CD206	TTCAGCTATTGGACGCGAGG	GAATCTGACACCCAGCGGAA
CD86	CTGTAGGCAGCACGGACTTG	CATGGTGCATCTGGGGTCCAT
CD200R1	TCAGTGGCTTCAGAAAATGCAAA	GTGCCATTGACTTCGCCTTG
FPR2	GAGACCTCAGCTGGTTGTGC	CATCCGGAATCCAGCTACCC
MMP9	CCGACTTTTGTGGTCTTCCC	TTTGGAATCGACCCACGTCT
CCR2	AGGAGCCATACCTGTAAATGC	GGCAGGATCCAAGCTCCAAT
YM1	GTTTGGACCTGCCCCGTTC	CCTTGGAATGTCTTTCTCCACAG
MHC-IIA	GAAGACGACATTGAGGCCGA	GGAACACAGTCGCTTGAGGA
IL13	GTATGGAGTGTGGACCTGGC	CTCTGGGTCCTGTAGATGGC
IL10	CTCGAATGTACCAGGAGCCA	AGGACGTTTGGCACATCCAT
IL4	GCATGGCCCAGAAATCAAGG	GAGAAATCGATGACAGCGCC
INOS	CTTGGTGAAGGGACTGAGCTG	CGTTCTCCGTTCTCTTGCAGT
CCL2	GATGCAGTTAACGCCCCACT	AGCTTCTTTGGGACACCTGC
ARG1	ACATTGGCTTGCGAGACGTA	ATCACCTTGCCAATCCCCAG
TNFA	CGCTGAGGTCAATCTGCCCAAG	GGTCAGAGTAAAGGGGTCAGAGTGG
B-ACTIN	GTACTCTGTGTGGATCGGTGG	AGGGTGTAAAACGCAGCTCAG
IL6	GGGACTGATGCTGGTGACAA	ACAGGTCTGTTGGGAGTGGT
CCL5	CTGCCTCCCCATATTCCTCG	TCGGGTGACAAAGACGACTG
CXCL5	TAAAAGGGGTGCAGTGGGTT	GAGCACCAGCTCGGGATATG
CD64	TCTGCTACTTTGGGTTCCAGTC	ATGTGTAGCGGTGTCTTCCC
MYOCD	ATGACATCAGCCAGGAACGC	GGACCTTTCAGTGGCGGTATT
CUL2	CCTGGACTGGACCATTGCATC	AAGTTTAGTGTTGAAACCTGCTCC
NF-KBIB	GACCTCAATAAACCGGAGCCT	ACCAAGCCTGAGAGAAGCCT
COMMD1	CTGCACAGCCAACTCTATCC	ACACAAAAATTCAGATTCCTGTCCA
GLUT1	GCTGTGCTTATGGGCTTCTC	CACAAGTCTGCATTGCCCAT
GLUT4	CTCCGCATCTTTCCCCCTC	AGTGTTCCAGTCACTCGCTG
AKT2	ACAGCCCTCAAGTATGCCTT	TCCAGCTTGATGTCACGGTA
IRS1	TGGACATCACAGCAGAATGAAGA	TTCCGGTGTCACAGTGCTTT
IRS2	TTTGCCCACAATTCCAAGCG	GTAGCGCTTCACTCTTTCACG
IRS3	GCTGCTACTGCTATGGGTTTC	CATGAATGCTTTGGGCCACC
IRS4	AGAATTCCAGGACCTTGCCG	GTGGCAGTGTAATAACTCTCATTT
INSR	AGATGTCCCATCAAATATTGCCAAA	CAAGAAGGCGGACCACATGA
FET-A	AGGGGCAGAGAGGTAATGGT	AGCACCTTTCAGAGTCGTGG
GLB1	CCGCTTCTACTGGGAGGACC	CCCGTACTCATTCTCAACCTGC
PAI-1	CACAACCCGACAGAGACAATC	TCTGTCTATCCGTTGCCCCT
P53	GCTCACCCTGGCTAAAGTTCT	TGAGGGGAGGAGAGTACGTG
CXCL10	CCACGTGTTGAGATCATTGCCA	CCACTGGGTAAAGGGGAGTG
MMP3	CCCTGCAACCGTGAAGAAGA	GACAGCATCCACCCTTGAGT

IL-8	TAGGCATCTTCGTCCGTCCC	CCTTCACCCATGGAGCATCA	
FAS	GTCCTGCCTCTGGTGCTTG	CAGCAAAATGGGCCTCCTTG	
TIMP	GACTTCATTGTGCCCTGGGA	ATGGGACAGCGAGTGATCTTG	
IL15	TTCTCTGCGCCCAAAAGACT	TTTCCTGACCTCTCTGAGCTG	
CCND1	AGAAGTGCGAAGAGGAGGTC	TTCTCGGCAGTCAAGGGAAT	
CCL20	CTGTGAACCTCCTCAGCCTAAGA	ACCCCAGCTGTGATCATTTCC	
P21	GTCCAATCCTGGTGATGTCC	GTTTTCGGCCCTGAGATGT	
Human Primers			
SOCS1	CACTTCCGCACATTCCGTTC	AGGCCATCTTCACGCTAAGG	
β-actin	GAGCACAGAGCCTCGCCTTT	ACATGCCGGAGCCGTTGTC	
SOCS1 3′ UTR primers			
SOCS1 (mut-1)	TAATGCTGCGTGCGGGCGCTGCCG	CGGCAGCGCCCGCACGCAGCATTA	
SOCS1 (mut-2)	GCCCGCCGTGCACGATTAACTGGGATGC	CATCCCAGTTAATCGTGCACGGCGGGC	
GLUT4 3′UTR primers			
GLUT4 (mut-1)	GTTTCACTGCCCATCTGGGCTGACACCTCC	GGAGGTGTCAGCCCAGATGGGCAGTGAAAC	
GLUT4 (mut-2)	ATCATGGGTTTCACTGCCCATCTAGTCACTGGGCTGACACCTCCCTCACAGAGTG	CACTCTGTGAGGGAGGTGTCAGCCCACAGTCAAGATGGGCAGTGAAACCCATGAT	
Cloning primers			
XbaI (Forward)	GCCGTGTAATTCTAGAGGGGCCAGGCAGGGGTGG		
SalI (Reverse)	AAGGGCATCGGTCGACTGTGGTCTTGGTCTCCATCTCTTC		
microRNA primer sequences			
U6 snRNA	GTGCTCGCTTCGGCAGCACATATACTAAATTGGAACGATACAGAGAAGATTAGCATGGCCCCTGCGCAAGGATGACACGCAAATTCGTGAAGCGTTCCATATTTT	001973	NR_004394
miR-210-3p	CUGUGCGUGUGACAGCGGCUGA	000512	MI0000286
miR-200b -3p	UAAUACUGCCUGGUAAUGAUGA	002251	MIMAT0000233
miR-27a-3p	UUCACAGUGGCUAAGUUCCGC	000408	MIMAT0000537
miR-126	CAUUAUUACUUUUGGUACGCG	000451	MIMAT0000137

Table C | Patient demographic details

Pathological features	
Non-obese non-diabetic patients:	
Number of patients	16
Age (median range)	43.6 ± 10.7 (19-65 years)
Gender	Male (n=6)
	Female (n=10)
BMI (median range)	24.3 ± 2.01 (19.4 - 27.4)
Fasting serum glucose (mmol/L)	4.7±0.78
Any other disease (Cancer and NAFLD)	No
Obese diabetic patients:	
Number of patients	14
Age (median range)	48.1 ± 12.2 (22-66 years)
Gender	Male (n=7)
	Female (n=7)
BMI (median range)	34 ± 3.6 (30.1- 44)
Fasting serum glucose (mmol/L)	8.07±3.1
Any other disease (Cancer and NAFLD)	No